UNIVERSITY OF CALIFORNIA, SAN DIEGO

A study of carbon-14 of paleoatmospheric methane for the last glacial termination from ancient glacial ice

A Dissertation submitted in partial satisfaction of the Requirements for the degree of Doctor of Philosophy

in

Earth Sciences

by

Vasilii Victorovich Petrenko

Committee in charge:

Professor Jeffrey P. Severinghaus, Chair
Professor Christopher Charles
Professor Ralph Keeling
Professor Devendra Lal
Professor Dave Lowe
Professor Mark Thiemens
Professor Ray F. Weiss

2008

The Dissertation of Vasilii Victorovich Petrenko is approved, and it is acceptable in quality and form for publication on microfilm:

_____

_____

_____

_____

_____

_____

_____

Chair

University of California, San Diego

2008

DEDICATION

I dedicate this dissertation to my father, Victor F. Petrenko, who always has been, and still is, a great inspiration, mentor and role model for me in science.

TABLE OF CONTENTS

LIST OF FIGURES

LIST OF TABLES

ACKNOWLEDGEMENTS

I would first of all like to thank my PhD advisor, Jeff Severinghaus. Jeff has been a terrific mentor in every possible way. At the start of my time at Scripps, he handed me an incredibly interesting and monstrously difficult project (I think he had no idea how difficult it really was), which has kept me motivated and busy for 6.5 years. This project, as well as Jeff's high standards for experimental research, data analysis, as well as writing, have challenged me and helped me grow as a scientist throughout my PhD. Despite being overloaded with his various academic responsibilities, Jeff was always very generous with his time. I felt like I could walk into his office for a discussion at any time; he was also quick with feedback on things like manuscripts. Jeff allowed me to take intellectual and logistical leadership of the project, especially in the later years, and encouraged me to work independently. He was always generous with compliments and encouragement. His enthusiasm for Earth Science is boundless and infectious. It is in very large measure Jeff's accomplishment that I have decided to continue along the research path beyond my PhD.

I would also like to thank Dave Lowe, who effectively became my advisor during the many months I spent at NIWA in New Zealand. Dave was a great role model with his enthusiasm for research, his amazing skill at working with people, and his belief that the science we are doing really can and will change the world for the better. He did everything he could to support me and my project with laboratory resources and with fantastic advice on all aspects of the work.

Over the summers we spent in the field together, Ed Brook also became an informal advisor to me. I was always amazed at Ed's ability to quickly and accurately assess any situation, however unexpected and complicated, and come up with the most reasonable approach to resolving it. Ed also has a very gentle, unassuming way of approaching people which I admire and have learned a lot from. He has been a great resource of ideas and has provided a great deal of laboratory and field support to the project.

I would also like to thank Andrew Smith, who made the high-precision ^{14}C measurements possible. Time after time, Andrew went out of his way to ensure that my

project continued to have access, free of charge, to ANSTO's ^{14}C facilities and that over a hundred (unplanned) test samples were processed during method development. He has taught me a great deal about ^{14}C and made me feel very welcome during my visits to ANSTO.

A special thanks goes out to Katja Riedel, who was my guardian angel while I was at NIWA and was always willing to help out with absolutely anything, including coming in on weekends to ensure that I could get access to the lab. She, much more than anyone else at NIWA, made me feel welcome during my stay in New Zealand.

This project would not have been possible at all without the ground-breaking work of Niels Reeh, who was the first to explore ablation margins as a source of ancient ice; and who enthusiastically helped us to find the ice we were after. Nor would have this project succeeded without the expertise and help of Gordon Brailsford. Gordon provided the most valuable practical laboratory advice with the NIWA part of the project, took the lead in designing and building a new CH_4 processing line, and did most of the testing and all of the air extractions for the ^{14}CO samples.

I would also like to thank all of my many collaborators for their numerous contributions to the project. They are listed below as well as in the "Acknowledgements" sections following individual chapters.

My family have always been a wonderful source of support and encouragement, and my Christmas-time escapes to New Hampshire were always rejuvenating. I was lucky to have my brother relatively nearby in Northern California, which facilitated many fun and sanity-restoring outdoor adventures.

Finally, I would like to thank Christie. I am lucky to have had her in my life for the past two years, and she has been the greatest source of warmth, love and support during the most trying times of this PhD.

Chapter 2, in full, is a reprint of the material as it appears in Quaternary Science Reviews, 25, Petrenko, V.V., Severinghaus, J.P., Brook, E.J., Reeh, N. and Schaefer, H., Gas records from the West Greenland ice margin covering the last glacial termination: a

horizontal ice core, pp. 865-875, Copyright (2006), with permission from Elsevier. The dissertation author was the primary investigator and author of this paper.

Chapter 3, in part, has been accepted for publication to Journal of Glaciology, 2008. Vasilii V. Petrenko, Jeffrey P. Severinghaus, Edward J. Brook, Jens Mühle, Melissa Headly, Christina M. Harth, Hinrich Schaefer, Niels Reeh, Ray F. Weiss, Dave Lowe and Andrew M. Smith, International Glaciological Society. The dissertation author was the primary investigator and author of this paper. The chapter is reprinted here from the Journal of Glaciology with permission from the International Glaciological Society.

Chapter 4, in part, has been accepted for publication to Radiocarbon, 2008. Vasilii V. Petrenko, Andrew M. Smith, Gordon Brailsford, Katja Riedel, Quan Hua, Dave Lowe, Jeffrey P. Severinghaus, Vladimir Levchenko, Tony Bromley, Rowena Moss, Jens Mühle and Edward J. Brook. The dissertation author was the primary investigator and author of this paper. It is reprinted here with permission from Radiocarbon.

Chapter 5, in part, will be submitted for publication to a yet-to-be-determined journal, as: Petrenko, V.V., A.M. Smith, J.P. Severinghaus, E.J. Brook, D. Lowe, Q. Hua, K. Riedel, G. Brailsford, N. Reeh, H. Schaefer, R.F. Weiss and D. Etheridge. "A study of C-14 of atmospheric methane for the last glacial termination."

VITA

Education

Ph.D. Scripps Institution of Oceanography, University of California, San Diego, March 2008. Ph.D. in Earth Sciences.

M. Ed. Individualized Focus on Teaching Science, Harvard University, June 2000.

B. A. Chemistry, University of New Hampshire, May 1997
Summa Cum Laude. Minor in Physics.

Publications

Petrenko, V.V., A.M. Smith, G. Brailsford, K. Riedel, Q. Hua, D. Lowe, J.P. Severinghaus, V. Levchenko, T. Bromley, R. Moss, J. Mühle and E.J. Brook. 2008. A new method for analyzing ^{14}C of methane in ancient air extracted from glacial ice. Accepted in *Radiocarbon*.

Smith, A.M., V.V. Petrenko, Q. Hua, J. Southon, and G. Brailsford. 2007. The effect of N2O, catalyst, and means of water vapor removal on the graphitization of small CO2 samples. *Radiocarbon*, **49** (2), 245-254.

Petrenko, V.V., J.P. Severinghaus, E.J. Brook, N. Reeh, and H. Schaefer. 2006. Gas records from the West Greenland ice margin covering the Last Glacial Termination: a horizontal ice core. *Quaternary Science Reviews*, **25** (9-10), 865-875.

Schaefer, H., M.J. Whiticar, E.J. Brook, V.V. Petrenko, D.F. Ferretti, and J.P. Severinghaus. 2006. Ice record of delta C-13 for atmospheric CH4 across the Younger Dryas-Preboreal transition. *Science*, **313** (5790), 1109-1112.

Petrenko, V.V., J.P. Severinghaus, E.J. Brook, J. Mühle, M. Headly, C.M. Harth, H. Schaefer, N. Reeh, R.F. Weiss, D. Lowe and A.M. Smith. 2008. A novel method for obtaining very large ancient air samples from ablating glacial ice for analyses of methane radiocarbon. Accepted in *Journal of Glaciology*.

ABSTRACT OF THE DISSERTATION

A study of carbon-14 of paleoatmospheric methane for the last glacial termination from ancient glacial ice

by

Vasilii Victorovich Petrenko

Doctor of Philosophy in Earth Sciences

University of California, San Diego, 2008

Professor Jeffrey P. Severinghaus, Chair

Ice core records from Greenland and Antarctica reveal large and rapid variations in atmospheric methane concentrations [CH_4] in response to abrupt climate change. Two such events occurred at the Oldest Dryas (OD) – Bølling and Younger Dryas (YD) – Preboreal (PB) climatic transitions during the last glacial termination. A record of ^{14}C of atmospheric CH_4 ($^{14}CH_4$) through these transitions can help to identify the sources of the [CH_4] increases and constrain the fossil fraction of paleo CH_4 budgets.

Very large (~100 L STP) samples of paleoatmospheric air are needed for such $^{14}CH_4$ measurements. To obtain these samples, ancient ice outcropping at an ice-margin ablation site in West Greenland was explored. Ice sections dating to the last glacial termination were identified and found to contain high-quality gas records. A new method for large-scale air extraction from glacial ice was developed and twelve large air samples from the YD-PB and the OD-Bølling transitions were obtained. New methods were also developed for processing this air for $^{14}CH_4$. $^{14}CH_4$ procedural blanks were greatly

reduced through the construction of a new CH_4 conversion line utilizing platinized quartz wool for CH_4 combustion and the use of an ultra high purity iron catalyst for graphitization. The overall $^{14}CH_4$ processing blank was 0.75 ± 0.38 pMC.

Measured $^{14}CH_4$ values were too high by 14 – 38% as compared to the highest expected values based on paleoatmospheric $^{14}CO_2$. In-situ production of CH_4 and direct cosmogenic production of $^{14}CH_4$ molecules in ablating ice were identified as the two most likely mechanisms that elevated $^{14}CH_4$. Sample $^{14}CH_4$ was then corrected for both mechanisms, however these corrections are speculative and do not allow any definite conclusions to be drawn from the results. Corrected $^{14}CH_4$ results suggest that there was a 7% increase in the fossil CH_4 fraction from the YD to the PB. The corrected $^{14}CH_4$ results also suggest no large changes in the fossil fraction between the OD and the YD. Finally, the corrected results suggest that up to 80% of the OD – Bølling [CH_4] rise (~100 ppb) was due to ^{14}C-free CH_4.

Chapter 1

Introduction to atmospheric methane: past and present budgets, isotopes and variations

1.1 Brief scope of dissertation and motivation

The main aim of this Ph.D. dissertation was to use measurements of ^{14}C of paleoatmospheric methane to test the clathrate hypothesis as well as to constrain the "fossil fraction" of the methane budget during the last glacial termination. The clathrate hypothesis states that several large and rapid increases in atmospheric methane concentration, observed during the last glacial period as well as the glacial termination at times of abrupt warming, were driven by massive destabilization of marine methane clathrates. If this hypothesis is correct it suggests that methane clathrates are potentially unstable during times of climatic warming. The amount of methane carbon contained in clathrates may be as large as the amount of carbon contained in all remaining fossil fuels combined. If clathrates are unstable at times of climatic warming, they present a substantial geo-hazard during the present global warming. Destabilization of a large amount of methane clathrates and direct release of methane to the atmosphere may result in a large positive feedback to the warming.

The fossil fraction of the methane budget is the fraction of the total global atmospheric methane source that is essentially free of ^{14}C. Such sources are methane emissions from clathrates and hydrocarbon seeps. Most natural sources of atmospheric methane, however, have a relatively high ^{14}C content, similar to that of atmospheric CO_2. For this reason ^{14}C of paleoatmospheric methane is an excellent tracer for testing the clathrate hypothesis as well as determining the fossil fraction of past methane budgets.

1.2 The role of methane in global climate and atmospheric chemistry

Methane (CH_4) is the most abundant organic molecule in the Earth's atmosphere and plays important roles in both the planet's radiative energy budget and global atmospheric chemistry (Brasseur et al., 1999). CH_4 is the third most important greenhouse gas after H_2O vapor and carbon dioxide (CO_2) and has a Global Warming Potential (GWP) 25 times that of CO_2 on a 100 –year timescale (Forster et al., 2007). The direct radiative forcing attributable to the CH_4 concentration ($[CH_4]$) increase in the anthropogenic era (after 1750 AD) is 0.48 W/m^2 (Forster et al., 2007). Increasing $[CH_4]$ also contributes a radiative forcing indirectly, through affecting tropospheric ozone concentrations, increasing stratospheric water vapor (of which it is the main source), as well as providing a small additional source of CO_2. If these indirect effects are taken into account, the radiative forcing due to anthropogenic $[CH_4]$ increase is estimated at ~ 0.85 W/m^2 , as compared to 1.66 W/m^2 for CO_2 (Forster et al., 2007).

CH_4 is involved in a large number of atmospheric chemistry processes. It is the second most important sink (after carbon monoxide (CO)) of tropospheric hydroxyl radicals (·OH) (Brasseur et al., 1999). Tropospheric ·OH is the "cleaning agent" of the atmosphere and is responsible for the oxidation and removal of most organic compounds. Substantial fluctuations in $[CH_4]$ have the power to affect ·OH concentrations ($[\cdot OH]$) and thereby change the lifetimes of many other atmospheric trace species (Forster et al., 2007). The oxidation of CH_4 by ·OH is also one of the main sources of CO and formaldehyde in the troposphere (Hobbs, 2000). Changes in $[CH_4]$ also influence tropospheric ozone production (Brasseur et al., 1999).

1.3 Brief overview of CH_4 sources and sinks

The main source of atmospheric CH_4 is from methanogenesis by anaerobic bacteria. CH_4 is produced in this way by two main pathways as follows (Reeburgh, 2007b):

$$CO_2 + 4H_2 \rightarrow CH_4 + 2H_2O \quad (1.1)$$

$$CH_3COOH \rightarrow CH_4 + CO_2 \quad (1.2)$$

Reaction 1.1 (CO_2 reduction) occurs primarily in marine sediments, while reaction 1.2 (acetate fermentation) occurs primarily in freshwater environments (Reeburgh, 2007b). Major non-microbial sources of methane include emissions from fossil fuel mining, biomass burning, as well as geologic sources such as gas seeps and methane hydrates (Reeburgh, 2007a).

The Intergovernmental Panel on Climate Change (IPCC) fourth assessment report estimates net total source of CH_4 to the modern atmosphere at 582 Teragrams / year (Tg yr^{-1}) (Denman et al., 2007). Estimates of the strengths of individual sources vary substantially between different studies. Anthropogenic sources are thought to account for 60 - 70% of the total source. The main anthropogenic sources are ruminants (20 – 45% of the anthropogenic source), energy (20 – 31%), rice agriculture (12 – 26 %) and biomass burning (5 – 25 %) (Denman et al., 2007). Natural sources are estimated to account for 30 - 40% of the total source, with the

main contributors being wetlands (69 – 89% of total natural source), geologic sources (~20%) and termites (9 – 14%) (Denman et al., 2007).

The main sink of atmospheric CH_4 is by reaction with tropospheric ·OH and accounts for ~85% of the total sink (Denman et al., 2007). The initial reaction step for this process is:

$$CH_4 + \cdot OH \rightarrow CH_3\cdot + H_2O \qquad (1.3)$$

A complex chain of chemical and photochemical reactions follows, with the major intermediate and final carbon products being formaldehyde, CO and CO_2 (Brasseur et al., 1999). The other known tropospheric CH_4 sinks are loss to the stratosphere (~7%), soil uptake (~5%), and oxidation by the chlorine radical in the marine boundary layer (~3%) (Denman et al., 2007).

1.4 Atmospheric CH_4 in the anthropogenic era and the use of stable isotopes in understanding the CH_4 budget

Humans have perturbed the atmospheric methane budget to a remarkable extent. Ice core records (see more detail in section 1.6) have shown that [CH_4] had remained between 350 and 800 parts per billion (ppb) for the past 650 thousand years (kyr) (Brook et al., 2000; Spahni et al., 2005); whereas presently global mean [CH_4] is 1775 ppb (Forster et al., 2007). The [CH_4] rise due to anthropogenic activities (rice agriculture, ruminants, biomass burning, coal mining) is generally considered to have

begun around 1750 AD, although some have argued that humans significantly affected the global methane budget much earlier, starting around 5 kyr before present (BP, where "present" = 1950 AD) (Ruddiman, 2003). Figure 1.1 shows methane concentrations for the past 1000 years. As can be seen, [CH_4] started to rise from ~ 700 ppb around 1750 AD and increased in an approximately exponential fashion until about the 1980s. In the 1990s, the rise slowed and [CH_4] leveled off around the year 2000, which has been attributed to the stabilization of the cumulative CH_4 emissions (Forster et al., 2007).

Measurements of stable isotopic composition of atmospheric CH_4 (the relative abundances of carbon-13 / carbon-12 ($\delta^{13}CH_4$) and deuterium / hydrogen-1 (δD)) can be used to constrain the relative contribution of various CH_4 sources and sinks to the overall budget. The δ notation for expressing isotopic ratios will be used extensively throughout this thesis; it is illustrated in Equation 1.4 below for the carbon-13 / carbon-12 ratio.

$$\delta^{13}C = \left[\frac{\frac{^{13}C}{^{12}C}\text{sample}}{\frac{^{13}C}{^{12}C}\text{standard}} - 1 \right] \times 1000 \qquad (1.4)$$

Table 1.1 shows a summary of $\delta^{13}CH_4$, δD, and ^{14}C of CH_4 ($^{14}CH_4$) of the main sources, as well as the fractionation effects for the main sinks. High-resolution records of $\delta^{13}CH_4$ are available for the entire anthropogenic era (Ferretti et al., 2005; Lassey et al., 2007a; Quay et al., 1999; Sowers et al., 2005) and show an increase in

$\delta^{13}CH_4$ from about –49 ‰ in 1900 AD to about – 47.2 ‰ today. This increase has been attributed to a higher overall contribution of anthropogenic biomass burning and fossil emissions to the global CH_4 budget (Lassey et al., 2007a; Sowers et al., 2005).

The variability in the $\delta^{13}CH_4$ and δD for each type of CH_4 source are quite large (Table 1.1), as they are influenced by environmental variables as well as by the isotopic composition of the source organic matter, which varies regionally. This makes it challenging to determine exact average $\delta^{13}CH_4$ and δD values for each type of source. Further, as can be seen from Table 1.1, the $\delta^{13}CH_4$ and δD isotopic signatures of several major sources are quite similar. For these reasons, large uncertainties still exist in the established methane budgets as illustrated by the disagreement between recent studies attempting to quantify this (see Table 7.6 in Denman et al. (2007)).

1.5 The use of carbon-14 in understanding the modern CH_4 budget

$^{14}CH_4$ is also a very useful tracer of CH_4 sources. Its main advantage over $\delta^{13}CH_4$ and δD is in being able to easily distinguish between fossil sources and sources of recent biogenic origin. Fossil CH_4 sources (leakage from fossil fuel mining, geologic sources such as natural gas seeps, clathrates) are very old and contain no measurable ^{14}C (Winckler et al., 2002). On the other hand, CH_4 that is produced biogenically from modern organic matter (e.g., wetlands, ruminants, rice paddies) will have $^{14}CH_4$ that closely follows the ^{14}C of atmospheric CO_2 ($^{14}CO_2$). A common unit

for reporting ^{14}C activities of CH_4 is percent of modern carbon (pMC), which was defined at the 8th International Conference on Radiocarbon Dating as (Stuiver and Polach, 1977):

$$pMC = \frac{A_{SN}}{A_{ON}} \times 100 \qquad (1.5)$$

A_{ON} is defined as 95% of the activity (in disintegrations per second per unit carbon mass) in the year 1950 AD of the IAEA Oxalic acid reference standard, normalized to a $\delta^{13}C$ of –19 ‰. This is given by Donahue et al. (1990):

$$A_{ON} = 0.95 A_{OX} \left\{ \frac{1 - \frac{19}{1000}}{1 + \frac{\delta^{13}C_{OX}}{1000}} \right\}^2 \qquad (1.6)$$

A_{SN} is the sample activity normalized to a $\delta^{13}C$ of –25 ‰. This is also given by Donahue et al. (1990):

$$A_{SN} = A_S \left\{ \frac{1 - \frac{25}{1000}}{1 + \frac{\delta^{13}C_S}{1000}} \right\}^2 \qquad (1.7)$$

The usefulness of normalizing the sample activity in this manner is that, after the normalization, the pMC activity of the sample is equal to that of its source carbon (correcting for radioactive decay) and the effects of mass-dependent fractionation are removed. For example, the ultimate source of carbon for CH_4 produced biogenically

is atmospheric CO_2. Suppose that CH_4 is produced microbially in the rumen of a cow from digestion of freshly-grown grass. $\delta^{13}C$ of atmospheric CO_2 is – 8 ‰ (Forster et al., 2007), and its current ^{14}C activity is 106 pMC. While the emitted CH_4 is likely to have a $\delta^{13}C$ of ~ - 60 ‰, its ^{14}C activity expressed in pMC will still be 106. In this case the delay between photosynthetic fixation of CO_2 by the grass and the emission of CH_4 from the cow is too short to affect the ^{14}C appreciably through decay. In the case of CH_4 emission from a northern peatland with a slow overturning of organic material, however, the delay ("lag time") may be significant and the ^{14}C activity of the emitted CH_4 would in fact be slightly lower than that of the CO_2 absorbed by plants.

One further ^{14}C reporting unit that will be used in this work is Δ, defined by Stuiver and Polach (1977) as:

$$\Delta = \left[\frac{A_{SN}e^{\lambda(1950-y)}}{A_{ON}} - 1\right] \times 1000 \text{ ‰} \qquad (1.8)$$

where λ is the ^{14}C decay constant and y is the sample age in years AD. This unit's usefulness lies in its incorporation of a decay correction for sample age. As can be seen from the equation, this unit also includes a normalization for $\delta^{13}C$.

In the last ~50 years, the cycling of $^{14}CH_4$ in the atmosphere has been strongly affected by the nuclear bomb test radiocarbon spike. Atmospheric $^{14}CO_2$ peaked at 170 pMC in 1964-1965, and has been decreasing rapidly since (Lassey et al., 2007a). Table 1.1 shows measured $^{14}CH_4$ for the main sources. All the measurements incorporated into the table were performed in the late 1980s or early 1990s. During

that period atmospheric $^{14}CO_2$ dropped from ~ 120 to ~ 112 pMC (Lassey et al., 2007a). $^{14}CH_4$ measurements for ruminant emissions were performed in 1986-88 by Wahlen et al. (1989), and the measured activities of 118-122 pMC agree well with atmospheric $^{14}CO_2$ for that period. $^{14}CH_4$ values measured for wetland emissions span a larger range (96 – 130 pMC), reflecting a range of lag times and the rapidly changing $^{14}CO_2$ since 1950. Lassey et al. (2007a) used the available atmospheric $^{14}CH_4$ measurements (Figure 1.2) to estimate the globally averaged biospheric CH_4 lag time at 6 yr (~50% uncertainty).

Starting in the 1970s, direct production of $^{14}CH_4$ molecules by nuclear power plants (primarily pressurized water reactors (PWRs)) became a significant contributor to the atmospheric $^{14}CH_4$ burden (Lassey et al., 2007a). Due to the growing influence of the PWR component, $^{14}CH_4$ continues to rise even while $^{14}CO_2$ is declining (Figure 1.2). Lassey et al. (2007b) applied a linear regression to the available atmospheric $^{14}CH_4$ measurements and data on electricity generation from PWRs world-wide for the period 1986 – 2000 to estimate both the fossil fraction of the methane budget (30.0 ± 2.3%) and the globally averaged efficiency of PWRs at producing $^{14}CH_4$ molecules.

1.6 Glacial-interglacial variations in [CH_4] from ice cores

Ice core records from Greenland and Antarctica show strong coupling between [CH_4] and climate on long timescales (Figures 1.3 a & b, (Brook et al., 2000; Spahni et al., 2005)). Figure 1.3a shows a combined 650 kyr record of [CH_4] and δD of ice (a

proxy for local temperature) from the Vostok and EPICA Dome C ice cores in Antarctica. As can be seen, [CH_4] generally follows the glacial-interglacial cycles, with high values during the interglacials.

The causes of the [CH_4] fluctuations observed in the ice cores on glacial-interglacial time scales are still a subject of active debate. One possibility is changes in the ·OH sink. Several modeling studies explored the effects of the changing climate on atmospheric chemistry and [·OH], and found only small reductions in [·OH] between the Last Glacial Maximum (LGM) and the Pre-industrial Holocene (PIH) (Crutzen and Bruhl, 1993; Martinerie et al., 1995; Thompson et al., 1993). It is thus likely that the main cause of the LGM -- PIH [CH_4] increase is a ramping up of CH_4 sources.

Figure 1.3b shows higher resolution records of [CH_4] and $\delta^{18}O_{ice}$ (also a proxy for local temperature) over the past 100 kyr from the GISP2 ice core in Greenland. Several large and rapid [CH_4] increases can be seen which coincide with many of the Dansgaard-Oeschger (D-O) abrupt warming events recorded in Greenland (Brook et al., 2000). The causes of rapid [CH_4] increases associated with rapid climate warming events are likewise still debated. Two such large and rapid [CH_4] events occurred during the last deglaciation, at the Oldest Dryas (OD) – Bølling (~14,700 yr BP) and Younger Dryas (YD) – Preboreal (PB) (~11,600 yr BP) climatic transitions (Severinghaus and Brook, 1999; Severinghaus et al., 1998), (Figure 1.3b).

Gases become thermally fractionated in the firn as a result of abrupt temperature change at the surface, and analyses of nitrogen and argon isotopic composition in the occluded air in the GISP2 ice core indicate that temperature at Greenland Summit rose by ~ 10˚C in just a few decades during each of these events (Grachev and Severinghaus, 2003, 2005; Severinghaus and Brook, 1999; Severinghaus et al., 1998). The YD-PB event is associated with a [CH_4] increase from ~500 to ~ 750 ppb; the OD-Bølling event with an increase from ~ 480 to ~650 ppb (Brook et al., 2000). Comparison of nitrogen and argon thermal fractionation signals with [CH_4] in the ice core allows for very accurate determination of the relative timing of the warming and [CH_4] rise. For each of these events, the [CH_4] rise started slightly (0-30 yrs) after the start of the temperature rise, and took longer than the temperature rise (>150 yrs for the YD-PB event and ~50 yrs for the OD-Bølling event) (Severinghaus and Brook, 1999; Severinghaus et al., 1998). This suggests that climatic change drove the change in [CH_4], rather than [CH_4] driving climate.

A further line of evidence suggesting that climate drives [CH_4] and not vice-versa is that not every one of the D-O events is associated with [CH_4] increases (Brook et al., 1996) (Figure 1.3 b). For example, at interstadial events 19 and 20, large temperature increases occurred without substantial accompanying [CH_4] increases.

Two main explanations for the rapid [CH_4] fluctuations associated with D-O events as well as for the overall glacial-interglacial [CH_4] increases have been proposed. The first invokes increased CH_4 emissions from wetlands in response to a warmer and wetter climate (the wetland hypothesis) (Brook et al., 2000; Brook et al.,

1996; Chappellaz et al., 1993). The second idea involves large and rapid releases of CH_4 from marine sedimentary CH_4 clathrates (the clathrate hypothesis) (Kennett et al., 2000, 2003).

1.7 Wetlands and millennial-scale [CH_4] oscillations

As discussed above, wetlands are the main natural source of CH_4 to the atmosphere. Many studies have shown that wetlands respond to warmer and wetter climatic conditions with increased methane production (e.g. Frolking and Crill, 1994; Schlesinger, 1997; Whalen, 2005). Increasing emissions from both northern and tropical wetlands have therefore been invoked by most workers to explain the glacial – interglacial [CH_4] differences (Chappellaz et al., 1997; Chappellaz et al., 1993; Crutzen and Bruhl, 1993).

On shorter time scales, [CH_4] also seems very responsive to Greenland climate, following both rapid temperature increases and decreases associated with the D-O events (Figure 1.3 b). Even climate events of centennial-scale duration recorded in Greenland ice cores, such as the Preboreal Oscillation (PBO) and the 8.2k event are accompanied by near-synchronous changes in [CH_4] (Figures 1.3 b and 1.5). This is consistent with the wetland hypothesis, as wetland productivity would respond quickly to changes in temperature and moisture conditions.

Ice core studies of the interpolar [CH_4] gradient indicate that the OD-Bølling [CH_4] transition was driven primarily by an increase in tropical emissions, while the YD-PB [CH_4] increase was driven by increases in both tropical and northern sources (Brook et al., 2000). This seems consistent with the wetland hypothesis. During the OD-Bølling transition, much of the area that is presently boreal wetlands was still glaciated, thus only tropical wetlands could have driven the [CH_4] rise. However, during the YD-PB transition, the ice sheets had already retreated considerably. A compilation of 1516 peatland initiation ^{14}C dates shows that a large burst in northern peatland development occurred around the time of the YD-PB transition (MacDonald et al., 2006).

Wang et al. (2001) discovered a remarkable resemblance between a $\delta^{18}O$ record from stalagmites in Eastern China (a proxy for East Asian summer monsoon intensity) and the GISP2 record. Virtually every D-O event in Greenland was coincident with a period of increased monsoon intensity. A large increase in East Asian monsoon intensity, for example, was coincident with the onset of the Bølling in Greenland. A more intense East Asian summer monsoon is associated with greater regional warmth and precipitation. It would thus be expected that wetlands in the monsoon-affected region would emit more CH_4 during the interstadials, providing support for the wetland explanation of D-O [CH_4] oscillations.

1.8 Methane clathrates, climate and millennial-scale [CH_4] oscillations

Methane clathrate (often referred to as "hydrate") is an ice-like solid composed of CH_4 and H_2O. In methane clathrate crystallographic structure I (most common), the $CH_4 : H_2O$ ratio is 1 : 5.75 (Kvenvolden, 1995). The largest amounts of methane clathrates are found in marine sediments, though substantial amounts are present in permafrost as well. CH_4 clathrates are thermodynamically stable at relatively low temperatures and high pressures; Figure 1.4 shows a diagram of CH_4 clathrate stability.

CH_4 clathrates in marine sediments form when CH_4 concentrations within the clathrate stability zone exceed CH_4 solubility (Buffett, 2000). For example, for a sediment temperature of 15˚C, clathrates can form at depths greater than ~1.2 km below sea level (Buffett and Archer, 2004). In the polar regions, with bottom water temperatures around –1.5 ˚C, clathrates can form at depths > ~250 m below sea level (Buffett and Archer, 2004). The two main sources of CH_4 for clathrate formation in the sediments are in-situ anaerobic microbial methanogenesis and natural thermogenic CH_4. Most documented CH_4 clathrate occurrences (direct recovery from coring) are at depths exceeding ~ 100 m below sea floor (mbsf); however clathrates have been recovered at some sites at depths as shallow as 2 mbsf (Kastner, 2001). The fact that CH_4 clathrates generally do not occur in the top-most part of the sediments is due to anaerobic CH_4 oxidation in the top-most part of the sediments by sulfate-reducing bacteria (Davie and Buffett, 2003).

Studies of clathrate $\delta^{13}CH_4$ have shown that most marine clathrate CH_4 originates from bacterial methanogenesis, with highly depleted $\delta^{13}CH_4$ due to isotopic fractionation by the methanogens. $\delta^{13}C$ values between –60 and –65 ‰ are most common (Miriam Kastner, personal communication). Measured δD of marine CH_4 clathrates is –189 ± 27 ‰ (Sowers, 2006). Because a minimum organic carbon content of ~ 1% dry weight is required for methanogenesis to happen in the sediments (Archer and Buffett, 2005), methane clathrates are generally restricted to high-productivity areas in the oceans such as the continental shelves. By recent estimates, the present amount of CH_4 carbon associated with marine clathrates is 500 – 5000 Gt (Buffett and Archer, 2004; Milkov, 2004); which at the upper end is comparable to the estimated carbon content of all the fossil fuels.

Less is known about CH_4 clathrates in the permafrost regions. In permafrost, CH_4 clathrates are stable at depths below ~200 m, and the stability zone (determined primarily by mean annual surface temperature and the geothermal gradient) is typically ~ 400 m thick (Macdonald, 1990). The existence of vast clathrate deposits in permafrost in Siberia as well as in North America has been inferred from borehole logging observations. For example, analysis of data from 150 wells drilled in the oil and gas-rich Beaufort-MacKenzie region of the Canadian Arctic led to the conclusion that CH_4 hydrates occur in 27 of these wells (Majorowicz and Hannigan, 2000). Macdonald (1990) estimated that ~400 Gt C may be stored in permafrost clathrates, although he referred to this estimate as “highly speculative”.

Methane clathrates are one of the key unknowns in predicting future climate. Because clathrates are stable at relatively cold temperatures, global warming may destabilize large amounts of clathrates both in the oceans and in the permafrost. If large-scale rapid destabilization of marine clathrates were somehow to happen, CH_4 would be released fast enough that it could escape to the atmosphere without being oxidized to CO_2 in the sediments or the water column. The modern atmosphere contains ~ 3.7 Gt of CH_4 carbon (Denman et al., 2007). If the upper limit of clathrate – bound CH_4 (~5000 Gt) is assumed, an instantaneous release of all of this CH_4 to the atmosphere would increase atmospheric [CH_4] by a factor of over 1000! This would produce a disastrously large positive feedback to climate warming because of the high effectiveness of CH_4 as a greenhouse gas. Even if the destabilization of existing clathrates is gradual and all the released CH_4 does get completely oxidized to CO_2 in the sediment or water column, the ocean carbonate system and atmospheric CO_2 would be substantially impacted because of the large amount of carbon present in clathrates.

Large-scale clathrate destabilization is one of the leading explanations for the Paleocene – Eocene Thermal Maximum (PETM) event about 55 Myr ago (Jansen et al., 2007). During the PETM, ocean temperatures warmed by 4 - 10 ˚C (depending on location) in ~ 10^3 to 10^4 yr (Zachos et al., 2003). The warming was accompanied by a globally recorded $\delta^{13}C$ excursion of > –2.5‰ of the oceanic carbon pool and widespread deep-sea carbonate dissolution (Zachos et al., 2003). Dickens et al. (1997) used a global carbon cycle model to demonstrate that the recorded $\delta^{13}C$ excursion

could be well reproduced with an injection of 1120 Gt of CH_4 from marine clathrates. This event is currently the subject of intensive research, as the implied amount of clathrate carbon added to the ocean-atmosphere system is of the same order of magnitude as the anthropogenic carbon release happening today. However, the ocean temperatures even before the start of the PETM were already much warmer than today (Zachos et al., 2001), so the distribution and stability regime of the clathrate reservoir may have been quite different.

A closer, however imperfect, analog to possible future climate-induced changes in the CH_4 reservoir may be found in the record of Quaternary glacial-interglacial and stadial-interstadial transitions. The temperature increases of intermediate and deep ocean waters (most clathrates are found at depths > 500 m, except in the polar regions (Kastner, 2001)) at the onset of interstadials and interglacials are likely to destabilize part of the clathrate reservoir. The rapid atmospheric [CH_4] increases observed in ice cores at the onset of most interstadial events, as well as the more gradual glacial-interglacial [CH_4] increases have therefore been interpreted by some workers as a result of massive clathrate destabilization events (Kennett et al., 2000, 2003).

The Clathrate Gun Hypothesis (Kennett et al., 2003) goes a step further to state that massive clathrate destabilization events caused not only the [CH_4] increases, but also initiated the warming events through CH_4 radiative forcing. The radiative forcing from even the largest of the observed [CH_4] increases (~250 ppb) is quite small,

however. For instance, the anthropogenic [CH_4] increase from 715 to 1774 ppb is estimated to have resulted in a direct radiative forcing of 0.48 W/m^2 (Forster et al., 2007). For comparison, the total anthropogenic radiative forcing is considered to be 2.63 W/m^2, accompanied by a surface warming of 0.74 ± 0.18˚C during the last century (Trenberth et al., 2007). So it seems very unlikely that CH_4 radiative forcing at the start of D-O events could have caused a noticeable warming or triggered a major climatic shift. Kennett et al. (2003), however, argued that the CH_4 radiative forcing was reinforced by multiple positive feedbacks. Any possibility that CH_4 increases actually caused the warming events was ruled out by high-resolution analyses of gases in the GISP2 ice core, however. As discussed above, nitrogen and argon isotopic analyses in the GISP2 core for the YD-PB and OD-Bølling transitions indicated that the warming started before the [CH_4] increase and was of shorter duration than the [CH_4] increase, proving that the warming drove the [CH_4] increase, and not the other way around (Severinghaus and Brook, 1999; Severinghaus et al., 1998).

Kennett et al. (2003) use two major lines of argument to show that clathrates may have been responsible for the [CH_4] increases at D-O event initiations as well as at glacial-interglacial transitions. The first is that substantial wetland development in the Northern Hemisphere did not occur until Early to Mid-Holocene and wetlands therefore could not have been responsible for the observed [CH_4] increases. Kennett et al. (2003) presented a compilation of ^{14}C dates of peat initiation as well as paleovegetation data to support their arguments. This has been called into question by others. Particularly, MacDonald et al. (2006) presented a comprehensive compilation

of 1516 ^{14}C dates of northern high-latitude peat initiation to show that a few peatlands did indeed start forming around the initiation of the Bølling, and a large burst of peatland development occurred around the time of the Younger Dryas – Preboreal transition.

The second major line of argument used by Kennett et al. (2003) to support a clathrate source of the [CH_4] increases is geological evidence of clathrate destabilization. The authors presented evidence of widespread submarine slumps on continental shelves (which typically harbor clathrates in the sediments). Submarine slumps of this nature may be capable of destabilizing large amounts of clathrate very quickly, as well as releasing the free CH_4 gas at the base of the clathrate stability zone, thus ensuring that [CH_4] makes it into the atmosphere without being oxidized. However, the authors state that although the slumps seem to date to sometime during the last deglaciation, accurate dating is not available for any of them. Kennett et al. (2000) interpreted negative $\delta^{13}C$ excursions in benthic and planktonic foraminifera observed at the initiation of several D-O events in the Santa Barbara Basin (SBB) sediments as evidence for clathrate CH_4 release. However, this interpretation has been shown to likely be incorrect. Stott et al. (2002) showed that in the SBB today, methane-derived CO_2 has no influence on $\delta^{13}C$ of benthic foraminifera. Yet modern $\delta^{13}C$ measured in one of the same benthic species that was used in the Kennett et al. (2000) study (*B. tenuata,* -2.8 ‰) is similar to the values observed during the interstadial excursions. Stott et al. (2002) further showed that the negative benthic $\delta^{13}C$ excursions observed for the interstadial events can be explained by increased

productivity and organic rain rate. Cannariato and Stott (2004) measured $\delta^{13}C$ of total organic carbon (TOC) in the same SBB sediment core as Kennett et al. (2000). Their results show that the interstadial negative $\delta^{13}C$ excursions in planktonic foraminifera, interpreted by Kennett et al. (2000) as addition of a large amount of clathrate carbon to surface waters, are most likely due to post-sedimentary overgrowths of calcite on the foraminifera. To summarize, neither of the Kennett et al. (2003) lines of argument for a clathrate source of the [CH_4] increases appear compelling.

A further argument against substantial clathrate involvement in interstadial and deglacial CH_4 changes has to do with the rapidity of clathrate decomposition during a warming. As discussed above, most clathrates in marine sediments are found at depths > 100 mbsf, and clathrates in permafrost only occur at depths > 200 m. Unless clathrates are destabilized suddenly by a massive submarine slump, the destabilization in response to a warming will be driven by the propagation of the thermal signal through the overlying sediments and will have a significant time lag. For example, Archer and Buffett (2005) note that it would take ~1000 years for the thermal signal to reach clathrates in response to a 3˚C deep ocean warming. In this case the clathrate destabilization would be very gradual and all the released CH_4 would be oxidized to CO_2 in the upper part of the sediment.

Recently, two studies of CH_4 budget changes during the glacial period as well as the last deglaciation have been conducted using $\delta^{13}C$ (Schaefer et al., 2006) and δD of CH_4 (Sowers, 2006) from glacial ice. The Schaefer et al. (2006) $\delta^{13}CH_4$ record

spans the abrupt [CH_4] increase which occurred at the Younger Dryas (YD) – Preboreal (PB) rapid climatic warming. No detectable shift in $\delta^{13}CH_4$ was observed for this transition as [CH_4] increased from about 500 to about 750 ppb, suggesting that the balance and cumulative $\delta^{13}CH_4$ of the CH_4 sources did not change significantly over the transition; rather the sources all increased proportionately. Schaefer et al. (2006) used an atmospheric box model to show that the $\delta^{13}C$ of the additional CH_4 source during the YD-PB transition was –50 to – 55 ‰. This is inconsistent with clathrate $\delta^{13}CH_4$ of –60 ‰ or lower, but may be consistent with a tropical wetland source (Schaefer et al., 2006).

The Sowers (2006) study spanned ~40 kyr and found an overall trend of decreasing (more negative) δD over the last deglaciation, without substantial shifts at times of abrupt [CH_4] increases at Interstadial 8 (~38.5 kyr BP), the OD – Bølling transition and the YD-PB transition. δD of marine CH_4 clathrates today (–189 ± 27 ‰) is much higher than that of wetlands (-320 ± 20 ‰) (Table 1.1). Assuming that wetlands were the dominant CH_4 source prior to the rapid [CH_4] increases, the lack of significant δD shifts during large [CH_4] increases argues strongly against any significant contributions from marine clathrates. Further, the overall decrease in δD of CH_4 over the deglaciation argues against major clathrate involvement in the deglacial [CH_4] increase.

To summarize, given the available geological evidence, it is very unlikely that CH_4 clathrates had a significant role in either the overall deglacial [CH_4] increase or the rapid [CH_4] increases associated with abrupt warming events.

1.9 Other hypotheses: melting thermokarst lakes, aerobic plant emissions and BVOCs

Recent work has shown that thermokarst lakes, located mainly in the permafrost regions of East Siberia, are a significant source of CH_4 to the atmosphere, emitting as much as 3.8 Tg yr^{-1}, mostly through ebullition (Walter et al., 2006). Most of the CH_4 is emitted from the thawing permafrost along the lake margins, and ^{14}C measurements indicate the released CH_4 carbon dates to 35 – 43 kyr BP (Walter et al., 2006). Thermokarst lakes form when frozen glacial-age loess and loess-related deposits in the permafrost regions begin to thaw. These loess deposits are particularly C-rich in East Siberia, and are known as the "yedoma ice-complex" (Walter et al, 2007). It has been estimated that modern yedoma contains ~450 Tg of organic C, and that these carbon stocks are readily decomposable upon melting of the permafrost (Zimov et al., 2006).

Walter et al. (2007) compiled 69 thermokarst lake ^{14}C initiation dates which show a first burst in thermokarst activity occurring at the initiation of the Bølling, a decline in the Younger Dryas, and another, much larger burst of thermokarst initiation in the Preboreal and Early Holocene. They estimated possible thermokarst CH_4

emissions at ~11 Tg yr^{-1} for the Bølling and up to 26 Tg yr^{-1} at the initiation of the Preboreal. This is qualitatively consistent with ice core studies of the interpolar [CH_4] gradient, which show a relatively stronger Northern Hemisphere (NH) source in the Preboreal and early Holocene than in the YD and Bølling (Brook et al., 2000; Chappellaz et al., 1997; Dallenbach et al., 2000). In this case thermokarst lakes would have been responsible for >40% of the global CH_4 source increase during the YD-PB transition (141 to 202 Tg, Brook et al. (2000)).

However, thermokarst lake emissions of this magnitude are unlikely given the YD-PB transition record of $\delta^{13}CH_4$. Schaefer et al. (2006) showed that $\delta^{13}CH_4$ remained unchanged through the YD-PB transition, with the lowest possible $\delta^{13}C$ of the transition CH_4 source being –55 ‰. The mean annual $\delta^{13}CH_4$ of thermokarst lake emissions today, on the other hand, is ~ -70 ‰ (Walter et al., 2006). Thus, the ice record of $\delta^{13}CH_4$ over the YD-PB transition does not appear to be consistent with a 26 Tg thermokarst lake source. A considerably smaller thermokarst source is more likely.

A previously unsuspected and potentially very large (62 – 236 Tg yr^{-1}) CH_4 source from plants with a $\delta^{13}C$ of ~ -50 ‰ (by an unknown aerobic production mechanism) was proposed by Keppler et al. (2006). If plants do in fact produce so much CH_4, it is possible that plants were the major driver of climate-induced atmospheric [CH_4] fluctuations on all timescales. However, Ferretti et al. (2007) used ice core $\delta^{13}CH_4$ and [CH_4] in a top-down approach to constrain the likely ranges of

aerobic plant emissions to 0 – 46 Tg yr^{-1} for the pre-industrial and 0 – 176 Tg yr^{-1} for the modern budgets. Further, Kirschbaum et al. (2006) examined the methods used by Keppler et al. (2006) for extrapolating their laboratory CH_4 emission determinations to the global scale, and found these to be "inappropriate and dimensionally inconsistent". Finally, Dueck et al. (2007) conducted experiments with ^{13}C-labelled plants which showed no evidence for CH_4 production and emission by terrestrial plants. They attribute the Keppler et al. (2006) findings of methane "production" to diffusion of CH_4 out of plant tissue. It thus seems unlikely that plant aerobic CH_4 production is real, and I will not discuss it further.

Recently Kaplan et al. (2006) proposed that changes in emissions of non-methane biogenic volatile organic compounds (BVOCs) could explain most of the glacial – interglacial [CH_4] increase via reducing tropospheric [·OH]. However, this hypothesis is based on the results of a coupled biosphere-atmosphere chemistry-climate model incorporating many simplifying assumptions. A key result from this model was that wetland CH_4 emissions increased only slightly at the end of the glacial, and then decreased again so that wetland emissions in the pre-industrial Holocene were comparable to those during the LGM. This is highly unlikely, given the evidence that wetlands expanded rapidly at the onset of the Bølling and the Preboreal (e.g. MacDonald et al., 2006) as well as that the LGM was a dry period in key methane-producing regions of the world (e.g. Wang et al., 2001). Although in principle increased BVOCs could substantially affect tropospheric [·OH], it appears unlikely that they were a major player and I will not discuss this idea further.

1.10 Using paleoatmospheric $^{14}CH_4$ to test the clathrate hypothesis and constrain the fossil fraction of the paleo CH_4 budget

It should be possible to test the clathrate hypothesis for the two rapid [CH_4] rise events which occurred at the YD-PB transition and the OD-Bølling transition by obtaining records of $^{14}CH_4$ through these transitions. The ultimate carbon source for wetland-produced CH_4 is essentially contemporaneous atmospheric CO_2 (Lassey et al., 2007b; Wahlen et al., 1989). If wetlands are the only source of the [CH_4] rise, there should be either no change or an increase in ^{14}C content of CH_4 the abrupt warming event (corrected for radioactive decay).

On the other hand, CH_4 clathrates contain little to no measurable ^{14}C, as discussed above. If clathrates are the only source of the ~50% [CH_4] increase at the YD-PB transition, for example, one would expect to see a 33% decrease in the $^{14}C/^{12}C$ ratio of methane over the [CH_4] transition (Figure 1.5). $^{14}CH_4$ measurements on ancient air should also allow for straightforward quantification of the fossil component of the CH_4 budget for various climatic intervals.

Measurements of $^{14}CH_4$ on modern ambient air are routinely done (Lowe et al., 1988; Quay et al., 1999; Wahlen et al., 1989). Typically, CH_4 in the air sample is either pre-concentrated on a low-temperature charcoal trap and then combusted to CO_2 on a platinized catalyst (Lowe et al., 1988; Quay et al., 1999; Wahlen et al., 1989), or combusted directly in the air stream with subsequent cryogenic trapping of the resulting CO_2 (Lowe et al., 1991). This CO_2 is then converted to graphite by reduction

with hydrogen, with Fe powder typically acting as the catalyst e.g., (Lowe et al., 1991). Finally, ^{14}C of the resulting graphite is measured by accelerator mass spectrometry (AMS). Air samples containing ~500 standard litres (SL) are typically processed for this, yielding a sample size of ~ 400 micrograms of carbon (μg C) (Lowe et al., 1991).

$^{14}CH_4$ measurements on ancient air samples required overcoming several formidable experimental challenges, however. First, sufficiently large ancient air samples had to be obtained. The only known source of well-preserved ancient air is glacial ice. For ice containing pre-Holocene air with ~500 parts per billion (ppb) [CH_4], at least 1000 kg of ice is required to provide ~25 μg C, barely enough for an AMS measurement of ^{14}C. This much ancient ice of a relatively uniform age is not available from ice cores, and another source of well-dated ancient ice with a well-preserved CH_4 record had to be found; this is the subject of Chapter 2. Second, apparatus had to be developed capable of extracting ~ 100 L of air from >1000 kg of ice in a reasonable amount of time and without significant CH_4 contamination. The development, testing and performance of this apparatus are discussed in Chapter 3. Third, CH_4 had to be extracted from this air and combusted to CO_2. This is routinely done for modern atmospheric samples as described above, but the relatively low [CH_4] (400 – 800 ppb) and $^{14}CH_4$ (~30 pMC) of the samples created a high risk of contamination from modern carbon and necessitated development of an improved technique. Fourth, the very small size of the samples (~20 μg) created difficulties with the graphitization reaction, and the small size and low ^{14}C of the samples again

created high risks of contamination from modern carbon and required further modification of existing graphitization techniques. Technique development and methods used for CH_4 extraction from the ancient air, combustion to CO_2 and graphitization are the subject of Chapter 4. Chapter 5 presents the $^{14}CH_4$ results obtained from ancient air samples dating to the last glacial termination and discusses the implications for past CH_4 budgets.

Acknowledgement

Figure 1.4 and caption are from Buffett (2000). Reprinted, with permission, from the *Annual Review of Earth and Planetary Sciences,* Volume 28 © 2000 by Annual Reviews. www.annualreviews.org.

Table 1.1 Isotopic signatures of modern CH_4 sources and fractionation associated with sinks. For the sink processes, the ε fractionation values are reported. The fractionation factor α for ^{14}C would be $\alpha_{14C} = (\alpha_{13C})^2$; but the resulting ε values in the units of pMC depend on the starting activity and are thus not reported.

Table 1.1

Sources	Mean global $\delta^{13}CH_4$, ‰ PDB	Mean global δD, ‰ SMOW	^{14}C activity, pMC
Natural			
Wetlands	-60 ± 5 [a]	-320 ± 20 [a]	96 - 130 [b, i]
Geologic sources	-40 ± 5 [b]	-185 ± 20 [g]	0 [g]
Clathrates	-60 ± 5 [b,c,d]	-189 ± 27 [e]	0 [h]
Wildfires	-25 ± 5 [b]	-225 ± 30 [a,f]	125 - 135 [a,f]
Anthropogenic			
Ruminants	-60 ± 5 [a,c]	-300 ± 10 [a, e]	118-122 [b,i]
Rice agriculture	-63 ± 5 [a,c]	-320 ± 30 [a, e]	106 - 129 [b,i]
Landfills	-55 ± 5 [b,c]	-310 ± 10 [a, e]	120 ± 5 [a]
Natural Gas	-43 ± 7 [a]	-185 ± 20 [a, e]	0 [a]
Coal Mining	-36 ± 7 [a]	-140 ± 20 [a, e]	0 [a]
Biomass Burning	-24 ± 3 [a]	-225 ± 30 [a, e]	117 - 141 [b,i]
Sinks			
OH radicals	-4.65 ± 0.75 [b]	-227 [j]	
Soil	-20 ± 2 [b]	- 80 [a]	
Loss to stratosphere	-3 ± 3 [b]	- 160 [a]	
Chlorine radicals	-60 ± 1 [b]	- 322 [j]	

[a] (Quay et al., 1999)
[b] (Lassey et al., 2007a)
[c] (Denman et al., 2007)
[d] Given uncertainty is a "best guess", the full range of $\delta^{13}C$ for clathrates is ~ -40 to- 100 ‰ (Maslin and Thomas, 2003)
[e] (Sowers, 2006)
[f] Here making an assumption that the isotopic signature of wildfire emissions is the same as in anthropogenic biomass burning
[g] Here making an assumption that isotopic composition of natural geologic emissions is the same as that from mined natural gas
[i] Converted from Lassey et al. (2007a) units of $\Delta^{14}C$ to pMC
[h] (Winckler et al., 2002)
[j] (Reeburgh, 2007a)

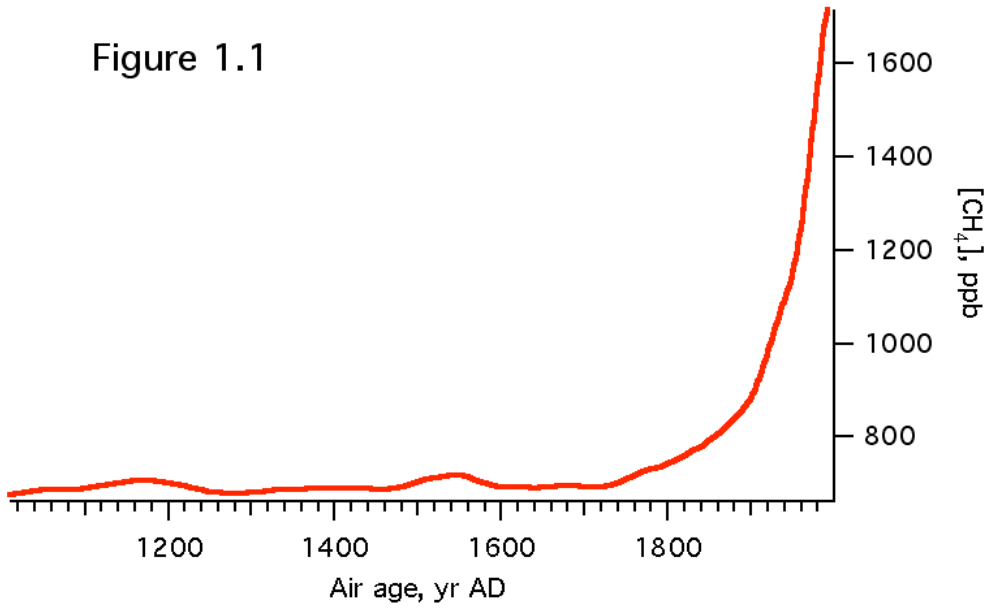

Figure 1.1. [CH_4] from the Law Dome ice core in Antarctica and Southern Hemisphere clean air measurements between 1000 and 1992 AD. Data are from Etheridge et al. (1998).

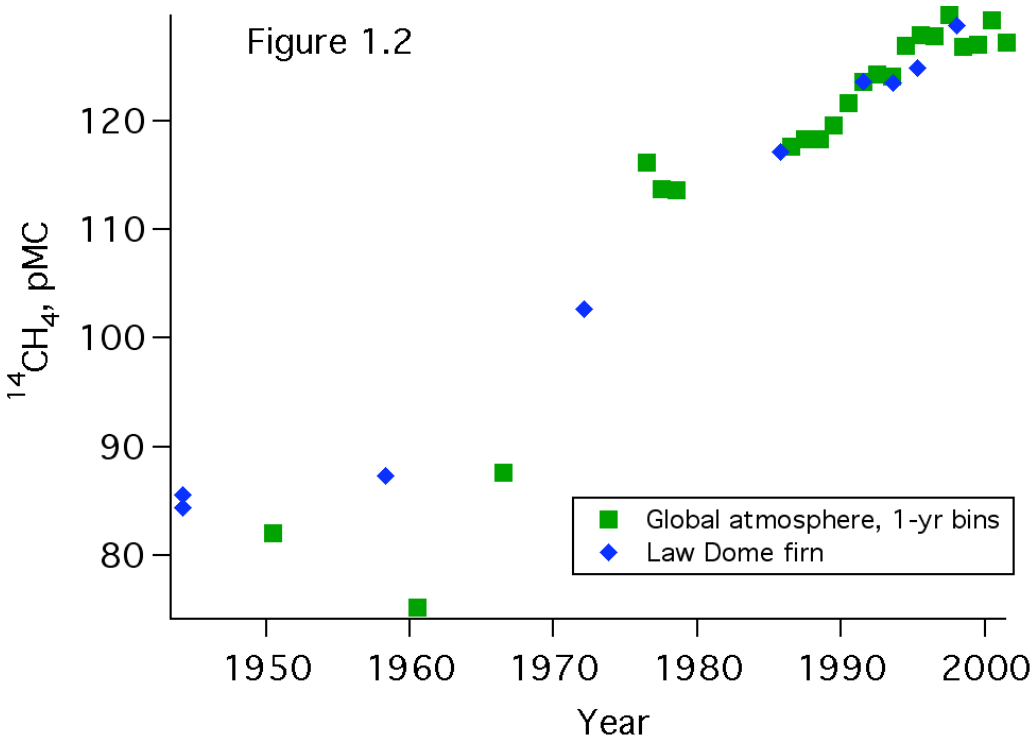

Figure 1.2 . Available atmospheric $^{14}CH_4$ data to date. Data are as published in Figure 5 of Lassey et al. (2007a), except here in units of pMC. The "global atmosphere" data are a composite of all available atmospheric measurements. Law Dome firn air data are courtesy of David Etheridge (personal communication).

Figure 1.3a

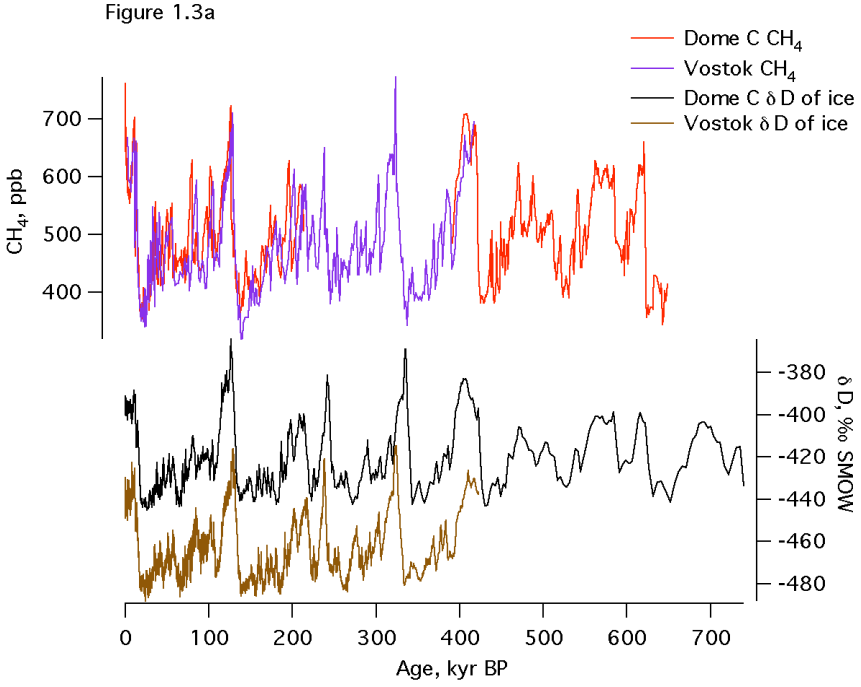

Figure 1.3b

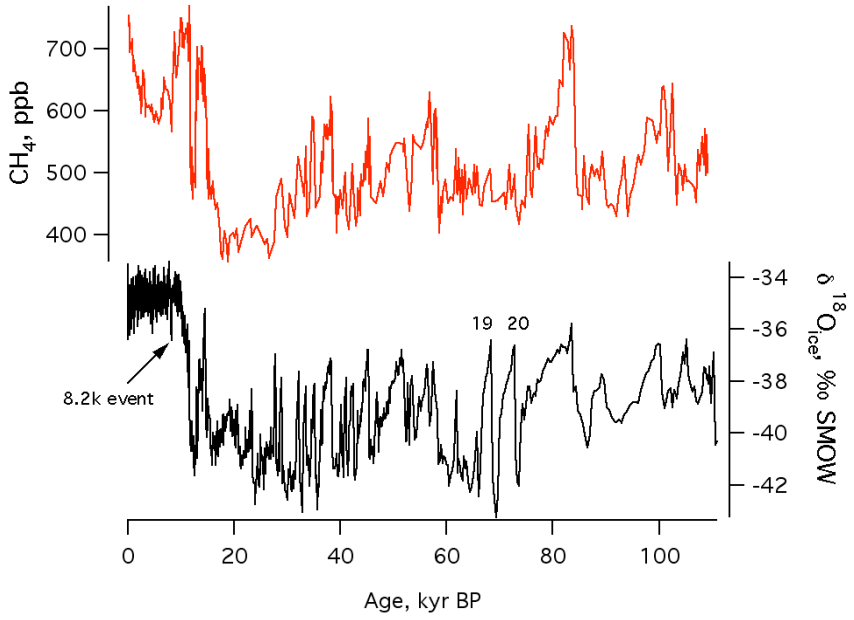

Figure 1.3. $[CH_4]$ and climate from ice core records. a) $[CH_4]$ (Spahni et al., 2005) and δD (Augustin et al., 2004) from EPICA Dome C; also $[CH_4]$ and δD from Vostok (Petit et al., 1999). b) $[CH_4]$ (Brook et al., 2000) and $\delta^{18}O_{ice}$ (Grootes and Stuiver, 1997) from GISP 2.

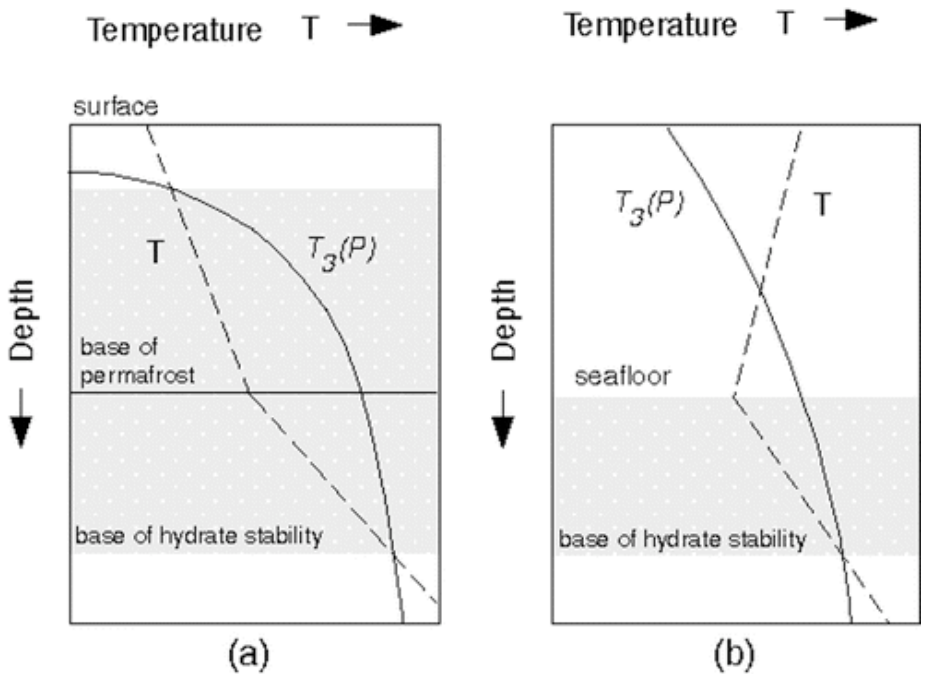

Figure 1.4. A schematic profile of temperature T in (*a*) continental permafrost and (*b*) marine sediments. Hydrate stability in the sediments (*shaded region*) is limited to depths where $T < T_3(P)$. T is the temperature profile in the sediments. T_3(P) is the maximum temperature at which hydrates are stable as a function of depth. Figure and caption are from Buffett (2000). Reprinted, with permission, from the *Annual Review of Earth and Planetary Sciences,* Volume 28 © 2000 by Annual Reviews. www.annualreviews.org.

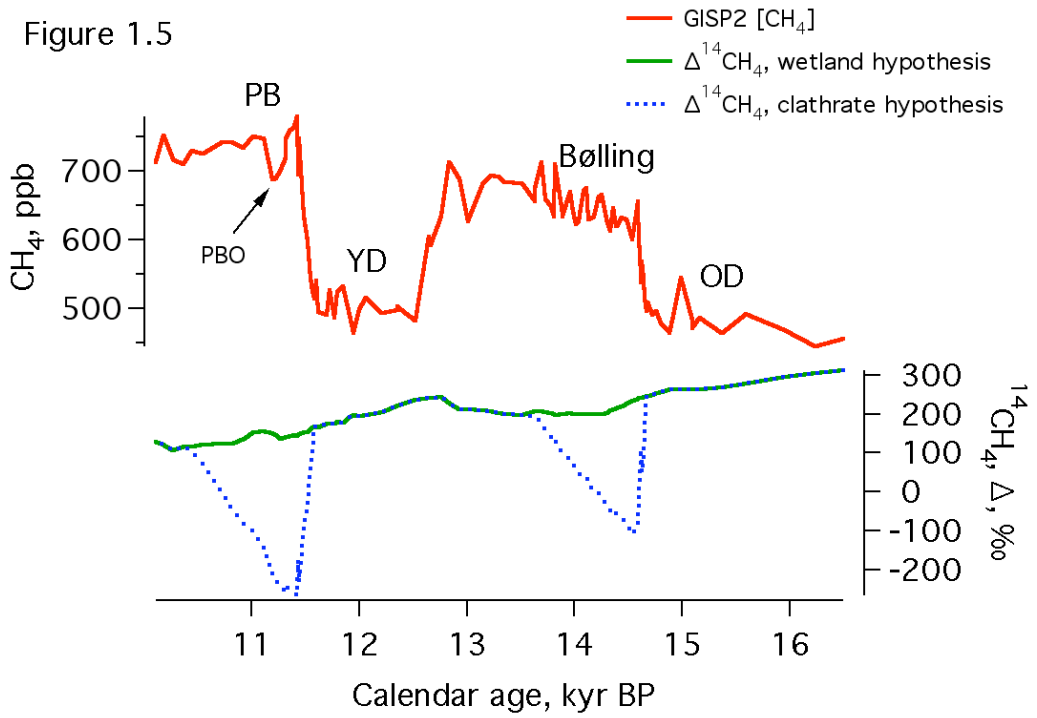

Figure 1.5. A simple model of atmospheric $^{14}CH_4$ during the last deglaciation under the wetland and clathrate hypotheses, in the age-corrected units of Δ. For the purposes of this model the lag time for biospheric CH_4 production is assumed to be zero, meaning that for biospheric CH_4 emissions, $^{14}CH_4 = {}^{14}CO_2$ of the contemporaneous atmosphere. The model assumes normally 0% fossil CH_4 emissions. For the wetland hypothesis, 100% biospheric CH_4 emissions are assumed for all times. For the clathrate hypothesis, it is assumed that the ^{14}C of released clathrate CH_4 is zero and that all of the CH_4 rise during the OD-Bølling and YD-PB transitions is due to clathrate emissions. Clathrate emissions are then assumed to decrease linearly to zero over 1000 years after peak $[CH_4]$ is reached. $[CH_4]$ is from (Brook et al., 2000), on the Schaefer et al. (2006) gas age scale. Paleoatmospheric $^{14}CO_2$ is from the Reimer et al. (2004) INTCAL04 compilation.

References

Archer, D., Buffett, B., 2005. Time-dependent response of the global ocean clathrate reservoir to climatic and anthropogenic forcing. Geochemistry Geophysics Geosystems 6, Q03002, doi:10.1029/2004GC000854.

Augustin, L., Barbante, C., Barnes, P.R.F., Barnola, J.M., Bigler, M., Castellano, E., Cattani, O., Chappellaz, J., DahlJensen, D., Delmonte, B., Dreyfus, G., Durand, G., Falourd, S., Fischer, H., Fluckiger, J., Hansson, M.E., Huybrechts, P., Jugie, R., Johnsen, S.J., Jouzel, J., Kaufmann, P., Kipfstuhl, J., Lambert, F., Lipenkov, V.Y., Littot, G.V.C., Longinelli, A., Lorrain, R., Maggi, V., Masson-Delmotte, V., Miller, H., Mulvaney, R., Oerlemans, J., Oerter, H., Orombelli, G., Parrenin, F., Peel, D.A., Petit, J.R., Raynaud, D., Ritz, C., Ruth, U., Schwander, J., Siegenthaler, U., Souchez, R., Stauffer, B., Steffensen, J.P., Stenni, B., Stocker, T.F., Tabacco, I.E., Udisti, R., van de Wal, R.S.W., van den Broeke, M., Weiss, J., Wilhelms, F., Winther, J.G., Wolff, E.W., Zucchelli, M., Members, E.C., 2004. Eight glacial cycles from an Antarctic ice core. Nature 429, 623-628.

Brasseur, G., Orlando, J., Tyndall, G. (Editors), 1999. Atmospheric Chemistry and Global Change. Topics in Environmental Chemistry. Oxford University Press, New York, 654 pp.

Brook, E.J., Harder, S., Severinghaus, J., Steig, E.J., Sucher, C.M., 2000. On the origin and timing of rapid changes in atmospheric methane during the last glacial period. Global Biogeochemical Cycles 14, 559-572.

Brook, E.J., Sowers, T., Orchardo, J., 1996. Rapid variations in atmospheric methane concentration during the past 110,000 years. Science 273, 1087-1091.

Buffett, B., Archer, D., 2004. Global inventory of methane clathrate: sensitivity to changes in the deep ocean. Earth and Planetary Science Letters 227, 185-199.

Buffett, B.A., 2000. Clathrate hydrates. Annual Review of Earth and Planetary Sciences 28, 477-507.

Cannariato, K.G., Stott, L.D., 2004. Evidence against clathrate-derived methane release to Santa Barbara Basin surface waters? Geochemistry Geophysics Geosystems 5, Q05007, doi:10.1029/2003GC000600.

Chappellaz, J., Blunier, T., Kints, S., Dallenbach, A., Barnola, J.M., Schwander, J., Raynaud, D., Stauffer, B., 1997. Changes in the atmospheric CH4 gradient

between Greenland and Antarctica during the Holocene. Journal of Geophysical Research-Atmospheres 102, 15987-15997.

Chappellaz, J.A., Fung, I.Y., Thompson, A.M., 1993. The Atmospheric CH4 Increase since the Last Glacial Maximum. Tellus Series B-Chemical and Physical Meteorology 45, 228-241.

Crutzen, P.J., Bruhl, C., 1993. A Model Study of Atmospheric Temperatures and the Concentrations of Ozone, Hydroxyl, and Some Other Photochemically Active Gases During the Glacial, the Preindustrial Holocene and the Present. Geophysical Research Letters 20, 1047-1050.

Dallenbach, A., Blunier, T., Fluckiger, J., Stauffer, B., Chappellaz, J., Raynaud, D., 2000. Changes in the atmospheric CH4 gradient between Greenland and Antarctica during the Last Glacial and the transition to the Holocene. Geophysical Research Letters 27, 1005-1008.

Davie, M.K., Buffett, B.A., 2003. A steady state model for marine hydrate formation: Constraints on methane supply from pore water sulfate profiles. Journal of Geophysical Research-Solid Earth 108 (B10), 2495, doi:10.1029/2002JB002300.

Denman, K.L., Brasseur, G., Chidthaisong, A., Ciais, P., Cox, P.M., Dickinson, R.E., Hauglustaine, D.A., Heinze, C., Holland, E., Jacob, D., Lohmann, U., Ramachandran, S., da Silva Dias, P.L., Wofsy, S.C., Zhang, X., 2007. Couplings Between Changes in the Climate System and Biogeochemistry. In: S. Solomon et al. (Editors), Climate Change 2007: The Physical Science Basis. Contribution of Working Group I to the Fourth Assessment Report of the Intergovernmental Panel on Climate Change. Cambridge University Press, Cambridge, U.K.

Dickens, G.R., Castillo, M.M., Walker, J.C.G., 1997. A blast of gas in the latest Paleocene: Simulating first-order effects of massive dissociation of oceanic methane hydrate. Geology 25, 259-262.

Donahue, D.J., Linick, T.W., Jull, A.J.T., 1990. Isotope-Ratio and Background Corrections for Accelerator Mass-Spectrometry Radiocarbon Measurements. Radiocarbon 32, 135-142.

Dueck, T.A., de Visser, R., Poorter, H., Persijn, S., Gorissen, A., de Visser, W., Schapendonk, A., Verhagen, J., Snel, J., Harren, F.J.M., Ngai, A.K.Y., Verstappen, F., Bouwmeester, H., Voesenek, L.A.C.J., van der Werf, A., 2007. No evidence for substantial aerobic methane emission by terrestrial plants: a C-13-labelling approach. New Phytologist 175, 29-35.

Etheridge, D.M., Steele, L.P., Francey, R.J., Langenfelds, R.L., 1998. Atmospheric methane between 1000 AD and present: Evidence of anthropogenic emissions and climatic variability. Journal of Geophysical Research-Atmospheres 103, 15979-15993.

Ferretti, D.F., Miller, J.B., White, J.W.C., Etheridge, D.M., Lassey, K.R., Lowe, D.C., Meure, C.M.M., Dreier, M.F., Trudinger, C.M., van Ommen, T.D., Langenfelds, R.L., 2005. Unexpected changes to the global methane budget over the past 2000 years. Science 309, 1714-1717.

Ferretti, D.F., Miller, J.B., White, J.W.C., Lassey, K.R., Lowe, D.C., Etheridge, D.M., 2007. Stable isotopes provide revised global limits of aerobic methane emissions from plants. Atmospheric Chemistry and Physics 7, 237-241.

Forster, P., Ramaswamy, V., Artaxo, P., Berntsen, T., Betts, R., Fahey, D.W., Haywood, J., Lean, J., Lowe, D.C., Myhre, G., Nganga, J., Prinn, R., Raga, G., M., S., Van Dorland, R., 2007. Changes in Atmospheric Constituents and in Radiative Forcing. In: S. Solomon et al. (Editors), Climate Change 2007: The Physical Science Basis. Contribution of Working Group I to the Fourth Assessment Report of the Intergovernmental Panel on Climate Change. Cambridge University Press, Cambridge, U.K.

Frolking, S., Crill, P., 1994. Climate Controls on Temporal Variability of Methane Flux from a Poor Fen in Southeastern New-Hampshire - Measurement and Modeling. Global Biogeochemical Cycles 8, 385-397.

Grachev, A.M., Severinghaus, J.P., 2003. Determining the thermal diffusion factor for Ar-40/Ar-36 in air to aid paleoreconstruction of abrupt climate change. Journal of Physical Chemistry 107, 4636-4642.

Grachev, A.M., Severinghaus, J.P., 2005. A revised +10 +/- 4 degrees C magnitude of the abrupt change in Greenland temperature at the Younger Dryas termination using published GISP2 gas isotope data and air thermal diffusion constants. Quaternary Science Reviews 24, 513-519.

Grootes, P.M., Stuiver, M., 1997. Oxygen 18/16 variability in Greenland snow and ice with 10^-3 to 10^5-year time resolution. Journal of Geophysical Research-Oceans 102, 26455-26470.

Hobbs, P., 2000. Introduction to Atmospheric Chemistry. Cambridge University Press, Cambridge, U.K., 262 pp.

Jansen, E., Overpeck, J., Briffa, K.R., Duplessy, J.-C., Joos, F., Masson-Delmotte, V., Olago, D., Otto-Bliesner, B.L., Peltier, W.R., Rahmstorf, S., Ramesh, R., Raynaud, D., Rind, D., Solomina, O., Villalba, R., Zhang, D., 2007. Palaeoclimate. In: S. Solomon et al. (Editors), Climate Change 2007: The Physical Science Basis. Contribution of Working Group I to the Fourth Assessment Report of the Intergovernmental Panel on Climate Change. Cambridge University Press, Cambridge, U.K.

Kaplan, J.O., Folberth, G., Hauglustaine, D.A., 2006. Role of methane and biogenic volatile organic compound sources in late glacial and Holocene fluctuations of atmospheric methane concentrations. Global Biogeochemical Cycles 20, GB2016, doi:10.1029/2005GB002590.

Kastner, M., 2001. Gas Hydrates in Convergent Margins: Formation, Occurence, Geochemistry and Global Significance, Natural Gas Hydrates: Occurence, Distribution and detection. Geophysical Monograph, 124. AGU.

Kennett, J.P., Cannariato, K.G., Hendy, I.L., Behl, R.J., 2000. Carbon isotopic evidence for methane hydrate instability during quaternary interstadials. Science 288, 128-133.

Kennett, J.P., Cannariato, K.G., Hendy, I.L., Behl, R.J., 2003. Methane Hydrates in Quaternary Climate Change: The Clathrate Gun Hypothesis. AGU, Washington, D.C., 216 pp.

Keppler, F., Hamilton, J.T.G., Brass, M., Rockmann, T., 2006. Methane emissions from terrestrial plants under aerobic conditions. Nature 439, 187-191.

Kirschbaum, M.U.F., Bruhn, D., Etheridge, D.M., Evans, J.R., Farquhar, G.D., Gifford, R.M., Paul, K.I., Winters, A.J., 2006. A comment on the quantitative significance of aerobic methane release by plants. Functional Plant Biology 33, 521-530.

Kvenvolden, K.A., 1995. A review of the geochemistry of methane in natural gas hydrate. Organic Geochemistry 23, 997-1008.

Lassey, K.R., Etheridge, D.M., Lowe, D.C., Smith, A.M., Ferretti, D.F., 2007a. Centennial evolution of the atmospheric methane budget: what do the carbon isotopes tell us? Atmospheric Chemistry and Physics 7, 2119-2139.

Lassey, K.R., Lowe, D.C., Smith, A.M., 2007b. The atmospheric cycling of radiomethane and the "fossil fraction" of the methane source. Atmospheric Chemistry and Physics 7, 2141-2149.

Lowe, D.C., Brenninkmeijer, C.A.M., Manning, M.R., Sparks, R., Wallace, G., 1988. Radiocarbon Determination of Atmospheric Methane at Baring Head, New-Zealand. Nature 332, 522-525.

Lowe, D.C., Brenninkmeijer, C.A.M., Tyler, S.C., Dlugkencky, E.J., 1991. Determination of the Isotopic Composition of Atmospheric Methane and Its Application in the Antarctic. Journal of Geophysical Research-Atmospheres 96, 15455-15467.

Macdonald, G.J., 1990. Role of Methane Clathrates in Past and Future Climates. Climatic Change 16, 247-281.

MacDonald, G.M., Beilman, D.W., Kremenetski, K.V., Sheng, Y.W., Smith, L.C., Velichko, A.A., 2006. Rapid early development of circumarctic peatlands and atmospheric CH4 and CO2 variations. Science 314, 285-288.

Majorowicz, J.A., Hannigan, P.K., 2000. Stability Zone of Natural Gas Hydrates in a Permafrost-Bearing Region of the Beaufort-Mackenzie Basin: Study of a Feasible Energy Source. Natural Resources Research 9, 3-25.

Martinerie, P., Brasseur, G.P., Granier, C., 1995. The Chemical-Composition of Ancient Atmospheres - a Model Study Constrained by Ice Core Data. Journal of Geophysical Research-Atmospheres 100, 14291-14304.

Maslin, M.A., Thomas, E., 2003. Balancing the deglacial global carbon budget: the hydrate factor. Quaternary Science Reviews 22, 1729-1736.

Milkov, A.V., 2004. Global estimates of hydrate-bound gas in marine sediments: how much is really out there? Earth-Science Reviews 66, 183-197.

Petit, J.R., Jouzel, J., Raynaud, D., Barkov, N.I., Barnola, J.M., Basile, I., Bender, M., Chappellaz, J., Davis, M., Delaygue, G., Delmotte, M., Kotlyakov, V.M., Legrand, M., Lipenkov, V.Y., Lorius, C., Pepin, L., Ritz, C., Saltzman, E., Stievenard, M., 1999. Climate and atmospheric history of the past 420,000 years from the Vostok ice core, Antarctica. Nature 399, 429-436.

Quay, P., Stutsman, J., Wilbur, D., Snover, A., Dlugokencky, E., Brown, T., 1999. The isotopic composition of atmospheric methane. Global Biogeochemical Cycles 13, 445-461.

Reeburgh, W.S., 2007a. Global Methane Biogeochemistry. In: H. Holland and K. Turekian (Editors), Treatise on Geochemistry. Elsevier, pp. 4.03: 01 - 32.

Reeburgh, W.S., 2007b. Oceanic methane biogeochemistry. Chemical Reviews 107, 486-513.

Reimer, P.J., Baillie, M.G.L., Bard, E., Bayliss, A., Beck, J.W., Bertrand, C.J.H., Blackwell, P.G., Buck, C.E., Burr, G.S., Cutler, K.B., Damon, P.E., Edwards, R.L., Fairbanks, R.G., Friedrich, M., Guilderson, T.P., Hogg, A.G., Hughen, K.A., Kromer, B., McCormac, G., Manning, S., Ramsey, C.B., Reimer, R.W., Remmele, S., Southon, J.R., Stuiver, M., Talamo, S., Taylor, F.W., van der Plicht, J., Weyhenmeyer, C.E., 2004. IntCal04 terrestrial radiocarbon age calibration, 0-26 cal kyr BP. Radiocarbon 46, 1029-1058.

Ruddiman, W.F., 2003. The anthropogenic greenhouse era began thousands of years ago. Climatic Change 61, 261-293.

Schaefer, H., Whiticar, M.J., Brook, E.J., Petrenko, V.V., Ferretti, D.F., Severinghaus, J.P., 2006. Ice record of delta C-13 for atmospheric CH4 across the Younger Dryas-Preboreal transition. Science 313, 1109-1112.

Schlesinger, W.H., 1997. Biogeochemistry: an analysis of global change. Academic Press, San Diego, California.

Severinghaus, J.P., Brook, E.J., 1999. Abrupt climate change at the end of the last glacial period inferred from trapped air in polar ice. Science 286, 930-934.

Severinghaus, J.P., Sowers, T., Brook, E.J., Alley, R.B., Bender, M.L., 1998. Timing of Abrupt Climate Change at the End of the Younger Dryas Interval from Thermally Fractionated Gases in Polar Ice. Nature 391, 141-146.

Sowers, T., 2006. Late quaternary atmospheric CH4 isotope record suggests marine clathrates are stable. Science 311, 838-840.

Sowers, T., Bernard, S., Aballain, O., Chappellaz, J., Barnola, J.M., Marik, T., 2005. Records of the delta C-13 of atmospheric CH4 over the last 2 centuries as recorded in Antarctic snow and ice. Global Biogeochemical Cycles 19, GB2002, doi:10.1029/2004GB002408.

Spahni, R., Chappellaz, J., Stocker, T.F., Loulergue, L., Hausammann, G., Kawamura, K., Fluckiger, J., Schwander, J., Raynaud, D., Masson-Delmotte, V., Jouzel, J., 2005. Atmospheric methane and nitrous oxide of the late Pleistocene from Antarctic ice cores. Science 310, 1317-1321.

Stott, L.D., Bunn, T., Prokopenko, M., Mahn, C., Gieskes, J., Bernhard, J.M., 2002. Does the oxidation of methane leave an isotopic fingerprint in the geologic record? Geochemistry Geophysics Geosystems 3(2), 10.1029/2001GC000196.

Stuiver, M., Polach, H.A., 1977. Reporting of C-14 Data - Discussion. Radiocarbon 19, 355-363.

Thompson, A.M., Chappellaz, J.A., Fung, I.Y., Kucsera, T.L., 1993. The Atmospheric Ch4 Increase since the Last Glacial Maximum .2. Interactions with Oxidants. Tellus Series B-Chemical and Physical Meteorology 45, 242-257.

Trenberth, K.E., Jones, P.D., Ambenje, P., Bojariu, R., Easterling, D., Klein Tank, A., Parker, D., Rahimzadeh, F., Renwick, J.A., Rusticucci, M., Soden, B., Zhai, P., 2007. Observations: Surface and Atmospheric Climate Change. In: S. Solomon et al. (Editors), Climate Change 2007: The Physical Science Basis. Contribution of Working Group I to the Fourth Assessment Report of the Intergovernmental Panel on Climate Change. Cambridge University Press, Cambridge, U.K.

Wahlen, M., Tanaka, N., Henry, R., Deck, B., Zeglen, J., Vogel, J.S., Southon, J., Shemesh, A., Fairbanks, R., Broecker, W., 1989. C-14 in Methane Sources and in Atmospheric Methane - the Contribution from Fossil Carbon. Science 245, 286-290.

Walter, K.M., Zimov, S.A., Chanton, J.P., Verbyla, D., Chapin, F.S., 2006. Methane bubbling from Siberian thaw lakes as a positive feedback to climate warming. Nature 443, 71-75.

Walter, K.M., Edwards, M.E., Grosse, G., Zimov, S.A., Chapin III, F.S., 2007. Thermokarst lakes as a source of atmospheric CH4 during the last deglaciation, Science 318, 633 - 636.

Wang, Y.J., Cheng, H., Edwards, R.L., An, Z.S., Wu, J.Y., Shen, C.C., Dorale, J.A., 2001. A high-resolution absolute-dated Late Pleistocene monsoon record from Hulu Cave, China. Science 294, 2345-2348.

Whalen, S.C., 2005. Biogeochemistry of methane exchange between natural wetlands and the atmosphere. Environmental Engineering Science 22, 73-94.

Winckler, G., Aeschbach-Hertig, W., Holocher, J., Kipfer, R., Levin, I., Poss, C., Rehder, G., Suess, E., Schlosser, P., 2002. Noble gases and radiocarbon in natural gas hydrates. Geophysical Research Letters 29, 1423.

Zachos, J., Pagani, M., Sloan, L., Thomas, E., Billups, K., 2001. Trends, rhythms, and aberrations in global climate 65 Ma to present. Science 292, 686-693.

Zachos, J.C., Wara, M.W., Bohaty, S., Delaney, M.L., Petrizzo, M.R., Brill, A., Bralower, T.J., Premoli-Silva, I., 2003. A transient rise in tropical sea surface temperature during the Paleocene-Eocene Thermal Maximum. Science 302, 1551-1554.

Zimov, S.A., Davydov, S.P., Zimova, G.M., Davydova, A.I., Schuur, E.A.G., Dutta, K., Chapin, F.S., 2006. Permafrost carbon: Stock and decomposability of a globally significant carbon pool. Geophysical Research Letters 33, L20502, doi:10.1029/2006GL027484.

Chapter 2

Gas records from the West Greenland ice margin covering the last glacial termination: a horizontal ice core

Abstract

Certain sites along ice sheet margins provide an easily accessible and almost unlimited supply of ancient ice at the surface. Measurements of gases in trapped air from ice outcropping at Pakitsoq, West Greenland, demonstrate that ancient air is mostly well preserved. No alterations in $\delta^{18}O_{atm}$ and $\delta^{15}N$ of N_2 are apparent, and alterations in methane are found in only a few ice sections. Using measurements of these gases, we have unambiguously identified a stratigraphic section containing ice from the end of last glacial period as well as Bølling-Allerød, Younger Dryas and Preboreal intervals. Extensive sections of ice from the Holocene and most ages within the last glacial period are probably also present. Very accurate dating has been possible in the ice section containing the Younger Dryas – Preboreal abrupt climate transition signal. The ice at Pakitsoq is folded and non-uniformly thinned, with many cross-cutting bands of bubble-free ice and dust. The cross-cutting features are associated with anomalies in both the gas and the ice records. With careful sampling to avoid these, the ice at Pakitsoq is suitable for recovery of large-volume samples of the ancient atmosphere for analysis of trace constituents such as $^{14}CH_4$.

2.1 Introduction

Ice cores from Greenland and Antarctica provide some of the best late Quaternary paleoclimatic records. They allow reconstruction of parameters such as temperature, trace gas concentrations, and precipitation in the polar regions, (e.g, Andersen et al., 2004; Petit et al., 1999) providing long-term perspective on modern climate change. Nonetheless, ice core records have several limitations. First, they

recover a relatively small amount of ice for any given time period, limiting the number and types of possible analyses. Second, ice coring is logistically complicated and expensive, particularly to depths where ice from the last glacial period can be recovered.

In this paper we present records of atmospheric composition from ancient ice outcropping in the ablation zone at the Greenland ice sheet margin, at a site called Pakitsoq (Reeh et al., 1991; Reeh et al., 2002). At this location essentially unlimited quantities of ancient ice can be collected on the ice sheet surface. The main challenges are the potential for post-depositional contamination of trapped gases, and determining an accurate chronology for the sampled section.

The motivation for this study comes from an uncertainty about the sources for rapid increases in atmospheric methane concentration associated with many of the abrupt warming events during the last glacial period, as well as at the Glacial – Holocene transition (Brook et al., 2000; Kennett et al., 2000). While most workers have attributed these variations to changes in methane emissions from wetlands, an alternative hypothesis holds that sea floor hydrates are the major source, and that they play an important role in late Quaternary climate change (Kennett et al., 2000, 2003). We are attempting to use the ^{14}C of atmospheric methane during two of these warming events (end of Younger Dryas 11,600 years ago and the transition into the Bølling warm interval 14,700 years ago) to constrain the possible methane sources. One major challenge is that about 2 m^3 of glacial ice must be processed in order to obtain enough methane carbon for a single accelerator mass spectrometry (AMS) ^{14}C measurement.

No ice core can provide that much sample, leading us to pursue samples from an ice sheet margin.

Ice sheet margins are potential sources of ancient ice because once deposited, ice flows within the ice sheet and eventually emerges in the ablation zone. In principle, if ice flow is unaffected by folding, faulting and basal melting, a complete sequence of all deposited ice layers should be available at the surface in the ablation zone, with the oldest ice emerging nearest to the margin (Figure 2.1). The most promising sites for finding ancient ice at the ice sheet margin are areas where a topographic obstacle results in flow stagnation. The slow ice flow at such sites ensures that the ice takes a relatively long time to travel from the site of deposition and is old by the time it becomes exposed at the margin. These sites are also compression zones, which prevents stratigraphy-disturbing crevasses from forming.

Reeh et al. (2002) summarized results for several ice margin sites around Greenland that have been sampled for $\delta^{18}O_{ice}$. Data from the Pakitsoq site in West Greenland are shown in Figure 2.2. A large portion of the Pakitsoq profile contains $\delta^{18}O_{ice}$ values that are lower than any found in modern Greenland precipitation, and are similar to values observed in the GISP2 and GRIP cores for the last glacial period (Grootes et al., 1993). Two large and abrupt shifts in $\delta^{18}O_{ice}$ between 500 and 550 meters in the Pakitsoq record have magnitudes similar to those found in GISP2 for the abrupt warming events at the initiation of the Bølling warm interval at 14,700 years BP (before present, where present is 1950 A.D.) and the termination of the Younger Dryas cold interval at 11,600 years BP. Together these features clearly show that this

record contains both Holocene and last glacial period ice, and suggest that Younger Dryas and Bølling-Allerød ice may also be present. However, assigning an absolute chronology to this record beyond a simple glacial / interglacial distinction is quite problematic when only $\delta^{18}O_{ice}$ and surface observations are available. A further complication is that ice at Pakitsoq appears to be disturbed by shearing and folding, and the sequence of outcropping layers may not be completely in stratigraphic order (Reeh et al., 2002).

Our objectives at the Pakitsoq site were to determine whether high-quality gas records could be obtained from the ice, as well as to establish a better chronology for ice of last glacial termination age. $\delta^{18}O_{ice}$, $\delta^{18}O_{atm}$, $\delta^{15}N$ of N_2, and methane concentration were determined in samples collected at Pakitsoq for this purpose. An ice-sheet flow-line model (Reeh et al., 2002) predicts that Pakitsoq ice dating to the last glacial termination originates near Greenland Summit, about 190 km south and 40 km west of the GISP2 site (Figure 2.3), in an area where modern $\delta^{18}O_{ice}$ values are about 3‰ heavier than at the GISP2 site. This proximity makes it probable that the GISP2 and Pakitsoq deposition sites experience similar surface temperature and accumulation rates, and that changes in these parameters during climatic transitions were synchronous and similar in magnitude at these two sites.

As is widely recognized, $\delta^{18}O_{ice}$ responds to variations in local temperature, moisture sources, seasonality of precipitation, and other influences (Jouzel et al., 1997). Although we expect Pakitsoq $\delta^{18}O_{ice}$ to be shifted toward more positive values with respect to GISP2, the magnitude of $\delta^{18}O_{ice}$ transitions should be very similar,

allowing for close correlation of the two records. $\delta^{15}N$ of N_2 in occluded air is primarily influenced by gravitational fractionation in the firn. The magnitude of this fractionation is in turn determined mainly by the firn diffusive column height (DCH) (Sowers et al., 1992). DCH appears to depend primarily on temperature and accumulation rate, with wind speed possibly also having an effect (Sowers et al., 1992; Schwander et al., 1997; Severinghaus et al., 2003). In addition, $\delta^{15}N$ of N_2 is affected by thermal fractionation, and can serve as an indicator of rapid temperature change at the deposition site (Severinghaus et al., 1998). Because of proximity of GISP2 and Pakitsoq deposition sites, we expect a similar climatic history for the two sites. We would therefore also expect similarity in the corresponding $\delta^{15}N$ of N_2 records for ice dating to the last glacial termination. This makes $\delta^{15}N$ particularly valuable for identifying known GISP2 abrupt climate change events in Pakitsoq ice (Severinghaus et al., 1998; Severinghaus and Brook, 1999).

The parameter $\delta^{18}O_{atm}$ denotes the true $\delta^{18}O$ of atmospheric molecular oxygen. Changes in $\delta^{18}O_{atm}$ reflect changes in fractionation (known as the Dole effect) as well as changes in the mean $\delta^{18}O$ of ocean water, which in turn reflect changes in the global ice volume (Bender et al., 1994; Malaize et al., 1999). During the last deglaciation, $\delta^{18}O_{atm}$ decreased steadily from about 1.1‰ to about – 0.2‰ (Bender et al., 1999). Atmospheric methane concentration exhibits large and rapid changes during the last deglaciation and closely follows Greenland temperature variations (Brook et al., 2000; Brook et al., 1996). Both atmospheric oxygen and methane are globally well-mixed, and have been widely used for correlating ice core

records from Greenland and Antarctica (Bender et al., 1994; Blunier and Brook, 2001). Barring in-situ alterations, we expect identical $\delta^{18}O_{atm}$ and methane records in Pakitsoq and GISP2 ice of the same age, which makes these two proxies especially valuable for establishing the Pakitsoq ice chronology.

2.2 Site Description

The Pakitsoq ice margin site is located about 40 km northeast of the town of Ilulissat in West Greenland (69˚25.83'N; 50˚15.20'W, Figure 2.3). Ice flowing westward from the Greenland Summit region encounters a mountain range here, creating a zone of compression. The ice flow velocity toward the margin is about 17 m / year at 1 km inland, and nearly zero at the margin (Reeh and Thomsen, 1994). The ablation rate is 2-3 m / year. At present, the site has a negative mass balance: the surface elevation has decreased by 9 meters in the past 12 years (Reeh et al, in preparation). The ice surface at the work site is nearly horizontal and free of crevasses. The main topographic features are small ice ridges and hummocks, as well as stream channels cut by the melt water. The elevation difference between the stream beds and the tallest hummocks is about 1 meter. There are several bands of ice with high sediment content ("dust bands"), typically 0.5 – 10 cm thick, present at our sampling site. The ice also contains "blue bands", which are 0.2 - 5 cm thick bands of bubble-free ice. Both dust bands and blue bands are mostly planar features, but show folding in some areas. Most dust bands strike parallel to the ice margin and dip at ~70˚ away from the margin; blue bands have more variation in their orientations. Surface melt features known as cryoconite holes are also abundant at the site.

2.3 Experimental

Ice samples were collected at the Pakitsoq site during the summers of 2001 – 03 for analysis of $\delta^{18}O_{ice}$, $\delta^{18}O$ of O_2, $\delta^{15}N$ of N_2, and methane concentration (Table 2.1). Initially, the most likely location of Younger Dryas ice was determined using $\delta^{18}O_{ice}$ records and high-accuracy GPS measurements from prior years, as well as surface ice appearance. The sample profile lines were oriented perpendicular to the ice margin. Positions of sampling profiles from different years were correlated by using permanent markers left in the ice.

Samples for $\delta^{18}O_{ice}$ were melted on site in leak-tight plastic bags and transferred into small bottles for shipment back to Denmark, where they were analyzed at the University of Copenhagen as in Reeh et al. (2002). Ice samples for gas analyses were stored in electric chest freezers at –10 to –21˚C while at Pakitsoq, and transported to the USA in thermally insulated boxes. Maximum temperature during transport was –12˚C. Samples were stored at -22 to -24˚C while in the USA.

Samples for $\delta^{18}O$ of O_2, $\delta^{15}N$ of N_2, and methane were analyzed in duplicate except in a few cases where insufficient good quality ice was available. For laboratory methane analyses, the samples were cleaned by removing 0.3-0.5 cm of the surface with either a clean steel chisel or an electric band saw with a clean blade. The methane concentration analyses were performed at Washington State University (WSU) using a wet extraction technique and gas chromatographic method described by Brook et al. (2000; 2005).

Field measurements of methane concentration were conducted in a laboratory tent at the site. The primary purpose of these measurements was to re-establish stratigraphic control at the beginning of each field season; we rely on laboratory-based measurements for more precise concentration data. Air was extracted by a melt/refreeze procedure, using glass vacuum vessels sealed to a 6-port stainless steel vacuum line using NW 40 clamp-flanges and Viton O-rings. An alcohol cold bath cooled with a probe chiller was used to keep the samples cold for initial evacuation of the flasks and refreezing (T= -30 to -40˚C). Air samples were expanded into a pre-evacuated 10 cc sample loop on a Shimadzu GC-14A gas chromatograph, pressure was measured with a capacitance manometer, and the sample was analyzed for methane with a flame ionization detector. No blank tests were performed in the field, but blanks for this apparatus in the laboratory range from about 10 to 20 ppb. Concentrations were quantified by comparison to an air standard of 1033 ppb methane (balance ultra zero air) purchased from Airgas Incorporated and calibrated at WSU against standard tanks previously calibrated at NOAA CMDL.

Measurements of $\delta^{18}O$ of O_2 and $\delta^{15}N$ of N_2 were carried out at the Scripps Institution of Oceanography. The samples were cleaned by removing 0.2-0.5 cm of the surface using an electric band saw with a clean blade. Sample sizes were between 10 and 16 grams of ice. The gas extraction was performed using a melt-refreeze method as described by Sowers et al. (1989), but with several modifications, as follows. Prior to melting the ice sample, the extraction vessel was kept at -20 to -24˚C by immersing it in a cold ethanol bath, and evacuated for 30 minutes with a turbo-

molecular pump. The ice was then melted using a water bath at or slightly above room temperature. The meltwater was refrozen within 2 hours, and the vessel was allowed to further cool for 10 minutes after the re-freezing was complete. During the cryo-transfer step, we used a trap at liquid nitrogen temperature (-196˚C) between the extraction vessel and the liquid helium-cooled sample tube to remove water vapor and carbon dioxide. The cryo-transfer was allowed to proceed for 10 minutes, and the air sample was then allowed to equilibrate for at least 40 minutes prior to the mass spectrometric measurement. The melt-refreeze cycle was not repeated for any of the samples.

The 2001 samples were analyzed on a Finnigan MAT 252 and the 2002-3 samples on a Finnigan MAT Delta XP; both instruments are dual dynamic-inlet isotope ratio mass spectrometers. We used air sampled outside of our laboratory building as the reference. In addition to the corrections described in Sowers et al. (1989), we corrected for the effects of pressure imbalance between the standard and sample bellows in the mass spectrometer.

Like nitrogen, oxygen in firn air is also affected by gravitational and thermal fractionation (Severinghaus et al., 1998). For this reason a correction is necessary to determine $\delta^{18}O_{atm}$ from $\delta^{18}O$ measured in occluded air. Gravitational fractionation is proportional to the isotopic mass difference, so the gravitational correction is $\delta^{18}O_{atm} = \delta^{18}O_{O2} - 2\,\delta^{15}N_{N2}$ (Sowers et al., 1989; Bender et al., 1994). The firn thermal diffusion sensitivity of the $^{18}O/^{16}O$ pair is about 1.6 times that of the $^{15}N/^{14}N$ pair (Severinghaus et al., 2001), so the above formula also incorporates a reasonable,

though not completely accurate correction for thermal fractionation. During the abrupt warming events at 11.6 and 14.7 kyr BP a thermal fractionation $\delta^{15}N$ signal of about + 0.15 ‰ would be expected, and the above correction would result in biasing the $\delta^{18}O_{atm}$ downward by about 0.05 ‰ (Severinghaus et al., 2001). The existing GISP2 $\delta^{18}O_{atm}$ record is only corrected using the above gravitational formula (Bender et al., 1999). Because we are using the Pakitsoq $\delta^{18}O_{atm}$ record for correlation with GISP2, and because we expect the $\delta^{15}N$ records at Pakitsoq and GISP2 to be very similar, we also use only the gravitational formula and do not attempt to correct for thermal diffusion.

2.4 Results and Discussion

2.4.1 High-resolution records covering the Younger Dryas – Preboreal transition

Figure 2.4 compares $\delta^{18}O_{ice}$, $\delta^{18}O_{atm}$, $\delta^{15}N$ of N_2, and methane concentration in samples collected in 2001 at Pakitsoq to GISP2 data for the Younger Dryas – Preboreal transition. The lowest $\delta^{18}O_{ice}$ values in the Pakitsoq sampling trench occur between about 1.7 and 4.3 meters. These values of –39.0 to –39.5‰ are close to the typical Younger Dryas GISP2 $\delta^{18}O_{ice}$ values of –40 to –41 ‰ (Stuiver et al., 1995). Higher $\delta^{18}O_{ice}$ values occur on either end of the trench (up to about -34 ‰ at 5.3 meters, and -36.5 ‰ at 0.6 meters), indicating that the trench contains a section of ice from a cold interval bounded on both sides by warm-interval ice. The magnitude of the GISP2 $\delta^{18}O_{ice}$ transition at the abrupt warming into the Preboreal is 3.75 ‰ (Stuiver et al., 1995). In comparison, the Pakitsoq $\delta^{18}O_{ice}$ transition between 4.4 and 5.2 meters has a magnitude of about 4.5 ‰. The exact magnitude of the $\delta^{18}O_{ice}$

transition in the Pakitsoq data, however, is difficult to interpret due to sections of unexpectedly high $\delta^{18}O$ values at about 4.0 m and 5.7 m.

A section with low methane values is found in the trench from about 1.1 to about 2.3 meters. The typical methane concentrations in this section are around 500 ppb, which is consistent with GISP2 Younger Dryas methane values. The higher methane values on either side of this section are again mostly consistent with pre- and post-Younger Dryas GISP2 values (700 and 750 ppb, respectively). The methane transition at 2.4 m coincides with a sharp rise in $\delta^{15}N$ of N_2 from 0.4 ‰ to about 0.57 ‰. A sharp rise in $\delta^{15}N$ is indicative of a rapid warming event (Severinghaus et al., 1998); and GISP2 data show a $\delta^{15}N$ increase of identical magnitude for the end-of-Younger Dryas event, also synchronous with the rise in methane (Severinghaus et al., 1998). Both the $\delta^{15}N$ and the methane transitions in GISP2 are contained in the "cold", low-$\delta^{18}O$ Younger Dryas ice as expected due to the ice-age gas-age offset. The methane and $\delta^{15}N$ transitions in our trench profile are also contained in ice with low $\delta^{18}O$ values.

Our measurements of $\delta^{18}O_{atm}$ in the Pakitsoq trench samples provide further evidence that the ice is of Younger Dryas age. Over the ice section that spans the low methane values, and the rise and fall of methane (0.6 m to 2.4 m), we observe that $\delta^{18}O_{atm}$ decreases from 0.84 ‰ to 0.54 ‰. GISP2 $\delta^{18}O_{atm}$ data for an equivalent time period (start of methane decline to end of methane rise) show a decrease from about 0.90 ‰ to about 0.54 ‰ (Bender et al., 1999). In the GISP2 record, $\delta^{18}O_{atm}$ values between 0.5 and 0.8 ‰ are not found at any other time in the past 25,000 years

(Sowers and Bender, 1995). To summarize, this unique combination of the four geochemical tracers is unequivocal evidence that the Pakitsoq section contains the Younger Dryas.

The data from the Pakitsoq trench suggest that ice age decreases toward the ice margin. This pattern is opposite of that expected in an idealized flow situation. This suggests that the sampled ice section is overturned and part of a large-scale fold.

Figure 2.5 shows a record of $\delta^{15}N$ of N_2 and methane concentration from trench sample profiles taken in 2001 – 3. Note the close match in the size, shape and position of the $\delta^{15}N$ peak and the methane transition at 2.4 meters for the three years. This shows that we are able to re-establish the position of Younger Dryas ice each season, as well as that Pakitsoq gas records are reproducible from year to year.

2.4.2 Quality of the ice and gas records at Pakitsoq

Alteration of the ice and gas records by processes at the ice sheet surface or during flow to the margin are clearly a concern at sites like Pakitsoq. The 3-year $\delta^{15}N$ record in Figure 2.5 indicates that the $\delta^{15}N$ record from 0.3 – 0.4 meters below the surface is as reliable as the record from 3 meters below the surface. Our samples from the 2003 surface profile (Table 2.1, Figure 2.8b**)**, some taken from depths of as little as 10 cm, also yield reasonable $\delta^{15}N$ values. This further suggests that as long as the ice sampled is solid and unaffected by surface melting, the depth does not matter for the quality of $\delta^{15}N$. Our 3-year trench sample profile data set for $\delta^{18}O_{atm}$ (not shown) along with the 2003 surface profile record suggest that the same is true for $\delta^{18}O_{atm}$. Any blue bands or dust bands in samples have always been carefully cut out prior to

gas isotopic analysis, so the effects of these features on $\delta^{15}N$ and $\delta^{18}O_{atm}$ have not been investigated.

$\delta^{18}O_{ice}$ is a very robust measurement and should not be affected unless the sample is contaminated by melt water or rainwater with different $\delta^{18}O$, or unless sublimation of ice occurs. Most $\delta^{18}O_{ice}$ samples at Pakitsoq were collected from solid ice only a few centimeters below the surface, and depth does not appear to be a factor in the quality of this record. However, earlier measurements by Reeh et al. (unpublished) indicate that $\delta^{18}O_{ice}$ of blue bands is several per mille higher than that of surrounding ice. Blue bands would therefore affect this measurement if included in the sample.

There is strong evidence that methane is elevated by the presence of dust bands and blue bands in the samples. Measurement of air extracted from blue band ice revealed elevated concentrations, in one case as high as 3743 ppb – more than twice modern ambient levels. Visible dust in ice samples was also correlated with high methane values. The origin of the dust bands is not currently known, but a neodymium and strontium isotope analysis on dust from one such band at our sampling site indicates that the dust is of local rather than Asian provenance (P. Biscaye, personal communication). We speculate that the dust bands form when subglacial dust is injected into fissures in the ice by subglacial meltwater.

A 6-meter vertical sample profile was taken in 2001 (Table 2.1; data not shown) along the ~ 70˚ dip of the stratigraphy, which ensured that the profile followed an isochron. This profile was taken in ice known to contain Younger Dryas methane

values (~500 ppb); and the results showed no evidence of the methane record being altered closer to the surface. Nine out of eleven samples had methane values between 470 and 505 ppb. The two remaining samples, one at 1.3 m and the other at 5.3 m depth, gave elevated methane values of 593 and 576 ppb, respectively. Both of these samples contained blue bands; and when one of these two samples was later re-analyzed by carefully cutting out all the blue band ice, it measured at 480 ppb. The very good agreement between methane values for the Younger Dryas – Preboreal transition (Figure 2.5) from three profiles at different depths provides further evidence that methane values are unaffected by depth in this ice section.

Some elevated methane concentrations can be seen in the trench profiles (Figure 2.5), such as between meter 0 and 2 and meter 5 and 6, especially in the 2001 and 2003 samples. Most of the samples with elevated methane contained no visible blue bands or dust bands. Elevated methane values in our trench profiles are found in a similar stratigraphic location from year to year, indicating that the high values are not due to sampling or analytical problems (we do not expect exact distance agreement, as the details of the stratigraphy change from year to year due to ablation and the fact that our sampling area is part of a large-scale fold – see discussion below). Sporadically elevated methane concentrations are not observed in Greenland ice core records around the time of the Younger Dryas (Brook et al., 2000; Brook et al., 1996; Chappellaz et al., 1993) and we speculate that in some Pakitsoq sections they may result from the presence of very small blue ice bands, which form after ice deposition. Some more recent measurements on ice sampled in 2004 and 2005 (not shown)

suggest that in ice sections where methane alteration is repeatedly observed, the extent of this alteration also increases with proximity to the surface.

Although much remains to be understood about the processes, patterns and extent of methane alteration in Pakitsoq ice, the results of laboratory methane analyses (Figure 2.5) as well as extensive field measurements (not shown) indicate that the methane record is intact in most of the ice at our sampling site.

2.4.3 Interpreting the stratigraphy and deformation of the Pakitsoq section

Figure 2.6 shows a large-scale aerial view of the sampling site. It is immediately apparent that there are well-defined boundaries between areas of darker and lighter-appearing ice. One of these boundaries is at our sampling site, about 500 meters from the ice margin. The darker, dustier ice is from the colder glacial period, while the cleaner ice is from the Holocene and the warm Bølling-Allerød (Reeh et al., 1993). We believe that the darker appearance of the ice is due to both higher dust content (due to drier and windier conditions during the glacial and lower accumulation rates) and a different distribution of dust on the ice surface. The relatively clean ice has coarser-grained crystals (Reeh et al., 2002), as well as a higher abundance of cryoconite holes. The cryoconite holes contain significant amounts of dust and we suspect that much of the surface dust in this ice is concentrated into the cryoconite holes, leaving the ice surface lighter in appearance. Another feature visible in the photograph is the folding of the ice layers, apparent because of the alternating lighter and darker bands in the ice. Folding is commonly observed in ice sheets and glaciers (e.g., Scambos et al., 2004; Hudleston, 1976). Several different causes of folding in a

variety of ice flow situations have been suggested, including bedrock topography (Hudleston, 1976; Whillans and Johnsen, 1983), transitions from ice sheet to ice stream flow (Jacobel et al., 1993; Scambos et al., 2004), anisotropy in ice rheological properties (Waddington et al., 2001) as well as advance and retreat of the ice margin (Hudleston, 1976). We suspect that the large-scale, sometimes overturned folds present at Pakitsoq are mostly the result of ice flow interaction with bedrock topography.

Figure 2.7, composed of two merged photographs, taken in 2004, shows a close-up view of the sampling site from above. Darker and lighter bands of ice, as well as the folding, are clearly visible. The well-defined fold beneath the laboratory tent is a syncline, with Preboreal age ice at its axis. The wide darker band of ice in the lower half of the image is from the last glacial period. The slim band of cleaner ice just above this is from the warm Bølling-Allerød interval. The narrow dusty layer above that is Younger Dryas ice, followed by the cleaner Preboreal ice. Unfortunately, the visual interpretation of ice layers by dust content is complicated by the presence of dust bands. Dust bands generally form small ridges on the surface, with the dust being washed out by melt water and deposited over the ice just downhill (toward the ice margin) of the dust band. It is therefore difficult to distinguish between truly dusty ice and ice that has picked up dust on its surface from a dust band nearby. We believe that the dustier band of ice slightly further up in the Preboreal section formed this way. The left side of the image shows a wedge of clean ice from the Bølling-Allerød interval near the hinge of the fold, and Younger Dryas ice

wrapping around to the other side of the fold. Above the main fold is a thin band of dusty ice that, according to field measurements of methane concentration (not shown), dates to the Oldest Dryas. This further shows that the section is not simply a single fold; rather, it appears to be a syncline-anticline pair, with the anticline located above the syncline in the image. The approximate positions of the 2001 – 3 trench profiles (green) and the 2003 surface profile (red), are also shown on the image.

Figure 2.8a shows the record of $\delta^{18}O_{ice}$, $\delta^{18}O_{atm}$, $\delta^{15}N$ of N_2 and methane concentration from the GISP2 ice core over the last glacial termination. We showed earlier how these four geochemical tracers may be used to uniquely identify the Younger Dryas and the Younger Dryas – Preboreal transition (Figure 2.4). In a similar way, other climatic intervals in GISP2 ice are also characterized by certain combinations of values of these four tracers, as can be seen from Figure 8a. Ice dating from the end of the last glacial period and before the transition into the warm Bølling is characterized by low $\delta^{18}O_{ice}$ (between –38.5 and –41 ‰), high $\delta^{18}O_{atm}$ (between 0.95 and 1.1 ‰) and low methane (between 400 and 500 ppb). This ice also contains the methane and $\delta^{15}N$ signals associated with the abrupt climate transition into the Bølling warm interval. The Bølling-Allerød interval ice is characterized by relatively high $\delta^{18}O_{ice}$ (though ranging from –35 to –41 ‰), $\delta^{18}O_{atm}$ that is gradually decreasing from about 1.07 to 0.78 ‰, and mostly high methane (between 600 and 700 ppb). This ice also contains the methane transition signal associated with the onset of the cold Younger Dryas. Ice from the Preboreal interval is characterized by high $\delta^{18}O_{ice}$

(between – 35 and –38 ‰), $\delta^{18}O_{atm}$ that is decreasing from about 0.55 to 0.0 ‰ and high methane (mostly between 700 and 750 ppb).

Figure 2.8b shows a record of $\delta^{18}O_{ice}$, $\delta^{18}O_{atm}$, $\delta^{15}N$ of N_2 and methane concentration measured in samples collected at Pakitsoq along a 50-meter profile in 2003. We have interpreted the ages of the ice sections along this profile by comparing our measurements to the GISP2 record, and the different climatic intervals along the profile are highlighted by grayscale bands in the figure. These data confirm our visual interpretation of the age of ice bands in the folds shown in Figure 2.7. Our $\delta^{15}N$ record from this profile contains two discrepancies from the GISP2 record. First, the expected $\delta^{15}N$ thermal fractionation peak near the Younger Dryas – Preboreal transition at –17 meters is missing. Second, the $\delta^{15}N$ peak at the Glacial – Bølling transition at around 16 meters does not reach its full GISP2 magnitude of 0.64 ‰. We believe that this is due to a combination of wide sample spacing and high degree of ice thinning in these sections of the profile.

The rising $\delta^{18}O_{atm}$ indicates that ice is getting older in our profile going from –24 to about – 1 meters. Note, however, that between about –1 and 12 meters the falling $\delta^{18}O_{atm}$ indicates that the ice is getting younger in the direction of the ice margin. Between 12 and 16 meters the rising $\delta^{18}O_{atm}$ again indicates ice getting older toward the margin. The fall in $\delta^{18}O_{atm}$ after meter 17 matches the GISP2 record going back in time beyond the Oldest Dryas (Bender et al., 1994; not shown). Reversals in the age-distance trend in our profile confirm our visual interpretation of folding in this ice section. The axis of one of the folds is located at about 11.5 meters in our profile

(indicated on Figures 2.7 and 2.8b). This is a syncline, with the youngest Preboreal ice in the middle, bounded by first Younger Dryas and then Bølling-Allerød ice on either side. The symmetry is not perfect -- ice in the lower (in Figure 2.7) side of this fold is more thinned than in the upper side; but features repeating on both sides make the determination of the axis position possible. For example, the sample at 11.5 meters has the lowest $\delta^{15}N$ value within this Preboreal section, with $\delta^{15}N$ rising on either side of 11.5 meters. Similar patterns are observed for $\delta^{18}O_{atm}$, with the exception of one sample at 10 meters, which may be an analytical artifact. High $\delta^{18}O_{ice}$ values are observed at 11.5 meters, with $\delta^{18}O_{ice}$ decreasing slightly to either side (at 9.5 and 12.8 meters; this may be the Preboreal Oscillation), then rising back to warm Preboreal values (at 8.5 and 13 meters) on both sides and finally decreasing again as Younger Dryas ice is encountered on both sides.

The second large fold included in our profile is an anticline with the oldest, Bølling-Allerød, ice section between about –14 and 0 meters at the center. Using the same lines of reasoning as above, we conclude that this fold has its axis between –0.5 and –1 meters in the profile. This interpretation is consistent with the visual evidence in Figure 2.7, which shows a thin wedge of darker ice (believed to date to the Oldest Dryas) at the center of this fold and to the left of our sampling profile.

Ice at our sampling site seems to be characterized by a variable time-distance relationship, as can most easily be seen from the $\delta^{18}O_{atm}$ record in Figure 2.8b. In the GISP2 record, $\delta^{18}O_{atm}$ decreases gradually from about 1.1 ‰ at the time of the Bølling abrupt warming (14.7 kyr BP) to about 0.0 ‰ at 10 kyr BP (Figure 2.8a). The slope

of this decrease steepens with time: $\delta^{18}O_{atm}$ is changing approximately twice as rapidly in the Preboreal than in the Bølling-Allerød (Bender et al., 1999). Taking this feature into account, the slope of the $\delta^{18}O_{atm}$ curve in the Pakitsoq surface profile can be used as a rough relative indicator of the time-distance relationship in the ice.

For example, the $\delta^{18}O_{atm}$ curve is particularly steep between –18 and –15 meters, as well as between 12 and 16 meters in the surface profile. Our sampling resolution (0.5 meters) does not allow us to completely rule out the possibility that ice of certain ages is simply missing from these sections, thereby causing the $\delta^{18}O_{atm}$ slope to be steep. However, the absence of large discontinuities in the $\delta^{18}O_{atm}$ record does suggest that this is not the explanation, and instead the ice is highly thinned in these sections as compared to other parts of the profile.

We suspect that differences in ice rheology are one of the main causes of variable thinning (Dahl-Jensen, 1985; Morgan et al., 1998; Thorsteinsson et al., 1999). It is also possible that non-uniform stresses at the time of folding resulted in enhanced thinning of certain ice sections. Unfortunately, with the limited data available, we are not able to identify any definite patterns linking greater thinning to particular ice types.

2.5 Conclusions

Pakitsoq is the first ice margin site in Greenland where the paleoatmospheric gas record has been explored to a significant extent. The Pakitsoq gas record appears to be intact for $\delta^{15}N$ of N_2 and $\delta^{18}O$ of O_2. Most of the ice sampled appears to contain an unaltered methane record as well; however some sections repeatedly show elevated

methane values. Proximity to the surface does not appear to affect $\delta^{15}N$ of N_2, $\delta^{18}O$ of O_2; methane also appears to be unaffected by this in most ice sections. The rapid ablation rate of almost 3 m / year might explain the preservation of gas records so near the surface. In ice sections that do show elevated methane, the degree of alteration appears to increase with proximity to the surface. Cross-cutting features in the ice margin stratigraphy, such as blue bands and dust bands, do appear to affect the gas record when included in samples. The Pakitsoq $\delta^{18}O_{ice}$ record appears to be intact with no dependence on proximity to the surface; however blue bands do affect this measurement if included in the sample.

The combination of $\delta^{15}N$ of N_2, $\delta^{18}O_{atm}$, methane and $\delta^{18}O_{ice}$ allows for unambiguous identification of different climatic intervals in the ice through comparison to central Greenland deep ice core records. Using this approach, the Last Glacial, Bølling – Allerød, Younger Dryas and Preboreal sections have been identified. It is also possible to obtain accurate dates for sections of the ice representing abrupt climate transitions, where the geochemical tracers are rapidly changing. The ice at Pakitsoq is folded and non-uniformly thinned. However, this has not been an obstacle in obtaining good quality gas records; in fact, the gas records have substantially increased our understanding of the fold geometry at Pakitsoq.

Much remains to be understood about the processes that produce the folding and cross-cutting features in Pakitsoq ice, as well as the methane record alterations in some of the ice sections. Nevertheless, the outcropping of good quality ancient ice at Pakitsoq opens the door to a large range of possibilities in paleoenvironmental studies.

Studies that have up until now been limited by availability of ancient ice may become feasible. In addition to our work on ^{14}C of methane, the possibilities include extracting wind-blown organic macroparticles for ^{14}C dating, ^{14}C dating of bulk organic matter in the ice, isotopic studies of dust, studies of trace gases present in part-per-trillion concentrations, and collection of extraterrestrial material. The ability to accurately date some sections in the outcrop also provides glaciologists with a powerful tool for studying ice margin stratigraphy, flow and deformation processes. We believe that this work demonstrates the viability of ice margin sites as easily accessible paleoenvironmental archives and paves the way for further studies at other such sites in Greenland, as well as Antarctica, where much older ice may be available at the surface (Popp et al., 2004).

Acknowledgements

We thank Jerome Chappellaz, Ralph Keeling, and Richard Alley for helpful discussions. VECO Polar Resources provided outstanding logistical support. We thank the Glaciology Group, Niels Bohr Institute, University of Copenhagen for performing the $\delta^{18}O_{ice}$ measurements. We would also like to thank Field Coordinator Paul Rose for his excellent help with logistics and sampling as well as his constant good cheer. The 109th Airlift Wing and Air Alpha provided reliable transport to and within Greenland. Ross Beaudette, Joseph Becker, Alexi Grachev, Melissa Headly, Takuro Kobashi, Jon Pompa, Margot Stiles, Derek Mastroianni, Neil Gordon and Koty Sharp assisted with field preparations. Leah Bjerkelund ably assisted with methane measurements. We thank Pierre Biscaye for Nd / Sr isotope measurements. Andreas Ahlstrøm participated in a valuable field collaboration. We would also like to thank Karl Kreutz for lending us his ECM unit, and Ice Coring and Drilling Services for developing the small ice sampling drill. We thank the Danish Polar Center and Greenland Home Rule for permission to carry out this research. This paper was greatly improved by suggestions from two anonymous reviewers. This work was supported by NSF grants OPP0221470 (to JPS) and OPP0221410 (to EJB), and by a Packard Fellowship (to JPS).

Chapter 2, in full, is a reprint of the material as it appears in Quaternary Science Reviews, 25, Petrenko, V.V., Severinghaus, J.P., Brook, E.J., Reeh, N. and Schaefer, H., Gas records from the West Greenland ice margin covering the last glacial termination: a horizontal ice core, pp. 865-875, Copyright (2006), with

permission from Elsevier. The dissertation author was the primary investigator and author of this paper.

Tables

Table 2.1. Summary of samples collected during the 2001 – 03 field seasons at Pakitsoq.

Table 2.1

Sample profile	Profile length	Sampling resolution	Depth below surface	Sampling method	Measured parameters	Notes
2001 trench	5.1 m	6-10 cm for $\delta^{15}N$, $\delta^{18}O_{atm}$ and CH_4; 15 cm for $\delta^{18}O_{ice}$	2.7 – 3.1 m	gasoline chainsaw for $\delta^{15}N$, $\delta^{18}O_{atm}$ and CH_4; steel chisel for $\delta^{18}O_{ice}$	$\delta^{15}N$, $\delta^{18}O_{atm}$, CH_4, $\delta^{18}O_{ice}$	
2001 vertical	6.0 m	40 – 70 cm		gasoline chainsaw to 3.5 m , hand auger from 3.5 – 6.0 m depth	CH_4	Profile taken at 70˚ angle to horizontal to match dip of stratigraphy
2002 trench	3.8 m	10 cm	0.6 – 0.8 m	gasoline chainsaw	$\delta^{15}N$, $\delta^{18}O_{atm}$, CH_4	
2003 trench	5.9 m	5 – 20 cm	0.3 – 0.4 m	electric core drill	$\delta^{15}N$, $\delta^{18}O_{atm}$, CH_4	
2003 surface	50 m	50 cm for $\delta^{15}N$ and $\delta^{18}O_{atm}$; 20 cm for $\delta^{18}O_{ice}$	5-10 cm for $\delta^{18}O_{ice}$; 10-20 cm for $\delta^{15}N$, $\delta^{18}O_{atm}$	electric core drill for $\delta^{15}N$ and $\delta^{18}O_{atm}$; steel chisel for $\delta^{18}O_{ice}$	$\delta^{15}N$, $\delta^{18}O_{atm}$, $\delta^{18}O_{ice}$	
2003 field methane	7.5 m	15 – 115 cm	5 - 10 cm	electric core drill	CH_4	analyzed in the field

Figures

Figure 2.1

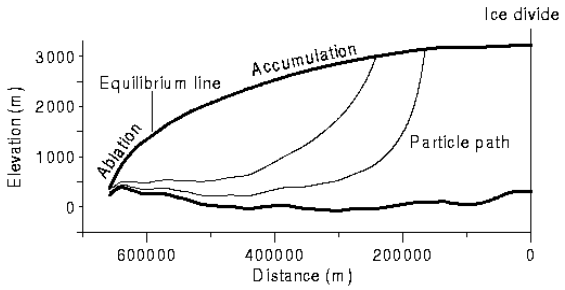

Figure 2.1. Cross-section of an ice sheet, showing particle paths connecting snow-deposition sites in the accumulation zone with locations where the ice resurfaces in the ablation zone.

Figure 2.2

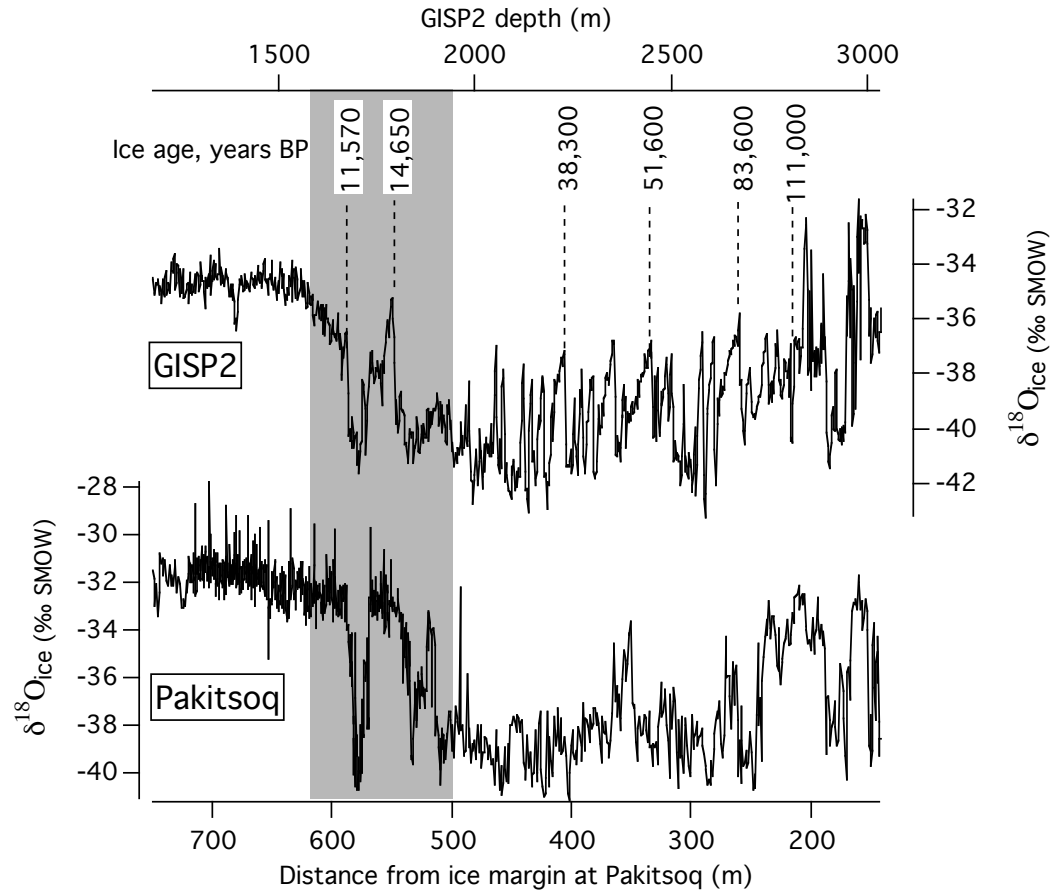

Figure 2.2. Comparison of a Pakitsoq ice margin $\delta^{18}O$ record from samples taken along a horizontal profile with GISP2. Pakitsoq data are from Reeh et al (2002); GISP2 $\delta^{18}O$ is from Grootes and Stuiver (1997); and GISP2 age scale is from Meese et al (1994). The age scale is in years before present (BP), where "present" is taken to be 1950 AD. The shaded rectangle highlights the area of interest at the Pakitsoq site that is examined in this paper.

Figure 2.3

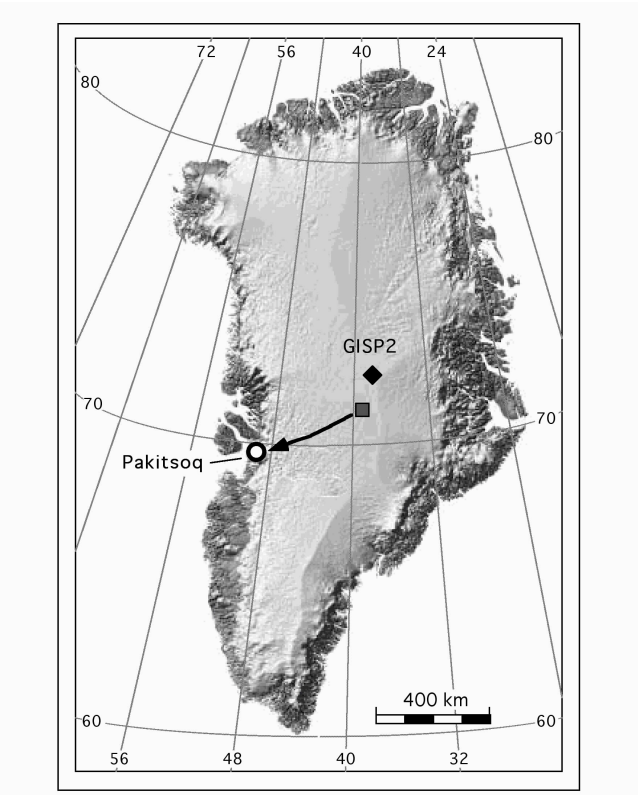

Figure 2.3. Location of the Pakitsoq ice margin site. The site of the GISP2 ice core as well as the approximate deposition site for Younger Dryas-age ice at Pakitsoq (gray square) are also shown (Reeh et al, 2002). Greenland image was from http://www.geus.dk/minex/mx22-03a.gif.

Figure 2.4

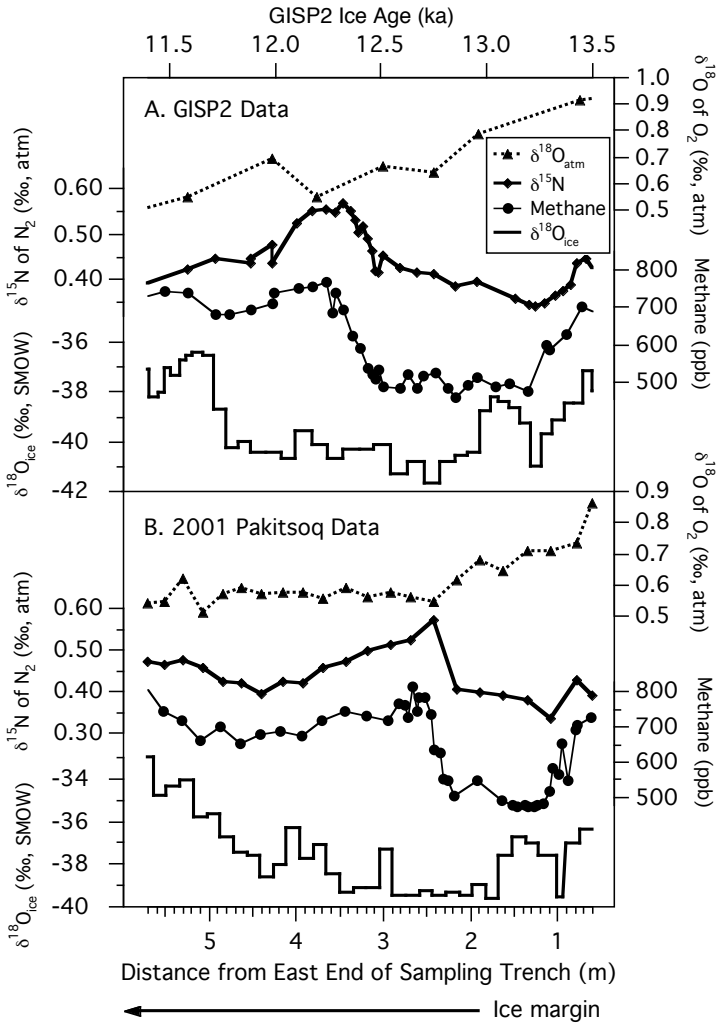

Figure 2.4. Comparison of GISP2 data with 2001 data from Pakitsoq. a) GISP2 oxygen isotopes of ice (Stuiver et al., 1995), methane (Brook et al., 1999), oxygen isotopes of molecular oxygen ($\delta^{18}O_{atm}$) (Sowers and Bender, 1995), and nitrogen isotopes (Severinghaus and Brook, 1999) are shown on the ice age timescale (Meese et al, 1994) for comparison with Pakitsoq ice. b) Record from the 2001 trench sample profile at Pakitsoq (Table 2.1). The pooled standard deviations (as defined in Severinghaus et al., 2003) for $\delta^{15}N$ and $\delta^{18}O_{atm}$ are 0.005 ‰ and 0.028 ‰ respectively. Methane blank correction was 20±9 ppb (2se, n=16) and pooled standard deviation was 19.3 ppb.

Figure 2.5

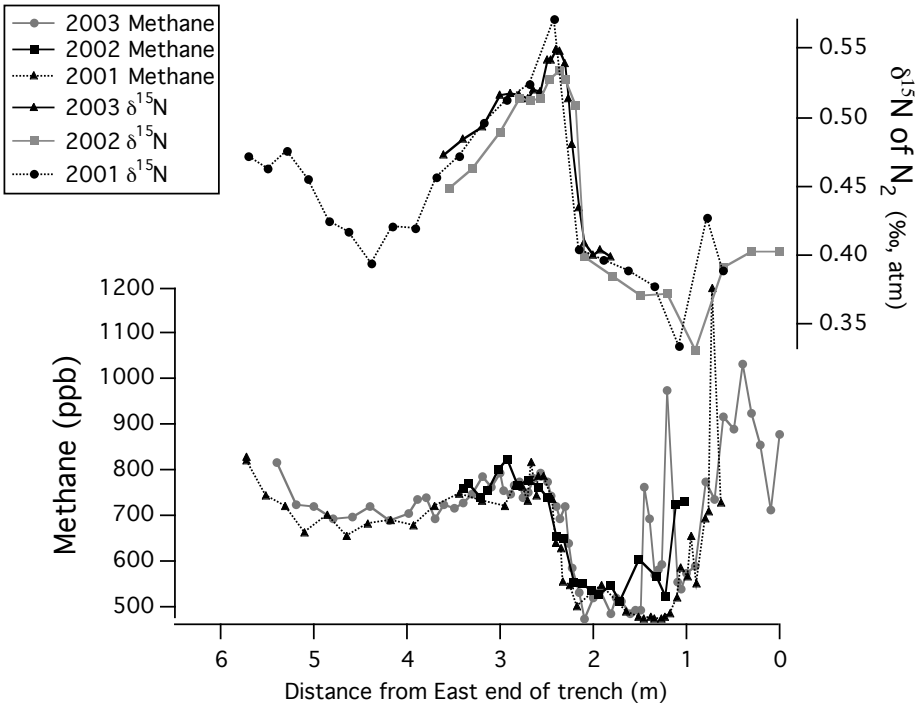

Figure 2.5. $\delta^{15}N$ of N_2 and methane concentration for the 2001, 2002 and 2003 trench sample profiles from Pakitsoq (Table 2.1). The sample profiles span the Younger Dryas – Preboreal transition in the gas record, going from right to left. The profiles are oriented perpendicular to the ice margin, with distance increasing toward the margin. Correlating the distance scales between profiles from different years is complicated by the 2.5 meters of annual ablation at the site – ice sampled one year is always gone by the following year. Field observations of planar features that mostly parallel the ice stratigraphy (dust bands and blue bands) show that the strike of the stratigraphy is about N 35˚ E and the dip is about 70˚ to the SE at our sampling site. At the end of each field season a 6-meter-long pole is placed in the ice along the dip of the stratigraphy, and its position in the profile noted. The distance scales are then correlated by assigning this pole the same position in the sampling profile the following year. The pooled standard deviations for the 2001, 2002 and 2003 $\delta^{15}N$ measurements are 0.005 ‰, 0.011 ‰ and 0.006 ‰ respectively. For 2001-03 methane measurements, the blank corrections are 20 ± 9 ppb (2se, n=16), 24 ± 21 ppb (2se, n=6) and 22 ± 5 ppb (2se, n=12) respectively. The pooled standard deviations for all methane samples from 2001, 2002 and 2003 are 19 ppb, 22 ppb and 17 ppb, respectively.

Figure 2.6

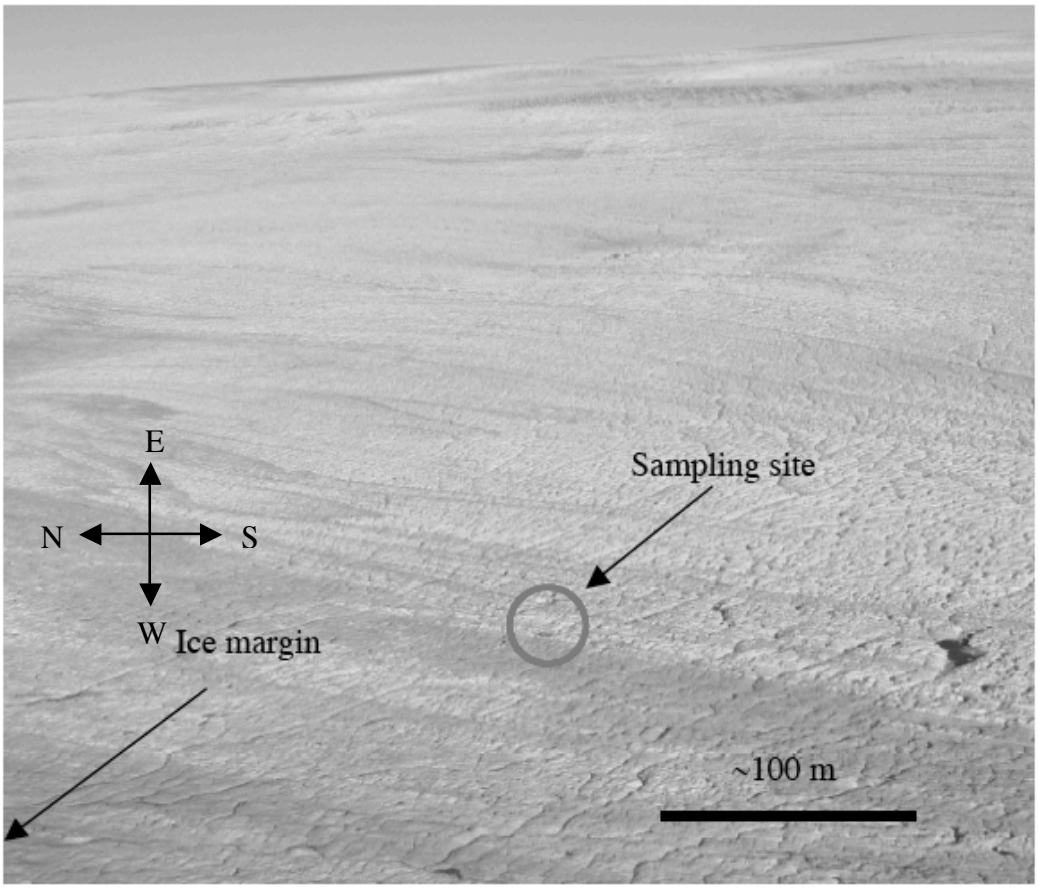

Figure 2.6. An aerial photograph of the Pakitsoq sampling area showing the boundary between darker, dustier ice from cold intervals and lighter-colored ice from warm intervals. Large-scale folding (center left) in the ice is also visible.

Figure 2.7

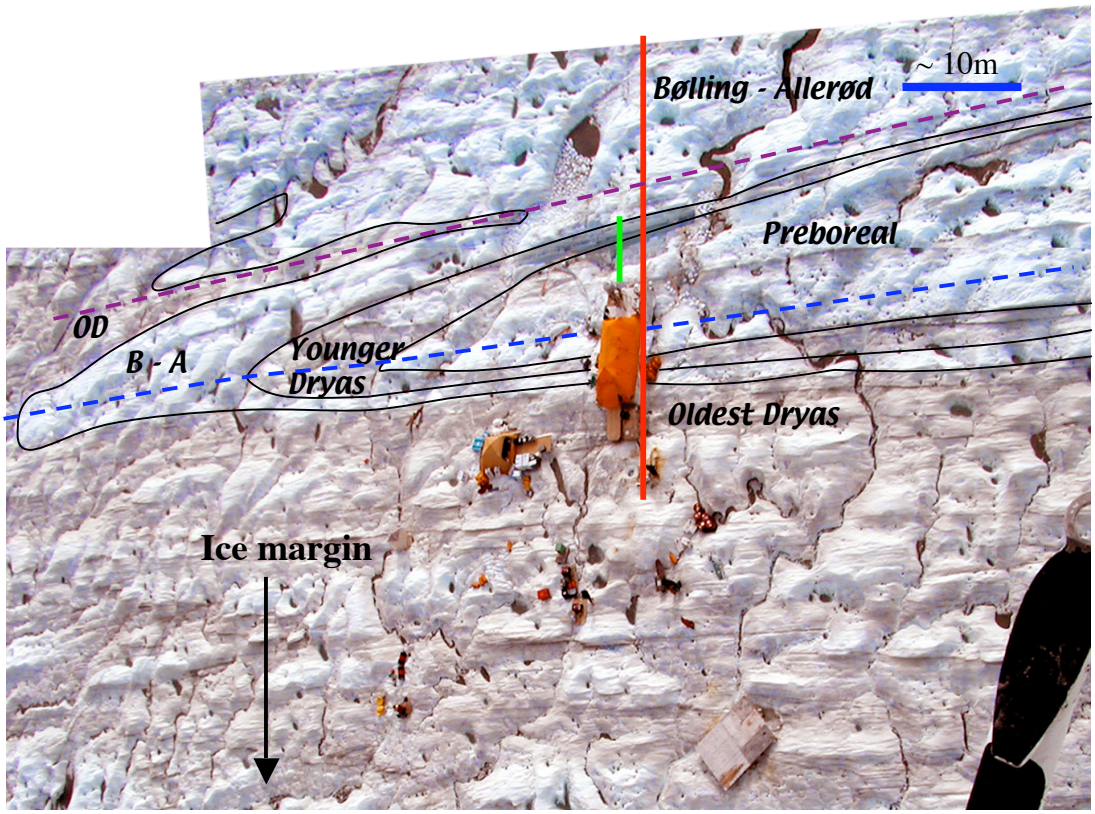

Figure 2.7. A view of the sampling site from above, illustrating the folding in the ice at the sampling site in 2004. The image is a composite of two photographs and the contrast and color intensity have been adjusted to enhance the visual difference between lighter and darker colored bands of ice. The orange object in the middle of the image is our main laboratory tent. The short green line shows the location and approximate span of the trench profiles. The red line shows the approximate position of the long sample profile taken in 2003 (the two profiles are parallel but offset by about 2 meters); an equivalent photo from 2003 was not available. The dashed blue and purple lines show the approximate axis positions of a syncline and an anticline fold, respectively.

Figure 2.8a

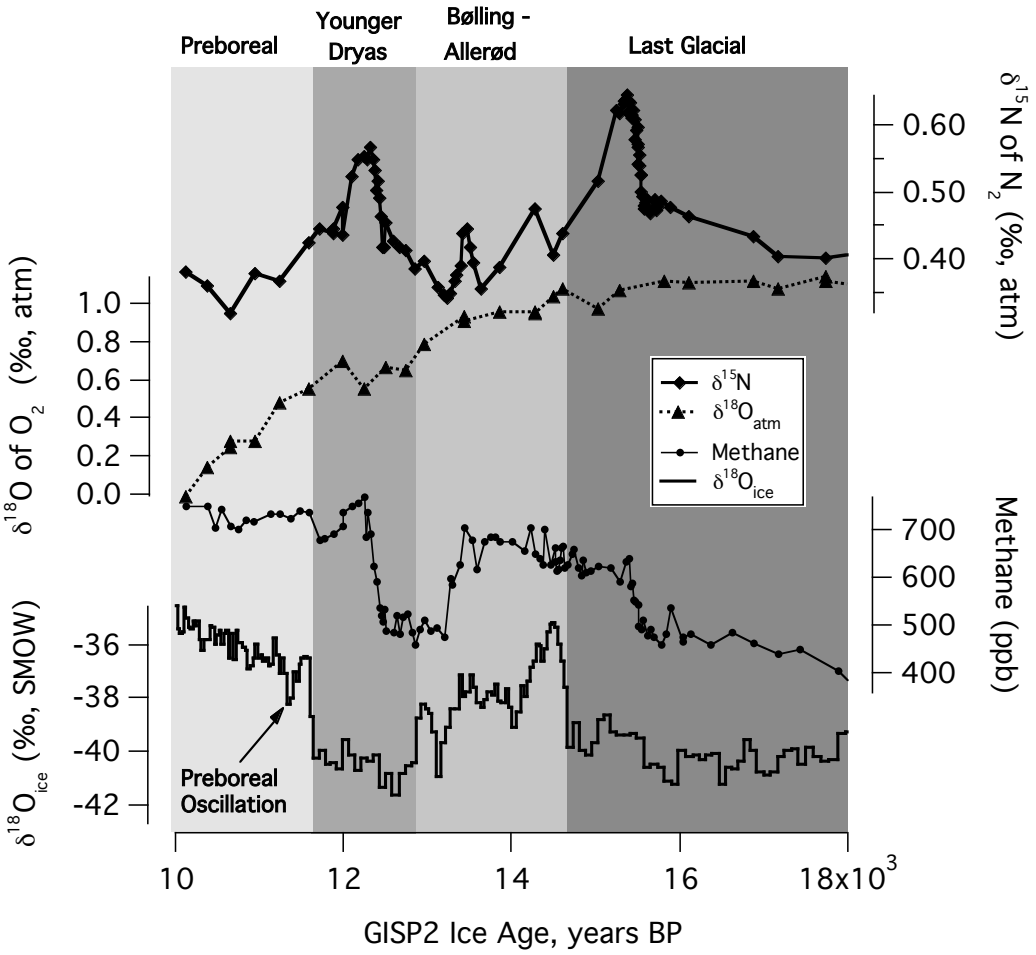

Figure 2.8a. $\delta^{18}O_{ice}$, $\delta^{18}O_{atm}$, $\delta^{15}N$ of N_2 and methane concentration from the GISP2 ice core over the Last Glacial Termination. Major climatic intervals on the ice age scale are highlighted with grayscale bands. Note the two large $\delta^{18}O_{ice}$ transitions corresponding to two abrupt warming events: the Bølling event at 14.7 kyr and the end-of-Younger-Dryas event at 11.6 kyr. The $\delta^{15}N$ and methane increases associated with these warming events are contained in older, low-$\delta^{18}O$ ice due to the gas age offset. Also note the monotonic decline in $\delta^{18}O_{atm}$ over the Glacial Termination, associated with decreasing global ice volume. The $\delta^{15}N$ data are from Severinghaus and Brook (1999) and Bender et al. (1994); $\delta^{18}O_{atm}$ data are from Bender et al. (1999); methane data are from Brook et al. (2000) and Severinghaus and Brook (1999); and $\delta^{18}O_{ice}$ data are from Grootes and Stuiver (1997). The GISP2 timescale is from Meese et al. (1994).

Figure 2.8b

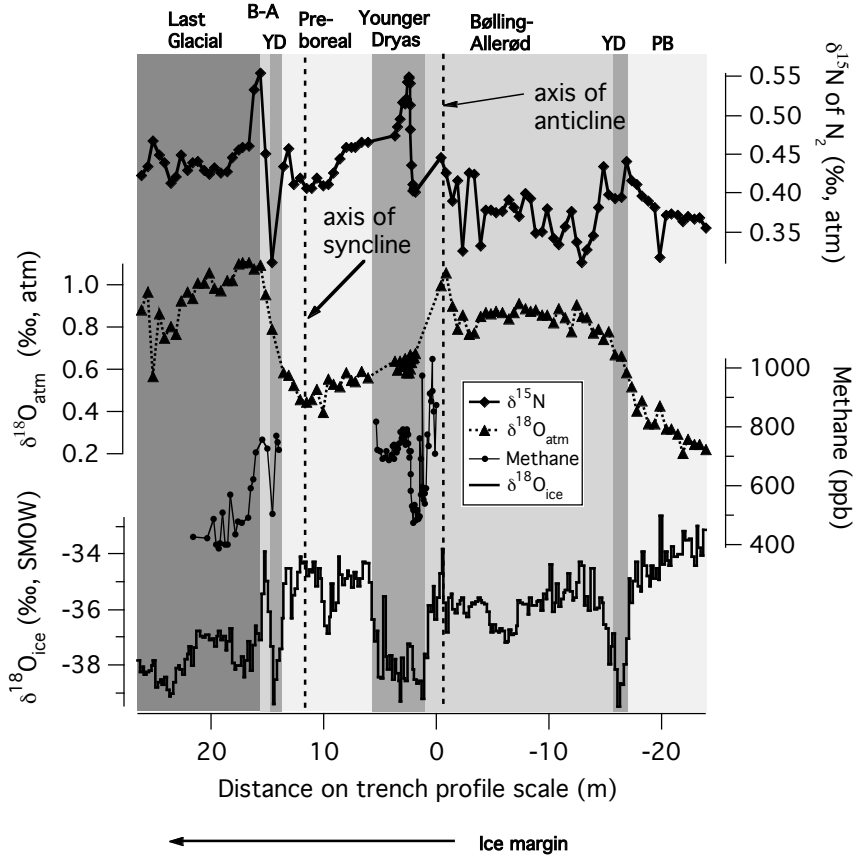

Figure 2.8b. Combined results from the 2003 surface, 2003 trench and 2003 field methane ice sample profiles at Pakitsoq (Table 2.1). $\delta^{18}O_{atm}$, $\delta^{15}N$ of N_2 and $\delta^{18}O_{ice}$ data are from the 2003 surface profile except for between 0 and 6 meters, where data for $\delta^{18}O_{atm}$ and $\delta^{15}N$ are from the 2003 trench profile. Methane data are from the 2003 trench profile between 0 and 6 meters and from the 2003 field methane profile between 14 and 22 meters. The section of the surface profile visible on Figure 2.7 is from about –10 to 26.5 meters. The 2003 trench profile was horizontally offset from the surface profile by 2 meters along the strike of the stratigraphy, as Figure 2.7 shows. The 2003 field methane profile was also offset from the surface profile by 2 meters and was in line with the 2003 trench profile. These offsets introduce some uncertainty in correlating the distance scales between the profiles, which we estimate to be up to 0.3 m.

The $\delta^{15}N$ and $\delta^{18}O_{atm}$ records have gaps from –0.4 to 1.8 and from 3.6 to 6.0 meters; samples from these sections of the profile have not yet been analyzed. The pooled standard deviations for 2003 surface profile $\delta^{15}N$ and $\delta^{18}O_{atm}$ measurements are 0.009 ‰ and 0.023 ‰ respectively. The field methane profile data are all single measurements. The different climatic intervals based on ice age are indicated at the top and are shown on the graph as different shades of gray.

References

Andersen, K.K., Azuma, N., Barnola, J.M., Bigler, M., Biscaye, P., Caillon, N., Chappellaz, J., Clausen, H.B., Dahl-Jensen, D., Fischer, H., Fluckiger, J., Fritzsche, D., Fujii, Y., Goto-Azuma, K., Gronvold, K., Gundestrup, N.S., Hansson, M., Huber, C., Hvidberg, C.S., Johnsen, S.J., Jonsell, U., Jouzel, J., Kipfstuhl, S., Landais, A., Leuenberger, M., Lorrain, R., Masson-Delmotte, V., Miller, H., Motoyama, H., Narita, H., Popp, T., Rasmussen, S.O., Raynaud, D., Rothlisberger, R., Ruth, U., Samyn, D., Schwander, J., Shoji, H., Siggard-Andersen, M.L., Steffensen, J.P., Stocker, T., Sveinbjornsdottir, A.E., Svensson, A., Takata, M., Tison, J.L., Thorsteinsson, T., Watanabe, O., Wilhelms, F., White, J.W.C., Project, N.G.I.C., 2004. High-resolution record of Northern Hemisphere climate extending into the last interglacial period. Nature 431, 147-151.

Bender, M., Malaize, B., Orchardo, J., Sowers, T., Jouzel, J., 1999. High precision correlations of Greenland and Antarctic ice core records over the last 100kyr. In: P.U. Clark, R. Webb and L. Keigwin (Editors), Mechanisms of global climate change at millennial timescales. American Geophysical Union, Washington, DC, pp. 149-164.

Bender, M., Sowers, T., Dickson, M.L., Orchardo, J., Grootes, P., Mayewski, P.A., Meese, D.A., 1994. Climate correlations between Greenland and Antarctica during the past 100,000 years. Nature 372, 663-666.

Blunier, T., Brook, E.J., 2001. Timing of millennial-scale climate change in Antarctica and Greenland during the last glacial period. Science 291, 109-112.

Brook, E.J., White, J.W.C., Schilla, A.S.M., Bender, M.L., Barnett, B., Severinghaus, J.P., Taylor, K.C., Alley, R.B., Steig, E.J., 2005. Timing of millennial-scale climate change at Siple Dome, West Antarctica, during the last glacial period. Quaternary Science Reviews 24, 1333 - 1343.

Brook, E.J., Harder, S., Severinghaus, J., Steig, E.J., Sucher, C.M., 2000. On the origin and timing of rapid changes in atmospheric methane during the last glacial period. Global Biogeochemical Cycles 14, 559-572.

Brook, E. J., Harder, S., Severinghaus, J., Bender, M., 1999. Atmospheric methane and millennial-scale climate change. In: P.U. Clark, R. Webb and L. Keigwin (Editors), Mechanisms of global climate change at millennial timescales. American Geophysical Union, Washington, DC, pp. 165-176.

Brook, E.J., Sowers, T., Orchardo, J., 1996. Rapid variations in atmospheric methane concentration during the past 110,000 years. Science 273, 1087-1091.

Chappellaz, J., Blunier, T., Raynaud, D., Barnola, J.M., Schwander, J., Stauffer, B., 1993. Synchronous changes in atmospheric CH4 and Greenland climate between 40-kyr and 8-kyr BP. Nature 366, 443-445.

Dahl-Jensen, D., 1985. Determination of the flow properties at Dye 3, South Greenland, by bore-hole-tilting measurements and perturbation modeling. Journal of Glaciology 31, 92-98.

Grootes, P.M., Stuiver, M., White, J.W.C., Johnsen, S., Jouzel, J., 1993. Comparison of oxygen-isotope records from the GISP2 and GRIP Greenland ice cores. Nature 366, 552-554.

Grootes, P.M., Stuiver, M., 1997. Oxygen 18/16 variability in Greenland snow and ice with 10^{-3} to 10^{5}-year time resolution. Journal of Geophysical Research-Oceans 102, 26455-26470.

Hudleston, P.J., 1976. Recumbent folding in base of Barnes-Ice-Cap, Baffin-Island, Northwest-Territories, Canada. Geological Society of America Bulletin 87, 1684-1692.

Jacobel, R.W., Gades, A.M., Gottschling, D.L., Hodge, S.M., Wright, D.L., 1993. Interpretation of radar-detected internal layer folding in West Antarctic ice streams. Journal of Glaciology 39, 528-537.

Jouzel, J., Alley, R.B., Cuffey, K.M., Dansgaard, W., Grootes, P., Hoffman, G., Johnsen, S.J., Koster, R.D., Peel, D., Shuman, C.A., Stievenard, M., Stuiver, M., White, J.W.C., 1997. Validity of the temperature reconstruction from water isotopes in ice cores. Journal of Geophysical Research - Oceans 102, 26471-26487.

Kennett, J.P., Cannariato, K.G., Hendy, I.L., Behl, R.J., 2000. Carbon isotopic evidence for methane hydrate instability during quaternary interstadials. Science 288, 128-133.

Kennett, J.P., Cannariato, K.G., Hendy, I.L., Behl, R.J., 2003. Methane hydrates in Quaternary climate change: The clathrate gun hypothesis. AGU, Washington, D.C., 216 pp.

Malaize, B., Paillard, D., Jouzel, J., Raynaud, D., 1999. The Dole effect over the last two glacial-interglacial cycles. Journal of Geophysical Research-Atmospheres 104, 14199-14208.

Meese, D.A., Alley, R.B., Fiacco, R.J., Germani, M.S., Gow, A.J., Grootes, P.M., Illing, M., Mayewski, P.A., Morrison, M.C., Ram, M., Taylor, K.C., Yang, Q.,

Zielinski, G.A., 1994. Preliminary depth-age scale of the GISP2 ice core. Special CRREL Report 94-1, US Army Cold Regions Research and Engineering Laboratory, Hanover, NH, 66pp.

Morgan, V., van Ommen, T.D., Elcheikh, A., Jun, L., 1998. Variations in shear deformation rate with depth at Dome Summit South, Law Dome, East Antarctica. Annals of Glaciology, Vol 27, 135-139.

Petit, J.R., Jouzel, J., Raynaud, D., Barkov, N.I., Barnola, J.M., Basile, I., Bender, M., Chappellaz, J., Davis, M., Delaygue, G., Delmotte, M., Kotlyakov, V.M., Legrand, M., Lipenkov, V.Y., Lorius, C., Pepin, L., Ritz, C., Saltzman, E., Stievenard, M., 1999. Climate and atmospheric history of the past 420,000 years from the Vostok ice core, Antarctica. Nature 399, 429-436.

Popp, T., Sowers, T., Dunbar, N., McIntosh, W., White, J.W.C., 2004. Radioisotopically dated climate record spanning the last interglacial in ice from Mount Moulton, West Antarctica, Poster presented at the AGU Fall Meeting, December 2004. AGU, San Francisco.

Reeh, N., Oerter, H., Letreguilly, A., Miller, H., Hubberten, H.W., 1991. A new, detailed ice-age O-18 record from the ice-sheet margin in Central West Greenland. Global and Planetary Change 90, 373-383.

Reeh, N., Oerter, H., Miller, H., 1993. Correlation of Greenland ice-core and ice-margin $\delta(^{18}O)$ records. In: W.R. Peltier (Editor), Ice in the Climate System. NATO ASI Series I: Global Environmental Change 12. Springer-Verlag, Berlin, pp. 481 - 497.

Reeh, N., Oerter, H., Thomsen, H.H., 2002. Comparison between Greenland ice-margin and ice-core oxygen-18 records. Annals of Glaciology, Vol 35, 136-144.

Reeh, N., Thomsen, H.H., 1994. Introduction to the Paakitsoq 1994 field programme, West Greenland. In: H.H. Thomsen and N. Reeh (Editors), Field report on palaeo-environmental studies at the Greenland ice sheet margin, Paakitsoq, West Greenland, 1994. Geological Survey of Greenland, Copenhagen.

Scambos, T., Bohlander, J., Raup, B., Haran, T., 2004. Glaciological characteristics of Institute Ice Stream using remote sensing. Antarctic Science 16, 205-213.

Schwander, J., Sowers, T., Barnola, J.-M., Blunier, T., Fuchs, A., Malaize, B., 1997. Age scale of the air in the summit ice: implication for glacial-interglacial temperature change. Journal of Geophysical Research - Atmospheres 102, 19483-19493.

Severinghaus, J.P., Grachev, A., Luz, B., Caillon, N., 2003. A method for precise measurement of argon 40/36 and krypton/argon ratios in trapped air in polar ice with applications to past firn thickness and abrupt climate change in Greenland and at Siple Dome, Antarctica. Geochimica et Cosmochimica Acta 67, 325-343.

Severinghaus, J.P., Grachev, A., Battle, M., 2001. Thermal fractionation of air in polar firn by seasonal temperature gradients. Geochemistry Geophysics Geosystems 2, 2000GC000146.

Severinghaus, J.P., Brook, E.J., 1999. Abrupt climate change at the end of the last glacial period inferred from trapped air in polar ice. Science 286, 930-934.

Severinghaus, J.P., Sowers, T., Brook, E.J., Alley, R.B., Bender, M.L., 1998. Timing of abrupt climate change at the end of the Younger Dryas interval from thermally fractionated gases in polar ice. Nature 391, 141-146.

Sowers, T., Bender, M., 1995. Climate records covering the last deglaciation. Science 269, 210-214.

Sowers, T., Bender, M., Raynaud, D., 1989. Elemental and isotopic composition of occluded O-2 and N-2 in polar ice. Journal of Geophysical Research-Atmospheres 94, 5137-5150.

Sowers, T., Bender, M., Raynaud, D., Korotkevich, Y.S., 1992. Delta N-15 of N_2 in air trapped in polar ice - a tracer of gas-transport in the firn and a possible constraint on ice age-gas age-differences. Journal of Geophysical Research-Atmospheres 97, 15683-15697.

Stuiver, M., Grootes, P.M., Braziunas, T.F., 1995. The GISP2 delta O-18 climate record of the past 16,500 years and the role of the sun, ocean, and volcanoes. Quaternary Research 44, 341-354.

Thorsteinsson, T., Waddington, E.D., Taylor, K.C., Alley, R.B., Blankenship, D.D., 1999. Strain-rate enhancement at Dye 3, Greenland. Journal of Glaciology 45, 338-345.

Waddington, E.D., Bolzan, J.F., Alley, R.B., 2001. Potential for stratigraphic folding near ice-sheet centers. Journal of Glaciology 47, 639-648.

Whillans, I.M., Johnsen, S.J., 1983. Longitudinal variations in glacial flow - theory and test using data from the Byrd-Station strain network, Antarctica. Journal of Glaciology 29, 78-97.

Chapter 3
A novel method for obtaining very large ancient air samples for analyses of methane radiocarbon

Abstract

We present techniques for obtaining large (~ 100 L STP) samples of ancient air for analysis of ^{14}C of methane ($^{14}CH_4$) and other trace constituents. Paleoatmospheric $^{14}CH_4$ measurements should allow to constrain the fossil fraction of past CH_4 budgets, as well as provide a definitive test of CH_4 clathrate involvement in large and rapid CH_4 concentration ($[CH_4]$) increases which accompanied rapid warming events during the last deglaciation. Air dating to the Younger Dryas-Preboreal and Oldest Dryas-Bølling abrupt climatic transitions was obtained by melt-extraction from old glacial ice outcropping at an ablation margin in West Greenland. The outcropping ice and occluded air were dated using a combination of $\delta^{15}N$ of N_2, $\delta^{18}O$ of O_2, $\delta^{18}O_{ice}$ and $[CH_4]$ measurements. The $[CH_4]$ blank of the melt-extractions was < 4 parts per billion. Measurements of $\delta^{18}O$ and $\delta^{15}N$ indicated no significant gas isotopic fractionation from handling. Ar/N_2, CFC-11 and CFC-12 in the samples indicated no significant $^{14}CH_4$ contamination from ambient air. Ar/N_2, Kr/Ar and Xe/Ar ratios in the samples were used to quantify effects of gas dissolution during the melt-extractions and correct the sample $[CH_4]$. Corrected $[CH_4]$ is elevated by up to 128 ppb over expected values for some samples, suggesting some in-situ CH_4 production in ice at this site.

3.1 Introduction

Glacial ice is the only known source of well-preserved ancient air. Analyses of air extracted from ice cores have demonstrated the coupling between global climate and greenhouse gases, and provided paleoenvironmental information ranging from changes in the global biospheric productivity to rapid temperature fluctuations over ice sheets (Bender, 2003; Petit et al., 1999; Severinghaus et al., 1998). One of the limitations of paleoatmospheric studies using ice cores is the relatively small amount of air available for analyses per sample (typically ≤1 kg of ice, yielding ≤ 100 cm^3 of air). For components present in very small (e.g., parts-per-trillion (ppt) or smaller) concentrations, this either severely limits the quality of possible analyses or makes the measurements entirely unfeasible. One of the measurements that has thus far been impossible due to insufficient ancient ice and air availability is carbon-14 of methane ($^{14}CH_4$).

Ice core records from Greenland and Antarctica show large and rapid variations in atmospheric [CH_4] in response to climate change (Brook et al., 2000; Chappellaz et al., 1993). Measurements of ambient atmospheric $^{14}CH_4$ in the past two decades have helped to constrain the fossil CH_4 contribution to the global budget, as well as reveal the $^{14}CH_4$ rise due to production from pressurized-water reactors (Conny and Currie, 1996; Lassey et al., 2007). ^{14}C can be a similarly powerful tool for understanding paleo CH_4 budgets and changes in the CH_4 sources during rapid climatic transitions at the end of the last glacial period. Recent studies of δD and $\delta^{13}C$ of CH_4 place constraints on CH_4 budgets during the last glacial termination (Schaefer

et al., 2006; Sowers, 2006). However, the uncertainties and similarities in the δD and $\delta^{13}C$ signatures of many CH_4 sources preclude definitive methane budget reconstructions. The great advantage of $^{14}CH_4$ is in being able to definitively separate the biogenic (wetlands, plants, animals) sources from geologic and clathrate sources. Biogenic $^{14}CH_4$ mostly follows atmospheric $^{14}CO_2$ (Quay et al., 1999; Wahlen et al., 1989), while most geologic and clathrate sources are very old and either contain no measurable ^{14}C or very low ^{14}C levels (Grabowski et al., 2004; Kessler et al., 2006; Winckler et al., 2002).

It has been suggested that several large and rapid atmospheric CH_4 increases during the last 100 kyr were the result of massive destabilization of marine CH_4 clathrates, which then in turn contributed to climatic warming (Kennett et al., 2000, 2003). Two such events occurred during the last glacial termination, during the Oldest Dryas (OD) – Bølling (~14,700 yr BP, where present = 1950 AD) and Younger Dryas (YD) – Preboreal (PB) (~11,600 yr BP) climatic transitions. Quantifying clathrate contributions to the CH_4 increases during abrupt warming events at the end of the last glacial period is particularly relevant in the light of current anthropogenic warming. By recent estimates, the present amount of CH_4 carbon associated with clathrates is 500 – 5000 Petagrams (Buffett and Archer, 2004; Milkov, 2004); which at the upper end is comparable to the estimated carbon content of all fossil fuels. Future warming of the ocean has the potential to destabilize large amounts of CH_4 clathrate, providing a positive feedback to the warming.

For ice containing pre-Holocene air with [CH_4] of ~500 parts per billion (ppb), at least 1000 kg of ice are required to provide ~25 micrograms of CH_4 carbon (μg C), which is near the lower limit required for an accelerator mass spectrometry (AMS) measurement of ^{14}C. Here we describe the techniques developed to extract and assess the quality of very large (~100 L STP each) samples of ancient air from glacial ice that are required for $^{14}CH_4$ analyses.

Several experimental challenges must be overcome to obtain air samples that are suitable for paleo $^{14}CH_4$ analyses. First, sufficient ice of the correct and well-constrained age with a well-preserved CH_4 record has to be obtained. Second, apparatus has to be developed capable of extracting ~ 100 L of air from >1000 kg of ice in a reasonable amount of time and without altering the CH_4. Finally, possible $^{14}CH_4$ contamination from ambient air as well as the effects of gas isotopic fractionation and air dissolution during the melt-extraction must be quantified.

3.2 The Pakitsoq ice outcrop

Previous work has demonstrated that large quantities of ice dating to the last glacial termination are exposed at the surface at an ice-margin ablation site called Pakitsoq in West Greenland (Petrenko et al., 2006; Reeh et al., 1991). An ice sheet flow-line model indicates that this ice originates near Greenland Summit, about 190 km south and 40 km west of the GISP2 site (Reeh, 1988; Reeh et al., 2002). The ice stratigraphy is rotated nearly 90˚ about an axis parallel to the ice margin, exposing a range of ages at the outcrop. In an idealized flow situation the oldest ice would be

found nearest to the ice margin in the ablation zone, with ice becoming younger with increasing distance from the ice margin, thus exposing a "horizontal ice core" on the ice surface. This is the general age pattern observed for Pakitsoq ablation ice. However, the situation is complicated locally by large-scale folding of the ice layers, which has been attributed mostly to ice flow interaction with bedrock topography (Petrenko et al., 2006). The ages for ice sections dating to the last glacial termination are established by correlating Pakitsoq surface ice records of $\delta^{15}N$ of N_2, $\delta^{18}O$ of O_2, $\delta^{18}O_{ice}$ and $[CH_4]$ with records from GISP2 (Petrenko et al., 2006). Very accurate dating is possible for ice dating from the YD-PB and OD-Bølling climatic transitions because of unique combinations of values for the four geochemical tracers observed in the GISP2 ice core for these periods, as well as the rapid changes in $\delta^{15}N$, $[CH_4]$ and $\delta^{18}O_{ice}$ during these transitions.

Five field seasons of ice sampling at Pakitsoq demonstrated that 1) despite 2-3m of annual ablation at the site, the ice surface stratigraphy remains mostly constant from year to year and 2) the $\delta^{15}N$, $\delta^{18}O_{ice}$, $\delta^{18}O_{atm}$ and $[CH_4]$ records in Pakitsoq ice and occluded air are mostly intact and suitable for paleoclimatic studies, although elevated $[CH_4]$ was observed in some ice sections (Petrenko et al., 2006). Pakitsoq ice contains thin planar bands with a high dust content (dust bands) as well as bands of bubble-free ice (blue bands). It was found that samples that contained dust bands as well as large ($>\sim$2 mm width) blue bands yielded elevated $[CH_4]$ with respect to contemporaneous GISP2 ice. Small, non-continuous blue bands ("cryptic blue bands") do not appear to result in elevated $[CH_4]$ when included in the samples (Petrenko et al., 2006).

3.3 Field procedures

3.3.1 Sample cutting and cleaning

Samples from the YD-PB transition were obtained in the summer of 2004, and samples from the OD-Bølling transition in the summer of 2005. The large ice samples were cut from near-surface Pakitsoq ice with oil-free electric chainsaws (Figure 3.1a). Saw bars and chains were pre-cleaned ultrasonically in acetone. Figure 3.1b shows the orientation of the ice cut for the large air samples with respect to the ice surface and stratigraphy, using the samples spanning the YD-PB climatic transition as an example. At the start of a sampling season, the approximate location of the YD-PB [CH_4] transition was identified by referencing to a marker pole placed in the ice at the end of the previous season. Several short near-surface ice sample profiles, oriented perpendicular to the stratigraphy, were collected at 5-20 cm resolution at the margins of and within the projected sampling area. The extracted air was analyzed immediately for [CH_4] by gas chromatography (GC) as described in (Petrenko et al., 2006) to re-determine the exact location and span of the [CH_4] transition, as well as [CH_4] in the ice to either side of the transition.

The ice stratigraphy at the Pakitsoq site dips East (away from the ice margin) at 50-70˚ to the horizontal. Guided by [CH_4] results from the field measurements, the sampling followed the spatial orientation of the stratigraphic layers with the aid of marker poles and geologic compasses for checking the dip of the ice layers cut. Most major blue bands and dust bands at Pakitsoq parallel the stratigraphy; these were also used to guide the sampling. As shown on Figure 3.1b, the overall shape of the ice

region cut for a sample was that of a parallelepiped with its long horizontal edges following the strike, and the inclined edges following the dip of the stratigraphy. At least the top 30 cm of ice was removed and discarded to reduce the risk of contamination from the modern atmosphere. Further sample profiles for field [CH_4] analyses were taken as the sampling progressed downward, to re-confirm the location of the YD-PB [CH_4] transition. The ice blocks were handled with vinyl gloves and placed on electropolished stainless steel-topped tables for cleaning. All dust bands as well as any blue bands > ~2mm in width were removed. 4-15 mm of ice was removed from all surfaces of each block with clean electropolished stainless steel chisels. Additional sample profiles and samples from corners of the ice areas cut were taken for laboratory analyses of $\delta^{15}N$ of N_2, $\delta^{18}O$ of O_2, $\delta^{18}O_{ice}$ and [CH_4].

3.3.2 Air extraction

The air was extracted at the field site immediately after the ice was cut. Ice was loaded into the 670 L melting tank (melter) constructed from chemically polished and surface anodized 6061 aluminum alloy (Figure 3.2). Some of the ice blocks were broken up once inside the melter to allow for tighter packing. The melter sealed with a lid on a double Viton® o-ring flange. Once sealed, the melter was evacuated first to ~130 hPa using two diaphragm pumps, and then to 8 hPa with a rotary vane pump. Pressure inside the melter was monitored with a piezo pressure transducer. Ultra high purity (u.h.p.) nitrogen (N_2; CH_4 - free) or argon (Ar; ~ 40 ppb of CH_4) was added to the melter to ~330 hPa, and the evacuation was repeated as above. The u.h.p. N_2 or Ar flush was done 3 times; at the end of the third flush the melter was evacuated for 30

min after the pressure reached 8 hPa, which allowed for further flushing out of ambient air with water vapor.

The melter was then isolated from the pumps and the propane burner underneath the melter was lit. A thin cylindrical steel shroud was placed around the burner and the lower part of the melter to facilitate efficient heat exchange. The flame was kept low at first to prevent overheating of the melter bottom. After 15-30 min enough ice melted to fill the bottom section of the melter with water, and the burner was turned on full strength (~290 kilowatts). The temperature of the melter walls was constantly monitored with a surface temperature probe. Because aluminum is an excellent conductor of heat, the melter walls (3.2 mm thick) remained at about the temperature of the water inside, which is close to 0˚C for most of the duration of the melting. A few small areas on the melter walls above the water occasionally reached ~50˚C, but were immediately cooled by spraying cold water from the outside. Melting progress was monitored through a glass window in the melter lid, and the burners were turned off when there were still a few ice blocks floating on top of the water. The melting process typically took 2 – 2.5 hr, with the final water temperature reaching 10-15 ˚C. Pressure inside the melter headspace and temperature of the walls was recorded.

Air transfer to 35 L electropolished stainless steel cylinders was done by two diaphragm pumps in series without drying the air. Immediately prior to the transfer, the line was flushed with u.h.p. N_2 or Ar for ~30 sec. With pumps running, leak checks were performed on the transfer line and the diaphragm pumps prior to each

transfer using a capacitance manometer. These leak checks indicated that air from leaks during transfer amounted to a maximum of 0.03% of total sample air. The transfer times were ~45 min per extraction for the YD, PB and YD-PB Transition samples, and ~30 min for the OD and Bølling samples. Pressure in the target cylinder was monitored with either a piezo pressure transducer or a mechanical high-pressure gauge. At the end of the transfer the pressures and temperatures of the melter and air cylinder were recorded.

The melter was closed and left overnight, with a further pressure and temperature reading taken in the morning, which served as a leak check of the melter itself. These leak checks indicated that ambient air possibly leaking into the melter amounted to < 0.15% of the total sample air for all extractions except one of the extractions for PB Sample 2, where this leak check indicated ~0.3% possible ambient air. However, the slight pressure increase sometimes observed in the melter overnight was always smaller than that expected from outgassing of dissolved air from the meltwater (see section 3.5.3). The water level was recorded and the melt water drained or filtered for particulates. 30-35 L STP of air was obtained from each melt extraction, and air from 2 or 3 melt-extractions was combined to form each sample listed in Table 3.2 (except for the LGM sample, which is from a single melt-extraction). For the YD, PB and YD-PB Transition samples, air from subsequent melt-extractions was added directly to air from previous extraction(s). For the OD and Bølling samples, air from each melt extraction was initially pumped into individual

cylinders, and then 2-3 extractions were later combined in a single cylinder using two diaphragm pumps in series.

3.3.3 Blank extractions

In order to assess the $^{14}CH_4$ contamination from the air extraction procedure, simulated extractions with a synthetic fossil CH_4-u.h.p. air mixture were conducted over the course of the sampling season as follows. For each sample of distinct age, blank extractions were conducted after the first melt-extraction and the last melt-extraction of that type of sample, to confirm that the extraction blank did not change over the sampling season. For example, the YD samples have an accompanying YD blank. Immediately after the melt-extraction was complete, the meltwater was heated to ~ 40-50˚C and boiled under vacuum (while pumping on the melter headspace) to de-gas for 1 hr. The melter was then closed and left to cool overnight.

Headspace pressure and melter temperature were recorded the following morning and served as a leak-check. The headspace was evacuated for 30 min with a diaphragm vacuum pump to remove any CH_4 that may have been produced as well as any remaining dissolved gases that may have equilibrated with the headspace overnight. A standard gas containing ~500 ppb of CH_4 in u.h.p. air was then introduced into the headspace. The gas stayed in the melter for the same duration as a typical melting time, and was then transferred into the same type of stainless steel cylinder as the sample air using exactly the same transfer procedure. Although the simulated extractions were done in batches of 2 or 3 (over meltwater from the same ice extraction), one simulated extraction was done for each melt extraction. The

amount of standard gas used in each simulated extraction was such that the amount of CH_4 was roughly equal to that in a real extraction. The amount of standard gas used and the duration of simulated extractions were adjusted so that the cumulative amount of CH_4 in all the sample extractions of a particular age (e.g., YD) as well as the cumulative sample time in the melter were equal to the cumulative amount of CH_4 and time spent in melter for the respective blank sample. For the OD and Bølling samples, where the sample air experienced an additional transfer between cylinders, this was also mimicked for the blanks.

3.4 Reducing the extraction [CH_4] blank and CH_4 production from aluminum

In previous work involving [CH_4] analyses of ice core air by melt-extraction either cleaned stainless steel or glass vessels were used, which both give acceptable [CH_4] blanks (Brook et al., 1996; Fluckiger et al., 2002). We chose to use an aluminum vessel for our large extractions to minimize vessel weight for easier field handling, as well as for the superior heat conductivity of aluminum, which is essential for fast ice melting times. However, an uncertainty remained about the [CH_4] extraction blank with an aluminum vessel. This blank indeed turned out to be a serious obstacle and several aluminum surface treatments were tested before the blank was successfully reduced. Table 3.1 summarizes the [CH_4] blank test results with the large vessel (melter) as well as with small-scale models (minimelters).

Initial tests were carried out in the field. Two melt-extractions were performed on ice containing gases of Preboreal age (first line in Table 3.1), which is known to have [CH_4] of ~700-750 ppb (Brook et al., 2000). The average resulting [CH_4] from

these two extractions was 2242 ppb. Further tests (not shown) determined that the observed high [CH_4] could not be explained be either elevated [CH_4] in the sampled ice or by CH_4 contamination from leaks, transfer lines or pumps, pointing to the melter itself as the contamination source. Additional field tests with a mostly dry melter demonstrated that much more CH_4 was produced if the melter was heated slightly; however the highest CH_4 production rates were clearly obtained in the presence of a large amount of water.

To investigate this problem further, five small-scale models of the melter (minimelters) were constructed. The minimelters were 6061 aluminum, sealed with Viton® o-rings and had an internal volume of ~1.5 L. Minimelter tests were conducted in the laboratory, which allowed for better-controlled experiments. The first two minimelter tests listed (Table 3.1) confirm the much higher CH_4 production rate in the presence of water. Such high rates of CH_4 production inside the aluminum vessels were puzzling and do not appear to have been described in the literature. One hypothesis is that some CH_4 is trapped near the aluminum surface during manufacturing and is slowly de-sorbed with time. This idea seems consistent with the observed higher CH_4 production rates when heat is applied. However, this doesn't seem to explain why much more CH_4 is produced in the presence of water and another mechanism is needed. Enhanced CH_4 production from untreated aluminum in the presence of water appears to be ubiquitous – we also observed this effect when pumping water-saturated air into a high-pressure aluminum cylinder (data not shown) that was known to not produce any detectable CH_4 when dry. Large amounts of oils

are used in the rolling of aluminum and it is possible that CH_4 is produced by cracking of the oil hydrocarbon chains. Water may be providing the extra hydrogen atoms required for this reaction. Commercial processes exist which utilize Ni-Al_2O_3 for catalytic hydrocarbon cracking in the presence of steam as well as for CH_4 synthesis from CO and H_2, however at much higher temperatures than in our tests (Catalysts and Chemicals, Inc., 1970; Esso Research and Engineering Co., 1969). It is possible that the 6061 alloy contains traces of Ni or other metals that result in a slow catalytic CH_4 production by one of these mechanisms, or that untreated aluminum itself acts as the catalyst.

Several commercially available and other aluminum surface treatments were investigated with the minimelters to eliminate the CH_4 production problem (Table 3.1). High CH_4 production rates remained after the initial cleaning with acetone and ethanol. Vacuum baking eliminated CH_4 production under dry conditions, but not under wet conditions. Neither soaking a minimelter in a hot acidic soap bath to clean the surface, nor applying a caustic etch (hot 50% NaOH bath for 1 min) followed by anodization decreased the wet CH_4 production rate. Coating the aluminum surface with a low-outgassing epoxy appeared to be very effective in reducing the wet CH_4 production, although later tests (not shown) suggested that CH_4 production was resuming slowly after a few weeks. The most effective CH_4 blank elimination was achieved by chemically polishing the aluminum for ~2.5 min. The chemical polishing process typically involves a ~90˚C bath containing ~80% phosphoric acid plus nitric and sulfuric acids. The untreated aluminum surface is very rough on a microscopic

level and chemical polishing results in a shiny appearance due to smoothing of the surface by removal of a few μm of the surface layer (Wernick et al., 1987). This both reduces the overall aluminum oxide surface area that may be involved in catalytic CH_4 production, as well as removes organic impurities (oil, CH_4) trapped in the surface layer from aluminum manufacturing, so it makes sense that this process was effective in reducing the CH_4 blank. Anodizing a chemically polished minimelter did not seem to make much difference in the already very low CH_4 production rate. Further passivating the surfaces of a chemically polished and anodized minimelter by boiling DI water in it for 8 hr did not appear to have an effect.

Interestingly, chemically polishing for 5 min resulted in about 3x the CH_4 production rate as compared to a 2.5 min process. This is probably tied to the fact that after the first few minutes of the chemical polish, surface roughness begins to increase again (Wernick et al., 1987). Electropolishing and anodizing, which are supposed to result in a similar finish to chemical polishing and anodizing, produced a dull surface (suggesting higher surface roughness) and a high CH_4 production rate compared to the chemically polished aluminum.

Based on the results of these tests, the treatment chosen for the large melter was a 2.5 min chemical polish followed by anodization. This drastically lowered CH_4 production in the presence of water (4^{th} line in Table 3.1). A further drop in the CH_4 production was observed the following year (see 2004 blanks in Table 3.2), suggesting that the melter surface was becoming further passivated with time.

3.5 Effects of melt-extractions and sample storage on air sample composition

3.5.1 [CH_4] blank of melt-extractions

The [CH_4] for all field blanks was < 4 ppb elevated over the [CH_4] of the standard gas (Table 3.2). The blank samples were saved for subsequent processing for ^{14}C to quantify any $^{14}CH_4$ blank from the melt-extractions. One potentially important shortcoming of the simulated blank extractions conducted in the field was that the ice-melting process (including the application of intense heat to the melter bottom) was not mimicked. To address this, a single simulated extraction was conducted at SIO with ~410 kg of gas-free ice obtained from a commercial ice-carving supplier. Small sub-samples of this ice were analyzed at OSU as described in Petrenko et al. (2006), and found to be free of CH_4. The gas-free ice was initially purchased in ~150 kg blocks, and was processed exactly as described above in the melt-extraction procedure. The chainsaw, bar, chain, ice scraping chisel and table were the same as used in the field. The major differences were that 1) about 2.5 times the usual amount of standard gas was used to provide sufficient pressure later for high-quality [CH_4] measurements and 2) the ambient temperature (+20˚C) was warmer than for a typical field extraction (+5˚C). Following the gas-free ice blank extraction, a further blank extraction was conducted over the meltwater using the usual blank procedure but again with ~2.5 times more than usual standard gas. These tests are listed together near the bottom of Table 3.2. As can be seen, the [CH_4] elevation over the standard gas value for both tests is <2 ppb. Because the blank results are similar

for both tests, we conclude that our field blank approach is adequate in determining the [CH_4] blank of ice melt-extractions for each sample.

Pakitsoq air samples and blanks were stored in electropolished steel cylinders for either 1 yr (OD – Bølling samples) or 2 yr (YD-PB samples) prior to processing for $^{14}CH_4$. Repeated measurements of [CH_4] in the samples over this time period (not shown) demonstrated that [CH_4] was unchanged in all sample cylinders over these time periods.

3.5.2 Remnant ambient air and isotopic fractionation during the melt-extraction

For three of the samples, u.h.p. Ar was used instead of the u.h.p. N_2 for flushing the ice-filled melter prior to starting the melting. This was done as a test of the amount of ambient air that the melter evacuation step may be leaving behind. As can be seen from Table 3.2, these three samples (YD 2, Transition 2 and Bølling 2) indeed show $\delta Ar/N_2$ that is higher by ~ 40‰ than in the corresponding replicate samples using N_2 as flushing gas, meaning that there is ~4% more argon due to the left-over flushing gas. Since Ar is only ~ 1% of air, this means that the residual flushing gas comprises only ~ 0.04% of the entire extracted air sample. The amount of residual ambient air in the melter should be much smaller than this because three Ar or N_2 flush and evacuation cycles were performed after the melter was sealed.

$\delta^{18}O$ of O_2 was measured in the large air samples and in Pakitsoq ice at SIO (Table 3.2). The procedure for air extraction from small ice samples as well as the mass spectrometry method for all samples was described in Petrenko et al. (2006).

For the large Pakitsoq air samples and blanks, 1-2 cm^3 STP aliquots were taken for the measurement by expanding the air sample into a small evacuated volume and allowing the air to equilibrate between this volume and the parent tank for at least 10 min. A second expansion and equilibration was performed for the blank tanks, which were at higher pressure, to reduce the aliquot amount. The air aliquot was then cryogenically transferred to a stainless steel dip tube in the same way as for air extracted from ice. The air aliquots from the CH_4 standard (a high-pressure cylinder) were collected by flowing the gas for 2 min through a regulator set to ~1.7 bar, then a ~4 m length of 6 mm OD Synflex® tubing, then through two small (~1.3 cm^3) sampling volumes, followed by another ~4 m length of Synflex® tubing. The sampling volumes were closed immediately after the gas flow was stopped and the air aliquots cryogenically transferred as for the rest of the samples.

The primary objective of $\delta^{15}N$ of N_2 and $\delta^{18}O$ of O_2 measurements on the large air samples was age determination. However, the isotopic measurements also serve to demonstrate that the melt-extraction procedure does not result in significant gas isotopic fractionation. The $\delta^{18}O$ of O_2 values shown for Pakitsoq ice in Table 3.2 are for Oldest Dryas – age ice and, as can be seen, they agree to within 0.1 ‰ with those in the large air samples. $\delta^{18}O$ of O_2 values measured in ice of other ages, as well $\delta^{15}N$ measurements (Figures 3.4 and 3.5) show similar or better agreement with values measured in the large air samples. Assuming that all isotopic fractionation during the melt-extraction is kinetic in nature, the effect on CH_4 isotopes should also be

negligible. This was confirmed by the good agreement of $\delta^{13}CH_4$ measured in the large air samples with $\delta^{13}CH_4$ measured in smaller ice samples (Schaefer et al., 2006).

3.5.3 Solubility loss of gases and corrections to [CH_4]

Some of the air from the gas bubbles in ice is lost to dissolution in the meltwater during the melt-extraction. At 0˚C, the solubility of CH_4 is close to that of Ar and O_2 and is about 2.5x that of N_2 (Table 3.3). Because of this, if a substantial fraction of air does dissolve in the meltwater, the [CH_4] in the headspace (and thus the extracted air sample) is effectively reduced. To determine the true [CH_4] in the sampled ice, a correction must be made for this effect. To better understand the solubility effects during the melt-extractions, we measured Kr/Ar and Xe/Ar ratios in the YD - PB large air samples, as well as in small samples of Pakitsoq ice using established methods described in Headly and Severinghaus (2007). Kr is about 2x more soluble than CH_4 and Ar, and Xe is about 4x more soluble (Table 3.3); thus these gases would show an enhanced solubility signature. $\delta Ar/N_2$ was also measured at SIO in all large air samples as well as in Pakitsoq ice. For $\delta Ar/N_2$ measurements, the procedure for air extraction from ice was described in Petrenko et al. (2006) and the decanting procedure for large air samples is the same as for $\delta^{18}O$ described above. The Ar/N_2 ratios were determined by measuring the 40/28 mass ratios using a Finnigan Delta XP dual dynamic inlet isotope ratio mass spectrometer. Corrections were made for sample/standard pressure imbalance and for O_2/N_2 ratio chemical slope as described by Severinghaus et al. (2003).

We expect the gases to be dissolving primarily by the following two mechanisms. 1) From the air bubbles as they rise through the water. During a melt extraction, the water level rises quickly to cover most of the ice blocks, and most of the melting and air release happens underwater. Because the air bubbles are released and rise near the surfaces of the ice blocks, the effective temperature of the water they exchange gases with is near 0˚C. 2) By dissolving directly into the water from the melter headspace. The surface water is constantly in contact with floating ice; thus we expect its temperature to be near 0˚C also. Thus, 0˚C is the most likely temperature of the water with which the gases equilibrate.

Knowing the typical water and headspace volumes for a melter extraction (484 L and 186 L, respectively) and the typical headspace temperature (284 K), it can be shown that the fraction of a particular gas that dissolves in the water at full equilibrium is:

$$F_W = \frac{K_H V_W}{K_H V_W + \frac{V_{AIR}}{1\ \text{atm}} \frac{273.15\ \text{K}}{T_{AIR}} \frac{1}{22.4\ \text{L mol}^{-1}}} \tag{3.1}$$

where F_w is the mole fraction of the total amount of a given gas which is dissolved, K_H is Henry's Law constant for the gas at dissolution temperature, V_W is the water volume in liters, V_{AIR} the headspace volume in liters, and T_{AIR} is the temperature of the gas in the headspace. The molar fractions of each gas dissolved can also be calculated for incomplete solubility equilibrium situations, e.g. if only 50% of the gas that could be

dissolved is actually dissolved. Knowing the starting $\delta Ar/N_2$, $\delta Kr/Ar$, and $\delta Xe/Ar$ in Pakitsoq ice (Table 3.2), the $\delta Ar/N_2$, $\delta Kr/Ar$, and $\delta Xe/Ar$ values expected in the samples extracted from the headspace for various fractions of full solubility equilibrium reached can then be determined (Figure 3.3a). We can then estimate the fraction of full solubility equilibrium achieved for the samples by plotting $\delta Kr/Ar$ and $\delta Xe/Ar$ vs $\delta Ar/N_2$ along with our model predictions (Figure 3.3b).

As can be seen, four of the samples fit the models well, while two samples (YD 2 and YD-PB Transition 2) are shifted strongly in $\delta Ar/N_2$. These are the two samples for which the melter flush was done with Ar, and, as discussed above, they have elevated Ar levels. This effect can be corrected for by assuming that the true Ar/N_2 ratio of these samples is as in their N_2-flushed duplicates (YD 1 and YD-PB Transition 1). When this is done, and the $\delta Kr/Ar$ and $\delta Xe/Ar$ values are corrected accordingly to account for lower true Ar levels, the plot becomes as on Figure 3.3c. As can be seen, there is excellent agreement between the data and the melter solubility model. Such agreement can only be achieved if all four gases (N_2, Ar, Kr and Xe) within any given sample are reaching the same fraction of full solubility equilibrium, despite their different solubilities and diffusivities in water. Although literature estimates for the gases of interest vary somewhat, the diffusivities in water of Ar, Kr and Xe in the range 0 – 10˚C are always slightly lower, while the diffusivity in water of N_2 is slightly higher than that of CH_4 at equivalent temperature; with the full range of measured diffusivities in water for all gases being $0.63 – 1.50 \times 10^{-5} cm^2 s^{-1}$ (Boerboom and Kleyn, 1969; Ferrell and Himmelblau, 1967; Jahne et al., 1987;

Maharajh and Walkley, 1973; Smith et al., 1955). The spread of samples along the model lines is most likely due to variability between samples of the fraction of full solubility equilibrium attained.

Because N_2, Ar, Kr and Xe all appear to achieve the same fraction of full solubility equilibrium within any given sample, we conclude that CH_4 in that sample will also achieve the same fraction of full solubility equilibrium. Based on δXe/Ar (Xe being the most soluble and therefore the best estimator), we estimate the full range of solubility equilibrium fractions observed in our samples to be 0.42 – 0.78 when sample δXe/Ar measurement errors are taken into account. Calculating the fractions of N_2, O_2, Ar and CH_4 dissolved for this range of equilibrium fractions, we can determine the minimum (1.02) and maximum (1.06) correction multipliers that need to be applied to the measured [CH_4]. These corrections, along with the blank corrections, are incorporated into the range of corrected [CH_4] values given in Table 3.2. Although Kr and Xe were not measured for the OD-Bølling samples, because the extraction procedure remained effectively the same during the 2004 and 2005 field seasons, we can expect the range of necessary solubility corrections to be the same. We have therefore applied the same solubility corrections to all samples.

Kr and Xe were not measured in the extraction blanks. However, δAr/N_2 in the samples shows a large Ar depletion as compared to Pakitsoq ice, so it can also serve as an indicator of dissolution of a substantial fraction of the gases. Interestingly, no significant δAr/N_2 depletion as compared to the CH_4 standard gas is observed in the YD - PB extraction blanks, and a slight enrichment is observed in the OD - Bølling

extraction blanks. This suggests that, unlike for the ice melt-extractions, there is no substantial exchange of gases between the headspace and the water for the extraction blanks. Therefore there is no need to correct the extraction blank [CH_4] for solubility effects.

The greatly enhanced gas exchange in the actual melt-extractions as compared to the blanks is most likely due to gas dissolution directly from the rising gas bubbles during melting. This is clear from a comparison of $\delta Ar/N_2$ in the actual samples with that for the gas-free ice blank (Table 3.2). The gas-free ice blank involved the same vigorous heating and water convection as for the actual samples, yet its $\delta Ar/N_2$ indicates 0.06 - 0.07 for the fraction on full solubility equilibrium reached, as compared to 0.42 – 0.78 determined for the actual samples.

After the solubility and blank corrections are applied, it can be seen from Table 3.2 that [CH_4] in some of the samples is higher than expected based on [CH_4] values (on the same measurement scale) in GISP2 ice of contemporaneous age. The expected [CH_4] values were determined as follows. First, the full gas age range of each sample was determined as described in section 3.6. Then, the average [CH_4] for all available GISP2 [CH_4] data points (Brook et al., 2000) within this gas age range was determined. Expected [CH_4] from GISP2 was also determined for the case where the youngest 25% of the age range on the young side (between mean age and minimum possible included age) was excluded. This exercise was then repeated for the old side of the age range (excluding the oldest 25% of the range on that side); as well as for the case where the end 25% from both the old and young sides were excluded.

The agreement between all of the above values was used to estimate the uncertainty of the expected [CH_4]. Expected [CH_4] for the LGM sample was not calculated as the dating for this sample is highly uncertain. The large uncertainties in the predicted [CH_4] of the YD-PB Transition samples are due to the fact that the [CH_4] is changing rapidly during this age interval; thus even small uncertainties in sample age span result in large predicted [CH_4] uncertainties.

In calculating the expected [CH_4], GISP2 [CH_4] values have been adjusted by +2 ± 1%, to correct for the melt-extraction solubility effect in the GISP2 data. Tests with 16 ice core samples recently performed in the laboratory of Ed Brook at Oregon State University (OSU) indicated that melt-extraction of ice core air results in an artificial lowering of true [CH_4] by 1.7 ± 0.5% (Ed Brook, personal communication, 2008). The melt-extraction vessels used in these tests, however, were different from the vessels used to generate the Brook et al. (2000) GISP2 [CH_4] data. To confirm that the melt-extraction solubility effect was similar for the GISP2 data set, comparisons must be made for pairs of samples from equivalent depths in GISP2, where one sample in each pair is measured using the new vessels, and one using the old vessels. Currently, 6 such pairs are available for GISP2 Early Holocene ice, with gas age difference of ≤10 years within each pair, which should result in essentially identical [CH_4] within the pairs. The mean [CH_4] difference for these 6 pairs is only 1.2 ppb, suggesting that the melt-extraction solubility effect is similar for old and new vessels, and that a correction of ~ +2% is needed for the GISP2 [CH_4] data set.

Further tests are in progress to increase the number of pair comparisons to 20 and confirm this 2% correction.

Some sections of ice with elevated [CH_4] have been previously observed at Pakitsoq (Petrenko et al., 2006). [CH_4] analyses on small ice samples taken from the same ice sections as the large samples also yield some values that are substantially elevated with respect to GISP2 [CH_4] (Figures 3.4 and 3.5). Further, two of the large air samples (Contaminated OD and Contaminated PB) have [CH_4] that is substantially elevated over replicate sample values. [CH_4] in the Contaminated PB sample is higher than the ambient atmospheric value, strongly indicating in-situ CH_4 production in the ice. In-situ CH_4 production has previously been observed and attributed to microbial sources in the ice (Campen et al., 2003; Price, 2007). It is thus possible that the apparent slight [CH_4] elevation over GISP2 in some samples is due to a small amount of microbial CH_4 production in Pakitsoq ice; however, this is not well understood.

3.5.4 CFC-based constraints on contamination from modern atmospheric CH_4

$^{14}CH_4$ of modern ambient air is ~130 percent modern carbon (pMC) (Quay and others, 1999), while the $^{14}CH_4$ for all Pakitsoq samples is expected to be < 30 pMC. It is therefore important to quantify the amount of modern ambient CH_4 that may somehow be included in our samples. The large size of the air samples enabled us to perform CFC-11 and –12 measurements for this purpose (Table 3.2). CFC-11 and -12 have been shown to only have recent anthropogenic sources (Butler et al., 1999). Neither the extraction blanks nor the methane standard gas contain measurable amounts of CFC-11 and –12. Any CFCs observed in the samples must therefore arise

either from contamination by modern air in the ice or from a handling-related process that is not mimicked by the blanks.

The maximum observed CFC-12 value in our samples is 2.8 ppt, or 0.5% of modern ambient air. The CFC-11/CFC-12 concentration ratio in ambient air is about 0.5, while in our samples this ratio is 1.53 ± 0.24. Because the CFC levels are so low in these samples, the measured values are comparable to the estimated uncertainties (Table 3.2 and caption). However, the fact that the above CFC-11/CFC-12 ratio is calculated on the basis of 12 different samples lends confidence to this value. The observed CFC-11/CFC-12 ratio is very different from the ambient ratio, demonstrating that direct leaks of ambient air are not the dominant source of the CFCs, and that ambient air leaks are therefore not a significant source of CH_4 contamination.

The observed CFC-11/CFC-12 ratio of 1.53 ± 0.24 is close to the value we calculate for CFC-11 and -12 dissolved in ~0˚C water at equilibrium with air containing modern CFC-11 and –12 concentrations (1.92) (Warner and Weiss, 1985). One possibility is that the CFCs are originating from the blue bands in Pakitsoq ice. The origin of blue bands is currently unknown, but it is possible that they are created when basal water is injected into cracks in the ice. This water may originate from moulins, and thus carry a recent atmospheric gas signature, which includes some modern CH_4. The effect of dissolved CFCs from blue bands equilibrating between the meltwater and headspace during a melt-extraction can be modeled, and our calculations (not shown) yield CFC concentrations of similar range to those observed, but the predicted CFC-11/12 ratios are ≤ 1, which argues against blue bands being a

major contributor of CFCs/modern air to the samples. Another line of evidence against the blue band source of CFCs comes from air samples extracted at Pakitsoq in 2003 (see Schaefer et al. (2006) for more on 2003 samples), for which even the smallest blue bands were removed. These show CFC-11 and –12 concentrations in the same range as the 2004-5 samples, and a CFC-11/12 ratio of 1.22 ± 0.25, which agrees with that for the 2004-5 samples within errors.

Another possible CFC source is dissolution of modern air in the liquid layer on the surface of all ice pieces that were loaded into the melter, as well as in the small amount of meltwater pooling at the melter bottom (the temperatures at Pakitsoq were always above freezing during our field campaigns). In this case the effective water volume for gas equilibration during a melt-extraction may be smaller than the overall meltwater volume, because CFCs are present in a thin liquid layer on the ice block surfaces and will equilibrate with the headspace before most of the ice is melted. The sample CFC-11/12 ratios predicted by this scenario match the observed ratios, and we therefore consider this to be the most likely source of CFCs in the samples. Of course some modern CH_4 would in this case be dissolved on the ice block surfaces as well. Based on CH_4 solubility in 0˚C water (2.56×10^{-3} M/atm, Table 3.3), we calculate that with this scenario, the added modern CH_4 would account for a maximum of ~0.4% of the total CH_4, resulting in a maximum ^{14}C shift of ~ 0.4 pMC in the samples. It is likely that even though a measurable amount of CFCs was trapped in the melter, most of the ambient CH_4 was removed during the flushing/ evacuation steps because CFCs are known to adhere to a variety of surfaces and dissolution on ice block surfaces may

not be the only process responsible for their presence. Because of this, as well as because the calculated ^{14}C correction is uncertain and small, we do not plan to include this correction in our ^{14}C calculations.

3.6 Ages of the large air samples

The ages of the large air samples were established by correlating records of $\delta^{15}N$ of N_2, $\delta^{18}O_{atm}$ ($\delta^{18}O$ of O_2, corrected for gravitational fractionation in the firn) (Bender et al., 1994), $[CH_4]$ and $\delta^{18}O_{ice}$ in Pakitsoq ice to the GISP2 ice core record of the same tracers. $\delta^{15}N$ of N_2, $\delta^{18}O$ of O_2 and $[CH_4]$ were measured in the large air samples as well as in small ice samples from horizontal profiles and from the corners of the sampling area (see the section 3.3.1). $\delta^{18}O_{ice}$ was also measured in the horizontal profile samples. The $\delta^{15}N$ of N_2 (Figures 4 and 5) and $\delta^{18}O_{atm}$ (Figure 4) values in the large air samples are consistent with values expected from the GISP2 ice core record, with the $[CH_4]$ values being higher than in GISP2 by up to 128 ppb in some samples as discussed above. To illustrate how the dating is accomplished, Figures 4 (YD – PB) and 5 (OD – Bølling) show $\delta^{15}N$, $[CH_4]$ and $\delta^{18}O_{atm}$ ($\delta^{18}O_{atm}$ in Figure 4 only) for the large air samples, as well as $\delta^{15}N$, $[CH_4]$, $\delta^{18}O_{ice}$ and $\delta^{18}O_{atm}$ ($\delta^{18}O_{atm}$ in Figure 4 only) for the small ice samples collected for age control. Records from contemporaneous GISP2 ice are also included in each figure for comparison.

As can be seen, the $[CH_4]$ values in the large air samples are mostly in good agreement with $[CH_4]$ measurements on stratigraphically equivalent small ice samples. Several of the small ice samples exhibit $[CH_4]$ that is elevated (by up to 500 ppb in

one case) with respect to the GISP2 record; this may be due to microbial in-situ production as mentioned above. $\delta^{15}N$ in the large air samples appears to be shifted down by ~ 0.02 ‰ with respect to the small ice samples, possibly due to fractionation, but this shift is close to the analytical uncertainty (0.009 ‰).

The best age determination for the large air samples is achieved through establishing gas age scales for sampled sections of Pakitsoq ice. Because all samples (except for LGM) are centered around climatic transitions involving large and rapid changes in several geochemical tracers, several good tie-points are available for correlating the Pakitsoq surface record with the GISP2 gas age scale. The main gas age tie points are listed in Table 3.4. We have found $\delta^{15}N$ to be the most robust and precise of the measurements on Pakitsoq ice. $\delta^{15}N$ peaks record rapid surface temperature changes (Severinghaus et al., 1998) that were almost certainly synchronous over all of Greenland. Further, the Pakitsoq deposition site is modeled to be within ~ 200 km of Summit, and Pakitsoq $\delta^{15}N$ shows a constant offset of only ~ -0.02 ‰ from GISP2 values during intervals of stable climate (YD and OD). These lines of evidence suggest that the Pakitsoq and GISP2 deposition sites for the climatic intervals of interest had similar firn thicknesses. We therefore make the assumption that the temporal evolution of the $\delta^{15}N$ peaks in GISP2 and Pakitsoq for the YD-PB and OD-Bølling abrupt warming events is the same and use $\delta^{15}N$ for most of the gas age tie points. We note that the other tracers are consistent with the ages so determined in all cases.

Once the gas age tie-points are established, the age-distance relationship for ice between any two tie points can then be determined from the stratigraphic positions of the tie points in the Pakitsoq profile. Based on these age-distance relationships, the average gas ages as well as the maximum possible age spans of the large air samples can be calculated (Table 3.5). This approach allows for mean age determination with < 1% absolute uncertainty for the YD-PB transition samples and ~2% absolute uncertainty for the OD-Bølling transition samples. The age of the LGM sample, however, is not well constrained because the four tracers we measured were not changing significantly around the time of the LGM.

3.7 Summary and conclusions

A novel method was developed for obtaining very large (~100 L STP) ancient air samples for paleoatmospheric $^{14}CH_4$ analyses. This air was extracted from ancient glacial ice outcropping at the Pakitsoq ablation site in West Greenland. The combination of $\delta^{15}N$ of N_2, $\delta^{18}O$ of O_2, $\delta^{18}O_{ice}$ and $[CH_4]$ allows for unambiguous dating of the air samples, especially at times of abrupt climatic transitions when several of these tracers are changing rapidly. The extraction method involves large-scale melt-extractions performed in the field accompanied by simulated extractions to test the procedural $[CH_4]$ and $^{14}CH_4$ blanks.

The field blank extraction procedure has been proven to simulate the $[CH_4]$ blank for actual melt extractions well, and $[CH_4]$ melt-extraction blanks for all large air samples are < 4 ppb. The amount of possible contamination to sample $^{14}CH_4$ from ambient air via several mechanisms was constrained using $\delta Ar/N_2$ and CFC-11 and

–12 measurements and found to be negligible for all samples. $\delta Ar/N_2$, $\delta Kr/Ar$ and $\delta Xe/Ar$ were measured in the samples to constrain gas loss to dissolution in water during the melt-extractions. The results show excellent agreement with a simple solubility model and indicate that all gases of interest were reaching the same fraction of full solubility equilibrium within a given sample, which allowed corrections to sample [CH_4] to be made.

Thirteen large air samples dating to the Younger Dryas-Preboreal and Oldest Dryas-Bølling rapid climatic transitions, as well as to the Last Glacial Maximum were obtained using these methods. After corrections for dissolved gases, some samples show higher [CH_4] (by up to 128 ppb) than contemporaneous ice samples from GISP2. This is most likely due to a small amount of microbial in-situ CH_4 production in Pakitsoq ice. However, it should be possible to correct the sample $^{14}CH_4$ for this in-situ production by determining the $^{14}CH_4$ of the contaminant from two samples that have elevated [CH_4] as compared to their replicates (Contaminated PB and Contaminated OD). Because of some in-situ produced CH_4 in the ice, Pakitsoq is not an ideal site for obtaining ancient air for $^{14}CH_4$ analyses. Colder glacier-margin sites in Antarctica where old ice is exposed at the surface (e.g., Mt. Moulton (Popp et al., 2004)) may provide higher-quality $^{14}CH_4$ records.

The large size of these air samples and the demonstrated lack of significant ambient air contamination lends them to a number of paleoatmospheric analyses beyond $^{14}CH_4$ that have not previously been possible due to insufficient air availability. For example, CF_4 which is known to have anthropogenic sources but is

suspected to have some natural sources as well, has been successfully measured in these samples (Mühle et al., in preparation). The meltwater from the ice extractions can also be filtered for particulates such as wind-blown dust and pollen.

Acknowledgements

This work was supported by NSF grants OPP 02-21470 (to J.P.S.) and OPP 02-21410 (to E.J.B.), a Packard Fellowship (to J.P.S.), and an American Chemical Society Petroleum Research Fund award (to E.J.B.).

We thank the UCSD Campus Research Machine Shop for an excellent job on constructing the melter and Benjamin Miller, Ralph Keeling, David Etheridge, Bruce Deck and Jack Marrin for helpful discussions. We thank Joe Melton and Matt Arsenault for their help with field sampling and CH_4 measurements. Katja Riedel performed some of the CH_4 analyses at NIWA. Leah Bjerkelund ably assisted with CH_4 measurements in minimelter tests. VECO Polar Resources provided outstanding logistical support in the field. Chuck Wiesman of Sapa Anodizing chemically polished test pieces free of charge and provided helpful discussions. We thank the Glaciology Group, Niels Bohr Institute, University of Copenhagen for performing the $\delta^{18}O_{ice}$ measurements. We would also like to thank Field Coordinator Paul Rose for his excellent help with logistics and sampling. Ross Beaudette and Marcel Croon helped with melter testing at SIO. We thank the Danish Polar Center and Greenland Home Rule for permission to carry out this research.

Chapter 3, in part, is in press in Journal of Glaciology, 2008, as: Vasilii V. Petrenko, Jeffrey P. Severinghaus, Edward J. Brook, Jens Mühle, Melissa Headly, Christina M. Harth, Hinrich Schaefer, Niels Reeh, Ray F. Weiss, Dave Lowe and Andrew M. Smith. Instruments and Methods: A novel method for obtaining very large ancient air samples from ablating glacial ice for analyses of methane radiocarbon. It is

reprinted here from the Journal of Glaciology with permission of the International Glaciological Society. The dissertation author was the primary investigator and author of this paper.

Tables

Table 3.1. Results of [CH_4] blank tests conducted with the large melter and small-scale models (minimelters). All melter tests shown were conducted in the field. [CH_4] measurements for the first three tests were done using a field GC setup as described in Petrenko et al. (2006), with typical [CH_4] uncertainties of 20 ppb. The [CH_4] measurements for the last melter test shown were conducted at NIWA, with uncertainties of ±1-5 ppb. All minimelter tests were carried out at Washington State University; [CH_4] measurements were performed using the same apparatus as in the field (Petrenko et al., 2006), but with better measurement uncertainties (± 1-6 ppb). Tests grouped together in the table were carried out concurrently. All minimelters eventually had more than one treatment applied. The treatments were applied in order from left to right as indicated by the dots. Minimelter tests are listed chronologically as conducted, from top to bottom. De-ionized (DI) water was used. De-gassed ice was produced by boiling DI water for ~1hr in a clean stainless steel vessel, followed by freezing. For minimelter tests, the vessels were initially evacuated, followed by the introduction of CH_4 standard gas, and then either spilling the DI water from a small beaker inside the vessel or placing the vessel into a 30˚C bath to start melting the ice. The amount of gas-free ice was increased and the amount of test standard gas decreased in later tests to increase CH_4 production detection sensitivity.

Table 3.1

Experimental conditions										Aluminum surface treatments applied											[CH4] results			
Melter	Minimelter	Gas amount	Dry	Glacial ice	Gas-free ice	Water	Heat applied	Test duration, hr		acetone and/or ethanol wash	Vacuum bake at 93°C for 24 hrs	hot acidic soap bath	chemical polish 2.5 min	epoxy coat	chemical polish 5 min	Caustic etch	Electropolish	anodize	Boil with DI water 8 hrs		Starting [CH4], ppb	End [CH4]	[CH4] production rate, ppb / hr	Notes
•		~25 L		~320 kg			•	1.3		•											~750	2242	1147.7	
•		~21 L				minimal		1.5		•											471	537	44.0	1
•		~21 L				minimal	•	2.75		•											471	1494	372.0	1,2
•		~30 L				~480 L		2		•			•					•			487	496	4.5	3
	•	~800 ml	•					0.58		•											378	407	50.0	4
	•	~800 ml				~40 ml		1.33		•											440	616	132.3	4
	•	~800 ml	•					2.13		•	•										378	378	0.0	5
	•	~800 ml	•					2.13		•		•	•								378	383	2.3	
	•	~800 ml				~40 ml		12.23		•	•										378	493	9.4	5
	•	~800 ml				~40 ml		12.24		•		•	•								378	397	1.6	
	•	~800 ml			~40 g			0.62		•											378	382	6.5	
	•	~800 ml			~40 g			0.72		•	•	•									378	385	9.7	
	•	~800 ml			~40 g			0.85		•		•	•					•			378	378	0.0	
	•	~800 ml			~40 g			21.7		•				•							378	507	5.9	
	•	~800 ml			~40 g			21.9		•	•			•							378	407	1.3	
	•	~800 ml			~40 g			21.8		•		•	•					•			378	401	1.1	
	•	~250 ml			~600 g			18		•	•	•			•						378	447	3.8	
	•	~250 ml			~600 g			18		•		•	•					•			378	406	1.6	
	•	~200 ml			~750 g			18		•						•		•			378	698	17.8	
	•	~200 ml			~750 g			18		•		•	•					•			378	397	1.1	
	•	~200 ml			~750 g			20		•		•	•					•	•		378	411	1.7	
	•	~200 ml			~750 g			18		•							•	•			378	567	10.5	
	•	~200 ml			~750 g			18		•		•	•					•	•		378	385	0.4	6

Notes: 1) Melter was drained but not dried 2) 20 min of gentle heating; up to 80°C in hottest spots; average of 2 tests
3) Blank test carried out in 2003 as described in blank extraction procedure in the text; result is an average of 10 blank extractions
4) Average result for 4 minimelters 5) Average result for 2 minimelters 6) Chemically polished aluminum strip inside minimelter

Table 3.2. Measured and corrected [CH_4], CFC-11, CFC-12, $\delta^{18}O$ of O_2, δAr/N2, δKr/Ar and δXe/Ar in Pakitsoq samples and melt-extraction blanks. [CH_4] was measured at NIWA using a HP 5890 gas chromatograph (GC) with a flame-ionization detector. [CH_4] values in the first column have been converted from the NIWA scale to the NOAA04 scale (Dlugokencky et al., 2005; Lowe et al., 1999) and corrected for the partial pressure of water vapor in the sample tanks. The CFC-11 and CFC-12 concentrations were measured at SIO as described in Mühle et al. (2007). The measurement uncertainties were estimated from concurrent reference gas measurements to be ± 2.0 parts per trillion (ppt) for CFC-12 measurements, and ± 2.8 ppt for CFC-11 measurements. $\delta^{18}O$ of O_2 and $\delta Ar/N_2$ were measured in duplicate; the pooled standard deviations (s_p) were 0.022 ‰ and 0.135 ‰, respectively. δKr/Ar and δXe/Ar were measured at SIO as described in Headly and Severinghaus (2007) and were single measurements; s_p estimated from concurrent reference air measurements was 0.26 ‰ for δKr/Ar and 2.03 ‰ for δXe/Ar. The reference for $\delta^{18}O$ of O_2, $\delta Ar/N_2$, δKr/Ar and δXe/Ar, as well as $\delta^{15}N$ of N_2 measurements was clean dry La Jolla air. The [CH_4] values in the "Corrected CH_4" column have been corrected for the melt-extraction blank and for dissolution during the melt-extractions as described in the text. [CH_4], CFC-11 and CFC–12 and $\delta Ar/N_2$ measurements on the CH_4 standard gas used in the blank extractions are also shown. Modern ambient air CFC-11 and CFC–12 concentrations are shown for comparison. [CH_4] for the gas-free ice blank and meltwater blank tests was measured at SIO. Typical $\delta^{18}O$ of O_2 (for ice containing Oldest Dryas-age air), $\delta Ar/N_2$, δKr/Ar and δXe/Ar measured in small Pakitsoq ice samples are shown for comparison with the large air samples. Expected [CH_4] values for all samples based on the GISP2 record (as described in Section 3.5.3), as well as differences from expected [CH_4] are also shown.

Table 3.2

Sample	CH_4, ppb	CFC-11, ppt	CFC-12, ppt	$\delta^{18}O$ of O_2, ‰	$\delta Ar/N_2$, ‰	$\delta Kr/Ar$, ‰	$\delta Xe/Ar$, ‰	corrected CH_4, ppb	CH_4 expected from GISP2, ppb	CH_4 elevation over GISP2, ppb
Younger Dryas 1	509.3 ± 1.1	2.0	1.5	1.37	-34.5	-33.28	-106.70	517 - 538	514- 537	-20 - +24
Younger Dryas 2	512.6 ± 0.7	3.6	2.4	1.38	8.4	-74.69	-140.52	520 - 541	514- 537	-16 - +27
YD-PB Transition 1	643.4 ± 0.7	2.2	1.7	1.54	-27.4	-22.14	-75.42	654 - 680	573- 699	-45 - +107
YD-PB Transition 2	662.2 ± 0.9	2.2	1.9	1.56	11.6	-60.61	-111.10	673 - 700	572- 716	-43 - +128
Preboreal 1	747.9 ± 0.8	2.9	2	1.46	-31.0	-31.98	-99.46	759 - 790	753- 778	-19 - +37
Preboreal 2	744.5 ± 1.2	4.7	2.8	1.42	-25.7	-21.37	-67.54	756 - 786	744- 769	-13 - +42
Contaminated PB	2117.2 ± 1.2							2154 - 2240	745- 770	+1383 - +1495
YD Blank	500.2 ± 0.2	0	0	0.00	-0.5					
Transition Blank	499.9 ± 0.7	0	0	0.00	-0.1					
PB Blank	501.0 ± 0.4	0	0	0.00	0.0					
Oldest Dryas 1	494.1 ± 1.0	2.9	1.7	1.97	-20.4			500 - 520	486- 509	-9 - +34
Oldest Dryas 2	501.0 ± 0.8	2.6	1.6	1.99	-20.3			507 - 527	486- 509	-2 - +41
Contaminated OD	564.4 ± 0.8	2.8	2	2.00	-22.4			571 - 594	484- 507	+64 - +110
Bølling 1	646.2 ± 0.4	5.1	2.5	2.22	-24.0			655 - 682	585- 618	+37 - +96
Bølling 2	662.5 ± 0.8	2.8	1.8	2.19	12.5			672 - 699	588- 621	+51 - +111
Last Glacial Maximum	406.6 ± 1.0	2.2	1.4	1.82	-32.8			411 - 427		
OD Blank	501.8 ± 0.8	0	0	0.01	2.1					
Bølling Blank	501.2 ± 0.4	0	0	0.02	2.1					
Methane standard gas	498.6 ± 0.8	0	0	-0.01	-0.1					
Gas-free ice blank	497.7 ± 0.5	0	0	0.01	-2.6			498 - 500		
Meltwater blank	499.9 ± 0.2	0	0	0.00	0.2					
Modern ambient air		246.0	545.0							
Typical values in Pakitsoq ice				2.07	5.8	25.9	50.4			

Table 3.3. Solubilities of gases of interest in terms of Henry's Law constant at 0°C. All solubilities are from Wilhelm et al. (1977), converted from units of molar fraction.

Table 3.3

Gas	K_H, M/atm
N_2	0.00106
O_2	0.00219
Ar	0.00239
Kr	0.00490
Xe	0.00934
CH_4	0.00256

Table 3.4. Main age tie-points used to establish the gas chronology of the sampled Pakitsoq ice sections. In addition to the points shown, more gradual changes in $\delta^{15}N$ from GISP2 were used to obtain additional age control points for the Preboreal, Oldest Dryas and Bølling samples. The GISP2 $\delta^{15}N$ data used for correlation with Pakitsoq records are from Severinghaus et al. (1998), Severinghaus and Brook (1999) and Kobashi (2007). $\delta^{18}O_{ice}$ data used are from Grootes and Stuiver (1997), and $\delta^{18}O_{atm}$ data used are from Bender et al. (1999) and Severinghaus et al. (2006). For each time period involved, the best available ice core gas age scale was used.

Table 3.4

Age tie point significance	GISP2 depth, m	GISP2 gas age, years BP (0 = 1950 AD)	Absolute age uncertainty, yr	Notes
Start of YD- PB $\delta^{15}N$ rise (last low value)	1700.58	11,570	40	1,2
YD-PB $\delta^{15}N$ peak	1697	11,464	42	1,3
$\delta^{18}O_{ice}$ drop into the YD (first low value)	1711	11,938	47	1,3
YD-age $\delta^{18}O_{atm}$ value of 0.785	1715.1	12,065	50	1,3
Start of OD-Bølling $\delta^{15}N$ rise (last low value)	1821.55	14,684	294	4
OD-Bølling $\delta^{15}N$ peak	1816.95	14,584	296	4
Start of $\delta^{18}O_{ice}$ rise into Bølling	1797	14,154	304	4
CH_4 values below 400 ppb not observed in GISP2 for samples younger than this	1878.2	17,263	695	5
Oldest pre-LGM $\delta^{18}O_{atm}$ value significantly below 0.95 per mil	737.16	23,674	850	6

Notes

1. Gas age scale as in Schaefer et al. (2006).

2. The termination of the YD is estimated from tree rings to be at 11,590 yr BP, with <1 year uncertainty (Kobashi, 2007). Because the Schaefer et al. (2006) gas age scale for GISP2 places the YD termination at 11,570 yr BP, we take a conservative estimate of the absolute age error of the YD termination as 40 yrs.

3. Absolute age uncertainty is calculated as the sum of the age uncertainty for the YD termination (40 years), plus 0.02 x the age difference from the YD termination point. The factor of 0.02 is used because this is the uncertainty in the GISP2 age scale for this depth range (Meese et al., 1997).

4. Gas age scale as in Severinghaus and Brook (1999)

5. Gas age scale as in Brook et al. (2000).

6. Depths and ages from Siple Dome, not GISP2. The Siple Dome data are used due to their better precision for $\delta^{18}O_{atm}$. Siple Dome gas age scale is as in Brook et al. (2005).

Table 3.5. Large air sample mean ages, uncertainties, and the maximum ranges of ages of ancient air possibly included in the large air samples. Yr BP is years before present, with present defined as 1950 AD.

Table 3.5

Sample	Mean age, yr BP	Mean age uncertainty	Absolute max. gas age possibly included in sample, yr BP	Absolute min. gas age possibly included in sample, yr BP
Younger Dryas 1	11,637	75	11,972	11,509
Younger Dryas 2	11,631	73	11,972	11,494
YD-PB Tranistion 1	11,535	54	11,592	11,368
YD-PB Transition 2	11,531	56	11,583	11,371
Preboreal 1	11,364	109	11,468	11,247
Preboreal 2	11,354	132	11,461	11,207
Contaminated PB	11,337	133	11,451	11,229
Oldest Dryas 1	14,760	300	16,240	14,390
Oldest Dryas 2	14,766	303	16,240	14,390
Contaminated OD	15,028	250	16,108	14,390
Bølling 1	14,599	298	14,978	14,119
Bølling 2	14,472	267	14,966	14,112
LGM	19,000*		24,524	16,568

*A best guess based on small variations in $\delta^{15}N$ and $\delta^{18}O_{ice}$

Figures

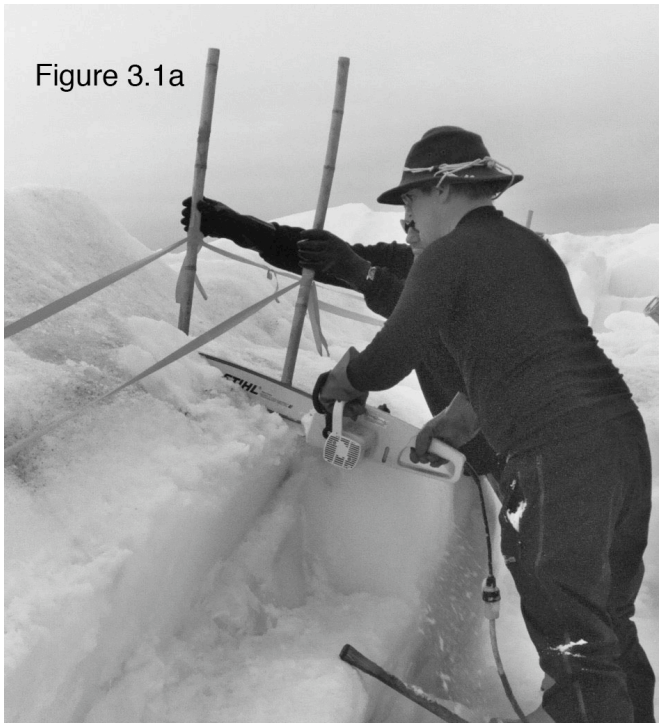

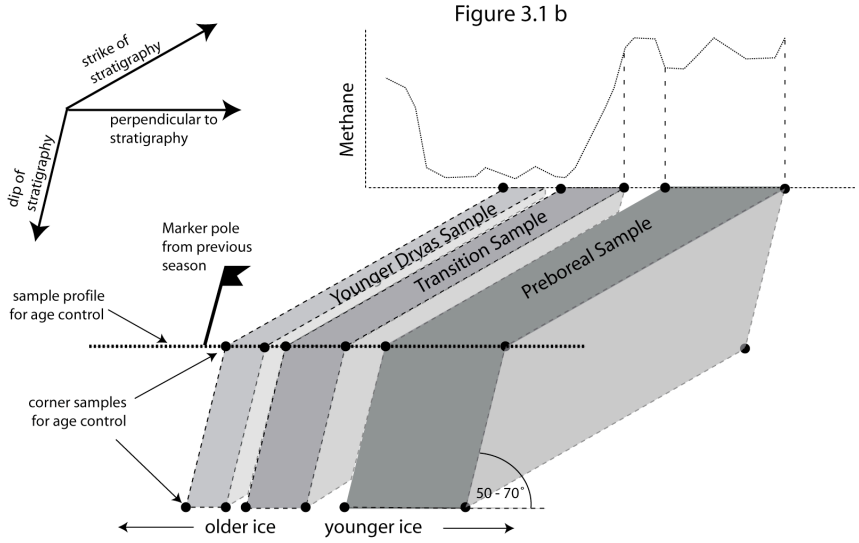

Figure 3.1. a) Field sampling of Younger Dryas ice. b) A simplified schematic illustration of the ice cut at Pakitsoq for the large air samples, using samples from the YD-PB transition as an example. The methane plot at the top does not represent real values and is used simply to illustrate the relative range of methane values spanned by each sample.

Figure 3.2

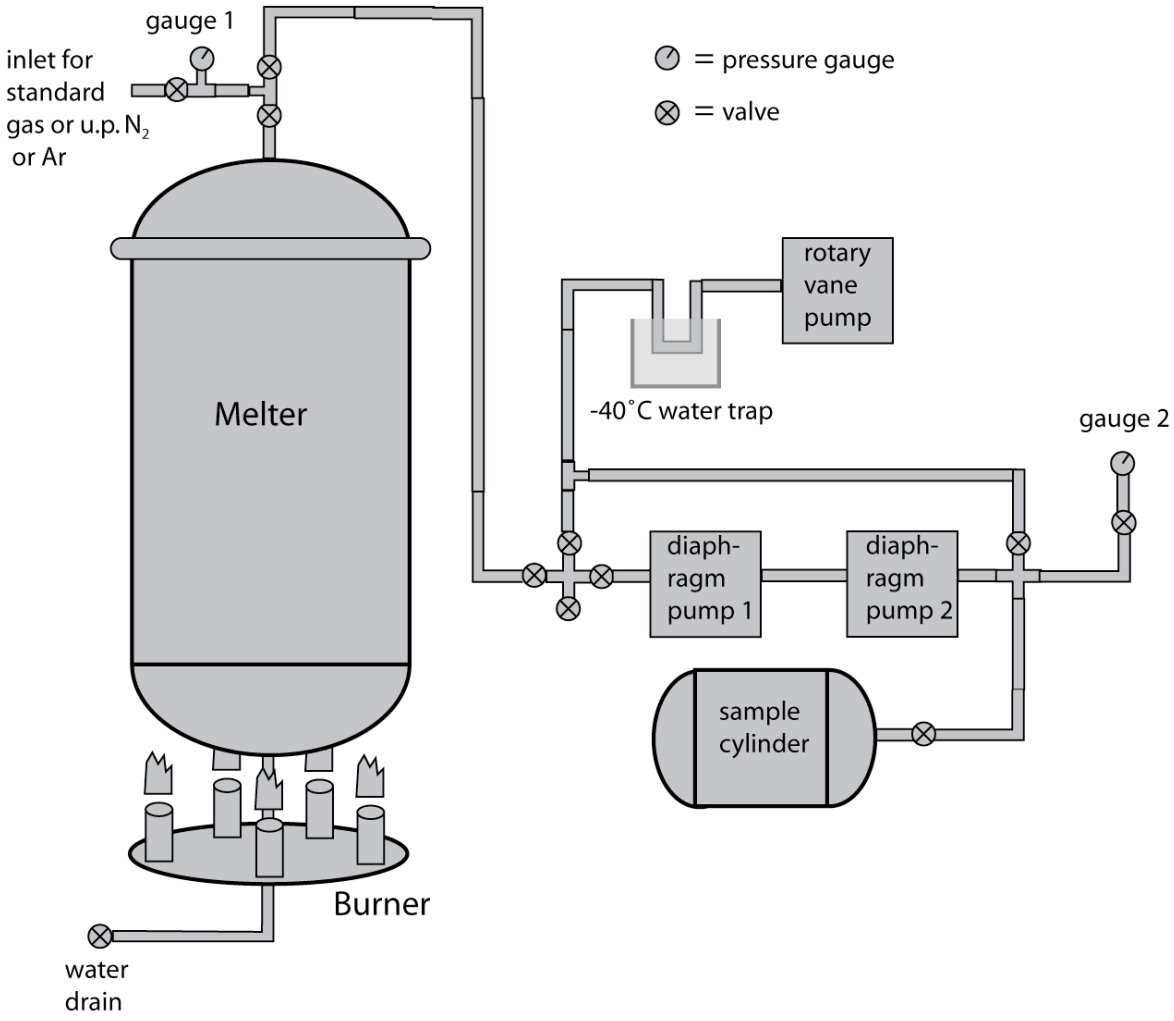

Figure 3.2. A schematic of the large air sample melt-extraction system. Gauge 1 is a 1300-hPa-range piezo pressure transducer. Gauge 2 is a schematic simplification of 3 available gauges: a 13-hPa-range capacitance manometer, a 1300-hPa-range piezo pressure transducer, and a 15-bar-range mechanical gauge. Diaphragm pumps 1 and 2 are KNF Neuberger models N860 and N145, respectively.

Figure 3.3. Solubility effects on gases during melter extractions. a) Modeled $\delta Ar/N_2$, $\delta Kr/Ar$, and $\delta Xe/Ar$ vs fraction of full solubility equilibrium reached for 0˚C. b) Measured and modeled $\delta Kr/Ar$ and $\delta Xe/Ar$ plotted vs $\delta Ar/N_2$. Data that plot off modeled curves are for samples Younger Dryas 2 and YD-PB Transition 2, which used argon flushing. Sample error bars are smaller than size of points and are not shown. c) Same as in b) but gas ratios for Younger Dryas 2 and YD-PB Transition 2 samples have been corrected for residual argon from flushing as described in the text.

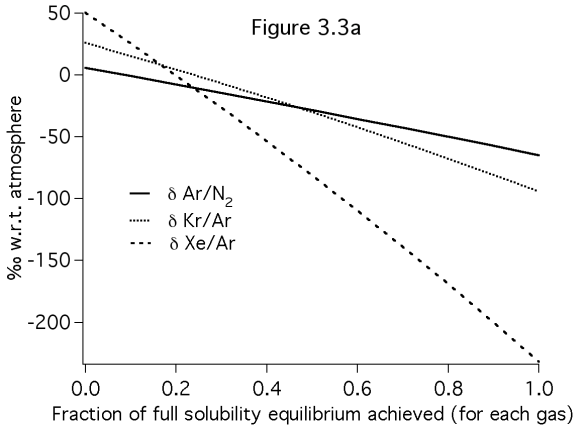
Figure 3.3a
50
0
-50
-100
-150
-200
‰ w.r.t. atmosphere
δ Ar/N2
δ Kr/Ar
δ Xe/Ar
0.0
0.2
0.4
0.6
0.8
1.0
Fraction of full solubility equilibrium achieved (for each gas)

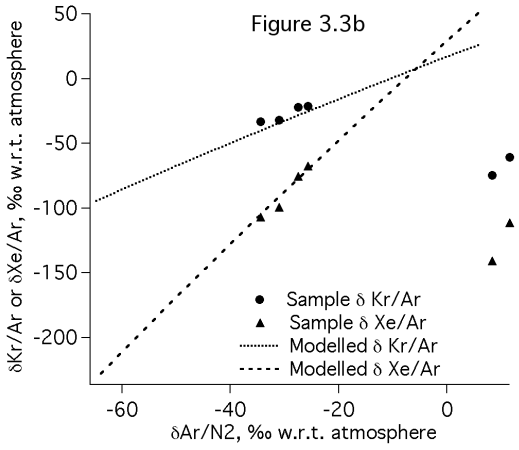
Figure 3.3b
50
0
-50
-100
-150
-200
δKr/Ar or δXe/Ar, ‰ w.r.t. atmosphere
Sample δ Kr/Ar
Sample δ Xe/Ar
Modelled δ Kr/Ar
Modelled δ Xe/Ar
-60
-40
-20
0
δAr/N2, ‰ w.r.t. atmosphere

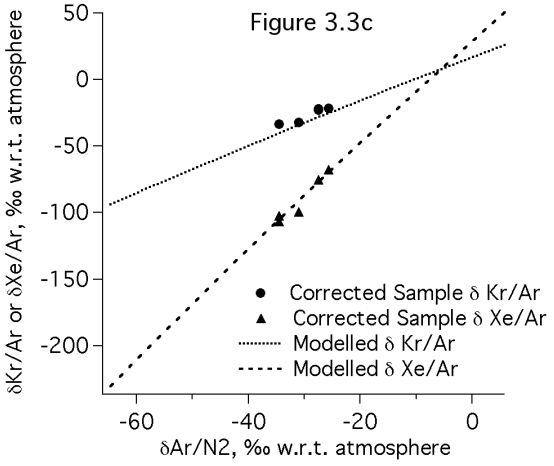
Figure 3.3c
50
0
-50
-100
-150
-200
δKr/Ar or δXe/Ar, ‰ w.r.t. atmosphere
Corrected Sample δ Kr/Ar
Corrected Sample δ Xe/Ar
Modelled δ Kr/Ar
Modelled δ Xe/Ar
-60
-40
-20
0
δAr/N2, ‰ w.r.t. atmosphere

Figure 3.4. Geochemical records of the Younger Dryas – Preboreal transition in the GISP2 ice core record (a) and at the Pakitsoq ice outcrop in 2004 (b). Both records are plotted versus gas age for easy comparison. The gas age scale for Pakitsoq was established as described in the text, and the distances of the main age tie points in the Pakitsoq horizontal profile are indicated. The age – distance relationship in Pakitsoq ice is variable (Petrenko et al., 2006). For example, for the Pakitsoq ice section shown on the plot, ice containing gases of Preboreal age is relatively less thinned.
a) GISP2 $\delta^{15}N$ of N_2 is from Severinghaus et al. (1998), $[CH_4]$ is from Brook et al. (2000), and $\delta^{18}O_{ice}$ is from Grootes and Stuiver (1997). All GISP2 data are plotted on the gas age scale as in Schaefer et al. (2006).
b) $\delta^{15}N$ of N_2, $\delta^{18}O_{atm}$ and $[CH_4]$ in the Pakitsoq large air samples and $\delta^{15}N$ of N_2, $\delta^{18}O_{atm}$, $[CH_4]$ and $\delta^{18}O_{ice}$ in small ice samples taken for stratigraphic age control. The horizontal error bars on the large air samples indicate the maximum possible range of gas ages included in the samples with respect to the GISP2 gas age scale. Measurements of $\delta^{15}N$ on the large air samples were performed simultaneously with measurements of $\delta^{18}O$ of O_2 as described in the text. Measurements of $\delta^{15}N$, $\delta^{18}O_{atm}$, $[CH_4]$ and $\delta^{18}O_{ice}$ on the small ice samples were performed as described in Petrenko et al. (2006). The pooled standard deviation for the small ice sample measurements was 0.009 ‰ for $\delta^{15}N$ and 0.024 ‰ for $\delta^{18}O_{atm}$. The average standard deviation of the small ice sample $[CH_4]$ measurements (includes reproducibility of repeated measurements on the same sample as well as variation in the methane blank) was 26 ppb. The age-control small ice sample set consisted of a single horizontal sample profile collected near the northern end of the sampling area (strike of the stratigraphy is approximately N-S), along with samples from the corners of ice areas cut for each large sample (not shown). Note that sample age decreases with profile distance for the YD-PB transect but increases with profile distance for the OD-Bølling transect (Figure 5). This is due to these transects lying on opposite sides of the axis of a large-scale fold in the ice; for a more detailed discussion see Petrenko et al. (2006). The Pakitsoq deposition site is slightly warmer than Summit (with $\delta^{18}O_{ice}$ higher by 1-2 ‰), with slightly thinner firn (as indicated by ~ 0.02 ‰ lower $\delta^{15}N$). This predicts a slightly lower gas-age – ice-age difference for Pakitsoq than for GISP2. This has been taken into account when using inflection points in the Pakitsoq $\delta^{18}O_{ice}$ record to establish gas age tie-points.

Figure 3.4: YD-PB Transition samples

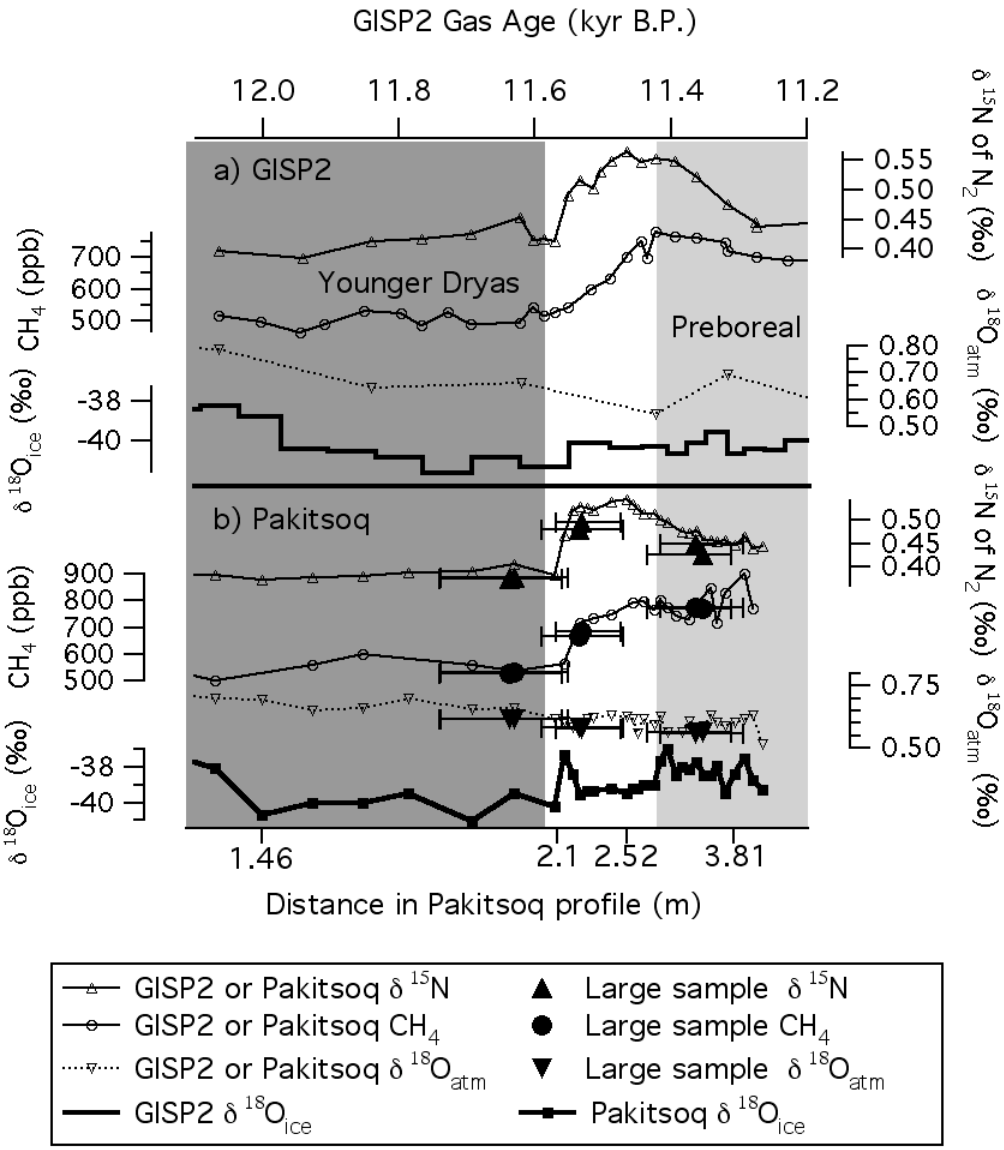

Figure 3.5. Geochemical records of the Oldest Dryas – Bølling transition in the GISP2 ice core record (a) and at the Pakitsoq ice outcrop in 2005 (b). As in Figure 3.4, both records are plotted versus gas age.
a) GISP2 $\delta^{15}N$ of N_2 is from Severinghaus and Brook (1999), [CH_4] is from Brook et al. (2000), and $\delta^{18}O_{ice}$ is from Grootes and Stuiver (1997). All GISP2 data are plotted on the gas age scale as in Severinghaus and Brook (1999).
b) OD-Bølling transition Pakitsoq large air samples and small ice samples taken for stratigraphic age control, similar to Figure 3.4b. The age-control small ice sample set in this case consisted of four horizontal profiles, collected along the top and bottom southern edges, near the center, and along the northern edge of the sampling area. Only the center profile is shown to avoid overloading the plot. The large Bølling samples included some gas from the OD- Bølling CH_4 transition.

Figure 3.5: OD - Bølling Transition samples

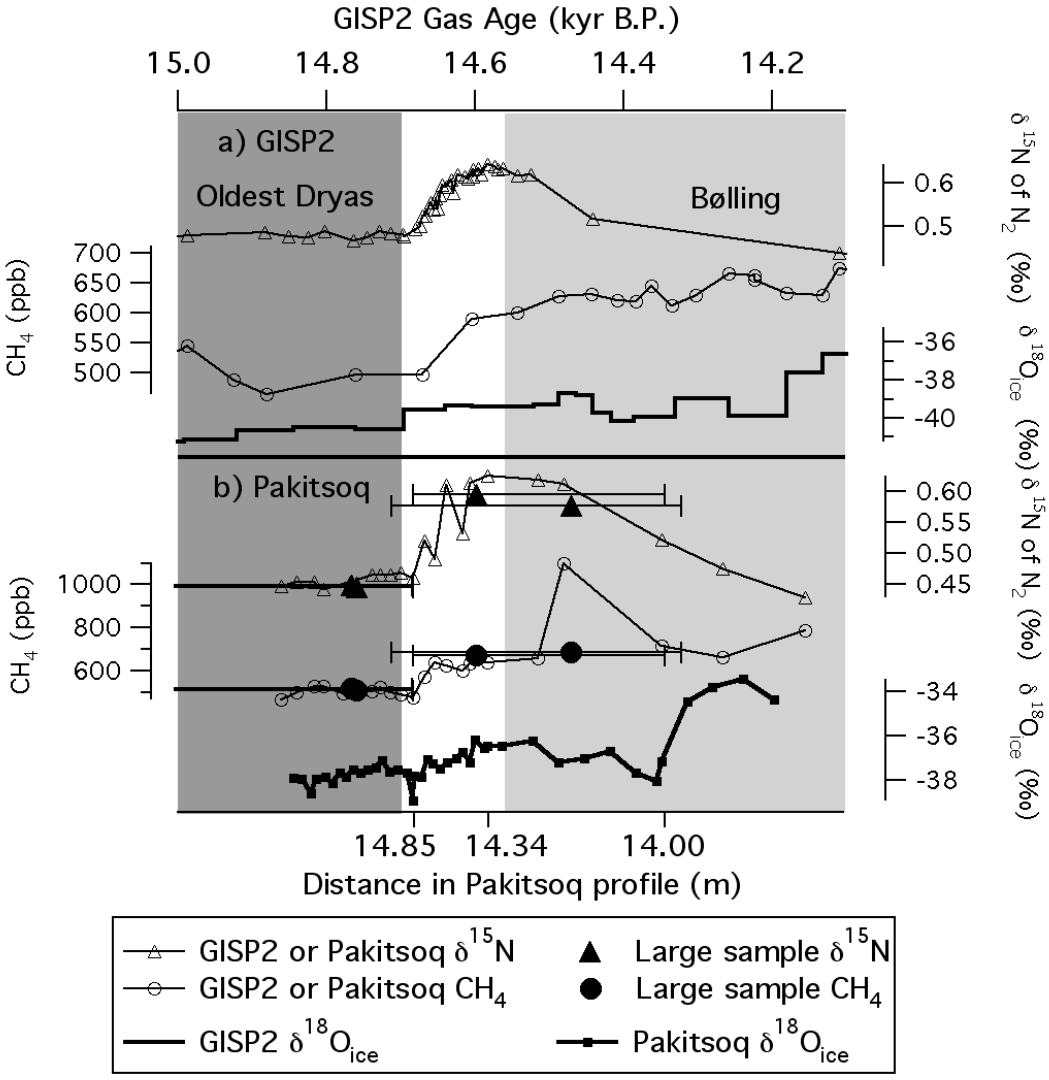

References

Bender, M., 2003. Climate-biosphere interactions on glacial-interglacial timescales. Global Biogeochemical Cycles 17 (3), doi: 10.1029/2002GB001932.

Bender, M., Malaize, B., Orchardo, J., Sowers, T., Jouzel, J., 1999. High Precision Correlations of Greenland and Antarctic Ice Core Records Over the Last 100kyr. In: P.U. Clark, R. Webb and L. Keigwin (Editors), Mechanisms of Global Climate Change at Millenial Timescales. American Geophysical Union, Washington, DC, pp. 149-164.

Bender, M., Sowers, T., Dickson, M.L., Orchardo, J., Grootes, P., Mayewski, P.A.,Meese, D.A., 1994. Climate Correlations between Greenland and Antarctica During the Past 100,000 Years. Nature 372, 663-666.

Boerboom, A.J.,Kleyn, G., 1969. Diffusion Coefficients of Noble Gases in Water. Journal of Chemical Physics 50 (3), 1086-1088.

Brook, E.J., Harder, S., Severinghaus, J., Steig, E.J.,Sucher, C.M., 2000. On the origin and timing of rapid changes in atmospheric methane during the last glacial period. Global Biogeochemical Cycles 14, 559-572.

Brook, E.J., Sowers, T.,Orchardo, J., 1996. Rapid variations in atmospheric methane concentration during the past 110,000 years. Science 273, 1087-1091.

Brook, E.J., White, J.W.C., Schilla, A.S.M., Bender, M.L., Barnett, B., Severinghaus, J.P., Taylor, K.C., Alley, R.B.,Steig, E.J., 2005. Timing of millennial-scale climate change at Siple Dome, West Antarctica, during the last glacial period. Quaternary Science Reviews 24, 1333-1343.

Buffett, B.,Archer, D., 2004. Global inventory of methane clathrate: sensitivity to changes in the deep ocean. Earth and Planetary Science Letters 227, 185-199.

Butler, J.H., Battle, M., Bender, M.L., Montzka, S.A., Clarke, A.D., Saltzman, E.S., Sucher, C.M., Severinghaus, J.P.,Elkins, J.W., 1999. A record of atmospheric halocarbons during the twentieth century from polar firn air. Nature 399, 749-755.

Campen, R.K., Sowers, T.,Alley, R.B., 2003. Evidence of microbial consortia metabolizing within a low-latitude mountain glacier. Geology 31, 231-234.

Catalysts and Chemicals, Inc., 1970. Pellet catalysts for methane production. Patent no. DE 1938079, Germany.

Chappellaz, J., Blunier, T., Raynaud, D., Barnola, J.M., Schwander, J.,Stauffer, B., 1993. Synchronous Changes in Atmospheric CH4 and Greenland Climate between 40-Kyr and 8-Kyr BP. Nature 366, 443-445.

Esso Research and Engineering Co., 1969. Catalyst for methane production. Patent no. 1055909, United Kingdom.

Conny, J.M.,Currie, L.A., 1996. The isotopic characterization of methane, non-methane hydrocarbons and formaldehyde in the troposphere. Atmospheric Environment 30, 621-638.

Dlugokencky, E.J., Myers, R.C., Lang, P.M., Masarie, K.A., Crotwell, A.M., Thoning, K.W., Hall, B.D., Elkins, J.W.,Steele, L.P., 2005. Conversion of NOAA atmospheric dry air CH4 mole fractions to a gravimetrically prepared standard scale. Journal of Geophysical Research-Atmospheres 110 (D18), doi: 10.1029/2005JD006035.

Ferrell, R.T.,Himmelblau, D.M., 1967. Diffusion Coefficients of Nitrogen and Oxygen in Water. Journal of Chemical and Engineering Data 12 (1), 111-115.

Fluckiger, J., Monnin, E., Stauffer, B., Schwander, J., Stocker, T.F., Chappellaz, J., Raynaud, D.,Barnola, J.M., 2002. High-resolution Holocene N2O ice core record and its relationship with CH4 and CO2. Global Biogeochemical Cycles 16 (1), doi: 10.29/2001GB001417.

Grabowski, K.S., Knies, D.L., Tumey, S.J., Pohlman, J.W., Mitchell, C.S.,Coffin, R.B., 2004. Carbon pool analysis of methane hydrate regions in the seafloor by accelerator mass spectrometry. Nuclear Instruments & Methods in Physics Research Section B-Beam Interactions with Materials and Atoms 223-24, 435-440.

Grootes, P.M.,Stuiver, M., 1997. Oxygen 18/16 variability in Greenland snow and ice with 10^-3 to 10^5 - year time resolution. Journal of Geophysical Research-Oceans 102, 26455-26470.

Headly, M.,Severinghaus, J., 2007. A method to measure Kr/N2 ratios in air bubbles trapped in ice cores and its application in reconstructing past mean ocean temperature. Journal of Geophysical Research-Atmospheres 112, doi:10.1029/2006JD008317.

Jahne, B., Heinz, G.,Dietrich, W., 1987. Measurement of the Diffusion-Coefficients of Sparingly Soluble Gases in Water. Journal of Geophysical Research-Oceans 92, 10767-10776.

Kennett, J.P., Cannariato, K.G., Hendy, I.L.,Behl, R.J., 2000. Carbon isotopic evidence for methane hydrate instability during quaternary interstadials. Science 288, 128-133.

Kennett, J.P., Cannariato, K.G., Hendy, I.L.,Behl, R.J., 2003. Methane Hydrates in Quaternary Climate Change: The Clathrate Gun Hypothesis. AGU, Washington, D.C., 216 pp.

Kessler, J.D., Reeburgh, W.S., Southon, J., Seifert, R., Michaelis, W.,Tyler, S.C., 2006. Basin-wide estimates of the input of methane from seeps and clathrates to the Black Sea. Earth and Planetary Science Letters 243, 366-375.

Kobashi, T., 2007. Greenland temperature, climate change, and human society during the last 11,600 years. Ph. D. Thesis, University of California, San Diego, La Jolla, 227 pp.

Lassey, K.R., Lowe, D.C.,Smith, A.M., 2007. The atmospheric cycling of radiomethane and the "fossil fraction" of the methane source. Atmospheric Chemistry and Physics 7, 2141-2149.

Lowe, D.C., Allan, W., Manning, M.R., Bromley, T., Brailsford, G., Ferretti, D., Gomez, A., Knobben, R., Martin, R., Mei, Z., Moss, R., Koshy, K.,Maata, M., 1999. Shipboard determinations of the distribution of C-13 in atmospheric methane in the Pacific. Journal of Geophysical Research-Atmospheres 104, 26125-26135.

Maharajh, D.M.,Walkley, J., 1973. Temperature-Dependence of Diffusion-Coefficients of Ar, CO2, CH4, CH3Cl, CH3Br, and CHCl2F in Water. Canadian Journal of Chemistry-Revue Canadienne De Chimie 51, 944-952.

Meese, D.A., Gow, A.J., Alley, R.B., Zielinski, G.A., Grootes, P.M., Ram, M., Taylor, K.C., Mayewski, P.A.,Bolzan, J.F., 1997. The Greenland Ice Sheet Project 2 depth-age scale: Methods and results. Journal of Geophysical Research-Oceans 102, 26411-26423.

Milkov, A.V., 2004. Global estimates of hydrate-bound gas in marine sediments: how much is really out there? Earth-Science Reviews 66, 183-197.

Mühle, J., Lueker, T.J., Su, Y., Miller, B.R., Prather, K.A.,Weiss, R.F., 2007. Trace gas and particulate emissions from the 2003 southern California wildfires. Journal of Geophysical Research-Atmospheres 112, Art. No. D03307.

Petit, J.R., Jouzel, J., Raynaud, D., Barkov, N.I., Barnola, J.M., Basile, I., Bender, M., Chappellaz, J., Davis, M., Delaygue, G., Delmotte, M., Kotlyakov, V.M.,

Legrand, M., Lipenkov, V.Y., Lorius, C., Pepin, L., Ritz, C., Saltzman, E.,Stievenard, M., 1999. Climate and atmospheric history of the past 420,000 years from the Vostok ice core, Antarctica. Nature 399, 429-436.

Petrenko, V.V., Severinghaus, J.P., Brook, E.J., Reeh, N.,Schaefer, H., 2006. Gas records from the West Greenland ice margin covering the Last Glacial Termination: a horizontal ice core. Quaternary Science Reviews 25, 865-875.

Popp, T., Sowers, T., Dunbar, N., McIntosh, W.,White, J.W.C., 2004. Radioisotopically Dated Climate Record Spanning the Last Interglacial in Ice from Mount Moulton, West Antarctica, Poster presented at the AGU Fall Meeting, December 2004. AGU, San Francisco.

Price, P.B., 2007. Microbial life in glacial ice and implications for a cold origin of life. Fems Microbiology Ecology 59, 217-231.

Quay, P., Stutsman, J., Wilbur, D., Snover, A., Dlugokencky, E.,Brown, T., 1999. The isotopic composition of atmospheric methane. Global Biogeochemical Cycles 13, 445-461.

Reeh, N., 1988. A Flow-Line Model for Calculating the Surface Profile and the Velocity, Strain-Rate, and Stress-Fields in an Ice-Sheet. Journal of Glaciology 34, 46-54.

Reeh, N., Oerter, H., Letreguilly, A., Miller, H.,Hubberten, H.W., 1991. A New, Detailed Ice-Age O-18 Record from the Ice-Sheet Margin in Central West Greenland. Global and Planetary Change 90, 373-383.

Reeh, N., Oerter, H.,Thomsen, H.H., 2002. Comparison between Greenland ice-margin and ice-core oxygen-18 records. Annals of Glaciology 35, 136-144.

Schaefer, H., Whiticar, M.J., Brook, E.J., Petrenko, V.V., Ferretti, D.F.,Severinghaus, J.P., 2006. Ice record of delta C-13 for atmospheric CH4 across the Younger Dryas-Preboreal transition. Science 313, 1109-1112.

Severinghaus, J., Beaudette, R.,Brook, E., 2006. Millennial-Scale Variations in Oxygen-18 of Atmospheric Molecular Oxygen. EOS Transactions, AGU 87, Fall Meet. Suppl., Abstract U34B-01.

Severinghaus, J.P.,Brook, E.J., 1999. Abrupt climate change at the end of the last glacial period inferred from trapped air in polar ice. Science 286, 930-934.

Severinghaus, J.P., Grachev, A., Luz, B.,Caillon, N., 2003. A method for precise measurement of argon 40/36 and krypton/argon ratios in trapped air in polar

ice with applications to past firn thickness and abrupt climate change in Greenland and at Siple Dome, Antarctica. Geochimica Et Cosmochimica Acta 67, 325-343.

Severinghaus, J.P., Sowers, T., Brook, E.J., Alley, R.B.,Bender, M.L., 1998. Timing of Abrupt Climate Change at the End of the Younger Dryas Interval from Thermally Fractionated Gases in Polar Ice. Nature 391, 141-146.

Smith, R.E., Friess, E.T.,Morales, M.F., 1955. Experimental Determinations of the Diffusion Coefficients of Gases through Water - Nitrogen and Argon. Journal of Physical Chemistry 59, 382-383.

Sowers, T., 2006. Late quaternary atmospheric CH4 isotope record suggests marine clathrates are stable. Science 311, 838-840.

Wahlen, M., Tanaka, N., Henry, R., Deck, B., Zeglen, J., Vogel, J.S., Southon, J., Shemesh, A., Fairbanks, R.,Broecker, W., 1989. C-14 in Methane Sources and in Atmospheric Methane - the Contribution from Fossil Carbon. Science 245, 286-290.

Warner, M.J.,Weiss, R.F., 1985. Solubilities of Chlorofluorocarbon-11 and Chlorofluorocarbon-12 in Water and Seawater. Deep-Sea Research Part a-Oceanographic Research Papers 32, 1485-1497.

Wernick, S., Pinner, R.,Sheasby, P.G., 1987. The surface treatment and finishing of aluminum and its alloys. ASM International, Metals Park, Ohio, 1273 pp.

Wilhelm, E., Battino, R.,Wilcock, R.J., 1977. Low-Pressure Solubility of Gases in Liquid Water. Chemical Reviews 77, 219-262.

Winckler, G., Aeschbach-Hertig, W., Holocher, J., Kipfer, R., Levin, I., Poss, C., Rehder, G., Suess, E.,Schlosser, P., 2002. Noble gases and radiocarbon in natural gas hydrates. Geophysical Research Letters 29, 1423.

Chapter 4

Methods for analyzing ^{14}C of methane in air extracted from ancient glacial ice

Abstract

We present a new method developed for measuring ^{14}C of methane ($^{14}CH_4$) in ancient air samples extracted from glacial ice and dating 11,000 - 15,000 calendar years before present. The small size (~20 μg CH_4 carbon), low CH_4 concentrations ([CH_4], 400 – 800 parts per billion (ppb)), high carbon monoxide concentrations ([CO]) and low ^{14}C activity of the samples created unusually high risks of contamination by extraneous carbon. Up to 2500 ppb CO in the air samples was quantitatively removed using the Sofnocat reagent. ^{14}C procedural blanks were greatly reduced through the construction of a new CH_4 conversion line utilizing platinized quartz wool for CH_4 combustion and the use of an ultra high purity iron catalyst for graphitization. The amount and ^{14}C activity of extraneous carbon added in the new CH_4 conversion line were determined to be 0.23 ± 0.16 μg and 23.57 ± 16.22 pMC. The amount of modern (100 pMC) carbon added during the graphitization step has been reduced to 0.03 μg. The overall procedural blank for all stages of sample handling was 0.75 ± 0.38 pMC for ~20 μg, ^{14}C-free air samples with [CH_4] of 500 ppb. Duration of the graphitization reactions for small (<25 μg C) samples was greatly reduced and reaction yields improved through more efficient water vapor trapping and the use of a new iron catalyst with higher surface area. ^{14}C corrections for each step of sample handling have been determined. The resulting overall $^{14}CH_4$ uncertainties for the ancient air samples are ~ 1.0 pMC.

4.1 Introduction

CH_4 is the most abundant organic molecule in the Earth's atmosphere and a key player in global atmospheric chemistry (Brasseur et al., 1999). It is also the third most important greenhouse gas after H_2O and CO_2, with a global warming potential 25 times that of CO_2 on a 100-yr timescale (Forster et al., 2007). Ice core records from Greenland and Antarctica show large and rapid variations in atmospheric CH_4 concentrations ($[CH_4]$) in response to climate change (Brook et al., 2000; Chappellaz et al., 1993). Ice core records, combined with measurements from firn air as well as instrumental measurements in the atmosphere, also capture the rapid rise of $[CH_4]$ starting around 1,750 AD, which is attributed to anthropogenic activity (Etheridge et al., 1998).

Measurements of atmospheric $^{14}CH_4$ in the past two decades have helped to constrain the fossil CH_4 contribution to the global budget, as well as reveal the $^{14}CH_4$ rise due to production from pressurized-water reactors (PWRs), though much uncertainty in these source terms remains (Conny and Currie, 1996; Lassey et al., 2007). ^{14}C can be a similarly powerful tool for understanding paleo CH_4 budgets and changes in the CH_4 sources during rapid climatic transitions at the end of the last glacial period. Recent studies of δD and $\delta^{13}C$ of CH_4 have been able to put constraints on CH_4 budgets during the last glacial termination (Schaefer et al., 2006; Sowers, 2006). However, the uncertainties and similarities in the δD and $\delta^{13}C$ signatures of many paleo CH_4 sources stand in the way of definitive CH_4 budget reconstructions. Here $^{14}CH_4$ has the great advantage of being able to definitively separate the biogenic

(wetlands, plants, animals) sources from geologic and clathrate sources. Biogenic $^{14}CH_4$ mostly follows atmospheric $^{14}CO_2$ (Quay et al., 1999; Wahlen et al., 1989), while most geologic and clathrate sources are very old and either contain no measurable ^{14}C or very low ^{14}C levels (Grabowski et al., 2004; Kessler et al., 2006; Winckler et al., 2002).

It has been suggested that several large and rapid atmospheric CH_4 increases during the last 100 kyr were the result of massive climate-driven destabilisation of marine CH_4 clathrates, which then in turn contributed to the warming (Kennett et al., 2000, 2003). Quantifying clathrate contributions to the CH_4 increases during abrupt warming events at the end of the last glacial period is particularly relevant in the light of current anthropogenic warming. By recent estimates, the present amount of CH_4 carbon associated with clathrates is 500 – 5,000 Gt (Buffett and Archer, 2004; Milkov, 2004); which at the upper end is comparable to the estimated carbon content of all the fossil fuels. Future warming of the oceans may destabilize large amounts of CH_4 clathrate, providing a substantial positive feedback to the warming.

At present, methods already exist for $^{14}CH_4$ analyses on modern atmospheric air, as well as on ocean water (Kessler and Reeburgh, 2005; Lowe et al., 1991). Here we describe the techniques developed to perform the first $^{14}CH_4$ measurements on ancient air extracted from glacial ice. Ice cores are commonly used for paleo-atmospheric studies, but at least 1,000 kg of ancient ice is required to provide ~25 micrograms of CH_4-derived carbon (μg C), barely enough for measurement of ^{14}C by

accelerator mass spectrometry (AMS). Such large amounts of ancient ice of a uniform age are not available from deep ice cores.

Previous work has shown that large amounts of ancient ice dating to the last glacial termination outcrop at the surface at the Pakitsoq ablation site in West Greenland (Petrenko et al., 2006; Reeh et al., 1991). The CH_4 record in Pakitsoq ice was shown to be mostly well preserved, however elevated CH_4 values (with respect to the GISP2 ice core record) were found in some ice sections (Petrenko et al., 2006). ~100 L ancient air samples for $^{14}CH_4$ analyses with ages between 11 – 15 calendar kyr before present (BP, where present = 1950 AD) were obtained from Pakitsoq ice by melt-extraction in the field (from here on referred to as "Pakitsoq samples") and details were presented in Chapter 3 of this thesis. The [CH_4] blank for the melt-extractions was found to be < 4 parts per billion (ppb) for all samples. Measurements of $\delta^{18}O$ of O_2 and $\delta^{15}N$ of N_2 in the samples indicated no significant gas isotopic fractionation from the melt-extraction. Ar/N_2, CFC-11 and CFC-12 measured in the samples indicated no significant $^{14}CH_4$ contamination from ambient air. Ar/N_2, Kr/Ar and Xe/Ar ratios in the samples were used to quantify effects of gas dissolution during the melt-extractions and correct the sample [CH_4]. [CH_4] values corrected for blank and solubility effects were slightly elevated over expected values for most samples. This may be due to a small amount of microbial in-situ CH_4 production in the ice (Price, 2007). Two of the samples had [CH_4] substantially elevated with respect to contemporaneous GISP2 ice (by >60 ppb). $^{14}CH_4$ measured in these two samples allows for $^{14}CH_4$ corrections to be made for other samples for in-situ produced CH_4.

In this paper we present the techniques developed for CH_4 extraction from air and combustion to CO_2 as well as for graphitization and measurement of these samples by AMS. Exceptionally low levels of extraneous ^{14}C from processing are essential for minimizing the result uncertainties with such small, ^{14}C-depleted samples. We discuss how this has been achieved, as well as the methods for accurately determining procedural ^{14}C corrections for each part of the sample handling.

4.2. Extraction of CH_4 from the air stream and combustion to CO_2

4.2 a. Pre-existing CH_4 extraction line description

To prepare the sample for $^{14}CH_4$ analysis by AMS, CH_4 was separated from the bulk air and combusted to CO_2 at the National Institute of Water and Atmospheric Research, Ltd (NIWA) in Wellington, New Zealand. This type of processing is common with modern atmospheric samples for both ^{13}C and ^{14}C of CH_4 measurements (Eisma et al., 1994; Lowe et al., 1988). The CH_4 extraction line and procedure used for atmospheric CH_4 work at NIWA was described in Lowe et al. (1991). Briefly, air entering this line passes first through two spiral traps at liquid nitrogen (LN_2) temperature to remove H_2O, CO_2 and other volatile organic compounds (VOCs). The air stream then passes through a Schuetze reagent (Stevens and Krout, 1972) which oxidizes CO to CO_2, and then through two additional traps at LN_2 temperature to remove the CO-derived CO_2. The air stream then enters a furnace at 700˚C containing platinized alumina pellets, where CH_4 is combusted to CO_2. The resulting CO_2 is then captured on three LN_2-cooled traps downstream of the furnace.

4.2 b. Pre-existing CH_4 line ^{14}C blank and sample memory

The pre-existing CH_4 line is used for ^{13}C and ^{14}C work on modern atmospheric samples. Because large amounts of sample air are easily obtainable, the combustion furnace is not evacuated between samples; instead ~40 standard liters (SL) of sample air are flushed through the line prior to starting CO_2 collection downstream of the furnace (although recently a furnace evacuation step has been added). Effects on C isotopes from small amounts of residual C from previous samples are negligible because the variation in $\delta^{13}CH_4$ and $^{14}CH_4$ activity from sample to sample is relatively small. It was this procedure (although with a smaller flush of ~8 SL to conserve sample) that was first applied as a test to 2 sets of blank (^{14}C-dead) samples. Each blank sample set was run following large volumes of modern atmospheric air having been processed through the line (typical $^{14}CH_4$ = 130 pMC). Figure 4.1 shows a plot of $^{14}CH_4$ versus total volume of blank test gas flushed since the start of the test set. $^{14}CH_4$ in all samples was significantly above 0 pMC, with ^{14}C content declining in an approximately exponential fashion as more blank gas is flushed through the line. This clearly demonstrated that the pre-existing CH_4 line has a substantial carbon "memory". The slightly higher $^{14}CH_4$ for the "NIWA line blanks" set as compared to the Greenland melt-extraction blanks is most likely due to slightly lower [CH_4] for that set, which results in the contaminating CO_2 that is being continuously outgassed from the line constituting a larger fraction of the total sample. Furthermore, the $^{14}CH_4$ for both test sets remained significantly above 0 pMC even after 400-500 SL of gas was flushed through the line. This showed that the line also has either a constant non-zero

^{14}C blank, or a long-term carbon memory due to the very large amounts of modern air it is routinely exposed to. The observed ^{14}C blank and sample C memory most likely arise from the relatively large amount (~200 g) of platinized alumina used as the catalyst for CH_4 combustion. Alumina is known to have very large surface area, which probably makes retention of significant amounts of CO_2 on the catalyst surface possible.

In an effort to eliminate the line ^{14}C memory and blank a modified procedure was developed which included the evacuation of the combustion furnace (down to 1 Pa with vacuum applied) and flushing of the entire line with 60 SL of CH_4-free ultra-high purity (u.h.p.) air in between samples. $\delta^{13}CH_4$ results from tests with this modified procedure (not shown) indicated that sample-to-sample carbon memory was no longer significant. The line $^{14}CH_4$ blank was then tested again with gas mixtures containing 511-613 ppb of CH_4 from a fossil gas field, which had been shown to have a $^{14}CH_4$ of 0.6 pMC or lower. For a total of 4 test samples of 20-30μg C size, the average $^{14}CH_4$, normalized to average [CH_4] (to account for greater relative contamination expected for lower-[CH_4] samples), was 2.6 pMC with a standard deviation of 0.9 pMC. This demonstrated that although the CH_4 line ^{14}C blank had been reduced with the modified procedure, significant blank and blank variability remained. A new CH_4 conversion line was therefore developed for processing the Pakitsoq samples and is described in detail below.

4.2 c. High [CO] and ^{14}C of CO in Pakitsoq ancient air samples

A further complication in processing air samples extracted from glacial ice for $^{14}CH_4$ is the possibility of ^{14}C contamination from CO. Any CO in the samples that breaks through the CO-oxidizing reagent in the line is oxidized to CO_2 in the furnace, and this CO_2 is then collected along with CH_4-derived CO_2. Air samples extracted from Pakitsoq ice contain very high [CO] (800 – 2,500 ppb) as compared to modern ambient air concentrations (40 – 200 ppb). The fact that this high [CO] is not an artefact of the melt-extraction is confirmed by the low [CO] in the extraction blanks (20-40 ppb), as well as by independent measurements of [CO] in Pakitsoq ice conducted at Washington State University, which yielded values in excess of 800 ppb (unpublished). The source of this extremely high [CO] is not well understood. Haan and Raynaud (1998) measured [CO] in Greenland ice core samples, and for gas ages between 1,000 and 1,600 AD found concentrations between 100 and 180 ppb, high variability, and a general trend of [CO] increasing with age. They suggest the slow oxidation of organic matter in Greenland ice as the most likely explanation for the elevated [CO] values. Colussi and Hoffmann (2003) suggested that elevated [CO] in Greenland ice can be explained by photolysis of organic matter by UV Cerenkov radiation from cosmic muons passing through the ice. It is thus likely that our very high [CO] originates from organic matter in the ice.

CO is mainly of concern for the $^{14}CH_4$ measurements because carbon-14 of CO (^{14}CO) in glacial ice can be elevated, owing to in-situ cosmogenic production in the upper ~10 m of the firn (Lal et al., 2000). Energetic ^{14}C is produced by neutron-induced spallation of oxygen nuclei in the ice crystals, and most of it is quickly

oxidized to either ^{14}CO or $^{14}CO_2$. Some of the resulting ^{14}CO remains trapped in the ice crystal lattice, however, it may also be expelled into the interstitial spaces and lost back to the atmosphere during re-crystallization. A study by Lal et al. (2000) on 12 GISP2 ice samples between 125 m and 1838 m depth found ^{14}CO concentrations ranging between 10 and 930 ^{14}CO molecules g^{-1} of ice, with an average of 298 molecules g^{-1} ice; although other studies on glacial ice have found lower values (Smith et al., 2000; Van de Wal et al., 2007). Two early measurements of ^{14}CO in Pakitsoq samples, done by dilution, yielded 38 ± 45 ^{14}CO molecules/gram ice (the large uncertainty arises from the dilution factor of ~1:600). For comparison, ice of Younger Dryas age (~12,000 calendar yr BP) is expected to contain only about 0.5 $^{14}CH_4$ molecules g^{-1} ice (in air bubbles). Thus, quantitative removal of CO was essential to ensure that ^{14}CO did not interfere with sample $^{14}CH_4$.

Tests of the Schuetze reagent (used in the pre-exisiting CH_4 line) CO conversion efficiency (not shown) indicated that up to 1% breaks through at high [CO] comparable to those in the Pakitsoq samples. At this CO break-through rate and ^{14}CO content, almost as much ^{14}C in the processed sample would be coming from CO as from CH_4, which is unacceptable.

To address this problem, two traps in series, each containing ~10 g of the Sofnocat 423 reagent (Molecular Products Group LTD, Essex, U.K.), were used as a replacement for the Schuetze reagent to oxidise CO to CO_2 at room temperature, followed by cryogenic removal with two LN_2-cooled Russian doll traps in series (Figure 4.2). Sofnocat has been previously shown to be very effective at CO oxidation

(Foulger and Simmonds, 1993). Table 4.1a summarises our preliminary tests with Sofnocat 423 and Table 4.1b shows the results of CO removal tests with Sofnocat conducted on the new CH_4 conversion line immediately prior to processing the Pakitsoq air samples for $^{14}CH_4$. As can be seen, even small amounts of Sofnocat can quantitatively remove up to 7,000 ppb of CO. The [CH_4] values in the test gas prior to and after passing through the Sofnocat indicate that CH_4 is unaffected. Tests conducted on the new CH_4 line indicate that the CO removal factor is at least 500x for each part of the Sofnocat trap (comparing test results with the [CO] blank and taking [CO] measurement errors into consideration). The minimal CO removal factor for the two parts of the Sofnocat trap combined in series is then 250,000. At this removal efficiency and assuming a maximum ^{14}CO of 83 molecules / gram ice for Pakitsoq samples (upper range of measurements listed above), the ^{14}C from CO that breaks through the Sofnocat would amount to $< 0.1\%$ of the expected ^{14}C from CH_4 and is thus negligible.

One further concern was whether the two Russian doll cryogenic traps downstream of the Sofnocat (Figure 4.2) were capable of quantitative removal of CO-derived CO_2. Brenninkmeijer (1993) described the use of Russian doll traps of very similar construction to ours for removing CO-derived CO_2. In his tests with a single trap containing two nested glass fibre thimbles with a 7 L/min flow rate, a 98% CO_2 removal efficiency was observed for a gas with [CO] of 20 ppb, and a 99.5% efficiency was observed for a gas with [CO] of 250 ppb. We take these values as a very conservative lower limit for the CO_2 trapping efficiency in our system, because

our Russian doll traps contained 3 nested glass fibre thimbles rather than 2; our flow rate was much lower at 0.8 SL/min, and our starting [CO] was much higher at 800 – 2,000 ppb, which should all result in better trapping than in the Brenninkmeijer (1993) tests. We then calculate that at the maximum possible ^{14}CO based on above measurements, the ^{14}C from CO which breaks through the Russian doll traps would amount to no more than 1.7% of the total ^{14}C from CH_4 in the samples. For $^{14}CH_4$ of ~30 pMC (typical for our samples), this would amount to an extra 0.5 pMC. However, as discussed above, this is almost certainly an overestimate.

4.2 d. The new CH_4 extraction line: description

To overcome the procedural issues described above, a new CH_4 extraction line was developed (Figure 4.2). This new line utilizes ~1 g of platinized quartz wool (Schimadzu Scientific Instruments, USA) packed to a length of ~55 mm into a 25 mm ID quartz tube at 700˚C for CH_4 combustion. Quartz wool has lower surface area than alumina; this combined with the much smaller overall amount of catalyst serves to minimize the carbon blank and sample memory in the line. The new line's smaller overall internal volume (< 700 cm^3) and surface area possibly also aids with reducing the blank. CO is oxidized by two Sofnocat traps in series, each containing ~10 g of the reagent; and the resulting CO_2 is then removed by two LN_2-cooled "Russian doll"-type traps. Air is pulled through the line by a two-stage rotary vane pump.

4.2 e. CH_4 conversion efficiency and N_2O production in the new line

Extensive testing of the new CH_4 line was conducted to optimize CH_4 conversion to CO_2, check line performance stability and ^{14}C blank, and investigate the possibility of interference from other hydrocarbons in the Pakitsoq samples. The initial phase of testing focused on optimizing CH_4 conversion efficiency while minimizing the production of N_2O in the combustion furnace. CH_4 conversion efficiency near 100% is important for maximum sample recovery as well as for avoiding significant isotopic fractionation, which occurs at lower conversion efficiencies. N_2O is produced from the N_2 and O_2 in the sample air stream on the platinized surface of the catalyst at high temperatures. We also observed this phenomenon in the pre-existing CH_4 line, and some test results suggested a link between relatively higher N_2O / CO_2 ratios in the combusted samples and extremely slow and incomplete graphitization of the sample CO_2 during AMS lab processing (Smith et al., 2007).

Figure 4.3a shows a comparison of furnace performance when packed with the platinized quartz wool to 35 vs 55 mm length. As expected, the CH_4 conversion efficiency as well as the rate of N_2O production both increase with temperature. It can be seen that in the 55 mm configuration (which also had a slightly lower gas flow rate of 0.8 SL/min as compared with 1.0 SL/min for the 35 mm case) essentially complete CH_4 combustion is achieved for lower values of N_2O / CO_2, which was desirable. Because of this we chose the 0.8 SL/min flow & 55mm catalyst configuration for further tests as well as actual sample processing. However, later experiments

demonstrated that N_2O does not in fact interfere with the graphitization reactions (Smith et al., 2007).

Figure 4.3b compares CH_4 conversion efficiencies for gases with different [CH_4]. The dependence of the CH_4 conversion efficiency on the sample [CH_4] as well as changes in the conversion efficiency over time are important to understand because they affect the line sample yield, which is an important indicator of line performance. For the 434 and 1740 ppb [CH_4] gases, the conversion efficiencies are essentially the same once the combustion is more than 99% efficient, but appear to be lower for the 434 ppb gas at lower temperatures where efficiencies start to decrease. This makes sense as we would expect a higher probability of reaction at the catalyst surface for gases with higher [CH_4]. Surprisingly, however, the conversion efficiencies for the 27,790 ppb test gas appear to be a few tenths of a percent lower than those for the 434 and 1740 ppb [CH_4] gases. This may be due to the available surface area on the catalyst being insufficient for such high [CH_4].

Further tests were conducted to monitor any changes in the performance of the new CH_4 line over time (Figure 4.3c). The March 2-4 tests were conducted less than a week after the catalyst was first loaded into the furnace. Approximately one month later (April 7 tests), both the CH_4 conversion efficiency and the rate of N_2O production had decreased slightly. This may be due to either a fraction of the platinized quartz wool surface becoming de-activated or to a slight gradual compaction of the quartz wool in the furnace tube, leaving less catalyst surface area available for interaction with the sample air stream. The tests from June 26 also show a CH_4 conversion

efficiency decrease as compared to the March 2-4 tests. It is unclear whether the conversion efficiency had decreased further since the April 7 tests, because the June 26 tests were conducted with a gas with lower [CH_4] (493 ppb), and the slightly lower observed conversion efficiencies as compared to the 1734 ppb test gas of April 7 are expected.

4.2 f. Sample yield and $\delta^{13}CH_4$ performance of the new line

Sample yield and $\delta^{13}CH_4$ are important indicators of the CH_4 line performance and can be used to characterise mass-dependent fractionation during processing as well as to identify addition of extraneous carbon (e.g., from air leaks), both of which may affect measured sample $^{14}CH_4$. Sample yield is defined as (amount CO_2 actually recovered) / (amount CO_2 expected) * 100%. Sample yield and $\delta^{13}CH_4$ were monitored during testing and sample processing.

Mass-dependent isotopic fractionation in the CH_4 line is linked closely to the sample yield and arises primarily due to 1) fractionation in the furnace due to incomplete combustion, 2) fractionation due to incomplete CO_2 trapping downstream of the furnace and 3) fractionation due to incomplete CO_2 transfers in the final stages of sample handling. All of the above effects decrease the sample yield, and our tests indicated that each of them also lowers the sample $\delta^{13}C$ (Table 4.2, Figure 4.4). Figure 4.4 shows changes in the sample yield and resulting $\delta^{13}C$ over time for a ~500 ppb [CH_4] test gas with no changes to the procedure. Changes in $\delta^{13}C$ follow the changes in sample yield, with lower $\delta^{13}C$ (more fractionation) observed for lower yields. Because no modifications to the procedure or the physical components of the

CH_4 line were made during this period, it is very unlikely that the decreasing yield and $\delta^{13}C$ are due to changes in CO_2 loss during trapping or CO_2 transfer. Instead, the CH_4 conversion efficiency of the furnace must be decreasing with time. This is consistent with our observations from direct GC measurements of gas exiting the CH_4 line (Figure 4.3c). Typical sample yields are 2-6% lower than the conversion efficiencies observed from GC tests. Part of this is probably due to the loss of some CO_2 during trapping and CO_2 distillation. In addition, the pressures in the furnace were slightly higher during the GC tests as compared to normal sample runs (due to different vacuum pumps used), which increases gas residence time in the furnace and may have resulted in higher conversion efficiencies.

Table 4.2 shows the results of several tests conducted to investigate the factors influencing sample $\delta^{13}C$ and yield, as well as to check the suitability of the overall procedure for handling the Pakitsoq $^{14}CH_4$ samples. Test 1 demonstrates that incomplete trapping of CO_2 downstream of the furnace results in a ^{13}C depletion of the trapped CO_2. ^{13}C depletion from incomplete CO_2 trapping has previously been observed by Brenninkmeijer and Rockmann (1996). The results of test 2 demonstrate that a sample ^{13}C depletion also occurs if a significant portion of the sample is left behind during CO_2 transfer between traps.

Overall, our tests demonstrated that although fractionation was occurring in the CH_4 line, its effect on the sample ^{14}C was negligible compared to the overall $^{14}CH_4$ measurement uncertainty for Pakitsoq samples (~1 pMC). For example, the maximum observed $\delta^{13}C$ shift due to processing fractionation for a ~ 500 ppb [CH_4] sample was -

0.6 ‰. A typical $^{14}CH_4$ value for the Greenland samples is ~ 30 pMC; assuming all the fractionation is mass dependent, this translates to a shift of -0.04 pMC in ^{14}C, or only 4% of the overall measurement uncertainty. $\delta^{13}CH_4$ was measured in the Greenland samples using GC-IRMS (Ferretti et al., 2005) and some of the values have been reported in Schaefer et al. (2006). Because our ^{14}C AMS measurements used the sample ^{13}C beam as a reference, a CH_4 line fractionation correction was made to the measured Pakitsoq sample $\delta^{13}CH_4$ values based on the test results.

The Pakitsoq air samples were saturated with H_2O vapor because the samples were not dried during the melt-extraction. Tests suggested that due to this, the upstream LN_2-cooled traps could become blocked with ice in the duration of a sample run. To lower the H_2O vapor pressure in the sample tanks and reduce the risk of ice build-up in traps, sample tanks were kept in a bucket of ice while being processed. However, this introduces the possibility of a slight thermal fractionation of the CH_4 isotopes between the top and the bottom of the tank. In addition, to utilize the maximum amount of sample possible, the sample tanks were run down to a pressure of 0.3 bar. It was suspected that some isotopic fractionation could also be caused by the mass flow controller at these low tank pressures. A test was conducted to check the possible effects on sample yield and $\delta^{13}C$ of cooling the sample tank and running it down to 0.3 bar. No significant differences relative to control runs were found in either yield or $\delta^{13}C$ (Test 4 in Table 4.2).

4.2 g. Tests of breakthrough of light non-methane hydrocarbons

The Pakitsoq samples contained 1 – 6 ppb each of ethane (C_2H_6), ethene (C_2H_4) and ethyne (C_2H_2), as indicated by gas chromatography – mass spectrometry (GCMS) measurements (technique described in Mühle et al. (2007). All the melt-extraction blanks contained less than 1 ppb of each of these, indicating that the light hydrocarbons originate mostly from the sample ice. Each of these compounds is volatile enough to possibly pass through LN_2-cooled traps in the upstream part of the CH_4 line and be combusted along with the sample CH_4 in the furnace. Since the ^{14}C of these C_2 hydrocarbons is unknown, this introduces a possible risk of contamination to the $^{14}CH_4$. To test whether any of the light C_2 hydrocarbons break through the upstream traps, a gas mixture containing 443 ppb of CH_4 and 114 ppb each of ethane, ethene and ethyne, as well as 5 other light hydrocarbons was run through the line dry as well as with H_2O vapor added to better simulate the Pakitsoq samples. The results (Table 4.2) show no noticeable increase in the yield for either of these tests, and indicate that any ^{14}C interference from C_2 hydrocarbons should be negligible. It is likely that the Sofnocat reagent plays a role in removing the C_2 hydrocarbons by oxidation to more condensable compounds, as the removal of C_2 and other hydrocarbons by Sofnocat was also observed by Ferretti et al. (November, 2005). Russian doll traps probably also play a role in the removal of C_2 hydrocarbons, as was observed by Brenninkmeijer (1991) and Pupek et al. (2005).

4.2 h. Final procedure used with the new CH_4 line

To minimize the carbon blank and sample memory, the line was kept evacuated while not in use. Quantitative leak-checks were performed on both the upstream and downstream parts of the line at the start of each day to ensure that any extraneous carbon added from leaks during a sample run would not exceed 0.1% of the total sample carbon. Leak checks were also performed on all connections to tanks containing sample, blank and reference gases. The furnace temperature was kept constant at 697-698° C. Prior to starting a sample run, the line was flushed with CH_4-free u.h.p. air at 0.8 SL/min for 15 min. A 1-h long flush followed any high [CH_4] (~28 ppm) samples or larger than usual (> 25 μg C) samples of modern air.

The flow of sample air (also at 0.8 SL/min) was started immediately after stopping the flow of the flush gas. CO_2 collection downstream of the furnace was started 3 min after starting the flow of the sample air. The LN_2 in all traps was topped up every 10 min and the glass stem valves downstream of the traps were warmed with a heat gun every 10 min (earlier tests determined that there was a risk of small leaks through the valves if they became too cold). Typical line pressures at gauges 2 and 3 (Figure 4.2) during a run were 260 and 55 mbar, respectively. After completing the sample collection, the resulting CO_2 was vacuum-distilled using LN_2 and an ethanol-dry ice mixture to separate it from the H_2O (produced during CH_4 combustion). The sample size was determined in a small calibrated volume using a capacitance manometer, and the sample CO_2 was then flame-sealed in a pre-cleaned 6mm Pyrex® tube. Prior to starting the next sample, the furnace was evacuated to < 0.05 mbar, and the entire line to <1 mbar. If the previous sample contained a lot of moisture (such as

all the Pakitsoq samples and melt-extraction blanks), all the upstream traps were also dried prior to starting the next sample.

4.3. Sample graphitization and AMS measurement

The CO_2 derived from CH_4 in the Pakitsoq samples was converted to graphite and measured by AMS at the Australian Nuclear Science and Technology Organisation (ANSTO) in Menai, Australia. A full description of the ANSTO graphitization procedures can be found in Hua et al. (2004) and Smith et al. (2007). ANSTO operates two machines for AMS, the 10 MV ANTARES accelerator (Fink et al., 2004), and the 2MV STAR accelerator, the latter manufactured by High Voltage Engineering Europa (HVEE). All Pakitsoq and test samples were measured on the ANTARES accelerator, utilizing the 4+ charge state, which gives a greater yield than the 3+ beams utilized on the STAR accelerator. Maximizing efficiency to produce the highest possible ^{14}C counting rate is essential for obtaining good measurement precision with low-^{14}C samples in the 20 μg range. Only the ^{13}C and the ^{14}C beams are normally measured on ANTARES, and the sample ^{14}C activity is corrected to the known $\delta^{13}C$ of the submitted sample.

Sample preparation procedures were modified from those given in Hua et al. (2004) in several ways in order to improve the graphitization rate, yield, and blank for small samples (10 – 45 μgC). First, the water vapor traps used with Pakitsoq samples consisted of an aluminum heat pipe immersed in a capped bath of ethanol and dry ice, giving cold trap temperatures of –60 to –70 ˚C during the graphitization reaction, as

opposed to the standard ANSTO procedure of using Peltier chillers with a minimum temperature of – 39˚C. Second, we used 1 mg of Sigma-Aldrich-400 (SA-400) 99.99+% purity Fe powder catalyst (SA-400) for the reduction of CO_2 to graphite in the presence of hydrogen (H_2) instead of 1 mg of Cerac-325 Fe powder (99.9% purity). Third, we added the step of pre-cleaning all flame-sealed Pyrex® tubes containing sample CO_2 with ethanol and handled the tubes only with vinyl gloves. Fourth, the pumping time on the sample tubes prior to cracking the tubes on the vacuum line to release the sample CO_2 was increased from 1 min to 5 min and a vacuum leak check step was added. Finally, a new system was developed for pressing the graphite from samples containing < 500 μgC into aluminum cathodes. The standard ANSTO procedure for such samples involves front-pressing the Fe-graphite mixture with a pin and hammer into a 1 mm recess. This results in considerable variation in the depth of the sample surface below the cathode surface, depending on the amount of the Fe-graphite mixture pressed. There is also variation in resultant sample density and surface finish. Eliminating this variability with the new pressing system results in much improved and reproducible behavior of the sample in the ion source.

In the course of work on the Pakitsoq samples and associated tests, over 100 samples containing < 45 μg C were processed using ~1 mg of SA-400 Fe powder as a catalyst and the described dry ice / ethanol cold trap. As a result of these procedural modifications, the graphitization reaction times for such small samples were decreased from 2.5 hr – 4 days to ≤ 80 min for all samples (Table 4.3). Such dramatic

improvement in the reaction rates was shown to be due to the more efficient water vapor trapping (Smith et al., 2007).

The graphitization reaction yields were also improved, from 61 – 90% to 80 – 95% for samples containing 15 – 45 μgC (Table 4.3). Prior tests (Smith et al., 2007) suggested that lower cold trap temperatures do not significantly affect the reaction yield; it is therefore most likely that the higher yields are due to the higher surface area of SA-400 than of Cerac-325 Fe catalyst. Improving graphitization yields was important because isotopic fractionation has been previously observed at ANSTO for samples with graphitization yields < 85% (Hua et al., 2001); low yields also mean less available graphite for the AMS measurement. One graphite sample prepared using the new technique from 20 μg of CO_2, which had been derived from the Oxalic-1 standard (OX-1), was measured for $\delta^{13}C$ by Elemental Analyzer – Isotope Ratio Mass Spectrometry. This sample had a graphitization yield of 82.7% and gave a $\delta^{13}C$ of –20.0 ‰. The consensus $\delta^{13}C$ value of OX-1 is -19.3 ‰ (Stuiver, 1983). This suggests that the amount of isotopic fractionation during graphitization of small samples with the new technique is small. This is further confirmed by the ^{14}C results on small test samples presented below.

Because of the low ^{14}C activity (~30 pMC) and the small size of the Pakitsoq samples (most between 15 – 25 μg C), minimizing the ^{14}C processing blanks was of key importance. Earlier determination of the graphitization blank at ANSTO (Hua et al., 2001) found an extraneous carbon mass of 0.14 ± 0.02 μg if a ^{14}C activity of 100 pMC is assumed. Our tests (see Section 4 b) show that with the modified procedure

this blank has been reduced to 0.03 μg of 100 pMC carbon. Although no tests were conducted to investigate the effect of each procedural modification on the blank by itself, it is likely that the most important factor in reducing the blank was the use of the very high purity (99.99+%) SA-400 Fe catalyst.

4.4. ^{14}C results for standards and process blanks and ^{14}C corrections

4.4 a. The general correction method and ^{14}C units used

The Greenland $^{14}CH_4$ samples underwent four major stages of handling, each of which is likely to be associated with the addition of extraneous carbon and/or isotopic fractionation. First, the ancient air trapped in glacial ice was obtained by the means of a vacuum melt-extraction in the field (see Chapter 3). Second, the CH_4 in this air was combusted and the resulting CO_2 collected. Third, the sample CO_2 was converted to graphite. Finally, the ^{14}C was measured by AMS. The simulated gas extractions, conducted in Greenland along with the actual air extractions from ice, were performed using a single standard gas mixture containing ~500 ppb CH_4 in u.h.p. air. These simulated extractions did not therefore mimic the full range of [CH_4] found in our real samples (~400 – 800 ppb), and can not be used to accurately assess the overall ^{14}C blank for all stages of sample handling. It is therefore necessary to assess each of these handling blanks separately.

Assuming that the effects of isotopic fractionation for each processing step are known or insignificant (see further discussion of this below), the general approach for correcting sample ^{14}C is as follows.

$$M_{final}\,{}^{14}C_{final} = M_{true}\,{}^{14}C_{true} + M_{extr}\,{}^{14}C_{extr} \quad (4.1)$$

Where M_{final} and $^{14}C_{final}$ are the carbon mass and ^{14}C specific activity of the processed sample, M_{true} and $^{14}C_{true}$ are the true carbon mass and ^{14}C specific activity of the unprocessed sample and M_{extr} and $^{14}C_{extr}$ are the carbon mass and ^{14}C specific activity of the extraneous carbon added during processing.

To stay consistent with prior work on atmospheric $^{14}CH_4$ (Lassey et al., 2007; Wahlen et al., 1989), we use the units of percent modern carbon (pMC) for reporting our results and making corrections to ^{14}C for extraneous carbon added during processing. As accepted at the 8th International Conference on Radiocarbon Dating, pMC is defined as:

$$pMC = \frac{A_{SN}}{A_{ON}} \times 100 \quad (4.2)$$

(Stuiver and Polach, 1977). Here A_{ON} is the normalized ^{14}C activity of the Oxalic-1 standard (Ox-1), and A_{SN} is the normalized ^{14}C activity of the sample, both also as defined in Stuiver and Polach (1977).

The pMC unit is not exactly mass-additive in the sense defined by Equation 4.1 because it is not a specific activity. It is, however, approximately mass-additive. For the very small levels of extraneous carbon added during the processing of Pakitsoq

samples (< 0.4 μg, see discussion below), the errors in ^{14}C correction calculations arising from using the pMC units amount to <0.3% of sample ^{14}C value, or < 0.1 pMC for samples with ^{14}C = 30 pMC (typical for Pakitsoq samples). As these errors are at least an order of magnitude smaller than the typical overall ^{14}C uncertainties after all corrections (~1.0 pMC), we find the pMC unit acceptable to use in the corrections calculations.

4.4 b. Corrections for processing blank and fractionation at ANSTO

36 blank and standard samples were measured to assess the fractionation and blank from processing at ANSTO (Table 4.4). Small (10, 20 and 40 μg C) samples of blanks and standards were decanted from larger "parent" samples (~220 - ~10,000 μg C) without affecting the sample ^{14}C through mass-dependent fractionation (see Table 4.4 caption), and both the small and parent samples were graphitised and measured for ^{14}C. As can be seen from the table, the agreement between the small samples and the larger parent samples is very good for all samples and often within the measurement errors. For the blank samples, if we assume that the average of the 4 large blanks represents the true ^{14}C of the marble (0.15 pMC), then the average of the four ~10μg blank samples (0.43 pMC) is only shifted by 0.28 pMC from the true value. This indicates a remarkably low ^{14}C blank. For example, assuming that the ^{14}C of the contaminant is 100 pMC, its mass is 0.03 μg. This low level of extraneous carbon and the fact that previous ANSTO work has demonstrated that no significant isotopic fractionation takes place for graphitization of samples ≥ 100 μgC (Hua et al., 2001), allows us to assume that the large "parent" samples represent the true ^{14}C values and

determine the blank corrections based on the observed shifts between the parent and small samples. Graphitization reactor #1 had a higher blank than the other reactors used (Table 4.4); this was further confirmed by the uncorrected ^{14}C observed in CH_4 line and Greenland melt-extraction processing blanks (not shown). We therefore treated reactor 1 separately in determining the ^{14}C corrections.

Assuming that $M_{final} = M_{true} + M_{extr}$, Equation 4.1 above can be re-arranged to yield:

$$(^{14}C_{final} - ^{14}C_{true})M_{true} = -^{14}C_{final}M_{extr} + ^{14}C_{extr}M_{extr} \quad (4.3)$$

In this case M_{final} and $^{14}C_{final}$ refer to the graphite sample as measured on the accelerator. Fractionation has negligible effects for blank samples, so the only process by which their ^{14}C can be shifted is addition of extraneous carbon. We know $^{14}C_{true}$ from the measurements on the (large) parent samples; M_{true} is also known for all samples. If $(^{14}C_{final}-^{14}C_{true})*M_{true}$ is plotted against $^{14}C_{final}$, the slope should be $-M_{extr}$ and the intercept $^{14}C_{extr}*M_{extr}$, so the mass and ^{14}C of the extraneous carbon added during processing can in principle be determined. When this is done for all blanks except those processed in reactor 1, however (plot not shown), a positive slope results, suggesting a negative M_{extr}, which has no physical meaning. We suspect that this is caused by the relatively small number of blanks measured for each mass which results in under-sampling of the full ^{14}C variability for the blanks and deviations in the calculated mean ^{14}C for each mass from the true mean.

All the blank and standard samples must therefore be considered together to determine the ^{14}C corrections for ANSTO processing. This complicates the situation somewhat because for non-blank samples, isotopic fractionation during graphitization, as well as during the accelerator measurement, may also have an effect on ^{14}C. The effect of isotopic fractionation alone on the ^{14}C of the processed sample will be proportional to the ^{14}C content of the sample:

$$^{14}C_{processed} = \alpha_0 {}^{14}C_{initial} \tag{4.4}$$

Here α_0 is a fractionation coefficient. In our case the mass of the small samples is variable; since larger fractionation had previously been observed at ANSTO for smaller samples (Hua et al., 2001), a good first-order approximation is that the effect of fractionation is inversely proportional to mass. This can be parameterized as follows:

$$^{14}C_{processed} = (1 + \frac{\alpha}{M_{true}}) {}^{14}C_{initial} \tag{4.5}$$

In this case α is a constant fractionation coefficient that has units of mass. To combine the effects of fractionation and addition of extraneous carbon we need to make some assumptions regarding whether the fractionation happens before or after the extraneous carbon is added (or both). However, considering that the amount of

extraneous carbon and its effects on the ^{14}C are clearly very small, this choice will have negligible effects on the ^{14}C correction. We will therefore assume that all fractionation happens after the extraneous carbon is added. Solving Equation 4.3 for $^{14}C_{final}$ and adding the effect of fractionation as parameterized in Equation 4.5, we get:

$$^{14}C_{final} = (1 + \frac{\alpha}{M_{true}}) \frac{^{14}C_{true} M_{true} + ^{14}C_{extr} M_{extr}}{M_{true} + M_{extr}} \tag{4.6}$$

Multiplying through by (M_{true} +M_{extr}) and expanding all the terms gives:

$$^{14}C_{final} M_{true} + ^{14}C_{final} M_{extr} = ^{14}C_{true} M_{true} + ^{14}C_{extr} M_{extr} + \frac{\alpha}{M_{true}} ^{14}C_{true} M_{true} + \frac{\alpha}{M_{true}} ^{14}C_{extr} M_{extr}$$

(4.7)

Based on how close to true ^{14}C values both the blank and standard samples measured, we know that both the mass of extraneous carbon and the effect of fractionation on ^{14}C must be quite small, meaning that $M_{extr} << M_{true}$ as well as $\alpha << M_{true}$. The last term in (4.7) is therefore negligible compared to the others, and the equation simplifies to:

$$^{14}C_{final} M_{true} + ^{14}C_{final} M_{extr} = ^{14}C_{true} M_{true} + ^{14}C_{extr} M_{extr} + \alpha ^{14}C_{true} \tag{4.8}$$

The $\alpha^{14}C_{true}$ term can be expanded to $\alpha^{14}C_{final}+ \alpha\ (^{14}C_{true}-^{14}C_{final})$. Because both α and $(^{14}C_{true}-^{14}C_{final})$ are very small, the term $\alpha\ (^{14}C_{true}-^{14}C_{final})$ is negligible compared to the other terms in Equation 4.8. The equation can then be re-written as

$$^{14}C_{final}M_{true}+^{14}C_{final}M_{extr}=^{14}C_{true}M_{true}+^{14}C_{extr}M_{extr}+\alpha^{14}C_{final} \quad (4.9)$$

Further re-arranging yields

$$M_{true}(^{14}C_{final}-^{14}C_{true})=^{14}C_{final}(\alpha - M_{extr})+^{14}C_{extr}M_{extr} \quad (4.10)$$

M_{true}, $^{14}C_{final}$ and $^{14}C_{true}$ are known, so $M_{true}(^{14}C_{final}-^{14}C_{true})$ can now be plotted against $^{14}C_{final}$ and a linear least-squares fit applied to find the slope $(\alpha-M_{extr})$ and the intercept $^{14}C_{extr}M_{extr}$.

Figure 4.5 shows these plots for all the blanks and standards processed through graphitization reactors 2, 3 and 5 (a) as well as for those processed through reactor 1 (b). Surprisingly, the slopes are positive, suggesting that $\alpha > M_{extr}$ and that there is a ^{14}C-enriching fractionation. We speculate that this may result from fractionation in the accelerator, since fractionation during graphitization results in a ^{14}C depletion. Knowing the slope and the intercept, the correction applied to determine the true ^{14}C prior to ANSTO processing is:

$$^{14}C_{true}=^{14}C_{final}-\frac{^{14}C_{final}\times \text{slope} + \text{intercept}}{M_{true}} \quad (4.11)$$

The effect of these corrections is small, and is illustrated for two samples in Table 4.7.

4.4 c. Corrections for CH_4 extraction line blank

Effects of mass-dependent fractionation on ^{14}C during the CH_4 combustion and separation from the air stream were shown above to be negligible for the Greenland samples; we therefore do not consider fractionation in determining the corrections for this stage of sample processing. There are, however, two possible mechanisms by which extraneous carbon can be added. The first is independent of the time it takes to run the air sample through the CH_4 extraction line; we will refer to the ^{14}C and mass of this type of extraneous carbon as $^{14}C_{fixed}$ and M_{fixed} and assume that both of these are constant. An example of this would be extraneous carbon added during the flame-sealing step. The second mechanism involves gradual addition of extraneous carbon with a ^{14}C activity of $^{14}C_{time}$ over time t at a rate of R μg/min. Examples of this are carbon from CO_2 in ambient air from leaks and gradual outgassing of CO_2 from the CH_4 line components. The mass ratio of extraneous carbon to sample CH_4 carbon for this second process will be inversely proportional to $[CH_4]$ of the air sample. The relationship between the $^{14}C_{final}$ post-processing and $^{14}C_{true}$ pre-processing can then be written as:

$$^{14}C_{final}M_{final} = {}^{14}C_{true}M_{true} + {}^{14}C_{fixed}M_{fixed} + {}^{14}C_{time}Rt \qquad (4.12)$$

Here $^{14}C_{final}$ is the ^{14}C with ANSTO processing corrections applied, and M_{final} is as determined at ANSTO prior to graphitization.

Table 4.5 gives a summary of the samples run to determine the CH_4 line procedural blank. As can be seen from the ^{14}C (corrected for ANSTO processing blank), the CH_4 line blanks are also very low, with very good agreement between large, high-[CH_4] samples and small, low-[CH_4] samples for which the CH_4 originated from the same air tank (Table 4.5 caption). In principle, the fixed and time-dependent components of extraneous carbon added can be determined by comparing the ^{14}C results between the sample sets shown. However, precise determination of the process blank is complicated by the fact that the magnitude of the ^{14}C differences between sets of samples containing identical CH_4 (all the ^{14}C-dead samples; all the modern samples) are similar to the ^{14}C uncertainties. A further complication is an outlier with a high ^{14}C in the 1,000 ppb ^{14}C-dead set (1.08 pMC, as compared to an average of 0.24 pMC for the other three samples in that set), for which we have no explanation. Nevertheless, a blank correction can still be determined as long as some simplifying assumptions are made. We first consider the two 500 ppb [CH_4] sets. These samples were all of approximately the same carbon mass (as measured immediately prior to graphitization), so M_{final} is the same. Because their [CH_4] is also the same, the $^{14}C_{time}Rt$ term is the same for both sets. $^{14}C_{fixed}$ and M_{fixed} are both constant; this also means that the total amount of extraneous carbon added is the same for both sets and M_{true} is the same. Writing out Equation 4.12 for both 500 ppb sets and subtracting the two equations, we get:

$$({}^{14}C_{\text{final modern}} - {}^{14}C_{\text{final "dead"}})M_{final} = ({}^{14}C_{\text{true modern}} - {}^{14}C_{\text{true "dead"}})M_{true} \quad (4.13)$$

because all the extraneous carbon terms cancel. Because the blanks are clearly small, we take $^{14}C_{\text{true "dead"}}$ as the ^{14}C of the large 28 ppm [CH_4] sample set. In the same manner, $^{14}C_{\text{true modern}}$ can be approximated by the ^{14}C of the large 1,750 ppb sample set. In this way the M_{true}/M_{final} can be determined and from that the overall mass of extraneous carbon is found to be 0.23 ± 0.16 μg. The overall ^{14}C of extraneous carbon can then be calculated by applying Equation 4.1 to the 500 ppb ^{14}C-dead set, obtaining 23.57 ± 16.22 pMC.

A further simplification can be made when considering the relative importance of the fixed and time-dependent components of extraneous carbon addition. The large and small 1,750 ppb [CH_4] modern sets show excellent agreement in their ^{14}C. The time-dependent component would be the same for these two sets, so only the fixed component would produce differences in the ^{14}C. When comparing the 500 ppb modern and small 1,750 ppb modern sets, however, the fixed component would not produce a difference in the ^{14}C because the sample mass is the same for these two sets. Here the ^{14}C shows a larger difference between the sets, however, and only the time-dependent component can explain it. We therefore make the assumption that the fixed component is negligible and that all of the extraneous carbon is added in a time-dependent fashion. Equation 4.12 then simplifies, and given that now $M_{final} = M_{true} + Rt$, it can be rearranged to yield:

$$\frac{(^{14}C_{true} - {}^{14}C_{final})M_{true}}{t} = {}^{14}C_{final}R - {}^{14}C_{time}R \quad (4.14)$$

The expression on the left side can now be plotted against $^{14}C_{final}$. Because the amount of extraneous carbon added is very small, the mass as determined prior to graphitization provides a good estimate of M_{true} for the purposes of this plot; $^{14}C_{true}$ for the "dead" samples in known from the 28 ppm set, and can be estimated for the "modern" samples from the large 1,750 ppb set. This plot for all the ~20μg samples is shown in Figure 4.6. From the slope and intercept, R = 0.00188 ± 0.00153 μg/min, and $^{14}C_{time}$ = 42.16 ± 72.96 pMC. The large uncertainty in the intercept and $^{14}C_{time}$ arises from the surprisingly high ^{14}C of one of the 1,000 ppb samples.

Corrections to sample ^{14}C for CH_4 line processing are made according to:

$$^{14}C_{true} = \frac{(^{14}C_{final}M_{final} - {}^{14}C_{time}Rt)}{M_{final} - Rt} \quad (4.15)$$

The effect of these corrections for two of the Pakitsoq samples can be seen in Table 4.7; sample ^{14}C changes very little as a result, but the uncertainties increase substantially.

4.4 d. ^{14}C corrections for Greenland melt-extractions

The air for paleo $^{14}CH_4$ analyses was obtained from large volumes of ancient glacial ice outcropping on the ice sheet margin in West Greenland, and the details are presented in Chapter 3. Briefly, glacial ice was melted under vacuum in the field, and the released ancient air transferred to storage cylinders. 2-3 melt-extractions were performed to obtain air for each sample. Simulated gas extractions were conducted to mimic the effects of this procedure on sample ^{14}C and $[CH_4]$. A mixture of 500 ppb CH_4 in u.h.p. air was used in the simulated extractions ("CH_4 standard gas" in Table 4.6), and separate blank extractions were conducted for each type of actual sample taken, as illustrated in Table 4.6. The blank extractions were conducted in such a way that the combined amount of extraneous carbon added for all blank extractions should have been equal to that for all the actual melt-extractions for a particular type of sample (e.g., Oldest Dryas blanks and Oldest Dryas samples) (see Chapter 3).

As can be seen from comparing the $^{14}CH_4$ of the CH_4 standard gas (corrected for ANSTO and CH_4 line blanks) with that of the extraction blanks (Table 4.6), the effect on ^{14}C of extraneous carbon added during the melt-extractions is not significant given the uncertainties. Comparison of $[CH_4]$ in the extraction blanks with the CH_4 standard gas shows that the extraneous carbon comprises $< 0.7\%$ of the total sample carbon in all cases. Despite the very small observed effects on ^{14}C, we use the data from the extraction blanks to further correct the ^{14}C of the actual samples. Measurements of $\delta^{18}O$ of O_2 and $\delta^{15}N$ of N_2 in the Pakitsoq samples demonstrated that the melt-extraction does not result in significant gas isotopic fractionation (Chapter 3), so only effects of extraneous carbon on ^{14}C need to be considered as presented in

Equation 4.1. M_{extr} is easily determined for each type of sample from the [CH_4] offsets between the extraction blanks and the CH_4 standard. The true ^{14}C of the CH_4 standard gas is taken to be 0 pMC based on the ^{14}C results with ANSTO and CH_4 line corrections included, which makes for straightforward determination of $^{14}C_{extr}$ for each type of sample. The true $^{14}CH_4$ of the air present in the sampled ice is then determined from

$$^{14}C_{true} = \frac{^{14}C_{final} M_{final} - ^{14}C_{extr} M_{extr}}{M_{final} - M_{extr}} \qquad (4.16)$$

Here $^{14}C_{final}$ is the ^{14}C with ANSTO and CH_4 line corrections incorporated and M_{final} is the mass as measured prior to graphitization and corrected for extraneous carbon added in the CH_4 extraction line.

To illustrate the effect of the step-wise ^{14}C corrections we show the results for the two Oldest Dryas samples in Table 4.7. As can be seen, the corrections are small for each of the processing steps, with the ^{14}C uncertainties growing with each correction.

4.5. Summary and Conclusions

A new method has been developed for measurements of $^{14}CH_4$ in ancient air samples obtained from glacial ice. A new CH_4 conversion line was constructed and tested extensively to minimize the $^{14}CH_4$ processing blank. Our tests indicated that the mass and ^{14}C activity of extraneous carbon added during the combustion and

separation of CH_4 from the air stream were 0.23 ± 0.16 μg and 23.57 ± 16.22 pMC for ~20μg C, 500 ppb [CH_4] samples. This represents a dramatic improvement over our early attempts at processing small, ~500 ppb [CH_4] samples when the mass of extraneous carbon added was up to 2.6 μg if ^{14}C activity of 100 pMC is assumed. The new CH_4 line utilizes a small amount (~1 g) of platinized quartz wool for CH_4 combustion, as opposed to a much larger amount (~200 g) of platinized alumina used for the same purpose in the pre-existing CH_4 line. The lower ^{14}C blank and no detectable carbon sample memory in the new line are most likely a result of less CO_2 being adsorbed onto the much lower overall surface area of the platinized quartz wool catalyst. Keeping the line and combustion furnace under high vacuum when not in use probably results in a further lowering of the ^{14}C blank. Very high [CO] in the Greenland air samples was of concern because of potentially high ^{14}CO, which was quantitatively removed using the Sofnocat reagent. In addition, it was demonstrated that there are no significant effects on sample $^{14}CH_4$ from mass-dependent fractionation or interference from non-methane light VOCs in the CH_4 conversion line.

Extensive testing and method development was also carried out at ANSTO to overcome the problem of unusually long (2-4 days) graphitization times for some small samples as well as to further reduce the processing ^{14}C blank. Graphitization times have been reduced to ≤ 1 hr for all samples < 25 μg C; with the most important factor being a colder trap for more efficient H_2O vapor trapping during the reaction. The amount of extraneous carbon added during graphitization (if assumed to have a ^{14}C activity of ~ 100 pMC) has been reduced to 0.03 μg, which is unprecedented to the

best of our knowledge. The most important factor in reducing the blank was likely the use of ultra high purity Sigma-Aldrich-400 Fe powder catalyst, though the development of a new cathode pressing system and increased care taken with each individual sample during processing probably also contributed.

Test results indicate that the amount of extraneous carbon added during the melt-extraction of air from ancient glacial ice in Greenland was comparably low. The average uncorrected ^{14}C for all the Greenland melt-extraction blank samples (all ~500 ppb CH_4, ~20 μg C, ^{14}C-dead to begin with) was 0.75 pMC, which represents a cumulative blank for overall sample processing. Such low blanks, as well as our demonstrated ability to make meaningful ^{14}C corrections for each step of the processing give us confidence in being able to accurately determine the $^{14}CH_4$ of the ancient air in sampled glacial ice. The methods developed for CH_4 extraction from relatively small, low-[CH_4] and low-$^{14}CH_4$ air samples will be useful for future paleo $^{14}CH_4$ work and may also find applications in modern atmospheric $^{14}CH_4$ monitoring. The methods developed for AMS preparation and measurement of very small, low-^{14}C activity CO_2 samples are likely to find broader paleoenvironmental and geochronological applications.

Acknowledgements

This work was supported by NSF grants OPP0221470 (to JPS) and OPP0221410 (to EJB), and by a Packard Fellowship (to JPS). We thank John Southon for making ^{14}C measurements on test samples at the U.C. Irvine accelerator facility. Alan Williams provided excellent training and help with sample graphitization at ANSTO. Ross Martin provided valuable advice on MS and GC systems at NIWA as well as assisted with some test sample processing. Ed Dlugokencky provided valuable advice as well as the Sofnocat reagent. Guaciara dos Santos and Dachun Zhang provided training and assisted with ^{14}C test sample preparation at UC Irvine. Susan Harder made the [CO] measurements in several ice samples at Washington State University. John McGregor unfailingly delivered dry ice to NIWA. We also thank Ingeborg Levin and Carl Brenninkmeijer for helpful discussions.

Chapter 4, in part, is in press in Radiocarbon, 2008, as: Vasilii V. Petrenko, Andrew M. Smith, Gordon Brailsford, Katja Riedel, Quan Hua, Dave Lowe, Jeffrey P. Severinghaus, Vladimir Levchenko, Tony Bromley, Rowena Moss, Jens Mühle and Edward J. Brook. A new method for analyzing ^{14}C of methane in ancient air extracted from glacial ice. It is reprinted here with permission from Radiocarbon. The dissertation author was the primary investigator and author of this paper.

Tables

Table 4.1. Summary of tests conducted with the Sofnocat 423 reagent. For tests shown in a), a gas mixture containing ~500 ppb CH_4 and high CO was passed first through the Sofnocat 423 reagent, then through a mass flow controller. 12.11 g of Sofnocat were packed into a 13 mm OD stainless steel tube to a length of 8 ± 0.5 cm. Gas aliquots were taken for gas chromatography (GC) measurements just upstream and just downstream of the Sofnocat. Pressure was maintained at 1 barg. The 3.4 ppb of CO remaining in the first test is most likely due to residual CO in the gas chromatograph from an immediately prior measurement of standard gas. The small variations in [CH_4] measured upstream and downstream of the Sofnocat are not significant. Tests shown in b) were conducted on the new CH_4 line. The gas flowed through the upstream part of the line at 0.8 SL/min and either bypassed the Sofnocat completely or flowed through only one part of the Sofnocat trap (the other part was replaced with an empty glass tube, see Figure 4.2); the gas was then delivered to the GC by a diaphragm pump. For testing part 1 of the trap, gas from an actual Pakitsoq air sample was used for a complete simulation of sample processing. For testing part 2, a synthetic high-CO gas mixture was used. The [CO] measurements were performed using a Hewlett-Packard 5890 gas chromatograph with a reducing gas detector. The [CO] measurement blank was determined by running a CO-free gas through part 1 of the Sofnocat trap. All measurements are from single GC injections except where [CO] errors are given, in which case 3 injections were performed. The CO detector is not calibrated to measure concentrations much above ~100 ppb, and the response may not be completely linear. All [CH_4] measurements were carried out using a Hewlett-Packard 5890 gas chromatograph with a flame-ionization detector.

Table 4.1 a

Flow rate, SL/min	Approx. gas residence time in Sofnocat, s	[CO] before Sofnocat, ppb	[CO] after Sofnocat, ppb	[CH_4] before Sofnocat, ppb	[CH_4] after Sofnocat, ppb
2	0.35	693	3.4	426.5	426.5
2	0.35	7,010	0	535.2	534.1
5	0.14	6,872	0	533.8	534.6
2	0.35	6,628	0	537.2	535.3
0.5	1.42	6,603	0	534.9	537.0
0.1	7.09	6,665	0	534.4	534.3

Table 4.1 b

	Bypassing Sofnocat: [CO], ppb	Through Sofnocat: [CO], ppb	[CO] error, ppb
Part 1 of Sofnocat trap	2,029	17.96	
Part 2 of Sofnocat trap	3,300	16.15	1.45
[CO] measurement blank		16.89	0.89

Table 4.2. Tests of factors influencing the sample yield and isotopic fractionation in the new CH_4 conversion line. CH_4 line configuration and procedure were as described in sections 4.2 d and 4.2 h, with the following exceptions. In test 1 only one LN_2 – chilled trap was used to capture CO_2 downstream of the furnace instead of the usual three. In test 2, a ~20μg aliquot of CO_2 with a known $\delta^{13}C$ was mixed with H_2O vapor from a previous sample run, and a CO_2 distillation was then performed as usual, except for the transfer into the manometer, which was cut short after 30 seconds (1 minute too short). The fraction of sample left behind in the transfer was not quantified. In test 4, one end of the sample gas cylinder sat in a bucket of ice; the pressures in the cylinder at the start and end of the run were 2.45 and 0.30 bar, respectively. In test 6, the sample gas was bubbled through milli-Q water at a gas pressure of 1200 mbar prior to entering the CH_4 line. All tests listed are single sample runs, except for the controls (#3). $\delta^{13}C$ measurements were made using a Finnigan MAT 252 dual dynamic inlet isotope ratio mass spectrometer. The true $\delta^{13}CH_4$ for some of the samples is known from previous analyses of air from the same cylinders using established methods (Lowe et al., 1991).

Table 4.2

Test	[CH_4], ppb	Yield, %	True $\delta^{13}CH_4$, ‰ PDB	Measured $\delta^{13}C$, ‰ PDB
1. Poor trapping of CO_2 downstream of furnace	517	69.1 ± 1.0	-47.23 ± .07	-48.83 ± .10
2. Incomplete transfer of CO_2			-47.02	-48.20 ± .10
3. Three control runs for tests #4-6 below	510	93.5 ± 0.2	-47.28 ± 0.15	-47.60 ± .03
4. Test gas run from a chilled cylinder down to low pressure	510	94.1 ± 1.0	-47.28 ± 0.15	-47.58 ± .08
5. Hydrocarbon-rich gas mixture	443	93.1 ± 1.0		
6. Hydrocarbon-rich gas mixture saturated with H_2O vapor	443	92.7 ± 1.0		

Table 4.3. Comparison of graphitization performance with small samples at ANSTO with earlier standard conditions (1 mg Cerac-325 Fe catalyst, -39˚C cold trap; shaded section) vs the new optimized conditions (1 mg SA-400 catalyst, -60 to -70˚C cold trap; unshaded). For standard conditions, only results for samples originating at NIWA are shown; all those samples were processed through the pre-existing CH_4 line. For the new optimized technique, slightly more than half the samples originated at NIWA (processed through the new CH_4 line); the rest were standards and blanks prepared at ANSTO and SIO. With the new technique, no significant differences in yields or reaction times were observed between samples that originated from NIWA and samples that originated from ANSTO or SIO.

Table 4.3

Sample size	Number of tests & samples	Graphitization yield	Reaction duration	Notes
15 - 25 μg C	6	65 – 87%	5 hr – 4 days	
25 – 45 μg C	26	61 – 90 %	2.5 hr – 4 days	
<15 μg C	9	76 – 85%	< 40 min	1 sample had a 69% yield
15-25 μg C	74	80 – 99%	30 – 60 min	1 sample had a 73% yield
25-45 μg C	28	82 – 95%	60 – 80 min	

Table 4.4. Samples processed to assess the ANSTO procedural blank. All masses were determined volumetrically prior to graphitization. For the marble blanks, CO_2 was evolved with 85% phosphoric acid from a single grain of IAEA C1 marble and subsequently decanted through a metal bellows valve to make the individual samples listed in the table. For IAEA-C8, a ~500μg sample was split into one 460 μg and two ~20μg samples by allowing the CO_2 to equilibrate between flasks in a vacuum line. The small OX-1-derived CO_2 samples and SIO 30 pMC CO_2 samples were prepared in a similar manner, with the 440 μg sample being the "parent" of all the ~20μg samples, and the 220 μg sample being the parent of all the ~10μg samples for OX-1, and the 560 μg sample being the parent of all small 30 pMC samples. The pMC value assigned to the average of all large OX-1 standards is 103.98. Samples that went through graphitization reactor 1 were treated separately when making ^{14}C corrections.

Table 4.4

Sample Type	Graphitization reactor(s)	N	Average mass, µg C	Larger of average mass uncertainty or stdev, µg C	Average ^{14}C, pMC	Larger of ^{14}C average uncertainty or stdev for the set, pMC
Marble blank	2,3	4	1,510	20	0.15	0.04
Marble blank	2,3,5	3	39.63	0.43	0.22	0.04
Marble blank	1	1	39.59	0.43	0.48	0.09
Marble blank	5	2	19.71	0.21	0.42	0.05
Marble blank	1	2	20.03	0.22	1.08	0.16
Marble blank	2,3	4	9.87	0.15	0.43	0.09
IAEA-C8	1	2	2,000	30	15.33	0.21
IAEA-C8	2	1	460	10	15.53	0.17
IAEA-C8	2,3	2	21.28	2.83	16.03	0.37
SIO 30 pMC CO_2	5	1	560	10	31.13	0.28
SIO 30 pMC CO_2	2,3,5	3	20.06	0.46	30.75	0.63
SIO 30 pMC CO_2	1	1	20.63	0.22	31.37	0.35
Large OX-1 avg			2,000		103.98	
OX-1	5	1	440	10	102.76	0.64
OX-1	1	1	220	10	104.70	0.51
OX-1	2,3,5	3	22.06	1.48	103.68	1.85
OX-1	1	1	21.64	0.23	104.78	0.95
OX-1	2,3	4	11.86	0.76	105.07	1.50

Table 4.5. A summary of the blank and modern samples processed to assess the CH_4 extraction line blank, using the procedure described in the text. "ppb" and "ppm" (parts per million) refer to [CH_4] of the gases used. The 500 ppb and 1000 ppb "^{14}C-dead" gases were prepared by diluting the 28 ppm gas with CH_4-free air and should thus have the same ^{14}C. The gas used for "large" and "small" modern sets was clean ambient air from the same tank, collected at Baring Head, New Zealand. The "500 ppb modern" gas was made by diluting air from this same tank with CH_4-free air. Run time is the total time for collection of CO_2 downstream of the CH_4 combustion furnace. Sample masses are as determined at ANSTO immediately prior to graphitization. The listed ^{14}C values have been corrected for the ANSTO processing blank as described in the text.

Table 4.5

Sample type	N	Average sample mass, µg C	Larger of average mass uncertainty or stdev of the set, µg C	Average run time, min	Run time stdev, min	Average ^{14}C corrected for ANSTO blank, pMC	Larger of ^{14}C average uncertainty or stdev of the set, pMC
Large 28 ppm ^{14}C-dead	3	190	10	16.51	0.01	0.22	0.04
1000 ppb ^{14}C-dead	4	19.39	0.37	45.11	0.23	0.45	0.42
500 ppb ^{14}C-dead	4	19.07	0.45	91.48	0.90	0.50	0.08
500 ppb modern	4	19.07	0.67	90.17	0.20	130.54	1.40
Small 1750 ppb modern	4	19.76	0.32	26.43	0.30	132.48	1.58
Large 1750 ppb modern	3	129.50	0.80	180.88	1.50	131.87	0.62

Table 4.6. Summary of samples processed to assess the field melt-extraction blank for each type of actual Pakitsoq ancient air sample. "CH_4 standard gas" was used in all the simulated extractions. All [CH_4] measurements were conducted at NIWA using a Hewlett-Packard 5890 gas chromatograph with a flame-ionization detector. Average ^{14}C uncertainties for the sample sets (after ANSTO and CH_4 line corrections were applied) are listed instead of ^{14}C standard deviations of the sets because the former are larger.

Table 4.6

Sample type	N	Average ^{14}C corrected for ANSTO and CH_4 line blanks, pMC	Average ^{14}C uncertainty for the set, pMC	Corrected average mass, µg C	Mass stdev, µg C	[CH_4], ppb	[CH_4] error, ppb
CH_4 standard gas	4	-0.02	0.60	19.05	0.26	500.41	0.84
Preboreal Blank	2	-0.09	0.61	19.03	0.14	502.82	0.38
Transition Blank	2	0.01	0.58	19.03	0.27	501.67	0.74
Younger Dryas Blank	2	-0.12	0.60	18.63	0.30	502.01	0.16
Bølling Blank	2	0.48	0.56	20.84	1.51	502.99	0.42
Oldest Dryas Blank	2	0.08	0.56	20.23	0.81	503.63	0.79

Table 4.7. The effect of progressive ^{14}C corrections for each processing step on two of the actual Pakitsoq samples.

Table 4.7

Sample	Uncorrected $^{14}CH_4$, pMC	Error, pMC	Graphitization reactor	Corrected for ANSTO blank, pMC	Error, pMC	Further corrected for CH_4 line blank, pMC	Error, pMC	$^{14}CH_4$ FINAL (further corrected for melt-extraction blank), pMC	Error, pMC
Oldest Dryas 1	28.54	0.44	5	28.29	0.45	28.17	0.88	**28.26**	**1.06**
Oldest Dryas 2	29.71	0.38	1	28.71	0.44	28.59	0.87	**28.69**	**1.05**

Figures

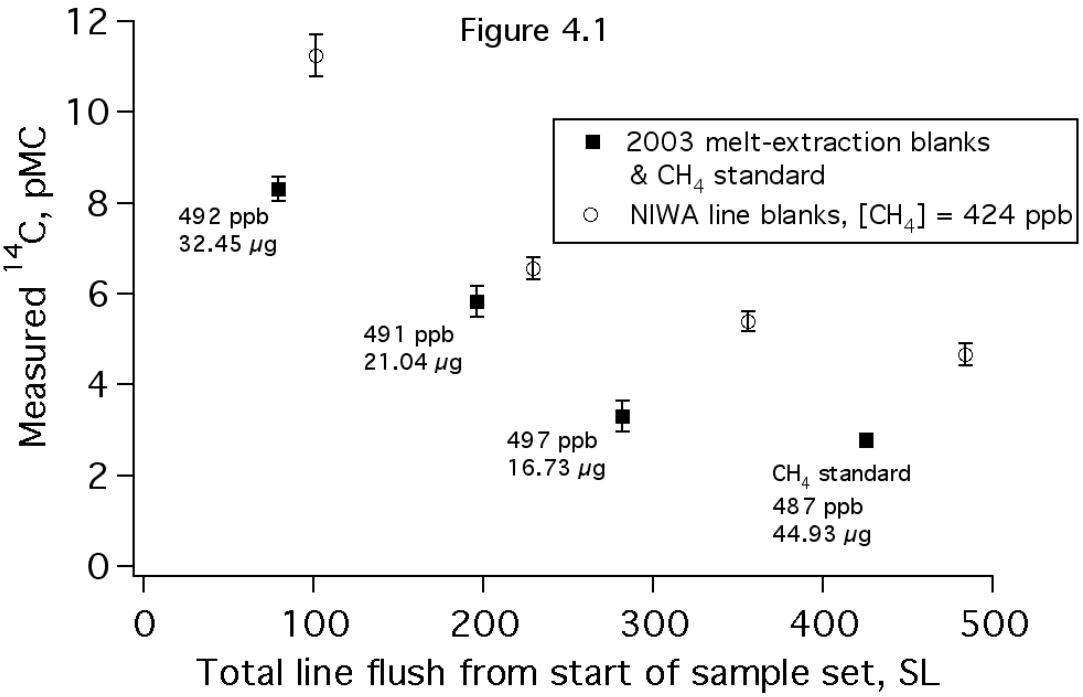

Figure 4.1. Tests of $^{14}CH_4$ blank on the pre-existing CH_4 line. The Greenland CH_4 standard gas used for the melt-extraction blanks during the 2003 field season is assumed to be ^{14}C-free. Although the source CH_4 used to make up this standard has never been directly measured for ^{14}C, a 28 part per million (ppm) CH_4 standard later made using CH_4 from the same source was measured for $^{14}CH_4$, yielding 0.2 pMC, indicating that it was effectively ^{14}C-free. The CH_4 used to make the gas mixture for the NIWA line blanks had likewise never been measured for ^{14}C; however the source of this methane is a fossil natural gas field in the North Sea; thus it is reasonable to assume that this should also be ^{14}C-free. The total volume of gas flushed through the line for each sample is calculated as total volume flushed prior to start of sample collection (since start of sample set) + 1/2 sample volume. Sample size for all NIWA line blank samples was 27 μg.

Figure 4.2

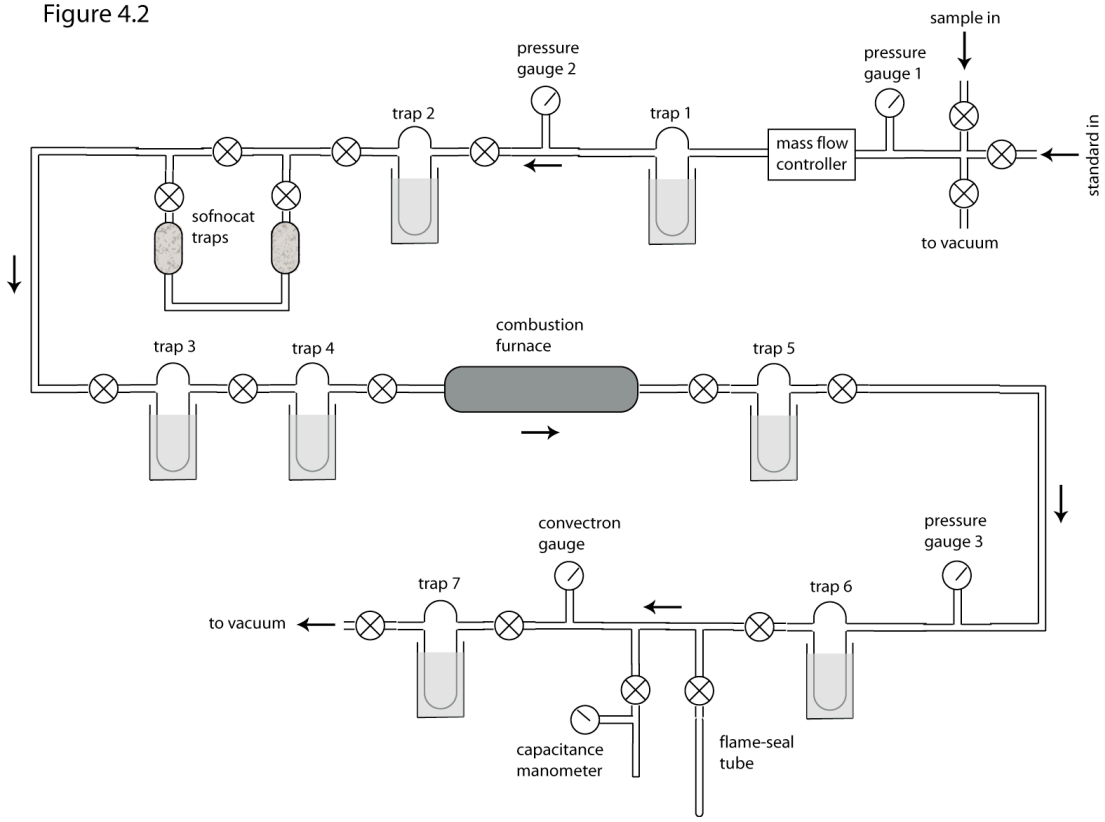

Figure 4.2. A schematic illustration of the new CH_4 extraction line developed for processing ancient Pakitsoq air samples for $^{14}CH_4$. The inlet allows for evacuation of the stainless steel flex hose which connects to the sample tank, minimizing the amount of gas wasted during the line flush. A 30-bar gauge is used to monitor the inlet pressure, and the air flow is kept at 0.8 SL/min with a Teledyne-Hastings mass flow controller (MFC). All the traps are cooled with liquid nitrogen. Trap 1 is a stainless steel thimble trap. Traps 2-4 are "Russian doll"-type traps (Brenninkmeijer, 1991). Traps 5 & 7 are Pyrex® U-traps, and trap 6 is a 6 mm OD Pyrex® multi-loop trap. Gauges 2 & 3 are pirani-type gauges. The Sofnocat 423 reagent is in 2 glass bulbs covered with aluminum foil to protect from direct light. The combustion furnace is a 25 mm ID quartz tube packed with platinum-coated quartz wool catalyst.

Figure 4.3. Tests of CH_4 conversion efficiency and N_2O production in the new CH_4 line. a) Tests with different amounts of catalyst. b) Tests with varying [CH_4]. c) Change in line performance with time. The flow rate of the test gas was set to 0.8 SL/min in all cases except the tests with 35 mm of catalyst in (a) when the flow was set to 1.0 SL/min. Upstream LN_2-cooled traps in the line (Figure 4.2) remove all CO_2 and N_2O originally present in the test gas, so all the CO_2 and N_2O exiting the line are due to CH_4 combustion and N_2O production in the furnace, respectively. Two oil-free diaphragm pumps in series were used to pull the gas through the line and deliver it to the GC system where [CH_4], [CO], [CO_2] and [N_2O] were continuously being measured. Typically 1-3 GC measurements were made at each furnace temperature. The CO_2 amount for the N_2O % of CO_2 calculation was estimated based on the amount of CH_4 combusted. [CH_4] and [N_2O] measurements for each set of tests were corrected for the respective blanks, which are most likely due to outgassing from pump diaphragms and/or small CH_4 and N_2O residuals in the GC system from the standard gases. All tests in (a) were conducted with gases with [CH_4] of around ~1740 ppb within a period of 4 days. All tests in (b) were conducted within a period of 5 days. All tests in (b) and (c) were conducted with 55mm of catalyst in the furnace and at 0.8 SL/min flow. All [N_2O] measurements were done using a Hewlett-Packard 6890 GC with an electron capture detector. All experiments were done in 2006.

Figure 4.3a

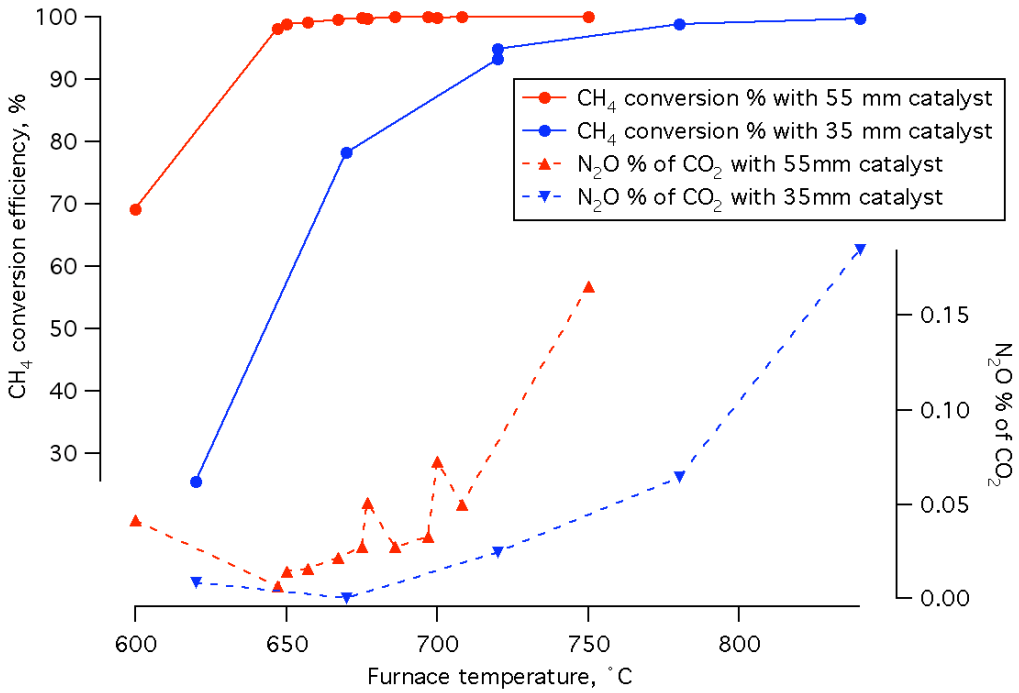

Figure 4.3b

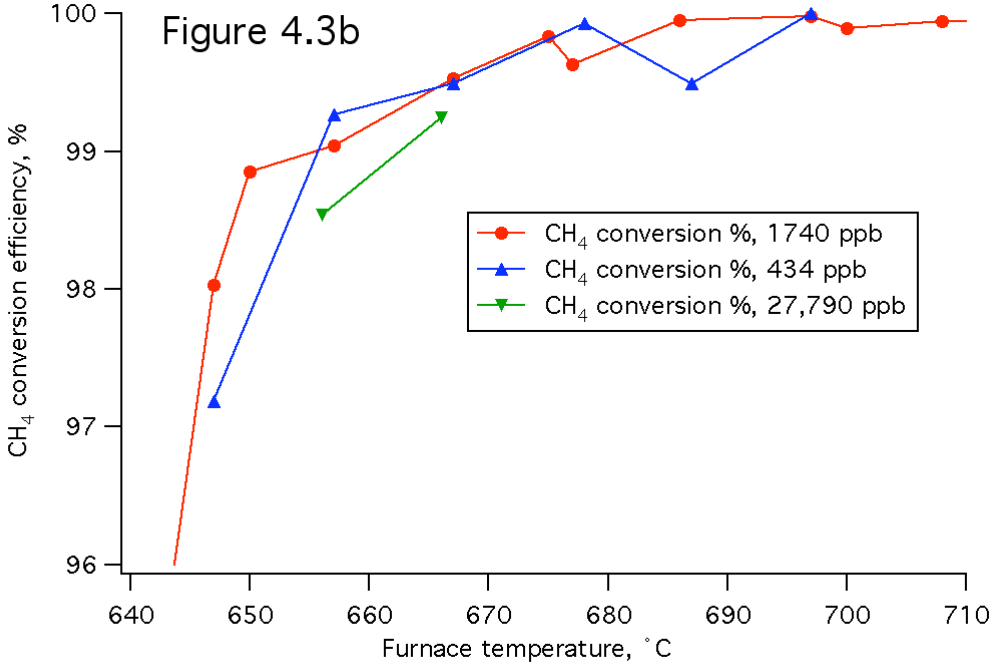

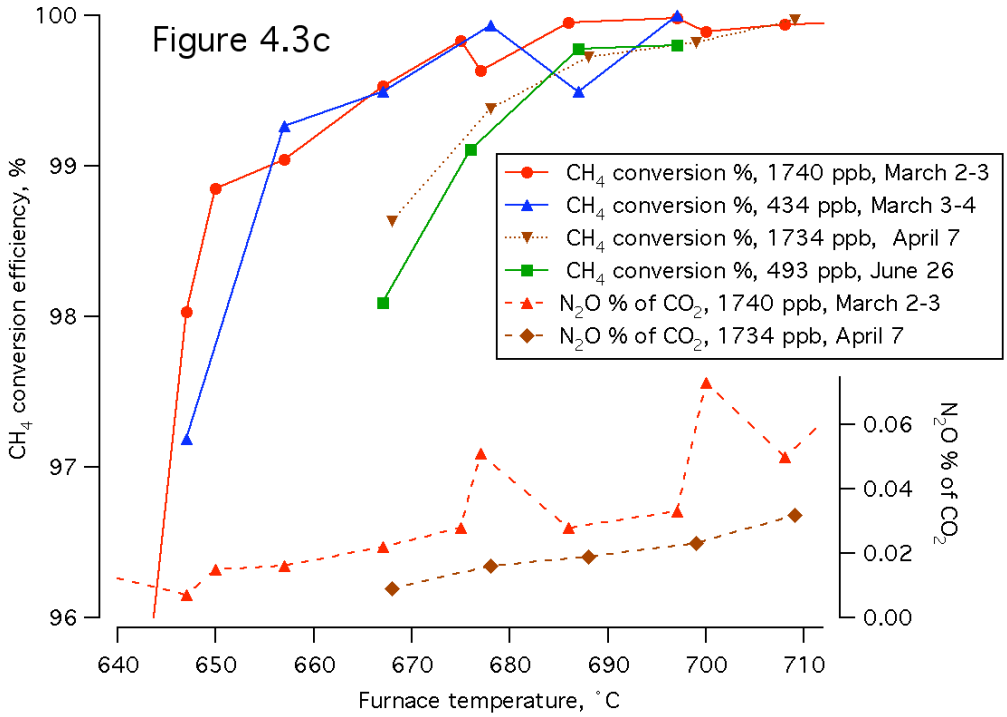

Figure 4.3, continued.

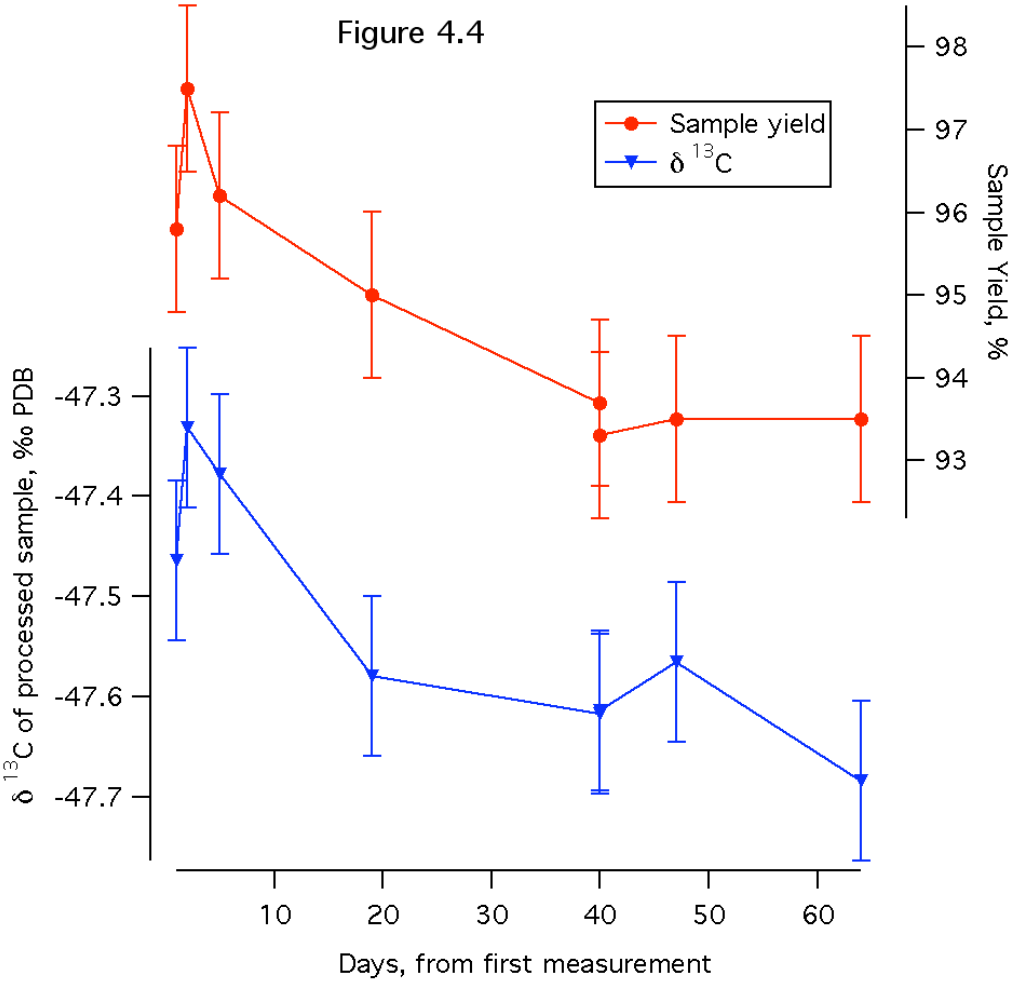

Figure 4.4. Changes in the sample yield and $\delta^{13}C$ of processed sample with time. Each data point represents a single test sample. Tests were carried out with two gas mixtures, each ~ 500 ppb in CH_4; the true $\delta^{13}CH_4$ of the gas is –47.28 ± 0.15 ‰. Day 1 is May 18, 2006. All tests used the same procedure and line configuration as for the Pakitsoq air samples. All sample sizes between 16.5 and 21.5 μg C.

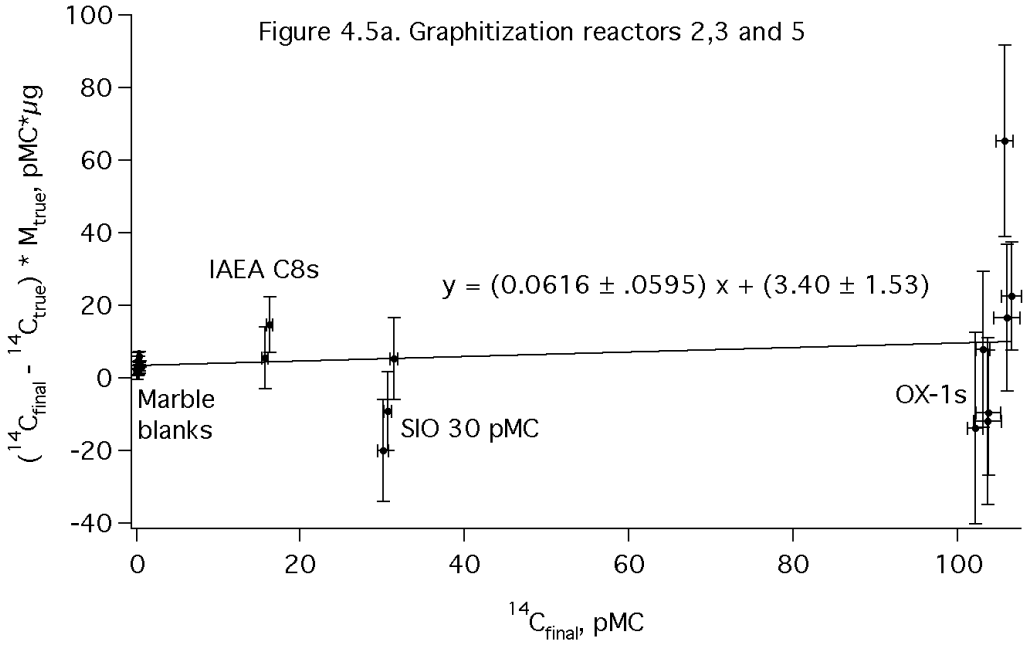

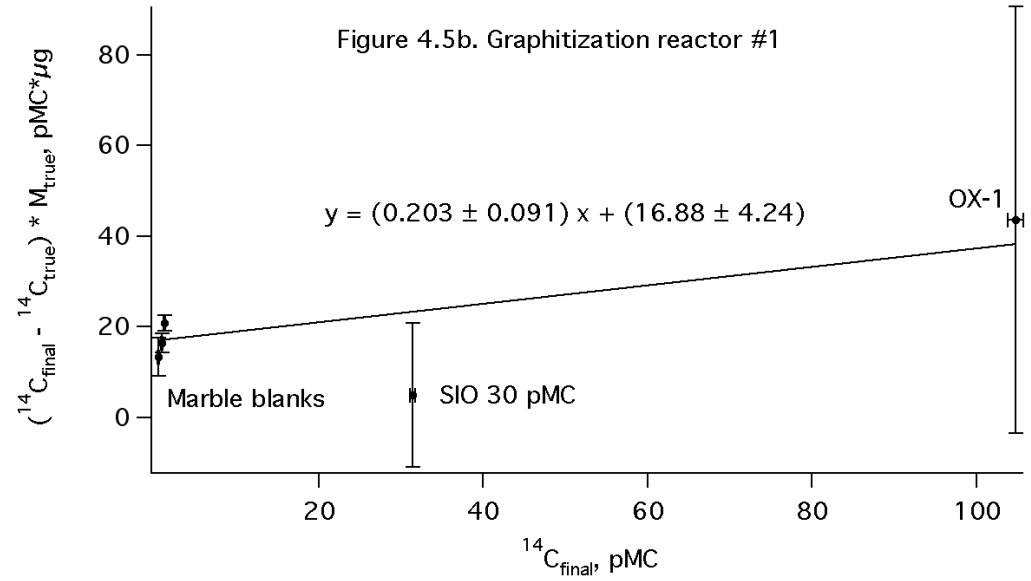

Figure 4.5. Plots of $M_{true}(^{14}C_{final}-^{14}C_{true})$ vs $^{14}C_{final}$ for ANSTO blanks and standards processed through reactors 2,3 and 5 (a) and 1 (b). Data for all individual samples are plotted. Errors for data points are as determined by error propagation. Least-squares line fits to the data with equations are shown. The intercept for each equation was set to the average $M_{true}(^{14}C_{final}-^{14}C_{true})$ for the blanks, and the intercept error is taken as the standard deviation of $M_{true}(^{14}C_{final}-^{14}C_{true})$ values for the blanks. The errors shown for the slopes are one standard deviation.

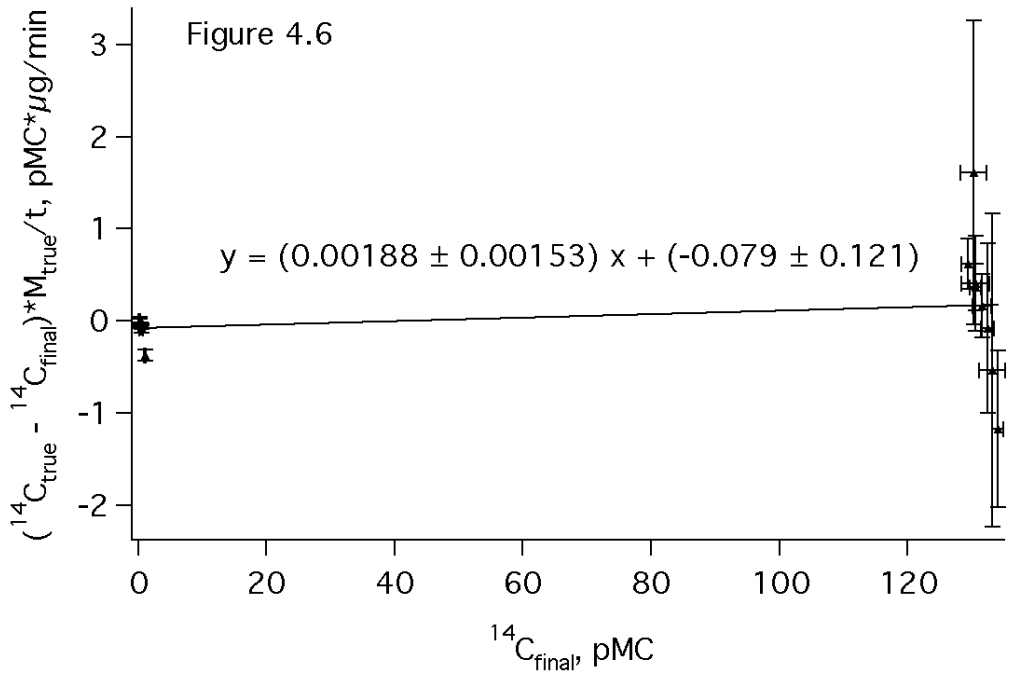

Figure 4.6. Determination of the NIWA processing blank from all individual ~20 μg-sized samples. The least-squares linear fit with equation is shown. The intercept is fixed at the average value of $(^{14}C_{true} - {}^{14}C_{final})*M_{true}/t$ for all the ^{14}C-dead samples; the uncertainty in the intercept is the standard deviation of all these values. The error shown for the slope is one standard deviation.

References

Brasseur, G., Orlando, J., Tyndall, G. (Editors), 1999. Atmospheric Chemistry and Global Change. Topics in Environmental Chemistry. Oxford University Press, New York, 654 pp.

Brenninkmeijer, C.A.M., 1991. Robust, High-Efficiency, High-Capacity Cryogenic Trap. Analytical Chemistry 63, 1182-1184.

Brenninkmeijer, C.A.M., 1993. Measurement of the Abundance of (CO)-C-14 in the Atmosphere and the C-13 / C-12 and O-18 / O-16 Ratio of Atmospheric CO with Applications in New Zealand and Antarctica. Journal of Geophysical Research-Atmospheres 98, 10595-10614.

Brenninkmeijer, C.A.M., Rockmann, T., 1996. Russian doll type cryogenic traps: Improved design and isotope separation effects. Analytical Chemistry 68, 3050-3053.

Brook, E.J., Harder, S., Severinghaus, J., Steig, E.J., Sucher, C.M., 2000. On the origin and timing of rapid changes in atmospheric methane during the last glacial period. Global Biogeochemical Cycles 14, 559-572.

Buffett, B., Archer, D., 2004. Global inventory of methane clathrate: sensitivity to changes in the deep ocean. Earth and Planetary Science Letters 227, 185-199.

Chappellaz, J., Blunier, T., Raynaud, D., Barnola, J.M., Schwander, J., Stauffer, B., 1993. Synchronous Changes in Atmospheric CH4 and Greenland Climate between 40-Kyr and 8-Kyr BP. Nature 366, 443-445.

Colussi, A.J., Hoffmann, M.R., 2003. In situ photolysis of deep ice core contaminants by Cerenkov radiation of cosmic origin. Geophysical Research Letters 30(4), doi: 10.1029/2002GL016112.

Conny, J.M., Currie, L.A., 1996. The isotopic characterization of methane, non-methane hydrocarbons and formaldehyde in the troposphere. Atmospheric Environment 30, 621-638.

Eisma, R., Vermeulen, A.T., Kieskamp, W.M., 1994. Determination of European Methane Emissions, Using Concentration and Isotope Measurements. Environmental Monitoring and Assessment 31, 197-202.

Etheridge, D.M., Steele, L.P., Francey, R.J., Langenfelds, R.L., 1998. Atmospheric methane between 1000 AD and present: Evidence of anthropogenic emissions

and climatic variability. Journal of Geophysical Research-Atmospheres 103, 15979-15993.

Ferretti, D., Fraser, A., Lassey, K., Martin, R., Brailsford, G., McGregor, J., November, 2005. Using electrical sensors to estimate methane emissions from farm animals, Meteorological Society of New Zealand Annual Conference, Wellington.

Ferretti, D.F., Miller, J.B., White, J.W.C., Etheridge, D.M., Lassey, K.R., Lowe, D.C., Meure, C.M.M., Dreier, M.F., Trudinger, C.M., van Ommen, T.D., Langenfelds, R.L., 2005. Unexpected changes to the global methane budget over the past 2000 years. Science 309, 1714-1717.

Fink, D., Hotchkis, M., Hua, Q., Jacobsen, G., Smith, A.M., Zoppi, U., Child, D., Mifsud, C., van der Gaast, H., Williams, A., Williams, M., 2004. The ANTARES AMS facility at ANSTO. Nuclear Instruments & Methods in Physics Research Section B-Beam Interactions with Materials and Atoms 223-24, 109-115.

Forster, P., Ramaswamy, V., Artaxo, P., Berntsen, T., Betts, R., Fahey, D.W., Haywood, J., Lean, J., Lowe, D.C., Myhre, G., Nganga, J., Prinn, R., Raga, G., M., S., Van Dorland, R., 2007. Changes in Atmospheric Constituents and in Radiative Forcing. In: S. Solomon et al. (Editors), Climate Change 2007: The Physical Science Basis. Contribution of Working Group I to the Fourth Assessment Report of the Intergovernmental Panel on Climate Change. Cambridge University Press, Cambridge, U.K.

Foulger, B.E., Simmonds, P.G., 1993. Ambient-Temperature Gas Purifier Suitable for the Trace Analysis of Carbon-Monoxide and Hydrogen and the Preparation of Low-Level Carbon-Monoxide Calibration Standards in the Field. Journal of Chromatography 630, 257-263.

Grabowski, K.S., Knies, D.L., Tumey, S.J., Pohlman, J.W., Mitchell, C.S., Coffin, R.B., 2004. Carbon pool analysis of methane hydrate regions in the seafloor by accelerator mass spectrometry. Nuclear Instruments & Methods in Physics Research Section B-Beam Interactions with Materials and Atoms 223-24, 435-440.

Haan, D., Raynaud, D., 1998. Ice core record of CO variations during the last two millennia: atmospheric implications and chemical interactions within the Greenland ice. Tellus Series B-Chemical and Physical Meteorology 50, 253-262.

Hua, Q., Jacobsen, G.E., Zoppi, U., Lawson, E.M., Williams, A.A., Smith, A.M., McGann, M.J., 2001. Progress in radiocarbon target preparation at the ANTARES AMS Centre. Radiocarbon 43, 275-282.

Hua, Q., Zoppi, U., Williams, A.A., Smith, A.M., 2004. Small-mass AMS radiocarbon analysis at ANTARES. Nuclear Instruments & Methods in Physics Research Section B-Beam Interactions with Materials and Atoms 223-24, 284-292.

Kennett, J.P., Cannariato, K.G., Hendy, I.L., Behl, R.J., 2000. Carbon isotopic evidence for methane hydrate instability during quaternary interstadials. Science 288, 128-133.

Kennett, J.P., Cannariato, K.G., Hendy, I.L., Behl, R.J., 2003. Methane Hydrates in Quaternary Climate Change: The Clathrate Gun Hypothesis. AGU, Washington, D.C., 216 pp.

Kessler, J.D., Reeburgh, W.S., 2005. Preparation of natural methane samples for stable isotope and radiocarbon analysis. Limnology and Oceanography-Methods 3, 408-418.

Kessler, J.D., Reeburgh, W.S., Southon, J., Seifert, R., Michaelis, W., Tyler, S.C., 2006. Basin-wide estimates of the input of methane from seeps and clathrates to the Black Sea. Earth and Planetary Science Letters 243, 366-375.

Lal, D., Jull, A.J.T., Burr, G.S., Donahue, D.J., 2000. On the characteristics of cosmogenic in situ C-14 in some GISP2 Holocene and late glacial ice samples. Nuclear Instruments & Methods in Physics Research Section B-Beam Interactions with Materials and Atoms 172, 623-631.

Lassey, K.R., Lowe, D.C., Smith, A.M., 2007. The atmospheric cycling of radiomethane and the "fossil fraction" of the methane source. Atmospheric Chemistry and Physics 7, 2141-2149.

Lowe, D.C., Brenninkmeijer, C.A.M., Manning, M.R., Sparks, R., Wallace, G., 1988. Radiocarbon Determination of Atmospheric Methane at Baring Head, New-Zealand. Nature 332, 522-525.

Lowe, D.C., Brenninkmeijer, C.A.M., Tyler, S.C., Dlugkencky, E.J., 1991. Determination of the Isotopic Composition of Atmospheric Methane and Its Application in the Antarctic. Journal of Geophysical Research-Atmospheres 96, 15455-15467.

Milkov, A.V., 2004. Global estimates of hydrate-bound gas in marine sediments: how much is really out there? Earth-Science Reviews 66, 183-197.

Mühle, J., Lueker, T.J., Su, Y., Miller, B.R., Prather, K.A.,Weiss, R.F., 2007. Trace gas and particulate emissions from the 2003 southern California wildfires. Journal of Geophysical Research-Atmospheres 112, Art. No. D03307.

Petrenko, V.V., Severinghaus, J.P., Brook, E.J., Reeh, N., Schaefer, H., 2006. Gas records from the West Greenland ice margin covering the Last Glacial Termination: a horizontal ice core. Quaternary Science Reviews 25, 865-875.

Price, P.B., 2007. Microbial life in glacial ice and implications for a cold origin of life. Fems Microbiology Ecology 59, 217-231.

Pupek, M., Assonov, S.S., Muhle, J., Rhee, T.S., Oram, D., Koeppel, C., Slemr, F., Brenninkmeijer, C.A.M., 2005. Isotope analysis of hydrocarbons: trapping, recovering and archiving hydrocarbons and halocarbons separated from ambient air. Rapid Communications in Mass Spectrometry 19, 455-460.

Quay, P., Stutsman, J., Wilbur, D., Snover, A., Dlugokencky, E., Brown, T., 1999. The isotopic composition of atmospheric methane. Global Biogeochemical Cycles 13, 445-461.

Reeh, N., Oerter, H., Letreguilly, A., Miller, H., Hubberten, H.W., 1991. A New, Detailed Ice-Age O-18 Record from the Ice-Sheet Margin in Central West Greenland. Global and Planetary Change 90, 373-383.

Schaefer, H., Whiticar, M.J., Brook, E.J., Petrenko, V.V., Ferretti, D.F., Severinghaus, J.P., 2006. Ice record of delta C-13 for atmospheric CH4 across the Younger Dryas-Preboreal transition. Science 313, 1109-1112.

Smith, A.M., Levchenko, V.A., Etheridge, D.M., Lowe, D.C., Hua, Q., Trudinger, C.M., Zoppi, U., Elcheikh, A., 2000. In search of in-situ radiocarbon in Law Dome ice and firn. Nuclear Instruments & Methods in Physics Research Section B-Beam Interactions with Materials and Atoms 172, 610-622.

Smith AM, Petrenko VV, Hua Q, Southon J, Brailsford G. 2007. The effect of N_2O, catalyst, and means of water vapor removal on the graphitization of small CO_2 samples. Radiocarbon 49 (2), 245-254.

Sowers, T., 2006. Late quaternary atmospheric CH4 isotope record suggests marine clathrates are stable. Science 311, 838-840.

Stevens, C.M., Krout, L., 1972. Method for the determination of the concentration and of the carbon and oxygen isotopic composition of atmospheric carbon monoxide. International Journal of Mass Spectrometry and Ion Physics 8, 265-275.

Stuiver, M., 1983. International Agreements and the Use of the New Oxalic-Acid Standard. Radiocarbon 25, 793-795.

Stuiver, M., Polach, H.A., 1977. Reporting of C-14 Data - Discussion. Radiocarbon 19, 355-363.

Van de Wal, R.S.W., Meijer, H.A.J., de Rooij, M., van der Veen, C., 2007. Radiocarbon analyses along the EDML ice core in Antarctica. Tellus Series B-Chemical and Physical Meteorology 59B, 157-165.

Wahlen, M., Tanaka, N., Henry, R., Deck, B., Zeglen, J., Vogel, J.S., Southon, J., Shemesh, A., Fairbanks, R., Broecker, W., 1989. C-14 in Methane Sources and in Atmospheric Methane - the Contribution from Fossil Carbon. Science 245, 286-290.

Winckler, G., Aeschbach-Hertig, W., Holocher, J., Kipfer, R., Levin, I., Poss, C., Rehder, G., Suess, E., Schlosser, P., 2002. Noble gases and radiocarbon in natural gas hydrates. Geophysical Research Letters 29(10), doi: 10.1029/2001GL014013.

Chapter 5:

Measurements of paleoatmospheric $^{14}CH_4$ from glacial ice covering the last glacial termination

5.1 Introduction

Chapter 1 presented the motivation for obtaining a record of ^{14}C of atmospheric methane ($^{14}CH_4$) for the last glacial termination, and Chapters 2 - 4 described the groundwork leading to these measurements. Briefly, a record of $^{14}CH_4$ for the last glacial termination would allow for better constraints on changes in the CH_4 budget during times of dramatic climate transitions, as well as provide a definitive test of the clathrate hypothesis.

It was shown in Chapter 2 that the Pakitsoq ablation site on the West Greenland ice margin offered virtually unlimited amounts of last-glacial-termination-age ice at the surface (Petrenko et al., 2006). The gas records in this ice were found to be mostly intact, however methane concentrations ($[CH_4]$) were found to be elevated in a few ice sections. Very accurate dating was possible in the ice sections containing the Younger Dryas – Preboreal and Oldest Dryas – Bølling abrupt climate transition signals.

~100 L STP ancient air samples for $^{14}CH_4$ analyses with ages between 11 – 15 calendar kyr before present (BP, where present = 1950 AD) were obtained from Pakitsoq ice by the means of a new method involving melt-extraction in the field and details were presented in Chapter 3 of this thesis (also in Petrenko et al. (2008a). The $[CH_4]$ blank for the melt-extractions was found to be < 4 parts per billion (ppb) for all samples. Ar/N_2, CFC-11 and CFC-12 measured in the samples indicated no significant $^{14}CH_4$ contamination from ambient air. Ar/N_2, Kr/Ar and Xe/Ar ratios in the samples were used to quantify effects of gas dissolution during the melt-

extractions and correct the sample [CH_4]. [CH_4] values corrected for blank and solubility effects were elevated by up to 128 ppb over expected values for some samples.

New methods were developed for measuring $^{14}CH_4$ in the ancient air samples, and details were presented in Chapter 4 (also in Petrenko et al. (2008b). ^{14}C procedural blanks were greatly reduced through the construction of a new CH_4 conversion line utilizing platinized quartz wool for CH_4 combustion and the use of an ultra high purity iron catalyst for graphitization. The amount and ^{14}C activity of extraneous carbon added in the new CH_4 conversion line were determined to be 0.23 ± 0.16 μg and 23.57 ± 16.22 percent modern carbon (pMC), respectively. The amount of modern (100 pMC) carbon added during the graphitization step has been reduced to 0.03 μg. The overall procedural blank for all stages of sample handling was 0.75 ± 0.38 pMC for ~20 μg, ^{14}C-free air samples with [CH_4] of 500 ppb.

5.2 ^{14}C corrections for in-situ CH_4 production in Pakitsoq ice

5.2.1 ^{14}C of in-situ produced CH_4

Table 5.1 shows $^{14}CH_4$, ^{13}C of CH_4 ($\delta^{13}CH_4$), and [CH_4] values measured in Pakitsoq samples, as well the [CH_4] values expected based on the GISP2 ice core record. As was discussed in Chapter 3, sample [CH_4] is higher than predicted from the GISP2 [CH_4] record (by up to 128 ppb) for some samples. It was demonstrated in Chapter 3 that elevated [CH_4] does not result from processing or ambient air leaks in these samples; thus this indicates that CH_4 production must occur in the ice by an

unknown mechanism. It is likely that $^{14}CH_4$ and $\delta^{13}CH_4$ have been affected by this in-situ component for samples with elevated [CH_4].

Price (2007) found evidence suggesting microbial CH_4 production in silty basal GISP2 ice. As was discussed in Chapter 2, Pakitsoq ice contains bands of silty ice (dust bands). Although all dust bands were carefully removed when sampling Pakitsoq ice, it is possible that fine-grained silt is present in smaller concentrations in ice outside of the dust bands. Thus, methanogenesis may be occurring in Pakitsoq ice via a mechanism similar to that proposed by Price (2007). Alternatively, a small amount of CH_4-rich sediment may have been entrained in Pakitsoq ice layers through ice flow processes, affecting [CH_4] in the ice.

For two of the samples (Contaminated PB and Contaminated OD), [CH_4] is substantially elevated in comparison to replicate samples of the same age (Table 5.1). $^{14}CH_4$ for these two samples is also significantly higher than that for other replicates. This allows a determination of ^{14}C of the contaminating CH_4. We assumed that, without the addition of extra in-situ [CH_4], the $^{14}CH_4$ and [CH_4] of the Contaminated PB sample would be the same as the corresponding averages for Preboreal 1 and Preboreal 2 samples. The mean ages of all Preboreal samples are within 27 years of one another, making this a robust assumption. Similarly, the values for the Contaminated OD sample were compared to the average values for Oldest Dryas 1 & 2 samples. The expected [CH_4] for all the Oldest Dryas samples is identical (Table 5.1). The mean age of the Contaminated OD sample is ~ 260 years greater than for

Oldest Dryas 1 & 2, and a decay correction was made for this to allow for comparison of $^{14}CH_4$ values.

A simple isotopic mass balance calculation then yields 79.3 ± 3.9 pMC for the ^{14}C of contaminating CH_4 in case of the Contaminated PB sample, and 84.1 ± 20.5 pMC in case of the Contaminated OD sample. The large uncertainty for the case of the Contaminated OD sample is due to relatively large uncertainties in measured and expected [CH_4] in comparison to the magnitude of [CH_4] elevation in the sample. The similarity in the calculated ^{14}C of the in-situ contaminant for both samples suggests a common production mechanism.

5.2.2. Additional clues from $^{14}CO_2$

In an attempt to understand this problem further, we performed measurements of ^{14}C of CO_2 ($^{14}CO_2$) on the remaining air in our samples, as CO_2 is a common substrate for methanogenesis. Also, if there is microbial in-situ production of both CH_4 and CO_2, the ultimate carbon source is likely to be the same for both and thus have the same ^{14}C isotopic signature. Because $^{14}CO_2$ was not part of the originally planned work, the method testing and development for this was not nearly as extensive as with $^{14}CH_4$.

Air processing was done at SIO in the Keeling lab. CO_2 was cryogenically extracted from the air samples on the extraction line that is normally used for work on dissolved inorganic carbon (DIC) of seawater, following the usual gas handling procedures for that line. The line and procedure were as described in Leuker (1998).

The initial pressure in Pakitsoq air sample tanks was ~0.3 bar. Only ~ 0.5 L STP of air was used per sample, resulting in sample sizes of 25 – 55 μg C, depending on sample [CO_2]. The remainder of the air was saved for subsequent processing for ^{14}C of CO (see Section 5.4). The recovered CO_2 was flame-sealed in 6 mm OD Pyrex tubes which had been pre-cleaned by rinsing with DI water and baking at ~510˚C for 8 hr. Graphitization and ^{14}C measurement by AMS were performed at ANSTO using methods described in Chapter 4. Two synthetic mixtures, each containing ~165 parts per million (ppm) of CO_2 in ultra-high purity (u.h.p.) air, were prepared at SIO and processed along with Pakitsoq samples to assess any ^{14}C blanks associated with the CO_2 extractions. One of the mixtures used fossil CO_2 ("Blank CO_2 Mix" in Table 5.2), and the other used modern CO_2 derived from ethanol manufacturing ("Modern CO_2 mix" in Table 5.2). One each "modern" and "blank" mixture was processed at the start of the sample sequence, and one each at the end of the sample sequence. Two large (~1000 μg C) sample aliquots were also taken from each of the source CO_2 tanks to obtain reliable ^{14}C values for these.

Table 5.2 shows the [CO_2] and $^{14}CO_2$ results for Pakitsoq samples as well as for the supporting samples discussed above. As can be seen from the ^{14}C results corrected for ANSTO processing, the average $^{14}CO_2$ of the "blank" synthetic mixture is in excellent agreement with the $^{14}CO_2$ of the parent CO_2 tank. The average $^{14}CO_2$ for the modern synthetic mixture, however, is ~ 3 pMC lower than that of the large samples; this is a significant difference given the errors. This set of results could be consistent with either addition of a small amount of extraneous ^{14}C-free carbon in the

CO_2 extraction line, isotopic fractionation in the extraction line, or both. Isotopic fractionation needed to explain such a shift would need to be quite substantial, however (~ 30 ‰ in $\delta^{13}C$), and is highly unlikely, given excellent sample yields (~100% for all samples, based on mass determinations at ANSTO). We thus assumed that this is due to addition of ^{14}C-free extraneous carbon. By simple mass-balance, the mass of this extraneous carbon is then 1.1 ± 0.5 μg. We then used this value to correct the Pakitsoq sample $^{14}CO_2$ for SIO processing.

It is possible that the field melt-extraction procedure also had an effect on $^{14}CO_2$. No attempt has been made to correct $^{14}CO_2$ for this effect. [CO_2] measured in the field blank extractions was 3 – 16 ppm, as compared to 2.5 ppm for the standard gas used in the blank extractions. It is not possible to say how much of the [CO_2] elevation in the field blanks was due to outgassing of CO_2 from the extraction apparatus, and how much was due to outgassing of left-over CO_2 from the meltwater. The low [CO_2] in the blanks as compared to the samples, however, suggests that if there is some CO_2 production in the extraction apparatus, the amount is relatively small and would not have a large effect on sample $^{14}CO_2$. No ^{14}C correction was attempted to account for effects of the melt-extraction.

Given the age of sample air and expected $^{14}CO_2$ between 20 and 29 pMC, the results were quite surprising, with all sample values between 66 and 78 pMC (Table 5.2), which is in good agreement with the determined ^{14}C of the in-situ CH_4. The much higher than expected sample $^{14}CO_2$ can in principle be explained by two

mechanisms: cosmogenic production of ^{14}C in the ice or addition of a large amount of high-^{14}C CO_2 in-situ.

Measured sample [CO_2] values are lower than expected from the ice core record (Table 5.2). Measured [CO_2] in these air samples, however, is probably a poor indicator of [CO_2] in sampled ice. Sample air is obtained by melt-extraction, and CO_2 is highly soluble. Because [CO_2] was never a major goal of this project, no attempts were made to quantify the effects of the field melt-extraction on sample [CO_2]. Nor are the pH or concentrations of carbonate, bicarbonate or other trace ions in Pakitsoq ice known, which may have allowed to estimate the extent of CO_2 dissolution during the melt-extractions. The following discussion of true [CO_2] in Pakitsoq ice is therefore speculative. A crude estimate may be obtained simply by considering the solubility of CO_2 in pure water. For this, we take the value of 0.0731 M/atm for K_H (the Henry's Law constant) at 0˚C, estimated from data in Lide and Frederikse (1995). We then use Equation 3.1 (Chapter 3) to estimate the fractions of CO_2 in the water and the headspace. For less soluble gases (N_2, Ar, Kr, Xe), it was shown in Chapter 3 that the fraction of full solubility equilibrium attained was 0.4 – 0.8. If it is assumed that CO_2 behaves in a similar manner, then ~50% of sample CO_2 will be in the meltwater. However, it is known that CO_2 does not behave the same way, as CO_2 dissolution involves chemical interactions. Thus CO_2 may dissolve faster and reach a full solubility equilibrium during the melt extractions. In this case, we calculate that only 20% of the CO_2 will be in the extracted air sample, with the rest remaining in the meltwater.

Thus, the true [CO_2] in sampled ice must be higher than what is measured in the air samples, and it is possible that it is much higher than the expected paleoatmospheric values. This leaves room for in-situ CO_2 production and $^{14}CO_2$ elevation by this mechanism. Figure 5.1 shows that sample [CO_2] does in fact explain a substantial fraction of the variance in $^{14}CO_2$, as well as in [CO]. However, both relationships are probably confounded to a large extent by [CO_2] dissolution during the melt-extraction. If we assume that all $^{14}CO_2$ elevation over expected values is due to in-situ CO_2 production, it is possible to make a (very speculative) estimate of the actual [CO_2] in sampled ice. For this estimate, we assumed that the ^{14}C of in-situ CO_2 is equal to that determined for in-situ CH_4 (79 pMC). These estimates are shown in the last column of Table 5.2, with all [CO_2] values > 1000 ppm.

There is some evidence to suggest that $^{14}CO_2$ in the samples was also elevated by cosmogenic ^{14}C production in the ice. This comes from the $^{14}CO_2$ vs [CO_2] relationship plotted in Figure 5.1 (a and b). The expected [CO_2] is essentially the same for all YD, YD-PB Transition, and PB samples (Table 5.2). Same applies for all OD and Bølling samples. The actual measured [CO_2] is then some function of the actual paleoatmospheric [CO_2], in-situ CO_2 production, and melt-extraction effects. Given the large range of measured [CO_2] values, it is likely that in-situ production was variable and samples with lower measured [CO_2] come from ice with less in-situ CO_2. Given the slopes of the $^{14}CO_2$ vs [CO_2] relationships in Figure 5.1, even if the linear fit lines were extended all the way to [CO_2] of zero, $^{14}CO_2$ would still be 60 – 65 pMC. This is not consistent with in-situ CO_2 production being the only mechanism

responsible for elevating $^{14}CO_2$ in the samples. Instead, this is consistent with sample $^{14}CO_2$ being elevated to ~ 65 pMC for all samples by cosmogenic ^{14}C production, with further slight elevation due to in-situ production of CO_2 with ^{14}C of ~ 79 pMC. However, we emphasize that the discussion of sample $^{14}CO_2$ and $[CO_2]$ is speculative because the melt-extraction effects on these parameters were not quantified.

It is interesting to note that sample $[CH_4]$ excess over expected does not seem to correlate with [CO], $[CO_2]$, or $^{14}CO_2$. This suggests the mechanism by which excess CH_4 is introduced in the ice is decoupled from the in-situ mechanisms for CO and CO_2.

A further piece of evidence comes from work which used ^{14}C dating of organic material to constrain past ice margin fluctuations in the Pakitsoq area (Weidick et al., 1990). This work showed that in the mid-Holocene the Pakitsoq ice margin had retreated, creating a marine fjord in an area which is upstream of our sampling site with respect to modern ice flow lines. The ice subsequently re-advanced between 2 – 3 kyr BP. Two ^{14}C dates of organic material (reindeer bone and a mollusk) are available from moraine material at the Pakitsoq ice margin within ~1 km of our sampling site, giving conventional ^{14}C ages of 3040 and 3420 yr, respectively, which translate to 68.5 and 65.3 pMC. This again is similar to the $^{14}CO_2$ and $^{14}CH_4$ of the contaminant we observe in the Pakitsoq samples. The common occurrence of dust bands in Pakitsoq ice indicates that material from the glacier bed is becoming entrained in the ice layers through folding and flow dynamics, probably near the ice margin. This then provides a mechanism to introduce organic matter (and microbial

communities) with similar ^{14}C activity to that described in Weidick et al. (1990) into Pakitsoq ice, which can then serve as a substrate for in-situ CH_4 and CO_2 production.

It is interesting to note that Pakitsoq ice (with a younger estimated calendar age of 9000 ± 1000 yr BP) has previously been measured for $^{14}CO_2$, yielding 67 ± 9 pMC (van de Wal et al., 1990). This agreement with our measurements is remarkable, considering that the van de Wal et al. (1990) measurements used a dry-extraction technique.

5.2.3. ^{14}C corrections for in-situ CH_4

The evidence available to us from the $^{14}CO_2$ measurements and the earlier Weidick et al. (1990) and van de Wal et al. (1990) work leaves many unknowns, and does not allow for definitive identification of the mechanism responsible for elevated CH_4 in some of the Pakitsoq samples. It does, however, seem to constrain the ^{14}C activity of in-situ CO_2, CH_4 and organic material in Pakitsoq ice between 65 and ~ 80 pMC. This is a narrow enough range to allow for meaningful corrections to be made to sample $^{14}CH_4$ based on the amount of $[CH_4]$ excess.

One question is how to choose the $^{14}CH_4$ of the in-situ component for each sample, to use in the corrections. Two estimates for ^{14}C of in-situ CH_4 are available (see above); and they may or may not reflect the same value, given the uncertainties. A further complication is that neither of these estimates come from samples that are actually to be corrected. $^{14}CO_2$ measurements are available for each sample, but these are somewhat uncertain due to the possible effects of the melt extraction; further they

do not agree perfectly with $^{14}CH_4$ of the in-situ contaminant (e.g., for Contaminated PB, in-situ $^{14}CH_4$ = 79.3 ± 3.9 pMC, $^{14}CO_2$ = 69.61 ± 2.72). It seems likely that the ^{14}C of in-situ CH_4 in ice sections which are physically close together should be uniform, especially if these sections are within the same stratigraphic layer. Sections within the same stratigraphic layer would have contacted the glacier bed at the same time and in the same place, entraining organic matter of likely uniform age. All of the samples spanning the YD-PB transition were taken from YD-age ice, all within just a few meters of each other. The situation is analogous for the OD-Bølling samples, where the ice sampled was all of OD age. Our choice is therefore to use the ^{14}C of in-situ CH_4 determined for the Contaminated PB sample (79.3 ± 3.9 pMC) to correct all the samples from the YD-PB transition, and the ^{14}C of in-situ CH_4 determined for the Contaminated OD sample (84.1 ± 20.5 pMC) to correct all the samples from the OD-Bølling transition. This correction is somewhat speculative because, despite the combined evidence from $^{14}CH_4$ of Contaminated OD and PB samples, $^{14}CO_2$, and ^{14}C of organic fossils, we cannot completely rule out that the actual $^{14}CH_4$ of in-situ CH_4 in the samples we corrected may be substantially different from the values we chose to use. For example, it may be possible that ^{14}C of in-situ CH_4 for some samples is closer to ^{14}C of organic matter deposited at the accumulation site (~ 20 – 30 pMC). However, the correction we applied represents a most-likely scenario given the available data.

The correction can be applied by using a simple mass-balance equation (e.g., Equation 4.1 in Chapter 4) as long as the ^{14}C of the contaminant as well as the true

expected [CH_4] are known. Determination of expected [CH_4] for the YD, PB, OD and Bølling samples is straightforward from the GISP2 [CH_4] record (Table 5.1) and was discussed in Chapter 3.

Determining the true [CH_4] for the YD – PB Transition samples proved more difficult. These samples spanned the ice containing the YD-PB [CH_4] rise, with [CH_4] changing rapidly from ~ 500 to ~ 750 ppb. Small errors in assigned ages can therefore result in large changes in expected true [CH_4]. We used our record of $\delta^{15}N$ in the horizontal profile spanning the sampling area (see Figure 3.4) to constrain the exact ages (and expected [CH_4]) of the YD-PB Transition samples. $\delta^{15}N$ is the most robust of the tracers we routinely measured in Pakitsoq ice, with pooled standard deviations of 0.010 ‰ or better for replicate samples (Petrenko et al., 2006). $\delta^{15}N$ also has a characteristic thermal diffusion peak at the YD-PB transition, which has been identified in both GISP2 and Pakitsoq ice. An ice sheet flow-line model indicates that ice outcropping at Pakitsoq originates near Greenland Summit (Reeh, 1988; Reeh et al., 2002); thus the temporal evolution in the abrupt warming at Summit and at the deposition site of Pakitsoq ice, as well as the evolution of firn thickness (both of which control $\delta^{15}N$) would be expected to be similar for both sites. Figure 5.2 shows the two plausible scenarios for a match between the $\delta^{15}N$ peak in Pakitsoq and GISP2, with the caption describing how the match was constructed in each scenario. Given the variability in degree of thinning in Pakitsoq ice (Petrenko et al., 2006), uncertainties in $\delta^{15}N$ in GISP2 (± 0.020 ‰) and this Pakitsoq profile (± 0.009 ‰) , as well as possible slight differences in the evolution of the $\delta^{15}N$ peak at the two deposition sites, either

scenario is plausible. However, it will be shown in section 5.6.1 that scenario A is unlikely.

As can be seen, scenario A predicts that Pakitsoq transition [CH_4] is highly elevated over expected, while scenario B predicts that Pakitsoq transition [CH_4] is very close to or slightly lower than that expected from GISP2. For each scenario, the expected [CH_4] of the YD-PB Transition large air samples was calculated by establishing a precise gas age scale for Pakitsoq based on the $\delta^{15}N$ match, and then integrating under the GISP2 [CH_4] curve for the age range spanned by each sample. As for the other samples, the uncertainties in predicted [CH_4] for each scenario were determined by alternatively removing a fraction of the age range (1/6th in this case) from the integral, either on the young or old end of the range. The resulting predicted [CH_4] values for each scenario are shown in Table 5.1.

The expected and measured [CH_4] values agree within the uncertainties for YD, PB, YD-PB Transition (Scenario B) and OD samples (Table 5.1). These samples thus may or may not contain in-situ CH_4, while Bølling samples definitely contain it. In the interest of treating all samples in a uniform manner, as well as to accommodate the increase in ^{14}C uncertainties associated with possible in-situ production, we applied the ^{14}C correction for in-situ CH_4 to all samples, regardless of the apparent [CH_4] excess over expected. The correction was applied following the simple mass-balance formula (Equation 4.1). The errors for the corrected values were determined using the standard error propagation techniques assuming 1-σ errors for all quantities. Because the ^{14}C of the contaminant is clearly higher than the ^{14}C of the

paleoatmospheric CH_4, the corrected value cannot be higher than the uncorrected value. This resulted in reduction of the calculated errors on the "plus" side of the distribution, and asymmetrical error bars for the corrected values. For YD-PB Transition samples under Scenario B, where the expected [CH_4] is a few ppb higher than measured [CH_4], the applied correction assumed zero for the amount of in-situ CH_4. The errors were still propagated to allow for the increase in uncertainty associated with possible in-situ production. The corrected $^{14}CH_4$ values and uncertainties are shown in Table 5.1, and the averages for replicate samples are plotted in Figure 5.3. Note that the only samples for which this correction makes a noticeable difference in $^{14}CH_4$ are the Bølling and, to a lesser extent, the OD.

Because the measured and expected [CH_4] do agree within errors for YD, YD-PB Transition (Scenario B), PB and OD samples, this correction may not be needed. We therefore also consider a scenario in which the $^{14}CH_4$ correction for in-situ CH_4 is applied only to the Bølling samples; this is discussed further below.

5.3 The case for direct cosmogenic production of $^{14}CH_4$ in Pakitsoq ice

Figure 5.3 shows the $^{14}CH_4$ averages for the replicate samples, corrected for in-situ CH_4 production, along with the predictive models introduced in Chapter 1 (Figure 1.5). The values can also be found in Tables 5.1 and 5.7. We use units of age-corrected Δ in the figures instead of pMC, because the pMC units are not meant to be used with age corrections. It is immediately apparent that, for most of the sample averages, $^{14}CH_4$ values are significantly higher than even the highest possible

paleoatmospheric $^{14}CH_4$ values (for a scenario where 100% of CH_4 emissions have the same ^{14}C signature as contemporaneous CO_2). There must therefore be another mechanism by which sample $^{14}CH_4$ is elevated *without* significantly affecting [CH_4]. We have considered several possibilities.

Procedural ^{14}C contamination has been demonstrated to be very small, and has been corrected for (Chapter 4). Further, it was shown in Chapter 4 that, given the expected levels of ^{14}CO in the samples, as well as the CO removal efficiency in the air processing line, any effect on $^{14}CH_4$ from ^{14}C in CO in the samples would be negligible. More accurate determinations of ^{14}CO in the Pakitsoq samples have since been made (see Section 5.4). These measurements revealed ^{14}CO levels ~10 times lower than what we used in the Chapter 4 estimates, further reinforcing our earlier conclusion that ^{14}C from CO did not affect $^{14}CH_4$ during sample air processing.

It is remotely possible that $^{14}CH_4$ is produced from ^{14}CO in the melter during the melt-extraction. Measurements of ^{14}CO in Pakitsoq samples (see section 5.4) indicate sample ^{14}CO activities of 200 – 450 pMC. If 10 ppb of CO with ^{14}C activity of 300 pMC is somehow converted to CH_4 in a YD sample, for example ([CH_4] of ~ 500 ppb; expected $^{14}CH_4$ of ~ 28 pMC under the zero-fossil emissions scenario) , sample $^{14}CH_4$ increases from 28.0 to 33.3 pMC. 10 ppb is a small enough amount to be undetectable given the uncertainties in measured and expected [CH_4]. Catalytic production of CH_4 from CO and steam is known (Johnson and Nelson, 1971; Rabo et al., 1980). However, the reaction conditions for such catalytic production are strikingly different from the environment in the melter. For example, aluminum is not

one of the metals used for catalysis, the reaction temperatures are always >100 ˚C, [CO] in the reactant stream is at least 1% (as compared to < 1 ppm in Pakitsoq samples), and the reactant stream does not appear to contain substantial amounts of oxygen. The reaction described in Rabo et al. (1980) proceeds in two steps, with the first step involving production of a layer of activated carbon on the catalyst surface, followed by methanation of this carbon by reaction with steam or hydrogen. From the descriptions of Johnson and Nelson (1971) and Rabo et al. (1980), it was unclear whether CH_4 could still be formed by these processes in the presence of substantial amounts of oxygen. However, it seems likely that in the presence of oxygen CO_2 would be formed instead of CH_4. We thus conclude that this mechanism is extremely unlikely. We further note that production of $^{14}CH_4$ from ^{14}CO in sample cylinders during storage on a scale greater than 1 ppb was ruled out by repeated high-precision measurements of $[CH_4]$ over the storage period.

Another possibility is that we are seeing a real paleoatmospheric signal, and that $^{14}CH_4$ was in fact higher than $^{14}CO_2$ in the ancient atmosphere. This would require direct cosmogenic production of $^{14}CH_4$ in the atmosphere. If such a natural mechanism operated in the past, it would still be expected to operate today. In this case, because cosmic ray intensity increases with altitude, we would expect to find higher $^{14}CH_4$ in the stratosphere than at the Earth's surface, similar to what is observed for ^{14}CO and $^{14}CO_2$ (e.g., Brenninkmeijer et al., 1995). However, measurements of $^{14}CH_4$ in the lower stratosphere and upper troposphere do not show values in excess of

surface $^{14}CH_4$ (Brenninkmeijer et al., 1995; Lowe et al., 1991). We can thus rule this possibility out.

A third possibility is production of $^{14}CH_4$ directly from ^{14}CO in the ice. In this case, again, it would be possible to raise $^{14}CH_4$ in the ice by this mechanism without a detectable effect on [CH_4]. All known natural processes of CH_4 production that do not require high temperatures are mediated by methanogens. CH_4 production by methanogens utilizing CO as a substrate has been observed (e.g. Moran et al., 2008; Rother and Metcalf, 2004). However, [CO] in these studies was 5% or higher, as compared with <1 ppm in Pakitsoq samples. More importantly, all studies examining microbial conversion of CO to CH_4 (Rother and Metcalf, 2004 and references therein) found that CO is first oxidized to CO_2, and CH_4 is subsequently produced by reduction of CO_2. [CO_2] in Pakitsoq ice is at least 100 x higher than [CO]. If conversion of CO_2 to CH_4 by methanogens does indeed occur in Pakitsoq ice, it would then be expected that only a very small fraction of this CO_2 is derived from CO. Finally, we show in section 5.4 that most or even all of cosmogenic ^{14}CO in Pakitsoq ice (which is the cause of high ^{14}CO activities) is produced during only a few years before the ice is sampled. It then follows that ^{14}CO activities in the ice would have been much lower than measured prior to these last few years preceding ice sampling. If methanogenesis occurs in Pakitsoq ice, it is likely that this process is ongoing from the time methanogens are injected into the ice by interaction with subglacial material, rather than happening only in the last few years before the ice becomes exposed at the surface. It then follows that any CH_4 production from CO would have utilized CO

with much lower ^{14}C activities than were measured in the samples. Taking all of the above arguments together, we conclude that it is very unlikely that any $^{14}CH_4$ elevation in the samples can be attributed to direct microbial production of CH_4 from CO in the ice.

A useful clue can be obtained by examining the amount of $^{14}CH_4$ elevation over the expected values (zero fossil emissions scenario) for different samples. It is clear from Figure 5.3, that in general, samples with lower [CH_4] have a greater $^{14}CH_4$ elevation over expected. This suggests a mechanism of $^{14}CH_4$ addition by which a fixed amount of $^{14}CH_4$ is added per gram of ice; so that $^{14}CH_4$ in samples with higher [CH_4] is less affected because of greater dilution.

One such mechanism is direct cosmogenic production of $^{14}CH_4$ molecules in the ice. Direct cosmogenic production of ^{14}CO and $^{14}CO_2$ molecules in ice in ablation and accumulation zones is well known (e.g. Lal et al., 1990; Smith et al., 2000; van der Kemp et al., 2002). ^{14}C is produced from oxygen atoms in the ice by neutron-induced spallation; production by muon capture has also been suggested (van der Borg et al., 2001; van der Kemp et al., 2002). The resulting "hot" ^{14}C atom can be involved in multiple chemical reactions before all of its energy is dissipated. To the best of our knowledge, cosmogenic production of $^{14}CH_4$ molecules in ice or water has never previously been observed under natural conditions on the Earth's surface. However, prior to our work no one has tried to investigate this; nor would it have been possible without the development of a large-scale ice sampling system similar to ours. Under laboratory conditions, several experiments in which water and/or ice were subjected to

intensive irradiation by protons to produce hot ^{11}C atoms or by $^{14}C^{+}$ or $^{14}CO^{+}$ beams did find that that a small fraction of the hot C atoms ended up as CH_4; other simple organics were also formed (Evans, 1970; Rossler et al., 1984; Stenstrom, 1970). It therefore seems possible that Pakitsoq ice contains $^{14}CH_4$ of cosmogenic origin. In absence of other plausible explanations, we consider this to be the most likely mechanism by which Pakitsoq sample $^{14}CH_4$ is elevated above the expected levels.

5.4 Measurements of ^{14}CO in Pakitsoq ice: understanding the cosmogenic ^{14}C component

To gain insight about the possible cosmogenic $^{14}CH_4$ production in Pakitsoq ice, we measured ^{14}C of CO (^{14}CO) on the air remaining in sample tanks after completion of $^{14}CH_4$ and $^{14}CO_2$ work. As with $^{14}CO_2$, these measurements were far beyond the original project plan. As time and resources were limited, method development and testing were not pursued as rigorously as with $^{14}CH_4$ measurements. Only ~10 L STP of air per sample was available for these measurements. [CO] in the samples was between 500 – 1300 ppb (Table 5.4); the resulting sample sizes were 3 – 7 μg C which necessitated dilution with ^{14}C-free CO_2 prior to graphitization and AMS measurement.

5.4.1 High [CO] in Pakitsoq samples

The high [CO] observed in the samples was unexpected (Table 5.4). Model results of Crutzen and Bruhl (1993) and Wang and Jacob (1998) as well as models

summarized in Haan et al. (1996) suggest that pre-industrial northern high latitude [CO] was 10 – 77 ppb. Elevated [CO] (up to ~ 180 ppb) has previously been observed in ice cores (Haan and Raynaud, 1998; MacFarling Meure, 2004), though never to such extent as in Pakitsoq ice. We are not aware of any prior measurements of [CO] in ablating glacial ice. Because elevated [CO] has been observed in ice accumulating at Greenland Summit (Haan and Raynaud, 1998), some of the in-situ CO production in Pakitsoq ice probably happened before the ice reached the Pakitsoq margin. However, given elevated CH_4, likely elevated [CO_2] and the presence of organic matter scraped from the glacier bed, as well as relatively warm ice temperatures near the margin (-7 ˚C in one measurement a few meters below surface), we speculate that much of the [CO] excess is probably a result of in-situ production near the Pakitsoq margin. The mechanisms of CO production in ice are unknown, though several hypotheses exist. First, Colussi and Hoffmann (2003) proposed that [CO] alterations can be explained by photochemical CO production from organics in the ice by ultraviolet (UV) radiation generated by fast muons passing through deep ice. Second, Haan and Raynaud (1998) hypothesized that the elevated [CO] was due to oxidation of organic impurities by H_2O_2. Third, several types of microbes are known to produce CO (e.g. Bowater et al., 2004; Tsunogai et al., 2005). Viable microbes are present in glacial ice and may be metabolically active (Price, 2007; Rohde and Price, 2007). Thus, microbial production may also be responsible for elevated [CO] in Pakitsoq ice.

5.4.2 ^{14}CO measurement methods

Carbon from CO for the AMS ^{14}C measurement was collected by combusting CO to CO_2, with subsequent cryogenic trapping of this CO_2. The CO extraction was performed at NIWA, using the same extraction line as for $^{14}CH_4$ work (see Chapter 4). The extraction procedure was largely similar to that for CH_4; however there were some modifications to the line and procedure and these are detailed below. Originally we attempted to oxidize CO using the Sofnocat reagent; however it was determined using $\delta^{13}C$ measurements with test samples that Sofnocat had a large carbon "memory", presumably due to the open alumina support structure of the catalyst, resulting in very high surface area. We therefore decided to use the platinized quartz wool furnace for CO oxidation, lowering the furnace temperature to 150˚C. It was found that at 150˚C, CO sample yields were 90 – 100%, while only 0.4% or less of CH_4 was combusted. The resulting contribution from CH_4 to total sample mass was 0.3% or less for all samples.

All Pakitsoq sample tanks were at ~0.3 bar after completion of $^{14}CH_4$ and $^{14}CO_2$ measurements. To boost the tank pressure and to reduce the CO mixing ratio for more reliable air processing and [CO] measurements, the sample air was diluted with CO-free u.h.p. air to bring the tank pressures to 3 bar. The u.h.p. air was passed through Sofnocat prior to entering the sample tanks, to ensure zero [CO] levels; the absence of [CO] in this air was confirmed several times by GC measurements.

When running the samples, diluted sample air was put through the extraction line at 0.99 L STP/min, first passing through the four upstream cryogenic traps, where H_2O, CO_2, N_2O and non-methane hydrocarbons were removed. Bypassing Sofnocat,

the air then entered the platinized quartz wool furnace at 150˚C where CO was combusted to CO_2; the resulting CO_2 was then captured on 3 cryogenic traps downstream of the furnace. The line was flushed with at least 10 L STP of u.h.p. air between the samples; this was followed with a flush of the sample air itself, for 1 min prior to starting the CO_2 collection. Small fans were installed to warm the glass stem valves downstream of the cryogenic traps (to prevent leaks, which have been shown to occur when these valves became too cold). An automated system was also added to maintain liquid nitrogen around the cryogenic traps at constant levels.

Prior to processing Pakitsoq samples, line performance was tested by processing several samples from a synthetic CO – u.h.p. air mixture ([CO] = 158 ppb) and monitoring the sample yields and $\delta^{13}C$. The sample yields were found to be in the 90 – 100% range, and $\delta^{13}C$ values agreed within measurement error with a sample from the same mixture that was processed on an extraction line routinely used at NIWA for CO isotopic work (Brenninkmeijer, 1993).

CO_2 derived from sample CO was flame-sealed in 6 mm OD Pyrex tubes and sent to ANSTO for ^{14}C processing. All samples were diluted with ~15 μg of ^{14}C-free CO_2 prior to graphitization, to bring the sample sizes to ~20 μg. Graphitization and AMS measurement were performed as described in Chapter 4.

5.4.3. ^{14}CO results and corrections for ANSTO processing

Table 5.3 shows the ^{14}CO results as measured, as well as after corrections for processing at ANSTO. Unfortunately, two of the Pakitsoq samples (Bølling 1 and 2)

as well as several further samples processed to assess the NIWA ^{14}CO blank, have not yet been measured. The ^{14}C results for all samples were normalized to a set of 3 ~20 μg C OX-1 standards (which were measured concurrently with the samples), which eliminates the need to make corrections for procedural fractionation, as samples of the same size will be fractionated similarly. Given the dilution factors, the inferred ^{14}CO activities for Pakitsoq samples are between 200 and 450 pMC. Since the objective of the ^{14}CO measurements was to gain insight into cosmogenic ^{14}C in Pakitsoq ice, it is useful to work in units of ^{14}C atoms. This was calculated from the ANTARES AMS raw data, which gives the $^{14}C/^{13}C$ ratio for sample versus the OX1 standard (times a constant), as follows:

$$^{14}\text{C atoms} = \frac{\frac{^{14}C}{^{13}C}_{\text{sample}}}{\frac{^{14}C}{^{13}C}_{\text{OX1}}} \times \frac{^{14}C}{^{13}C}_{\text{OX1}} \times \frac{\text{Mass (g)} \times 6.02 \times 10^{23}}{13 + 12 \times \frac{^{12}C}{^{13}C}_{\text{sample}}} \qquad (5.1)$$

The $^{14}C/^{13}C$ ratio for OX1 in 2007 was 1.126×10^{-10}. $\delta^{13}CO$ values (not shown) have been measured in all samples except for Preboreal 1 (a procedural problem) in the laboratory of John Mak at the State University of New York at Stony Brook, and were used in the ^{14}CO calculations; it was assumed that $\delta^{13}CO$ for Preboreal 1 was the same as for Preboreal 2 sample. $\delta^{13}C$ of the dilutant CO_2 was measured to be -4 ± 1 ‰ (approximate measurements obtained along with ^{14}C on ANSTO's STAR accelerator).

Two large (2 mg and 1 mg C) samples of the dilutant CO_2 were processed to assess the amount of ^{14}C added to the samples with the dilutant. Three small (~20 μg C) samples of this same dilutant were also processed to assess the procedural ^{14}C

blank. The average ^{14}C activity for the large samples was 0.12 pMC; for the small samples it was 0.27 pMC, confirming that the dilutant was quite ^{14}C-depleted and the ANSTO processing blanks were low. As can be seen from Table 5.3, ^{14}C in Pakitsoq samples that originates from the dilutant or from the ANSTO blank amounts to < 1% of total ^{14}C for all samples.

To check whether there was a ^{14}C blank associated with the dilution procedure itself, 3 ~7 μg C samples of the OX-2 standard were prepared and diluted to ~ 20 μg as for the Pakitsoq samples. 3 ~20 μg C undiluted samples of OX-2 were also prepared for comparison. The calculated ^{14}C atoms per unit mass values (not shown) for these two sets were in excellent agreement, indicating no significant ^{14}C blank associated with the dilution.

5.4.4 ^{14}CO corrections for air processing at NIWA

Data from NIWA processing of Pakitsoq sample air for ^{14}CO are shown in Table 5.4. The remaining sample air in all tanks was stored at ~0.3 bar for 1 yr prior to processing for ^{14}CO. Pressure measurements in all sample tanks at the start and end of this storage period showed excellent agreement for all samples, demonstrating that no significant ambient air leaks into the tanks had taken place.

[CO] in the sample tanks shown in Table 5.4 was calculated based on [CO] measurements after dilution with CO-free u.h.p. air; however earlier [CO] measurements (up to 3 years earlier) on the tanks were also attempted as described in Chapter 4. These earlier measurements yielded [CO] values 1.5 – 3 times higher than

what was determined based on [CO] in the diluted tanks. This may be viewed as suggestive of slow CO consumption in the electropolished stainless steel sample tanks over time. If this CO consumption is real, it presents a problem for the interpretation of the results, as ^{14}CO will of course also be consumed and the calculations will then underestimate the ^{14}CO content in sampled Pakitsoq ice. However, the [CO] values measured in the undiluted samples (800 – 2500 ppb) are quite far out of the calibration range of the mercuric oxide (HgO) reducing detector used at NIWA for measurements of ambient [CO]. The HgO detectors are well known to be non-linear (Novelli, 1999), and the measurements thus do not indicate actual values. For example, one dry, high-concentration synthetic mixture of CO in u.h.p. air, stored in a Scott-Marrin Al cylinder, was measured for [CO] several times in October-November 2004, and then again in March 2006. The earlier measurements yielded 5800 – 7000 ppb; while the later measurement was 3961 ppb; an apparent [CO] decrease similar to that observed for the Pakitsoq samples over the same time period. Although it is in principle possible that CO can be adsorbed or consumed in some way in a cylinder, [CO] growth in cylinders over time is much more common (Gordon Brailsford, personal communication, 2007). Further, the electropolished stainless steel cylinders of the same kind that are used for Pakitsoq samples have been shown to be very stable for [CO] (Paul Novelli, personal communication, 2007). It thus seems likely that the apparent [CO] decrease over time in Pakitsoq sample tanks is a measurement artefact; we thus assume that no actual CO consumption has occurred.

A problem was encountered in the processing of the Pakitsoq samples for CO which, unfortunately, was not identified until after all the samples had been processed. A reinforced teflon hose, which was used to connect sample tanks to the extraction line, had developed a leak, probably due to repeated connecting and disconnecting of the hose. This resulted in substantial leaks of lab air into the line during processing, which can be seen from looking at the sample yields in Table 5.4. The yields for the first three samples listed, which were processed to assess the line ^{14}C blanks, are similar to those in earlier line tests. The leak appears to have developed after the processing of these first samples, as indicated by the high and variable yields for Pakitsoq samples. As this leak was established to be the major source of extraneous ^{14}C added during NIWA processing, the corrections we applied focus on this single source of contamination.

Because the leak did not appear to affect the initial three samples (or at least not to the same extent), they cannot be used for their intended purpose of quantifying the line processing blank. However, some estimates of the maximum and minimum amounts of extraneous ^{14}C which was added can be obtained by considering the sample yields as well as the air volume processed. The yield determination for these samples is less certain than in the $^{14}CH_4$ work (see Chapter 4), due mostly to smaller sample size; and the uncertainties in both the expected and measured sample size are both ~ 5%. Because 90% was the typical yield in successful line tests (which gave the correct $\delta^{13}C$), we took this as the expected value for any sample that was not affected by extraneous carbon. The amount of extraneous carbon introduced was then

calculated based on the difference of the yield from 90%, with the errors in expected and measured sample size defining the possible range of values (not shown in the table).

The next step is to estimate the number of extraneous ^{14}CO molecules that may have been included via this leak. Although 3 samples of NIWA laboratory air were processed after the Pakitsoq samples, in order to understand the lab air ^{14}CO content, these have not yet been measured for ^{14}C. One source of ^{14}CO in lab air is known quite well: clean ambient air. Pakitsoq samples were processed in November, when the clean ambient air near NIWA is known to have ^{14}CO of ~ 15 molecules cm^{-3} (Manning et al., 2005). The maximum and minimum amounts of ^{14}CO added to the samples from this source can be estimated by considering the discrepancy between the volume of air actually taken from the sample tanks (based on starting and ending tank pressures) and the volume of air processed through the line (based on the mass flow controller). As can be seen from Table 5.4, the comparison of these two sample air volume estimates confirms substantial air leaks for most samples.

The amount of extraneous CO introduced from clean ambient air could not account for the high yields observed for most samples, thus other sources of CO in leaking air must also be present. Laboratory air can have elevated [CO] due to a number of sources. The NIWA laboratory does not work with radioactive tracers; it is thus reasonable to assume that extra CO emitted in the laboratory would have a ^{14}C activity between zero and "modern" (i.e. ~ 106 pMC).

The estimates of maximum and minimum number of ^{14}CO molecules that could have been introduced were then arrived at as follows. The maximum ^{14}CO estimate assumed the largest possible air leak allowed for by errors, a clean ambient air [CO] of 50 ppb (typical for November in New Zealand (Novelli et al., 1998)) and ^{14}CO of 15 molecules cm^{-3}. The maximum allowable amount of extraneous carbon (based on expected & measured sample sizes and associated errors) was also assumed; it was further assumed that all the extraneous carbon not accounted for by CO from clean ambient air was 106 pMC in ^{14}C activity. The minimum ^{14}CO estimate assumed the smallest allowable amount of extraneous carbon (based on expected & measured sample sizes and associated errors). The smallest possible amount of leaked air was zero for most samples given the errors. It is thus possible, under this scenario, to have a leak that is small in volume but high in [CO]. It was then further assumed that the ^{14}C activity of the leaked CO was 100 times lower than in ambient air, due to 100x dilution by ^{14}C-free CO in the lab. For the Younger Dryas 2 sample, the yield measurement allows for the minimum possible amount of extraneous carbon to be zero, and this is what we adopted for that sample.

The number of ^{14}CO molecules for each Pakitsoq sample from Table 5.3 was then corrected for the estimated range of extraneous ^{14}C; the corrected maximum and minimum estimates are shown in Table 5.4. As can be seen, this increases the ^{14}C uncertainties to 25 - 30% of sample values.

No attempt was made to correct the ^{14}CO data for possible ^{14}C blanks associated with the field melt extraction. The [CO] melt extraction blanks were 13 –

41 ppb, as compared to 3 ppb for the standard gas used in the simulated extractions. As with [CO_2] for these blanks, it is unclear whether the observed [CO] represents outgassing by the extraction system components or outgassing of dissolved sample CO from the melt water. However, the [CO] in the blanks is clearly very low compared to that in the samples. Further, $^{14}CH_4$ of the blanks (Chapter 4) indicates that any extraneous carbon added in the melt-extractions is likely ^{14}C-free.

5.4.5. Possible sources of ^{14}CO in Pakitsoq ice and the cosmogenic component

Direct cosmogenic production is not the only source of ^{14}CO in Pakitsoq ice. There is also ^{14}CO from the ancient air in the ice, as well as from (non-cosmogenic) in-situ production of CO. These components must be constrained before the cosmogenic ^{14}CO component can be quantified.

The number of ^{14}CO molecules expected in each sample from occluded ancient air can be easily calculated based on sample size, [CO], expected paleo [CO], ^{14}C activity of paleoatmospheric CO and gas age. No existing records of paleo [CO] reach this far back in time. Based on model predictions for the pre-industrial, described above, we chose a value of 50 ppb. A value of 900 pMC was chosen for the ^{14}C activity, as this is a typical ^{14}CO activity in clean background air today (Manning et al., 2005). The choices of both the paleoatmospheric [CO] and ^{14}CO are speculative. However, as can be seen from Tables 5.5 and 5.4, the estimated amount of ^{14}CO from paleoatmospheric air in the samples is 10 – 40 times smaller than the total ^{14}CO content. Thus, even if our estimate was 2 times too low, paleoatmospheric ^{14}CO

would still not be a major contributor to overall ^{14}CO content. The uncertainty in ^{14}CO content arising from this component is minor as compared to the overall ^{14}CO content uncertainty, and is ignored.

The ^{14}CO contribution from in-situ produced CO depends on the ^{14}C of the organic substrate, for which there are two main possibilities. The first is that this substrate is organic matter that was injected into Pakitsoq ice near the margin via ice-tectonic or subglacial hydrological processes. In this case the ^{14}C activity of this organic matter is likely to be similar to that of in-situ produced CH_4 as well as that of $^{14}CO_2$ in Pakitsoq ice. We therefore choose a value of 75 pMC for ^{14}C activity of CO produced in this manner. It was assumed that 50 ppb of the [CO] was a real paleoatmospheric signal and that the rest of CO was produced in-situ. This scenario (with paleoatmospheric ^{14}CO included) provides the maximum estimate of the amount of non-cosmogenic ^{14}CO in the ice (Table 5.5).

The second possibility is that the substrate is organic matter that was wind-deposited at the accumulation site. In this case the ^{14}C activity of organic matter is likely to be similar to the ^{14}C activity of contemporaneous atmospheric CO_2. We thus used the INTCAL04 compilation (Reimer et al., 2004) and the mean age of the ice (not the gas) included in each sample to determine the ^{14}C activity of CO produced in this way. Again, it was assumed that 50 ppb of the [CO] was a real paleoatmospheric signal and that the rest of CO was produced in-situ. This scenario (again, with paleoatmospheric ^{14}CO included) provides the minimum estimate of the amount of

non-cosmogenic ^{14}CO in the ice (Table 5.5). In reality, it is likely that CO is produced from both types of substrate.

One other correction is still needed to the ^{14}CO results. ^{14}CO is produced in air cylinders by interaction of cosmogenic neutrons with ^{14}N, the same mechanism by which ^{14}CO is produced in the Earth's atmosphere (Lowe et al., 2002). The ^{14}CO production rates for inside and outside storage in Wellington, New Zealand, as well as for air transport were estimated by(Lowe et al. (2002). The Pakitsoq sample tanks were stored for either ~3 yr (YD-PB) or ~2 yr (OD-Bølling) prior to processing for ^{14}CO, as well as transported several times by air between Greenland, USA, and New Zealand. Fortunately, almost all of the storage time was in the same actual laboratory (or just outside the building) for which Lowe et al. (2002) estimated the ^{14}CO production rates. We thus use their estimates of production rates and associated uncertainties, as well as known storage and transport histories of the Pakitsoq sample tanks to estimate the necessary corrections to Pakitsoq sample ^{14}CO. These corrections are 13.8 ± 2.8 ^{14}CO molecules cm^{-3} STP air for the YD – PB samples and 9.0 ± 1.8 ^{14}CO molecules cm^{-3} STP air for the OD – Bølling samples, and have been incorporated into the maximum and minimum ^{14}CO values shown in the last two columns of Table 5.5.

As can be seen from Table 5.5, the fraction of ^{14}CO in Pakitsoq samples that is from paleoatmospheric and in-situ produced CO may be quite high, up to 55% in one case. The correction for this non-cosmogenic ^{14}CO in ice is uncertain and of the same order of magnitude as the total ^{14}CO content. The result is that the ranges between the

maximum and minimum values for ^{14}CO from direct cosmogenic production in ice for each sample are as large as 100% of the average values for most samples. ^{14}CO concentrations in ice are commonly expressed in the units of molecules g^{-1} ice in the literature (e.g., Lal et al., 2000; van der Borg et al., 2001). This is easily calculated for Pakitsoq samples based on the total number of ^{14}CO molecules, volume of (undiluted) air sample processed, and the typical air content of glacial ice (here taken as 0.09 cm^3 STP g^{-1}).

5.4.6. Is observed ^{14}CO produced in the accumulation or ablation zone?

The observed cosmogenic ^{14}CO could have been produced either in the accumulation zone, the ablation zone, or both. Lal et al. (1987) derived estimated ^{14}C production rates at various altitudes in the high latitude regions. Following their work, it can easily be shown that the total amount of ^{14}C produced (ignoring decay) at a site at steady state with a constant ice accumulation rate A_0 is given by:

$$^{14}C_{produced} = \frac{P_0 \Lambda}{\rho A_0} \tag{5.2}$$

Where P_0 is the (constant) production rate at the surface, Λ is the absorption mean free path in ice (~150 g cm^{-2} (van der Kemp et al., 2002)) , and ρ is the ice density. This equation also holds for ablation zones for the total amount of ^{14}C produced in ice being brought up from depth to the surface, with a constant ablation rate A_0. The elevation of the Pakitsoq site is ~ 350 m above sea level, while that for the accumulation site of Pakitsoq ice is predicted by a flow-line model from Reeh (1988) to be ~3000 m. This means a ^{14}C surface production rate ~7 times higher at the

accumulation site due to altitude only (assuming a constant cosmic ray flux in time) (Lal et al., 1987). The Pakitsoq ablation rate is ~ 2.5 m ice / yr (Petrenko et al., 2006); while the accumulation rate at Summit during the YD or the OD was ~ 0.07 m ice / yr. Because of the gas age – ice age offset, the age of the ice from which all the air samples were extracted is either Younger Dryas (YD, Transition, PB samples) or Oldest Dryas (OD, Bølling samples). A quick calculation shows that, even with 15 kyr of decay of ^{14}C produced in the accumulation zone, we would expect at least 70 times more cosmogenic ^{14}C in Pakitsoq ice from production in the accumulation zone than in the ablation zone, assuming that all of the ^{14}C produced in the firn is retained in the ice.

Different ice core studies of cosmogenic ^{14}C produced in the accumulation zone disagree regarding how much of the cosmogenic ^{14}C is retained in the firn, however. Studies in the GISP2 ice core, for example, suggest that almost all of the cosmogenic ^{14}C is retained (e.g. Lal et al., 1997). Studies of several Antarctic cores with a large range of mean-annual temperatures and accumulation rates, on the other hand, suggest that no or very little cosmogenic ^{14}C is retained in the firn, presumably because of loss to the atmosphere via firn recrystallization processes (e.g. Smith et al., 2000; van der Kemp et al., 2000). It is therefore possible that, despite the much higher expected ^{14}C production at the accumulation zone, most or even all of the cosmogenic ^{14}CO in Pakitsoq samples is from ablation zone production.

5.4.7. Modeled cosmogenic ^{14}CO production in the ablation zone

It does not seem possible to make accurate predictions regarding cosmogenic ^{14}CO produced in the accumulation zone, due to the uncertainty about ^{14}C retention in the firn. However, all studies that looked at ablation ice suggest that cosmogenic ^{14}C is quantitatively retained (e.g. Lal et al., 1990; van der Kemp et al., 2002). We thus created a simplified model to investigate how well the measured ^{14}CO values in Pakitsoq samples compare to theoretical predictions of ^{14}CO production in the ablation zone. ^{14}C production by neutrons in ice is well known; production by muon capture has also been suggested (van der Borg et al., 2001; van der Kemp et al., 2002). We therefore included both production mechanisms in our model. ^{14}C production rates at the surface at the Pakitsoq elevation of 350 m were approximated from values given in van der Kemp et al. (2002) and the altitude – production rate relationship given in Lal et al. (1987); the approximated values are 40 ^{14}C atoms g^{-1} yr^{-1} for production by neutrons (P_{0n}) and 5.5 ^{14}C atoms g^{-1} yr^{-1} for production by muons ($P_{0\mu}$).

Production by both muons and neutrons decreases exponentially with depth due to shielding from overlying ice. The absorption mean free path in ice for neutrons (Λ_n) is ~150 g cm^{-2}, and for muons it is ~ 1365 g cm^{-2} (Van Der Kemp et al., 2002). Using a density of 0.90 g cm^{-3} for glacial ice, these translate to e-folding depths of 1.67 m and 15.17 m, respectively. Our model follows parcels of ice at the Pakitsoq ablation margin, which start at a depth of ~ 40 m below surface (^{14}C production is negligible below this depth). The model proceeds in monthly increments, with ice parcels moving upward as the overlying ice melts. Almost all of the ablation at Pakitsoq happens by melting during the warmest summer months of June through

August. The model thus assumes zero ablation for September – May, and a constant ablation rate of 0.833 m per month during June – August. For the final summer, when the ice is sampled, the model proceeds in daily increments with the same ablation rate. Detailed field records allow us to determine the mean date of sampling, as well as the mean depth below surface of the ice taken for each sample. In the model, the starting depth of the ice parcel is adjusted slightly (by up to ± 1 m) for each sample to make the depth below surface on the sampling date during the last model summer match the actual depth below surface during sampling.

One final parameter in the model is the fraction of produced ^{14}C which goes to CO (F_{CO}) as compared to CO + CO_2 (assuming that almost all of cosmogenic ^{14}C goes to one of these two species). Several estimates of this have been made in ablation ice, and they range from 0.23 (VanRoijen et al., 1995) to 0.57 (Lal et al., 1990). Somewhat arbitrarily, we chose a value of 0.25 for our purposes.

Measured and modeled cosmogenic ^{14}CO concentrations are compared in Table 5.6. We emphasize that the absolute modeled values are associated with considerable uncertainties, due to the unknown actual F_{CO} in Pakitsoq ablation ice, as well as uncertainties in P_{0n} and $P_{0\mu}$. Cosmogenic ^{14}C production rates in glacial ice have never been directly measured; most workers have used theoretical estimates (e.g., Lal et al., 1987) or transferred values from rates determined for quartz (correcting for oxygen composition difference) (e.g. van der Kemp et al., 2002). Further, the ^{14}CO values measured in Pakitsoq samples are probably an underestimate due to incomplete efficiency of the melt- extraction in recovering ^{14}CO. Cosmogenic ^{14}CO is locked in

the ice lattice, and thus first ends up in the water, not the air bubbles, upon melting of the ice. The efficiency of the extraction of this ^{14}CO then depends on how efficient the air bubbles rising through the melt water are at stripping out the dissolved gases. (This would apply only to ^{14}CO produced in the ablation zone which is still locked in the ice lattice. ^{14}CO produced at the accumulation zone would have had enough time to diffuse into the air bubbles. The melter technique has no trouble extracting gases that are already in the air bubbles). Despite all of these uncertainties, some insights can still be gained from the model results.

Modeled ^{14}CO (from neutrons and muons) is higher than mid-range measured cosmogenic ^{14}CO values by about a factor of 2. If the model parameters are correct, and if the ^{14}CO melt-extraction efficiency is ~0.5 or greater, all of the observed ^{14}CO can be explained by production in the ablation zone. This makes the presence of cosmogenic ^{14}CO from the accumulation zone seem less likely and suggests that all ^{14}CO that was produced in the accumulation zone may have been lost to the atmosphere through re-crystallization near the top of the firn. However; given the uncertainties in the model and data, presence of some ^{14}CO from the accumulation zone is of course possible.

5.5. Corrections to $^{14}CH_4$ for cosmogenic production

One of the questions that needs to be considered in applying the correction for cosmogenic $^{14}CH_4$ production is whether or not we can assume that the fraction of cosmogenic ^{14}C which goes to CH_4 is constant. It may be possible that variations in

impurity loading in different Pakitsoq ice sections would affect the cosmogenic $^{14}CH_4$ yield relative to other products. Although impurity loading in Greenland ice over the last glacial termination varies substantially, the impurity concentrations are very small. For example, the maximum summed concentration of all major ions in the GISP2 ice core (Na^+, NH_4^+, K^+, Mg^{2+}, Ca^{2+}, Cl^-, NO_3^-, SO_4^{2-}) is < 1 ppm by weight (Mayewski et al., 1997). The concentration of insoluble dust particles is similarly small, with a value of 650 ppb (by weight) in Oldest Dryas ice in the GRIP ice core (DeAngelis et al., 1997). Even though only "clean" ice (i.e. without visible dust bands or large blue bands) was sampled at Pakitsoq, it is likely that the impurity concentration in our samples was somewhat higher than in the deep ice cores due to addition of subglacial material.

The only prior study we are aware of that attempted to quantify the effects of adding low-concentration impurities to H_2O on CH_4 yield from hot C atom reactions was done by Stenstrom (1970). In this work ^{11}C was produced by proton bombardment of water and dilute (1 mM) aqueous solutions of a variety of solutes. Although this study provides a rather imperfect comparison with our setting (proton vs neutron or muon bombardment, water vs ice, ^{11}C vs ^{14}C, much higher bombardment intensities than in our case), it showed no significant changes in the primary yield of $^{11}CH_4$ (0.06 ± 0.02 %) between tests. A 1mM concentration for a major ice-core ion such as Ca^{2+} translates to 40 ppm by weight, i.e. at least 40 x higher than the impurity loading of YD and OD-age ice in the Greenland Summit ice cores. This suggests that

any differences in impurity loading of Pakitsoq ice are unlikely to affect the $^{14}CH_4$ cosmogenic yield.

A further line of argument for this comes from considering the likelihood of a hot ^{14}C atom encountering anything other than H_2O molecules in the ice. If this likelihood is scaled simply (and somewhat crudely) by the mass ratio of impurities to H_2O, and a value of 10 ppm is assumed for the impurity loading of Pakitsoq ice (10 x the ice core values, to account for possible inclusion of subglacial material), the hot ^{14}C atom is still 100,000 times more likely to collide with an H_2O molecule than with an impurity. To conclude, it seems unlikely that there is variability between Pakitsoq samples in the yield of cosmogenic $^{14}CH_4$ relative to other cosmogenic ^{14}C products.

Since the ^{14}CO results leave open the possibilities of cosmogenic $^{14}CH_4$ production in both the accumulation and ablation zones, any correction for this effect should ideally take into account both possibilities. For the case of production in the ablation zone, the relative amounts of ^{14}C, and thus $^{14}CH_4$ produced in each sample are accurately predicted by the model (the uncertain parameters in the model affect the absolute, not relative values). The absolute amount of cosmogenic $^{14}CH_4$ produced is not possible to determine, however. By applying the cosmogenic correction, therefore, it should be possible to compare the relative strengths of the fossil components of the CH_4 budgets for each climatic interval sampled. It would not, however, be possible to determine the absolute magnitudes of the fossil components.

The situation is more complicated for the case of possible $^{14}CH_4$ production in the accumulation zone. Here, even for a relative correction to be applied, it is

necessary to know the relative rates of cosmogenic ^{14}C production as well as the fractions of ^{14}C retained in the firn for all samples. ^{14}C production rate is controlled by altitude, accumulation rate, and the cosmic ray flux. The altitude of the accumulation sites for Pakitsoq ice spanning the last glacial termination has been determined using a flow-line model from Reeh (1988), and is within 50 m for all $^{14}CH_4$ samples, which would not affect production rates significantly. The accumulation rates for the Summit region are also known from GISP2, though some uncertainties in these exist. Changes in the cosmic ray flux are subject to considerable uncertainty, however. The flux of cosmic rays in the high latitudes is modulated mostly by solar activity, as geomagnetic shielding for cosmic rays of interest is essentially zero in latitudes above 60˚ (Lal and Peters, 1967). (Lal et al. (2005) used measurements of ^{14}CO and $^{14}CO_2$ in the GISP2 ice core to estimate the relative strength of the cosmic ray flux at Summit for several discrete age points in the GISP2 record. These results, however, do not have the time resolution we require to compare accumulation-zone ^{14}C production rates between Pakitsoq samples.

Several high-resolution records of ^{10}Be from Summit ice cores are available (e.g., Finkel and Nishiizumi, 1997; Yiou et al., 1997). ^{10}Be is produced cosmogenically mainly in the stratosphere and lower troposphere, and is rapidly scavenged by aerosols, with subsequent deposition on the Earth's surface (Field et al., 2006). Because ^{10}Be is produced at all latitudes, ^{10}Be fluxes (flux = concentration / accumulation rate) recorded in ice cores are a function of solar activity and geomagnetic intensity (both of which modulate the cosmic ray flux) as well as

climate-related transport and deposition processes. The record of ^{10}Be flux at Summit for ice of YD and OD age does in fact show substantial variability (up to factor of 2 for OD ice) within each time period, on the timescale of several hundred years (which is the difference in ice ages between YD and PB or Bølling and OD samples) (Muscheler et al., 2004). However, because ^{10}Be flux at Summit is affected by so many variables (Field et al., 2006), it is uncertain whether this represents actual changes in cosmic ray flux in the polar regions or climatic effects.

In addition, there would be uncertainties associated with the fraction of cosmogenic ^{14}C that is retained in the firn at the accumulation site. Any correction for cosmogenic $^{14}CH_4$ originating from the accumulation zone would thus be highly uncertain. Pakitsoq ^{14}CO data do not require the presence of any ^{14}CO from the accumulation zone to explain the values; nor do they rule out the presence of ^{14}CO from the accumulation zone. Given the good agreement of results with the ablation-zone production model, it seems unlikely that ^{14}CO from the accumulation zone accounts for a greater fraction of the total than ^{14}CO from the ablation zone. Further, it seems reasonable to assume that the processes affecting the loss of cosmogenic ^{14}CO and $^{14}CH_4$ in the firn (such as recrystallization) would have a similar effect on each species. It then follows that it is unlikely that cosmogenic $^{14}CH_4$ from the accumulation zone accounts for a greater fraction of the cosmogenic total than $^{14}CH_4$ from the ablation zone. We therefore choose to apply the cosmogenic $^{14}CH_4$ correction under the assumption that all cosmogenic $^{14}CH_4$ is produced in the ablation zone. This correction is well determined (by the model), but speculative considering

that some $^{14}CH_4$ from the accumulation zone may be present. However, it constitutes our best attempt at quantifying the true paleo $^{14}CH_4$ signals and is therefore worthwhile.

The correction is illustrated in Table 5.7 and the approach is as follows. We take the YD sample average as a reference and assume that, without the cosmogenic component, average $^{14}CH_4$ for the YD samples would fall along the wetland hypothesis scenario shown in Figure 5.3 and discussed in Chapter 1. The YD samples are the best reference to use because in-situ CH_4 production in these samples, if any, is very small and the associated corrections to $^{14}CH_4$ almost negligible (see Table 5.1). We then determine a "cosmogenic correction factor" for each sample, which is the ratio of predicted cosmogenic ^{14}CO for that sample to average ^{14}CO predicted for YD samples (Tables 5.6 and 5.7). Sample $^{14}CH_4$ (in pMC) is first un-normalized for $\delta^{13}C$, and then multiplied by the $^{14}C/^{12}C$ ratio of the standard (1.19×10^{-12}) to obtain the sample $^{14}C/^{12}C$ ratios. The number of $^{12}CH_4$ molecules per gram of ice is then determined from the air content (assumed 0.09 cm^3 STP g^{-1} for all samples) and sample $[CH_4]$; followed by a calculation of the number of $^{14}CH_4$ molecules per gram of ice for each sample (Table 5.7). The expected number of $^{14}CH_4$ molecules per gram of ice for YD sample average, based on the wetland scenario is then calculated, and from that the cosmogenic excess of $^{14}CH_4$ for the YD sample average is found. This excess is then multiplied by the cosmogenic correction factor for each type of sample to determine the respective excesses of $^{14}CH_4$. These are then subtracted for each

sample, and the results are converted back to pMC (Table 5.7) or age-corrected Δ (Figure 5.4).

5.6. Discussion of $^{14}CH_4$ results after all corrections

In the following discussion it is important for the reader to keep in mind that, although each of the two corrections (in-situ CH_4 and cosmogenic) applied to the $^{14}CH_4$ results represents a "most-likely" scenario, both corrections are somewhat speculative, especially the one addressing cosmogenic production. Due to this, the following discussion should be considered somewhat speculative as well. Because the cosmogenic correction assumed a wetland hypothesis $^{14}CH_4$ value for the YD sample average, nothing can be said about the absolute magnitudes of the fossil component of CH_4 budgets for each climatic interval.

It is, however, possible to examine the relative changes in the magnitude of the fossil fraction of the CH_4 budget between pairs of climatic intervals. For simplicity, it is assumed that the fossil fraction is zero for the Younger Dryas. To calculate the % change in the fossil fraction, the $^{14}CH_4$ values from Figure 5.4 are first converted from Δ to pMC, but keeping the age correction. The % change in the fossil fraction of the CH_4 budget from one interval to another is then calculated as:

$$\%\ \text{change} = \frac{{}^{14}CH_{4,\text{sample 1}} \times \frac{{}^{14}CH_{4,\text{wetland 2}}}{{}^{14}CH_{4,\text{ wetland 1}}} - {}^{14}CH_{4,\text{sample 2}}}{{}^{14}CH_{4,\text{sample 1}} \times \frac{{}^{14}CH_{4,\text{wetland 2}}}{{}^{14}CH_{4,\text{ wetland 1}}}} \times 100\% \qquad (5.3)$$

The "sample 1" and "sample 2" subscripts refer to the determined $^{14}CH_4$ values for the two intervals being compared, and the "wetland 1" and "wetland 2" refer to $^{14}CH_4$ values (also in pMC & with an age correction) predicted for each interval under the wetland hypothesis. Multiplying "sample 1" by the "wetland 2/ wetland 1" ratio corrects for the effect of changing paleoatmospheric $^{14}CO_2$. The results of these comparisons are listed in Table 5.8. The relative changes in fossil fractions were calculated for the scenario where all the corrections were applied to sample $^{14}CH_4$, as well as for the scenario where YD, YD-PB Transition (Scenario B), PB and OD samples were not corrected for in-situ CH_4 production.

5.6.1. The Younger Dryas – Preboreal transition

From Figure 5.4, it is apparent that, even given the large error bars, Scenario A for the YD-PB Transition samples is unrealistic, as the possible range of $^{14}CH_4$ values falls entirely outside the envelope predicted by the all-wetland and all-clathrate scenarios for the transition. Scenario B, which predicts higher $[CH_4]$ and a slightly younger age for these samples, is therefore more likely.

The relatively large error bars for the samples arise mostly from the uncertainty associated with the correction for in-situ CH_4 production. Given these error bars (1 σ, capped on the "+" side for several samples by measured $^{14}CH_4$ values), the YD, YD-PB Transition, and PB samples are not distinguishable from one another. However, the errors may be overestimated for the YD and YD-PB Transition (scenario B) samples, as the amount of in-situ CH_4, if any, is quite small (Table 5.1),

and the in-situ corrections have a very small effect on $^{14}CH_4$ for these samples (Table 5.1 and Figure 5.3). Further, the fact that each of the values shown is an average of two replicates, with excellent agreement within all replicate pairs (Table 5.7), lends extra confidence to the values.

As can be seen from Table 5.8, no change in the fossil fraction as compared to the YD is suggested by the data for the YD-PB Transition even after [CH_4] had risen by 30% and regardless of whether or not the correction for in-situ CH_4 is applied to YD and YD-PB Transition samples. This argues against any substantial clathrate involvement in the YD-PB CH_4 transition, consistent with the findings of Sowers (2006) and Schaefer et al. (2006). However, the results suggest that a ~6-7% increase in the fossil CH_4 fraction is likely in the early Preboreal (with the full possible range of change in the fossil fraction being –4.5 to +17%). The 6-7% increase is relatively small compared to the 31% increase in [CH_4] (relative to PB values) since the YD. This further argues against major clathrate involvement in the YD-PB CH_4 transition.

Figure 5.5 shows [CH_4] and all available data for CH_4 isotopes over the YD-PB transition. All the $\delta^{13}CH_4$ data are from Pakitsoq (see Figure 5.5 caption). One $\delta^{13}CH_4$ data point from GISP2 dating to the very end of the CH_4 transition (not shown) is in perfect agreement with the Pakitsoq data (Todd Sowers, personal communication, 2008), consistent with our finding that for the YD-PB transition, the amount of in-situ produced CH_4 in Pakitsoq ice (if any), is quite small.

Remarkably, as was discussed in Schaefer et al. (2006) and Sowers (2006) neither $\delta^{13}CH_4$ nor δD show any significant changes over this large climatic transition

which drove the CH_4 increase. Assuming no significant changes in the overall CH_4 sink fractionation, this could be consistent with a scenario where the relative strengths of individual sources remain the same while the absolute source strength increases; or a scenario where a relative increase in an isotopically light source (e.g. boreal wetlands) is balanced by a similar relative increase in an isotopically heavy source (e.g. biomass burning).

Where could a ~7% increase in the fossil fraction of the CH_4 source in the PB arise? The uncertainties and variability in $\delta^{13}CH_4$ and δD data do not allow us to rule out a 7% contribution from marine clathrates or geologic CH_4 seeps; although a 14% contribution, for example, would shift the δD of the source mixture by +18 ‰ (assuming source values in Table 1.1 and an all-wetland scenario for the YD), which would have been evident from the δD data.

An interesting possibility is emissions from melting thermokarst in Eastern Siberia and Alaska, following the hypothesis of Walter et al. (2007), described in Chapter 1. Only a limited number of CH_4 isotopic measurements of this source are available, but using the data presented in Walter et al. (2006), we estimate the overall $^{14}CH_4$ at ~28 pMC, $\delta^{13}CH_4$ at ~ - 73 ‰ PDB and δD at ~ - 386 ‰ SMOW. If we assume that, during the Preboreal, the $^{14}CH_4$ activity of the thermokarst source was also 28% of the contemporaneous $^{14}CO_2$ activity, then a 10% contribution from the thermokarst source would result in the same overall ^{14}C as a 7% contribution from a ^{14}C-free source. For δD, this would cause a shift of – 7 ‰ for the source mix (assuming –320 ‰ for the source mix at YD), and for $\delta^{13}C$ a shift of – 2 ‰ for the

source mix (assuming –55 ‰ for the source mix at YD). While such a shift in δD would go undetected, it should be detectable in $\delta^{13}C$, which may be a weakness for this hypothesis. However, of course it is possible that the overall $\delta^{13}CH_4$ of thermokarst lake emissions during the PB was different than the $\delta^{13}CH_4$ of the selected lake emissions sampled recently by Walter et al. (2006). A further attractive feature of this hypothesis is that it provides a built-in time lag for the release of ^{14}C-depleted CH_4 (note that no ^{14}C lowering is observed in our data during the transition itself). The lag would arise from the time necessary to melt sufficient permafrost in order for the lakes to develop and active CH_4 ebullition to begin. However, a time lag could also be consistent with CH_4 release from clathrates (the time required for the thermal signal to reach the clathrate zone in the sediments).

5.6.2. The Oldest Dryas – Bølling transition

Figure 5.6 shows the $^{14}CH_4$ data for the OD – Bølling transition along with the GISP2 δD data of Sowers (2006). The $^{14}CH_4$ error bars are even larger here than for the YD-PB case, owing to the larger uncertainty in the determined $^{14}CH_4$ of the in-situ produced CH_4, as well as to the lower overall measured ^{14}C (due to greater sample age). Given the error bars, the OD and Bølling values are indistinguishable from one another. However, the errors may be overestimated for the OD sample, as the amount of in-situ CH_4, if any, is quite small (Table 5.1). As for the YD – PB samples, the OD – Bølling $^{14}CH_4$ data points represent averages of replicate samples, with excellent

agreement between the replicates (Table 5.7), which lends extra confidence to the values.

Unlike for the YD – PB, no published $\delta^{13}CH_4$ data are available for the OD – Bølling. $\delta^{13}CH_4$ for the large Pakitsoq samples before any corrections are shown in Table 5.1. The $\delta^{13}CH_4$ correction for in-situ CH_4 is highly uncertain in this case, because of the large uncertainty in the determined $\delta^{13}CH_4$ of the contaminant (-67.0 ± 15.7 ‰, determined using the same approach as for $^{14}CH_4$). The corrected values are thus highly uncertain and will not be discussed.

From Table 5.8 it can be seen that the fossil fraction of the CH_4 budget during the OD was possibly higher than during the YD, by ~ 7%, if the scenario with all $^{14}CH_4$ corrections is considered (with the full range of possible changes in the fossil fraction being –10 to +21 %). However, if we consider the scenario where the corrections for in-situ CH_4 are not applied to YD and OD samples, the data suggest no difference in the fossil fraction between the two intervals (Table 5.8).

The average δD for the YD values (Figure 5.5) is -90 ‰. δD during the OD is highly variable (Figure 5.6), but the average of measured GISP2 values is – 85 ‰. As was already suggested by Sowers (2006), it is possible that the slightly higher δD during the OD is due to increased CH_4 emissions from marine hydrocarbon seeps on exposed continental shelves during a time of lower sea level as compared to the YD, as hypothesized by Luyendyk et al. (2005). If 7% of the OD CH_4 budget was from geologic emissions, it would raise the δD of the source mix by ~ 9 ‰ as compared to the YD (assuming all-wetland emissions for YD, no significant change in $[CH_4]$, and

δD values as in Table 1.1). Given the disagreement between the two scenarios in Table 5.8, our data cannot lend conclusive support to the increased hydrocarbon emission hypothesis, but do suggest that large changes in the fossil fraction between the OD and the YD were unlikely.

With all corrections applied, the $^{14}CH_4$ results suggest that an increase of ~14% in the fossil fraction is likely during the OD – Bølling transition (Table 5.8), with the full range of possible change in the fossil fraction being –11 to 36%. For the scenario where the OD samples are not corrected for in-situ CH_4 production, the results suggest a 21% increase in the fossil fraction, with the full possible range being +3 to +37%. Since the [CH_4] increase for this same time period is only 17.5% (Table 5.8, relative to Bølling value), this suggest that most or all of the [CH_4] rise was likely due to fossil (or ^{14}C-depleted) CH_4. We note that this result depends heavily on the substantial (23% of original $^{14}CH_4$ value, see Table 5.1) correction for in-situ CH_4 which was applied to the Bølling samples. The uncorrected Bølling and OD $^{14}CH_4$ values (see Fig. 5.3 or 5.4) are essentially identical. We are confident that Bølling samples have elevated [CH_4], and it is highly likely that the $^{14}CH_4$ of the contaminant we used in the correction is representative of the real value. However, we cannot rule out the possibility that the $^{14}CH_4$ of the contaminant is actually closer to ^{14}C of organic matter wind-deposited at the accumulation site (~ 20 pMC), in which case the corrected Bølling $^{14}CH_4$ values would in fact be slightly higher than the OD values.

The melting thermokarst lake emission hypothesis seems unlikely to explain the $^{14}CH_4$ decrease for the OD-Bølling transition suggested by our results, because ice

core studies of the interpolar [CH_4] gradient suggest that the [CH_4] increase into the Bølling was driven almost entirely by increasing emissions in the low latitudes (Brook et al., 2000). If we assume a 7% fossil fraction for the OD (based on $^{14}CH_4$ data with all corrections applied), and allow for all of the [CH_4] rise to Bølling sample values (17.5% rise, w.r.t. Bølling values) to be due to clathrates or hydrocarbon seeps, we would expect a 21 ‰ increase in the δD of the source mix during the OD – Bølling transition. Assuming no significant changes in δD sink fractionation, this should be detectable in the GISP2 δD data, even given the surprisingly high variability in the GISP2 δD values during the OD (standard deviation of 9 ‰). Thus, based on GISP2 δD it is unlikely that all of the CH_4 increase from OD into the Bølling was due to increased emissions from clathrates or hydrocarbon seeps. However, the δD data may allow for ~50% of the CH_4 increase to be derived from clathrates or geologic sources. Provided that the other 50% of the CH_4 increase was from sources with δD similar to the OD source mix, this would result in a 10.5 ‰ increase in the δD of the source mix, which may not be detectable in the GISP2 δD data given the high variability.

It may be possible that such a large burst of ^{14}C – depleted CH_4 at the start of the Bølling came from regions affected by the monsoons, where large areas with accumulations of aged organic matter (possibly as loess) were transformed into wetlands at the onset of the Bølling. No large shifts in the δD of the source mix would be required in this case. Cave records of stalagmite $\delta^{18}O$ indicate that the largest single increase in the intensity of the East Asian summer monsoon during the last

deglaciation occurred at the onset of the Bølling (Wang et al., 2001). We are currently looking further into this hypothesis.

5.7 Summary and Conclusions

The usefulness of the Pakitsoq $^{14}CH_4$ record for interpreting changes in the paleo CH_4 budgets is limited by in-situ production of CH_4 as well as by what is very likely direct cosmogenic production of $^{14}CH_4$ molecules in the ice. Sample $^{14}CH_4$ activities as measured were too high by 14 – 38% as compared to the highest possible expected $^{14}CH_4$ based on the record of paleoatmospheric $^{14}CO_2$.

Sample $^{14}CH_4$ has been corrected for in-situ production by estimating the ^{14}C of the contaminant from two samples with much higher $[CH_4]$ than their respective replicates, and estimating the $[CH_4]$ excess for the other samples by comparisons with the GISP2 ice core $[CH_4]$ record. $^{14}CO_2$ values measured in the samples show good agreement with the inferred $^{14}CH_4$ of the contaminant, as well as with ^{14}C values measured on two samples of organic matter deposited by the glacier at the Pakitsoq margin within 1 km of the sampling site. The combined evidence suggests that Pakitsoq ice contains a substantial amount of organic matter with a ^{14}C activity of 65 – 80 pMC, which has been incorporated into the ice through ice-margin flow and possibly hydrological processes, and which serves as a substrate for both CH_4 and CO_2 production in Pakitsoq ice.

Measurements of ^{14}CO were carried out on the samples to investigate the possible cosmogenic production of $^{14}CH_4$. Cosmogenic ^{14}CO was detected, in the

range of 0 – 8 ^{14}CO molecules g^{-1} ice. Large uncertainties in the determination of the cosmogenic ^{14}CO component arose from undetected lab air leaks during sample processing, as well as from the uncertain non-cosmogenic ^{14}C content of CO in the ice; as a result the possible range of ^{14}CO values for each sample was typically as large as ~100% of the mean ^{14}CO value in the range. A comparison of measured ^{14}CO was carried out with a model of in-situ cosmogenic production in the ablation zone (at the sampling site), using published values of ^{14}C production rates by neutrons and muons in ice. The model predictions agreed well with the measured values (allowing for incomplete ^{14}CO recovery in the melt-extraction), indicating that all of the observed ^{14}CO could be explained by ablation-zone production, and accumulation-zone production was not necessary (although still possible). On the basis of this comparison, a correction for cosmogenic $^{14}CH_4$ was applied to all samples, using model predictions to determine the relative amount of cosmogenic ^{14}C produced in each sample in the ablation zone.

The correction for in-situ CH_4 production increases the $^{14}CH_4$ errors (1-σ) by a factor of 2 or more for all samples. This may be an overestimate of the errors, as the measured and expected [CH_4] ranges overlap for all samples except the Bølling. In-situ CH_4 production thus may not have taken place for YD, YD-PB Transition, PB and OD samples. For this reason a scenario was also considered where only the cosmogenic correction was applied for YD, YD-PB Transition, PB and OD samples.

Both corrections (in-situ CH_4 and cosmogenic ^{14}C) are somewhat speculative, although each represents a most likely scenario. This does not allow us to be

completely certain in our corrected $^{14}CH_4$ results and their interpretations. The large error bars, due mostly to the correction for in-situ CH_4, make the $^{14}CH_4$ data points within the YD-PB transition indistinguishable from each other. The same applies for the OD and Bølling samples. However, as discussed, the errors may be overestimated. Further, $^{14}CH_4$ for each climatic interval is represented by a pair of replicate samples. Even after all corrections, the agreement within all pairs is excellent, with the average pair difference being 0.82 pMC, and the largest pair difference being 1.74 pMC, which is within the combined ^{14}C measurement uncertainty. Such excellent agreement between replicates lends extra confidence to the results.

Keeping the above caveats in mind, the $^{14}CH_4$ results for the YD-PB transition are consistent with the earlier findings of Sowers (2006) (using δD of CH_4) and Schaefer et al. (2006) (using $\delta^{13}CH_4$) that clathrates did not play a substantial role in the YD-PB CH_4 transition, and that the CH_4 source mix did not change substantially from the YD to the PB. The $^{14}CH_4$ results suggest no change in the fossil CH_4 fraction about two thirds of the way through the CH_4 transition, but a small (6-7%) increase in the fossil fraction during the early Preboreal. Considering the available isotopic data and associated uncertainties, this 6-7% increase could be consistent with either emissions from marine clathrates or melting thermokarst lakes in eastern Siberia and Alaska.

The $^{14}CH_4$ results suggest a similar fossil fraction in the OD as compared to the YD. If the scenario with all $^{14}CH_4$ corrections is considered, the results suggest a ~7% higher fossil fraction in the OD. However, if the correction for in-situ CH_4 is not

made for the YD and OD samples, the results suggest no change in the fossil fraction between the two intervals.

The $^{14}CH_4$ results also suggest that 80-100% of the OD – Bølling [CH_4] rise (~100 ppb) was due to ^{14}C-free CH_4; this result hinges on the accuracy of the correction for in-situ CH_4 for the Bølling samples. This is surprising, as the interpolar gradient indicates that the extra CH_4 most likely originated in the low latitudes during this transition. Available GISP2 δD data rules out clathrates or hydrocarbon seeps as the sole source of this fossil CH_4, but allows for up to ~50% of the CH_4 increase to be from these sources. However, a large burst of clathrate CH_4 exclusively in the low latitudes seems unlikely, considering that the magnitude of the OD-Bølling abrupt climate events was greatest in the northern high latitudes. Even allowing for large emissions from clathrates or hydrocarbon seeps, up to 50% of the CH_4 increase (which also has to come from ^{14}C-dead or highly ^{14}C-depleted sources) is still unexplained. It may be possible that the large and abrupt increase in summer monsoon intensity in East Asia activated wetlands in areas with substantial deposits of aged organic matter, contributing to the inferred $^{14}CH_4$ decrease.

Acknowledgements

I plan to submit this Chapter, in part, for publication to a yet-to-be-determined journal, as: Petrenko, V.V., A.M. Smith, J.P. Severinghaus, E.J. Brook, D. Lowe, Q. Hua, K. Riedel, G. Brailsford, N. Reeh, H. Schaefer, R.F. Weiss and D. Etheridge. "A record of C-14 of atmospheric methane for the last glacial termination."

I thank the Keeling laboratory for their permission to use their sea water line for $^{14}CO_2$ processing of Pakitsoq samples. I thank the NIWA TROPAC group for hosting me during the $^{14}CH_4$ sample processing. I thank Gordon Brailsford and Katja Riedel for developing the method for CO extractions from Pakitsoq air and for processing the sample air for ^{14}CO. I thank Andrew Smith, Quan Hua and Alan Williams at ANSTO for graphitizing and measuring the ^{14}C in Pakitsoq CO and CO_2 samples. I thank all my co-authors as well as Devendra Lal for valuable discussions. I also thank Zhihui Wang and John Mak for measuring ^{13}C of CO in Pakitsoq samples.

Tables

Table 5.1 $^{14}CH_4$, $\delta^{13}CH_4$ and $[CH_4]$ for Pakitsoq samples, as well the $[CH_4]$ values expected based on the GISP2 ice core record. $^{14}CH_4$ values in the first column have been corrected for processing as described in Chapter 4. $\delta^{13}CH_4$ was measured at NIWA as described in Ferretti et al. (2005). $\delta^{13}CH_4$ values shown are as measured, without gravitational or diffusion corrections. All $[CH_4]$ values throughout this chapter are on the NOAA 04 scale (Dlugokencky et al., 2005). ^{14}C values corrected for in-situ CH_4 production are also shown. The LGM sample was not measured for $^{14}CH_4$.

Sample	$^{14}CH_4$, pMC	$\delta^{13}CH_4$, ‰ PDB	$[CH_4]$, ppb	$[CH_4]$ expected from GISP2, ppb	$^{14}CH_4$, corrected for in-situ CH_4, pMC	+ Error	- Error
Younger Dryas 1	35.42 ± 1.21	-45.22 ± 0.15	527 ± 10	525 ± 11	35.24	1.39	2.82
Younger Dryas 2	35.10 ± 1.19	-45.34 ± 0.14	531 ± 10	525 ± 11	34.64	1.65	2.82
YD-PB Transition 1A	34.40 ± 1.05	-46.05 ± 0.09	667 ± 13	584 ± 12	28.05	2.89	2.89
YD-PB Transition 2A	33.72 ± 1.04	-46.07 ± 0.13	687 ± 13	583 ± 12	25.66	2.95	2.95
YD-PB Transition 1B				677 ± 21	34.40	1.05	3.42
YD-PB Transition 2B				695 ± 22	33.72	1.04	3.35
Preboreal 1	32.11 ± 1.00	-45.10 ± 0.11	774 ± 15	765 ± 13	31.55	1.56	2.43
Preboreal 2	33.66 ± 1.03	-45.34 ± 0.09	771 ± 15	756 ± 13	32.78	1.92	2.48
Contaminated PB	62.98 ± 1.53	-51.74 ± 0.05	2197 ± 43	758 ± 13			
Oldest Dryas 1	28.26 ± 1.06	-43.25 ± 0.16	510 ± 10	497 ± 11	26.87	2.45	2.94
Oldest Dryas 2	28.69 ± 1.05	-43.08 ± 0.15	517 ± 10	497 ± 11	26.51	3.02	3.02
Contaminated OD	34.30 ± 1.07	-45.99 ± 0.18	583 ± 11	496 ± 11			
Bølling 1	29.65 ± 0.97	-46.08 ± 0.17	669 ± 13	602 ± 16	23.62	3.97	3.97
Bølling 2	29.11 ± 1.03	-46.37 ± 0.18	686 ± 13	605 ± 16	21.78	4.27	4.27
Last Glacial Maximum		-41.86 ± 0.18	419 ± 8				

Table 5.2. Pakitsoq sample [CO_2] and $^{14}CO_2$. First column: [CO_2] measured in sample tanks; measurements were performed at NIWA using a Hewlett-Packard 6890 GC equipped with a methanizer and flame-ionization detector. [CO_2] in the "Modern" and "Blank" CO_2 mixes was not measured; the value of 165 ppm was calculated from volumetric determinations of the amount of CO_2 and u.h.p. air used for preparing the mixtures. Second column: sample $^{14}CO_2$, corrected for ANSTO processing as described in Chapter 4. Third column: sample $^{14}CO_2$, further corrected for processing the air at SIO. Fourth column: expected $^{14}CO_2$ in the samples from INTCAL04 radiocarbon calibration (Reimer et al., 2004), based on mean sample air age. Fifth column: expected sample [CO_2], based on the Dome C ice core record (Monnin et al., 2001). Last column: inferred [CO_2] in sampled ice if all $^{14}CO_2$ elevation is assumed to arise from in-situ CO_2 production; see text for explanation. "Modern" and "dead" CO_2 samples at the bottom of the table were ~1000 μg C samples of pure CO_2.

Sample	[CO_2] in air sample, ppm	$^{14}CO_2$, pMC, corrected for ANSTO processing	$^{14}CO_2$, pMC, further corrected for SIO processing	Expected $^{14}CO_2$, pMC	Expected [CO_2], ppm	Speculated [CO_2] in sampled ice, ppm
Younger Dryas 1	109.68	68.45 ± 0.63	71.18 ± 2.75	28.52	251	1568
Younger Dryas 2	131.02	71.69 ± 0.75	74.04 ± 2.33	28.57	251	2417
YD - PB Transition 1	162.55	71.95 ± 0.98	73.85 ± 2.71	28.63	250	2321
YD - PB Transition 2	209.36	72.35 ± 0.77	73.85 ± 2.14	28.68	250	2320
Preboreal 1	154.50	65.47 ± 0.67	67.30 ± 2.53	28.86	254	1067
Preboreal 2	215.27	75.85 ± 0.72	77.36 ± 2.15	28.94	254	6566
Contaminated PB	147.17	67.62 ± 0.75	69.61 ± 2.72	28.93	254	1319
Oldest Dryas 1	160.17	70.69 ± 0.70	72.62 ± 2.25	21.00	223	1943
Oldest Dryas 2	213.76	74.01 ± 0.68	75.50 ± 2.20	21.00	223	3415
Contaminated OD	181.57	73.71 ± 0.70	75.46 ± 2.26	20.53	221	3374
Bølling 1	141.89	69.83 ± 0.72	71.96 ± 2.41	21.20	225	1779
Bølling 2	149.02	64.56 ± 0.70	66.44 ± 2.26	21.27	225	1014
Blank CO_2 mix #1	~165	-0.04 ± 0.20				
Modern CO_2 mix #1	~165	105.16 ± 1.34				
Modern CO_2 mix #2	~165	103.71 ± 1.45				
Blank CO_2 mix #2	~165	0.16 ± 0.22				
SIO modern CO_2		106.71 ± 1.19				
SIO modern CO_2		107.64 ± 1.20				
SIO dead CO_2		0.13 ± 0.14				
SIO dead CO_2		0.11 ± 0.15				

Table 5.3. Measured ^{14}CO values and corrections for ANSTO processing. Results are based on preliminary ^{14}C data from the ANTARES AMS run. Following quality control on individual sample measurements (to be done at ANSTO), the numbers may change slightly. First column: ^{14}C of the diluted sample (pMC), as measured. Sample and dilutant masses are as determined volumetrically at ANSTO. The errors for sample and dilutant masses have been increased to 5% (from the usual 1% error for ANSTO mass determinations) to account for some observed discrepancies between the calculated and measured total mass of sample + dilutant. The "Dead CO" samples are from a synthetic mixture of fossil CO and u.h.p. air. The "BHD" sample is clean ambient air sampled at Baring Head, New Zealand.

Sample Name	Measured ^{14}C of diluted sample, pMC	Sample Mass, µg C	Mass of dilutant, µg C	Dilution Factor	^{14}C atoms in diluted sample in 2007, not blank-corrected	^{14}C atoms in undiluted sample in 2007, blank-corrected
Dead CO mix#1 19 Nov 07	0.80 ± 0.09	5.96 ± 0.30	15.86 ± 0.79	3.7	1.05E+04 ± 1.16E+03	6.68E+03 ± 2.65E+03
BHD 6655	211.87 ± 1.57	5.17 ± 0.26	14.53 ± 0.73	3.8	2.51E+06 ± 2.87E+04	2.51E+06 ± 2.88E+04
Dead CO mix#1 20 Nov 07	1.50 ± 0.17	7.01 ± 0.35	16.44 ± 0.82	3.3	2.11E+04 ± 2.36E+03	1.73E+04 ± 3.35E+03
Younger Dryas 1	70.03 ± 1.25	3.64 ± 0.18	15.40 ± 0.77	5.2	8.08E+05 ± 1.62E+04	8.05E+05 ± 1.64E+04
Younger Dryas 2	49.10 ± 0.50	2.08* ± 0.10	15.77 ± 0.79	8.6	5.33E+05 ± 7.47E+03	5.29E+05 ± 7.84E+03
YD-PB Transition 1	78.03 ± 0.62	3.63 ± 0.18	15.30 ± 0.77	5.2	8.96E+05 ± 1.05E+04	8.92E+05 ± 1.08E+04
YD-PB Transition 2	67.48 ± 1.14	3.56 ± 0.18	15.10 ± 0.76	5.2	7.63E+05 ± 1.45E+04	7.60E+05 ± 1.47E+04
Preboreal 1	82.66 ± 0.87	3.31 ± 0.17	14.71 ± 0.74	5.4	9.03E+05 ± 1.26E+04	9.00E+05 ± 1.29E+04
Preboreal 2	70.98 ± 0.74	3.87 ± 0.19	15.03 ± 0.75	4.9	8.13E+05 ± 1.10E+04	8.09E+05 ± 1.13E+04
Contaminated PB	74.96 ± 0.60	4.5 ± 0.23	15.30 ± 0.77	4.4	8.99E+05 ± 1.05E+04	8.95E+05 ± 1.08E+04
Oldest Dryas 1	68.27 ± 0.73	4.95 ± 0.25	14.27 ± 0.71	3.9	7.94E+05 ± 1.07E+04	7.90E+05 ± 1.10E+04
Oldest Dryas 2	61.99 ± 0.73	4.31 ± 0.22	14.87 ± 0.74	4.5	7.20E+05 ± 1.06E+04	7.16E+05 ± 1.08E+04
Contaminated OD	69.46 ± 0.80	5.47 ± 0.27	15.07 ± 0.75	3.8	8.63E+05 ± 1.22E+04	8.59E+05 ± 1.25E+04

* Mass determination may not have been reliable

Table 5.4. Data from Pakitsoq sample processing for ^{14}CO at NIWA. Sample [CO] was calculated from [CO] measured in samples after dilution with CO-free u.h.p. air and the dilution factor. The error in [CO] is estimated to be 2%. [CO] measurements were performed as described in Chapter 4. The error in the yield may be up to 10%, due to extremely small sample size and uncertainties in [CO] and temperature of sample tanks (see text).

Sample	[CO], ppb	Yield, %	Volume of air put through the line, L STP	Volume of air used from sample tank, L STP	Maximum number of ^{14}CO molecules added from lab air	Minimum number of ^{14}CO molecules added from lab air	Maximum number ^{14}CO molecules in sample, corrected for NIWA processing	Minimum number ^{14}CO molecules in sample, corrected for NIWA processing
Dead CO mix #1 19 Nov 07	158.36	89.36						
BHD 6655	64.44	99.56						
Dead CO mix #1 20 Nov 07	158.36	90.43						
Younger Dryas 1	671.38	110.55	91.2 ± 4.6	86.6 ± 3.1	2.32E+05	2.20E+03	8.19E+05	5.56E+05
Younger Dryas 2	583.86	95.70	98.1 ± 4.9	79.5 ± 2.9	2.35E+05	0.00E+00	5.37E+05	2.86E+05
YD-PB Transition 1	636.37	110.00	94.1 ± 4.7	93.2 ± 3.4	1.87E+05	2.11E+03	9.01E+05	6.94E+05
YD-PB Transition 2	735.53	104.81	86.2 ± 4.3	84.9 ± 3.1	1.74E+05	1.18E+03	7.73E+05	5.70E+05
Preboreal 1	566.69	105.70	92.2 ± 4.6	90.9 ± 3.3	1.73E+05	1.13E+03	9.11E+05	7.14E+05
Preboreal 2	879.17	112.88	75.3 ± 3.8	72.6 ± 2.6	2.03E+05	2.93E+03	8.18E+05	5.95E+05
Contaminated PB	672.04	102.69	88.2 ± 4.4	87.0 ± 3.1	1.66E+05	6.97E+02	9.05E+05	7.18E+05
Oldest Dryas 1	998.17	120.12	89.2 ± 4.5	88.3 ± 3.2	2.46E+05	5.87E+03	7.95E+05	5.33E+05
Oldest Dryas 2	967.89	102.73	87.2 ± 4.4	86.9 ± 3.1	1.73E+05	9.80E+02	7.26E+05	5.32E+05
Contaminated OD	1286.09	104.87	88.3 ± 4.4	86.5 ± 3.1	2.20E+05	1.96E+03	8.70E+05	6.26E+05
Bølling 1	569.34	109.03	79.3 ± 4.0	78.6 ± 2.8	1.50E+05	1.48E+03		
Bølling 2	734.02	114.63	89.2 ± 4.5	89.0 ± 3.2	1.87E+05	3.18E+03		

Table 5.5. ^{14}CO sources in sampled Pakitsoq ice and the amount of ^{14}CO from direct cosmogenic production in ice. Sample gas ages are as in Chapter 3; sample mean ice ages were calculated using the mean sample gas age and the gas age – ice age difference for the corresponding GISP2 depth (as in (Schaefer et al., 2006)). Other columns are explained in the text. Maximum and minimum values in last two columns include a correction for ^{14}CO production in sample tanks during storage.

Sample	Mean sample ice age, yr BP	Mean sample gas age, yr BP	^{14}CO molecules from paleoatmospheric CO	Maximum ^{14}CO molecules from in-situ CO	Minimum ^{14}CO molecules from in-situ CO	Maximum fraction of ^{14}CO from paleoatmospheric and in-situ CO	Maximum ^{14}CO molecules per gram ice from cosmogenic production in ice	Minimum ^{14}CO molecules per gram ice from cosmogenic production in ice
Younger Dryas 1	12530	11637	3.87E+04	1.64E+05	5.95E+04	0.36	6.49	1.92
Younger Dryas 2	12523	11631	3.07E+04	1.12E+05	4.07E+04	0.50	4.27	0.02
YD-PB Transition 1	12420	11535	4.13E+04	1.63E+05	5.97E+04	0.29	6.83	2.96
YD-PB Transition 2	12416	11531	3.64E+04	1.68E+05	6.14E+04	0.36	6.17	2.12
Preboreal 1	12108	11364	4.02E+04	1.37E+05	5.16E+04	0.25	7.10	3.44
Preboreal 2	12082	11354	3.45E+04	1.88E+05	7.21E+04	0.37	7.78	2.76
Contaminated PB	12047	11337	3.74E+04	1.53E+05	5.85E+04	0.26	7.39	3.58
Oldest Dryas 1	15660	14760	2.82E+04	2.66E+05	7.07E+04	0.55	6.73	1.37
Oldest Dryas 2	15666	14766	2.38E+04	2.17E+05	5.80E+04	0.45	6.25	1.91
Contaminated OD	15952	15028	2.24E+04	2.84E+05	7.58E+04	0.49	8.02	2.34

Table 5.6. Modeled vs measured ^{14}CO in Pakitsoq samples. Ice for each sample was cut on two or more different days, which is why a "mean" sampling date is given. The measured values are as in Table 5.5. All ^{14}CO values are per gram ice.

Sample	Mean sampling depth, m	Mean sampling date	Predicted ^{14}CO, molecules/g, neutrons only	Predicted ^{14}CO, molecules/g, neutrons + muons	Predicted $^{14}CO_2$ molecules/g , neutrons + muons	Measured max cosmogenic ^{14}CO, molecules/g	Measured min cosmogenic ^{14}CO, molecules/g
Younger Dryas 1	1.13	6-Aug	2.53	9.49	28.46	6.49	1.92
Younger Dryas 2	1.12	10-Aug	2.44	9.36	28.09	4.27	0.02
YD-PB Transition 1	0.65	2-Aug	3.52	10.74	32.23	6.83	2.96
YD-PB Transition 2	1.63	6-Aug	1.87	8.61	25.82	6.17	2.12
Preboreal 1	0.34	21-Jul	4.85	12.33	36.98	7.10	3.44
Preboreal 2	0.58	28-Jul	3.87	11.17	33.51	7.78	2.76
Contaminated PB	0.68	23-Jul	3.87	11.17	33.51	7.39	3.58
Oldest Dryas 1	1.22	27-Jun	3.83	11.11	33.34	6.73	1.37
Oldest Dryas 2	1.65	8-Jul	2.58	9.55	28.66	6.25	1.91
Contaminated OD	0.83	27-Jun	4.84	12.31	36.94	8.02	2.34
Bølling 1	0.83	27-Jun	4.84	12.31	36.94		
Bølling 2	1.51	6-Jul	2.88	9.94	29.83		

Table 5.7. $^{14}CH_4$ corrections for direct cosmogenic production, assuming all production happens in the ablation zone. $^{14}CH_4$ values in first column are as in Table 5.1. The "wetland hypothesis" values assume $^{14}CH_4$ values equal to contemporaneous $^{14}CO_2$ and are based on mean sample ages and the INTCAL04 data (Reimer et al., 2004). All errors are 1-σ; but capped on the "+" side for some samples by actual $^{14}CH_4$ values measured in the samples as discussed in the text. Sample $^{14}CH_4$ values here are given in pMC and without age corrections. A scenario is also shown in which the cosmogenic correction, but not the correction for in-situ CH_4 is applied for the YD, YD-PB Transition (scenario B), PB and OD samples. These are samples for which the measured and expected [CH_4] values agree within errors; thus the correction for in-situ CH_4 may not be needed. Cosmogenic correction factors are relative to YD average.

Sample	$^{14}CH_4$, pMC, corrected for in-situ CH_4 production	+ Error	- Error	Expected $^{14}CH_4$, pMC, under wetland hypothesis	Number of $^{14}CH_4$ molecules per gram ice	+ Error	- Error	Cosmogenic $^{14}CH_4$ correction factor	$^{14}CH_4$, further corrected for cosmogenic production, pMC	+ Error	- Error	$^{14}CH_4$, pMC, with cosmogenic correction but w/o in-situ CH_4 correction	Error
Younger Dryas 1	35.24	1.39	2.82	28.52	0.51	0.02	0.04	1.01	28.78	1.55	2.91	28.64	1.40
Younger Dryas 2	34.64	1.65	2.82	28.57	0.51	0.03	0.04	0.99	28.31	1.78	2.90	28.45	1.37
YD-PB Transition 1 A	28.05	2.89	2.89	28.63	0.51	0.05	0.05	1.14	22.26	2.94	2.94		
YD-PB Transition 2 A	25.66	2.95	2.95	28.68	0.48	0.06	0.06	0.91	21.15	3.00	3.00		
YD-PB Transition 1 B	34.40	1.05	3.42	28.70	0.63	0.02	0.06	1.14	28.60	1.25	3.48	28.32	1.25
YD-PB Transition 2 B	33.72	1.04	3.35	28.74	0.64	0.02	0.06	0.91	29.21	1.23	3.41	28.98	1.23
Preboreal 1	31.55	1.56	2.43	28.86	0.67	0.04	0.05	1.31	25.83	1.68	2.51	26.11	1.18
Preboreal 2	32.78	1.92	2.48	28.94	0.70	0.04	0.05	1.19	27.58	2.02	2.56	28.20	1.23
Oldest Dryas 1	26.87	2.45	2.94	21.00	0.38	0.04	0.04	1.18	19.07	2.51	2.99	20.08	1.19
Oldest Dryas 2	26.51	3.02	3.02	21.00	0.38	0.04	0.04	1.01	19.91	3.07	3.07	21.76	1.19
Bølling 1	23.62	3.97	3.97	21.20	0.43	0.07	0.07	1.31	16.99	4.00	4.00		
Bølling 2	21.78	4.27	4.27	21.27	0.41	0.08	0.08	1.06	16.56	4.30	4.30		

*Excess 14CH4 over wetland hypothesis for Younger Dryas = 0.093 molecules g^{-1} ice

Table 5.8. Relative changes in the fossil fraction of the CH_4 budget for different pairs of climatic intervals. Calculations were performed using $^{14}CH_4$ data incorporating all corrections (top half of the table), as well as using the data set where YD, YD-PB Transition, PB and OD samples are not corrected for in-situ CH_4 production (bottom half of the table). % increase in $[CH_4]$ is calculated relative to the value for the second interval in each pair from the expected average $[CH_4]$ values for each type of sample, listed in Table 5.1. % change in fossil fraction is calculated as described in the text, except for the Oldest Dryas – Bølling pair, where Younger Dryas values instead of Oldest Dryas values are used in the denominator of Equation 5.3. This allows to incorporate the assumption that the fossil fraction during the OD is already non-zero. Maximum and minimum % increases in the fossil fraction are calculated using the maximum and minimum $^{14}CH_4$ values allowed for each type of sample by the error bars.

Periods compared	**% increase in $[CH_4]$**	**% change in fossil fraction**	**Max % increase in fossil fraction**	**Min % increase in fossil fraction**
ALL SAMPLES CORRECTED FOR BOTH IN-SITU CH4 AND COSMOGENIC PRODUCTION				
Younger Dryas - YD-PB Transition (B)	23.42	-0.68	11.48	-11.77
Younger Dryas - Preboreal	30.95	7.59	17.22	-4.47
Younger Dryas - Oldest Dryas	-5.59	7.17	20.65	-10.19
Oldest Dryas - Bølling	17.54	13.79	35.56	-11.02
ONLY BØLLING SAMPLES CORRECTED FOR IN-SITU CH4; ALL SAMPLES CORRECTED FOR COSMOGENIC PRODUCTION				
Younger Dryas - YD-PB Transition (B)	23.42	0.24	6.51	-6.46
Younger Dryas - Preboreal	30.95	6.04	12.00	-0.36
Younger Dryas - Oldest Dryas	-5.59	0.37	7.55	-7.33
Oldest Dryas - Bølling	17.54	20.67	37.07	2.89

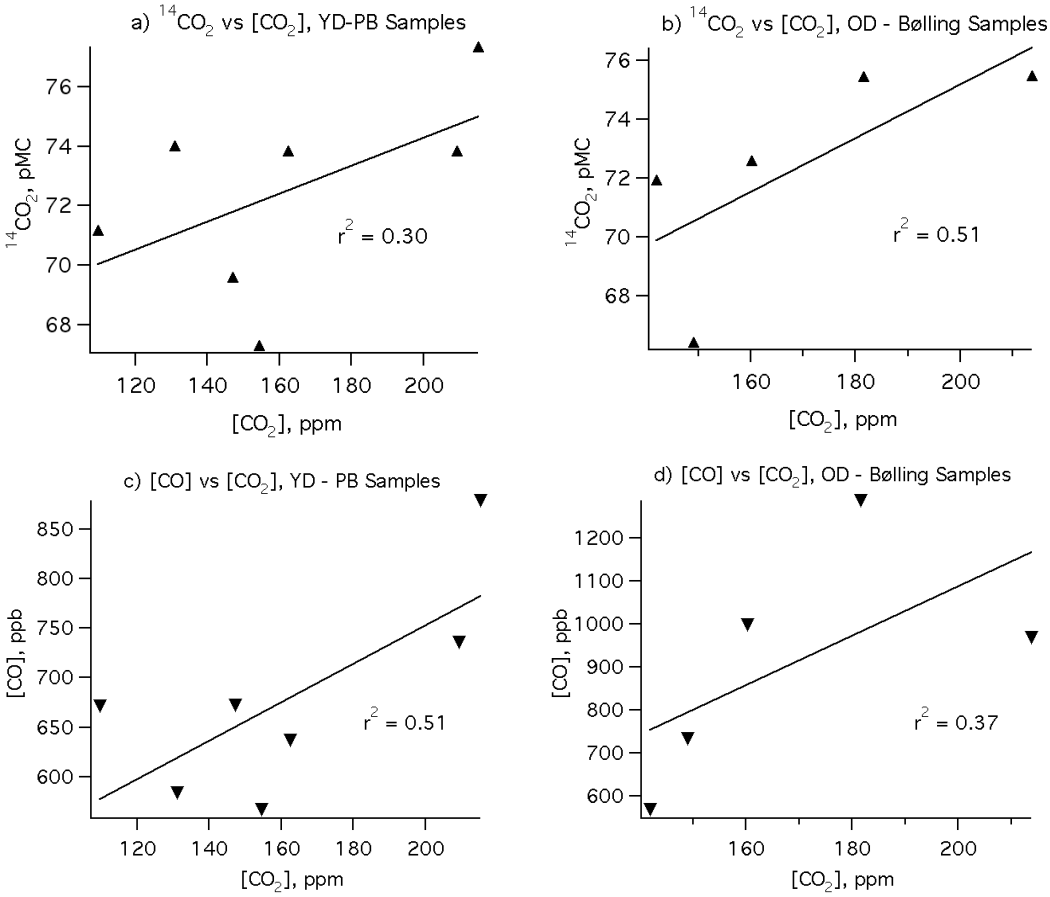

Figure 5.1. Relationship between [CO_2] and $^{14}CO_2$ or [CO] for the YD – PB and OD – Bølling samples.

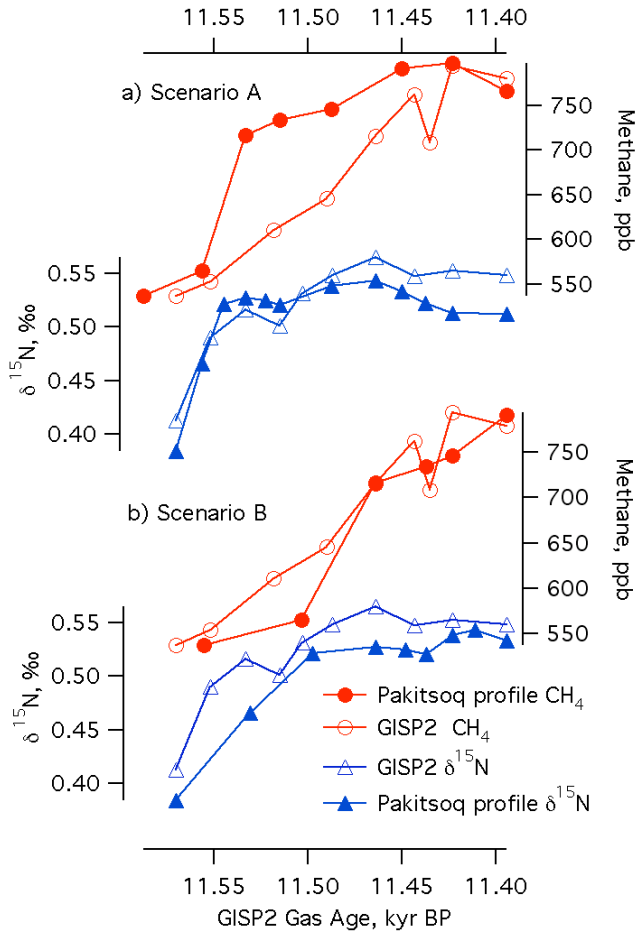

Figure 5.2. GISP2 and Pakitsoq records of $\delta^{15}N$ and $[CH_4]$ over the YD-PB transition, both on the GISP2 gas age scale as in (Schaefer et al., 2006). GISP2 $[CH_4]$ is from Brook et al. (2000), corrected up by 2% as described in Chapter 3; GISP2 $\delta^{15}N$ is from Severinghaus et al. (1998). All $[CH_4]$ values are on the NOAA04 scale. In scenario A, the highest $\delta^{15}N$ value in the Pakitsoq profile was matched to the highest value in the GISP2 $\delta^{15}N$ peak, and the "plateau" on the old (rising) side of the GISP2 $\delta^{15}N$ peak was matched to a similar feature in the Pakitsoq $\delta^{15}N$. The GISP2 $\delta^{18}O_{ice}$ record (Stuiver et al., 1995) indicates that the YD-PB abrupt warming at Greenland Summit was a 2-step event, so this transient plateau in $\delta^{15}N$ is a real feature of the record. In Scenario B, it was assumed that the plateau on the rising side of the $\delta^{15}N$ peak in Pakitsoq corresponded to the highest $\delta^{15}N$ value in the GISP2 record, while the plateau in $\delta^{15}N$ on the "falling" side of the peak in the GISP2 record (with very slightly lower $\delta^{15}N$ than the highest value) corresponded to the highest values in Pakitsoq.

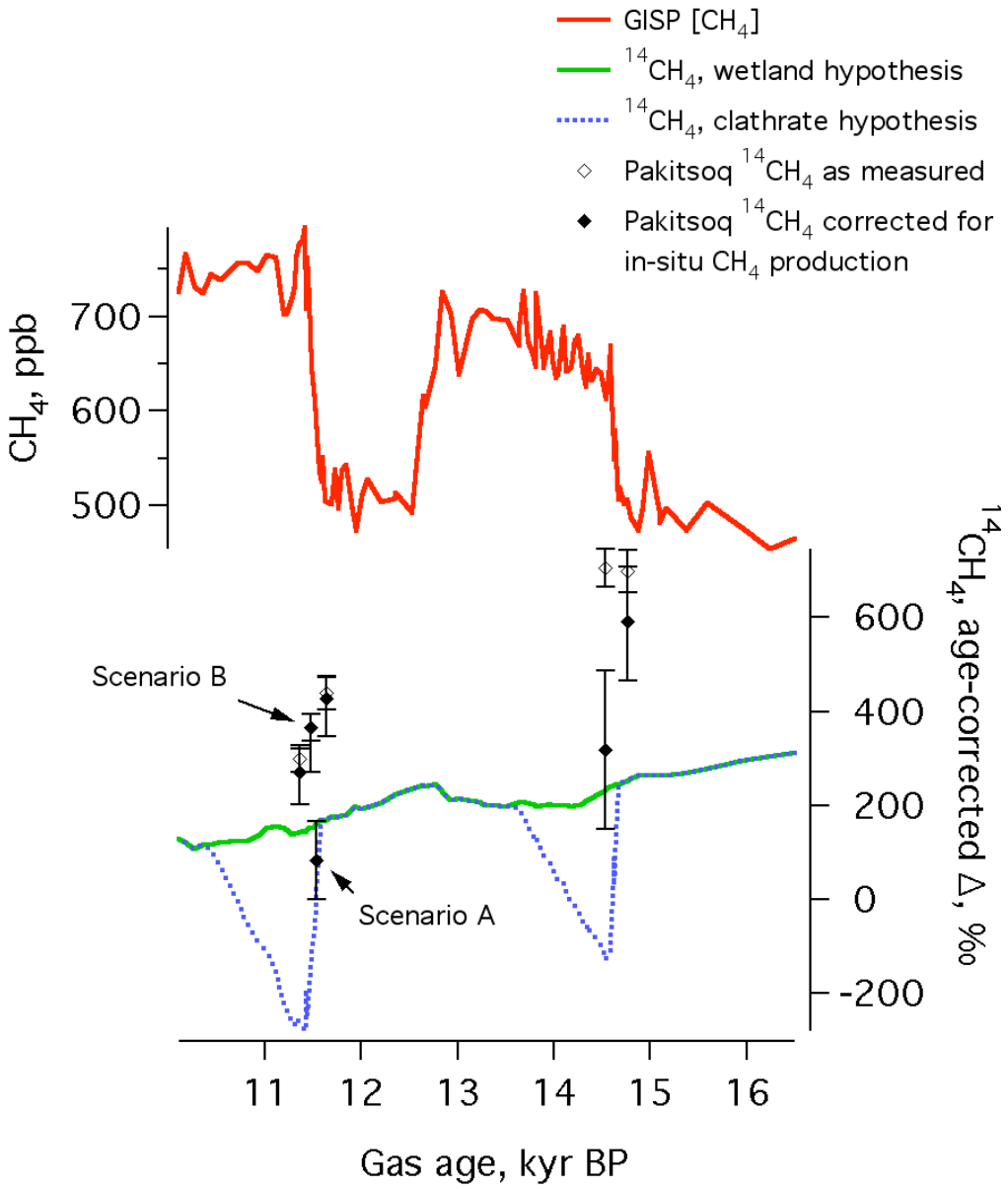

Figure 5.3. Pakitsoq sample $^{14}CH_4$, corrected for in-situ CH_4 production, compared with predictive $^{14}CH_4$ models discussed in Chapter 1 (Figure 1.5). Averages of replicate samples are shown (not individual samples). The uncorrected and corrected value for YD-PB Transition (scenario B) overlap completely. Note that no change or a drop in $^{14}CH_4$ through the transitions, depicted by the two models, are not the only possibilities. It is also possible to have an increase in $^{14}CH_4$ during the transitions. For example, if there is a substantial fossil CH_4 source during the YD, and the absolute magnitude of the fossil source stays unchanged through the YD-PB transition, $^{14}CH_4$ during the PB would actually be higher than during the YD.

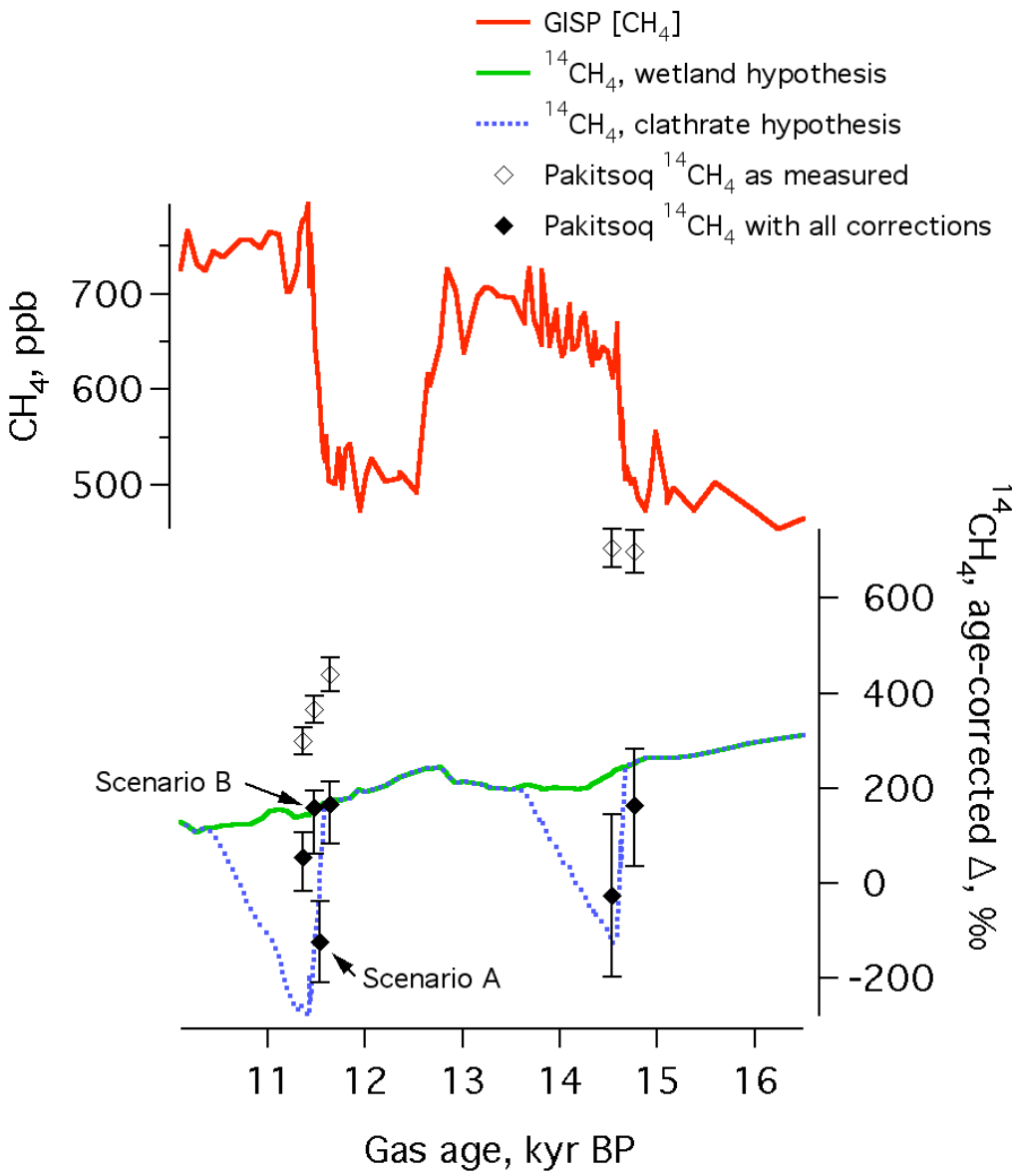

Figure 5.4. Pakitsoq sample $^{14}CH_4$, as measured (procedural corrections only), as well as with corrections for in-situ CH_4 production and cosmogenic production of $^{14}CH_4$ in the ablation zone. Average values for replicate samples are shown. The predictive $^{14}CH_4$ models are as in Chapter 1 and Figures 1.5 and 5.3.

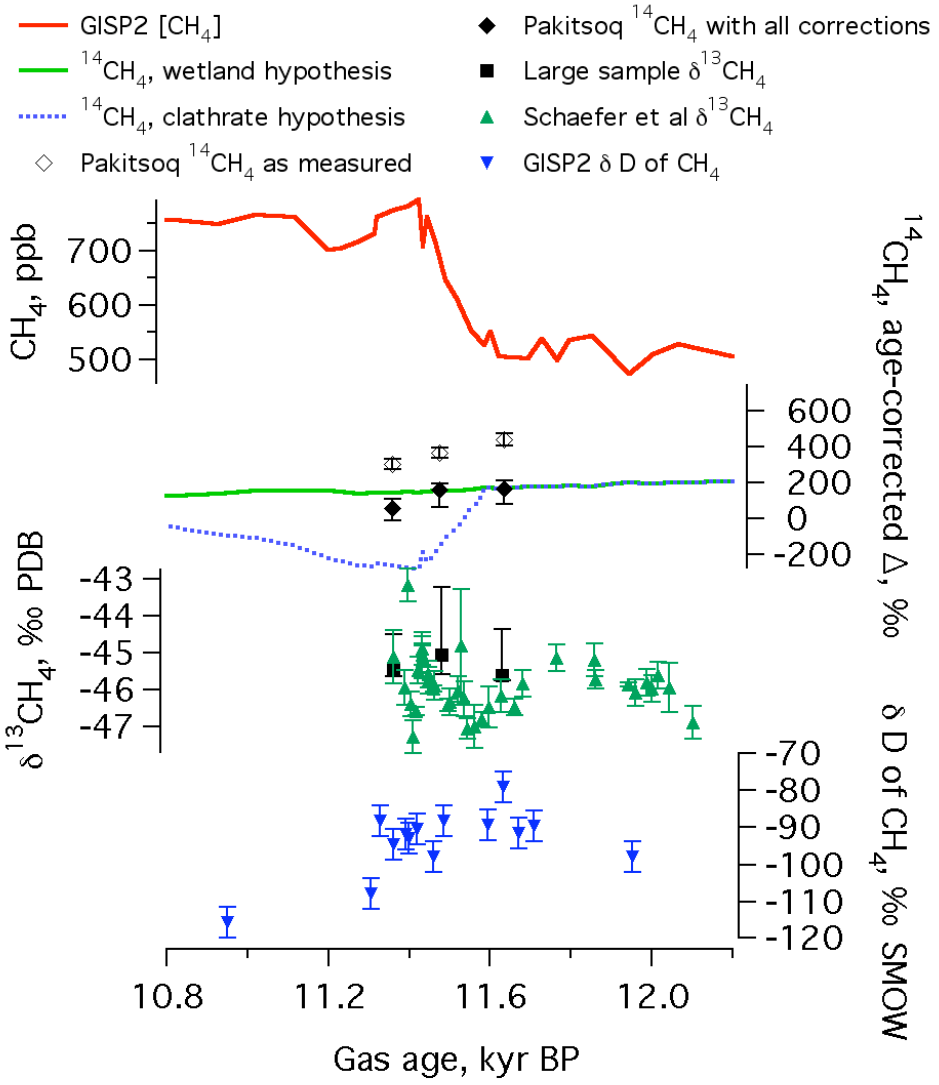

Figure 5.5. A record of [CH_4] and its isotopes over the YD-PB transition. [CH_4] is from GISP2 (Brook et al., 2000), corrected up by 2% for solubility effects as described in Chapter 3. Pakitsoq $^{14}CH_4$ values with and without corrections are as in Figure 5.4; Scenario A for YD-PB Transition has been removed. $\delta^{13}CH_4$ values for the large Pakitsoq YD-PB samples have been presented in Schaefer et al. (2006); here they are further corrected for possible in-situ CH_4 production using the same approach as was detailed for ^{14}C. The determined $\delta^{13}CH_4$ of the in-situ contaminant was –55.3 ± 2.3 ‰. Errors for corrected $\delta^{13}CH_4$ on the "-" side are limited by measured $\delta^{13}CH_4$ values. Other $\delta^{13}CH_4$ data are also from Pakitsoq ice (Schaefer et al., 2006). δD data are from Sowers (2006), placed on the Schaefer et al. (2006) age scale.

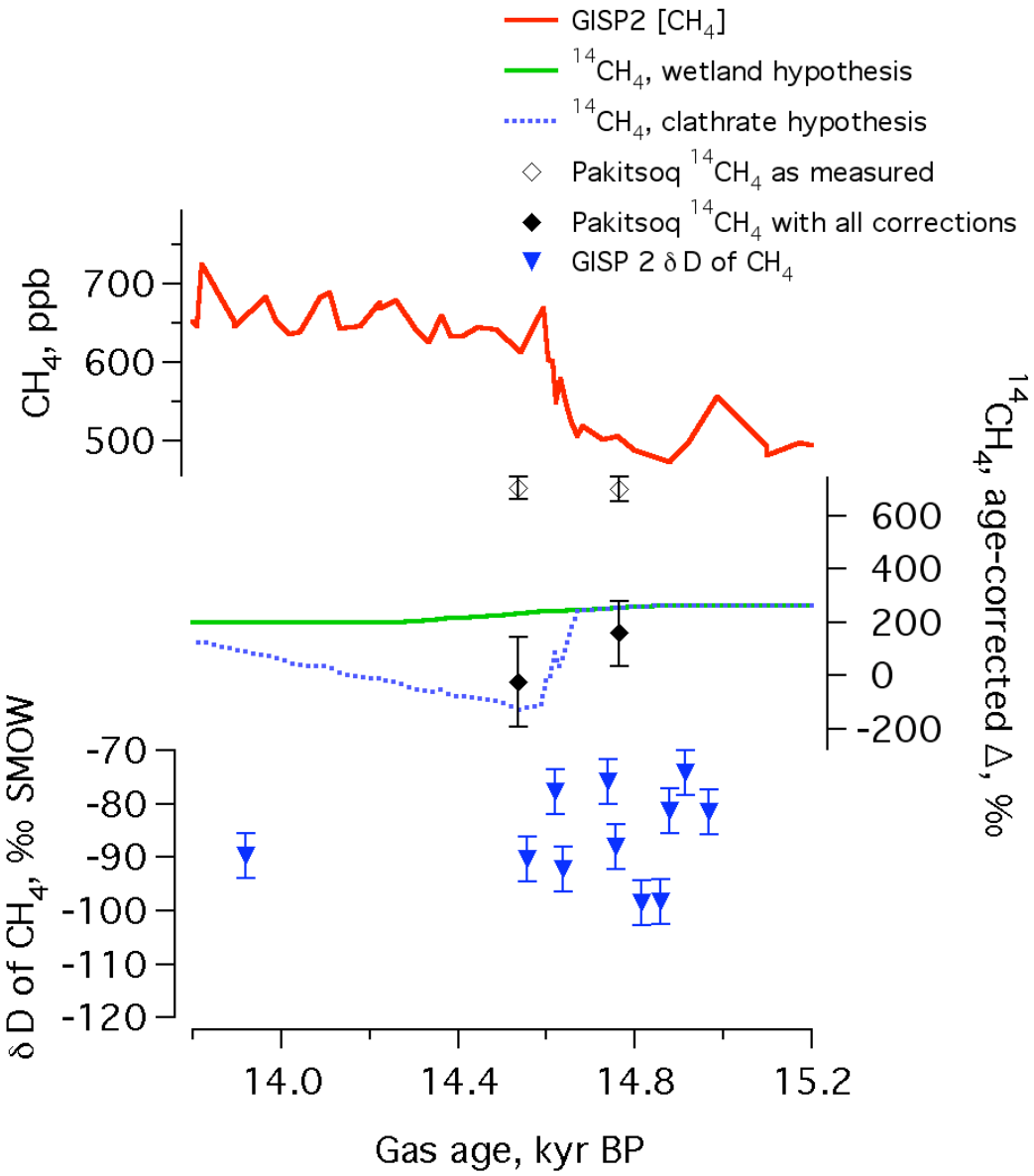

Figure 5.6. [CH_4] and its isotopes over the OD – Bølling transition. GISP2 [CH_4] and $^{14}CH_4$ models are as in preceding figures in this Chapter. Pakitsoq $^{14}CH_4$ is shown as measured as well as with all corrections applied. δD data are from Sowers (2006).

References

Bowater, L., Fairhurst, S.A., Just, V.J., Bornemann, S., 2004. Bacillus subtilis YxaG is a novel Fe-containing quercetin 2,3-dioxygenase. Febs Letters 557, 45-48.

Brenninkmeijer, C.A.M., 1993. Measurement of the Abundance of (CO)-C-14 in the Atmosphere and the C-13 C-12 and O-18 O-16 Ratio of Atmospheric CO with Applications in New-Zealand and Antarctica. Journal of Geophysical Research-Atmospheres 98, 10595-10614.

Brenninkmeijer, C.A.M., Lowe, D.C., Manning, M.R., Sparks, R.J., vanVelthoven, P.F.J., 1995. The C-13, C-14 and O-18 isotopic composition of CO, CH4, and CO2 in the higher southern latitudes lower stratosphere. Journal of Geophysical Research-Atmospheres 100, 26163-26172.

Brook, E.J., Harder, S., Severinghaus, J., Steig, E.J., Sucher, C.M., 2000. On the origin and timing of rapid changes in atmospheric methane during the last glacial period. Global Biogeochemical Cycles 14, 559-572.

Colussi, A.J., Hoffmann, M.R., 2003. In situ photolysis of deep ice core contaminants by Cerenkov radiation of cosmic origin. Geophysical Research Letters 30 (4), doi: 10.1029/2002GL016112.

Crutzen, P.J., Bruhl, C., 1993. A Model Study of Atmospheric Temperatures and the Concentrations of Ozone, Hydroxyl, and Some Other Photochemically Active Gases During the Glacial, the Preindustrial Holocene and the Present. Geophysical Research Letters 20, 1047-1050.

DeAngelis, M., Steffensen, J.P., Legrand, M., Clausen, H., Hammer, C., 1997. Primary aerosol (sea salt and soil dust) deposited in Greenland ice during the last climatic cycle: Comparison with east Antarctic records. Journal of Geophysical Research-Oceans 102, 26681-26698.

Dlugokencky, E.J., Myers, R.C., Lang, P.M., Masarie, K.A., Crotwell, A.M., Thoning, K.W., Hall, B.D., Elkins, J.W., Steele, L.P., 2005. Conversion of NOAA atmospheric dry air CH4 mole fractions to a gravimetrically prepared standard scale. Journal of Geophysical Research-Atmospheres 110 (D18), doi: 10.1029/2005JD006035.

Evans, I.M., 1970. The reactions of low energy 14C+ and 14CO+ ion beams with ice. PhD Thesis Thesis, University of Cambridge, 205 pp.

Ferretti, D.F., Miller, J.B., White, J.W.C., Etheridge, D.M., Lassey, K.R., Lowe, D.C., Meure, C.M.M., Dreier, M.F., Trudinger, C.M., van Ommen, T.D.,

Langenfelds, R.L., 2005. Unexpected changes to the global methane budget over the past 2000 years. Science 309, 1714-1717.

Field, C.V., Schmidt, G.A., Koch, D., Salyk, C., 2006. Modeling production and climate-related impacts on Be-10 concentration in ice cores. Journal of Geophysical Research-Atmospheres 111, doi: 10.1029/2005JD006410.

Finkel, R.C., Nishiizumi, K., 1997. Beryllium 10 concentrations in the Greenland Ice Sheet Project 2 ice core from 3-40 ka. Journal of Geophysical Research-Oceans 102, 26699-26706.

Haan, D., Martinerie, P., Raynaud, D., 1996. Ice core data of atmospheric carbon monoxide over Antarctica and Greenland during the last 200 years. Geophysical Research Letters 23, 2235-2238.

Haan, D., Raynaud, D., 1998. Ice core record of CO variations during the last two millennia: atmospheric implications and chemical interactions within the Greenland ice. Tellus Series B-Chemical and Physical Meteorology 50, 253-262.

Johnson, M.M., Nelson, W.T., 1971. Catalytic production of methane from carbon monoxide and steam. Patent no. US 3600145. Phillips Petroleum Co., U.S.

Lal, D., Jull, A.J.T., Burr, G.S., Donahue, D.J., 1997. Measurements of in situ C-14 concentrations in Greenland Ice Sheet Project 2 ice covering a 17-kyr time span: Implications to ice flow dynamics. Journal of Geophysical Research-Oceans 102, 26505-26510.

Lal, D., Jull, A.J.T., Burr, G.S., Donahue, D.J., 2000. On the characteristics of cosmogenic in situ C-14 in some GISP2 Holocene and late glacial ice samples. Nuclear Instruments & Methods in Physics Research Section B-Beam Interactions with Materials and Atoms 172, 623-631.

Lal, D., Jull, A.J.T., Donahue, D.J., Burtner, D., Nishiizumi, K., 1990. Polar Ice Ablation Rates Measured Using Insitu Cosmogenic C-14. Nature 346, 350-352.

Lal, D., Jull, A.J.T., Pollard, D., Vacher, L., 2005. Evidence for large century time-scale changes in solar activity in the past 32 Kyr, based on in-situ cosmogenic C-14 in ice at Summit, Greenland. Earth and Planetary Science Letters 234, 335-349.

Lal, D., Nishiizumi, K., Arnold, J.R., 1987. In-situ Cosmogenic H-3, C-14, and Be-10 for Determining the Net Accumulation and Ablation Rates of Ice Sheets. Journal of Geophysical Research-Solid Earth and Planets 92, 4947-4952.

Lal, D., Peters, B., 1967. Cosmic ray produced radioactivity on the Earth. In: S. Flugge (Editor), Handbuch der Physik. Springer-Verlag, Berlin, pp. 551 - 612.

Leuker, T.J., 1998. The ratio of the first and second dissociation constants of carbonic acid determined from the concentration of carbon dioxide in gas and seawater at equilibrium. PhD Thesis, University of California, San Diego, La Jolla, CA, 155 pp.

Lide, D.R., Frederikse, H.P.R. (Editors), 1995. CRC Handbook of Chemistry and Physics. CRC Press, Boca Raton, FL.

Lowe, D.C., Brenninkmeijer, C.A.M., Tyler, S.C., Dlugkencky, E.J., 1991. Determination of the Isotopic Composition of Atmospheric Methane and Its Application in the Antarctic. Journal of Geophysical Research-Atmospheres 96, 15455-15467.

Lowe, D.C., Levchenko, V.A., Moss, R.C., Allan, W., Brailsford, G.W., Smith, A.M., 2002. Assessment of "storage correction" required for in situ (CO)-C-14 production in air sample cylinders. Geophysical Research Letters 29, doi: 10.1029/2001GL014719.

Luyendyk, B., Kennett, J., Clark, J.F., 2005. Hypothesis for increased atmospheric methane input from hydrocarbon seeps on exposed continental shelves during glacial low sea level. Marine and Petroleum Geology 22, 591-596.

MacFarling Meure, C., 2004. The Variation of Atmospheric Carbon Dioxide, Methane and Nitrous Oxide During the Holocene from Ice Core Analysis. Ph.D. Thesis, The University of Melbourne, Melbourne, 189 pp.

Manning, M.R., Lowe, D.C., Moss, R.C., Bodeker, G.E., Allan, W., 2005. Short-term variations in the oxidizing power of the atmosphere. Nature 436, 1001-1004.

Mayewski, P.A., Meeker, L.D., Twickler, M.S., Whitlow, S., Yang, Q.Z., Lyons, W.B., Prentice, M., 1997. Major features and forcing of high-latitude northern hemisphere atmospheric circulation using a 110,000-year-long glaciochemical series. Journal of Geophysical Research-Oceans 102, 26345-26366.

Monnin, E., Indermuhle, A., Dallenbach, A., Fluckiger, J., Stauffer, B., Stocker, T.F., Raynaud, D., Barnola, J.M., 2001. Atmospheric CO2 concentrations over the last glacial termination. Science 291, 112-114.

Moran, J.J., House, C.H., Vrentas, J.M., Freeman, K.H., 2008. Methyl sulfide production by a novel carbon monoxide metabolism in Methanosarcina acetivorans. Applied and Environmental Microbiology 74, 540-542.

Muscheler, R., Beer, J., Wagner, G., Laj, C., Kissel, C., Raisbeck, G.M., Yiou, F., Kubik, P.W., 2004. Changes in the carbon cycle during the last deglaciation as indicated by the comparison of Be-10 and C-14 records. Earth and Planetary Science Letters 219, 325-340.

Novelli, P., 1999. CO in the atmosphere: measurement techniques and related issues. Chemosphere: Global Change Science 1, 115-126.

Novelli, P.C., Masarie, K.A., Lang, P.M., 1998. Distributions and recent changes of carbon monoxide in the lower troposphere. Journal of Geophysical Research-Atmospheres 103, 19015-19033.

Petrenko, V.V., Severinghaus, J.P., Brook, E.J., Reeh, N., Schaefer, H., 2006. Gas records from the West Greenland ice margin covering the Last Glacial Termination: a horizontal ice core. Quaternary Science Reviews 25, 865-875.

Petrenko, V.V., Severinghaus, J.P., Brook, E.J., Muhle, J., Headly, M., Harth, C.M., Schaefer, H., Reeh, N., Weiss, R.F., Lowe, D., Smith, A.M., 2008a. A novel method for obtaining very large ancient air samples from ablating glacial ice for analyses of methane radiocarbon. Journal of Glaciology 54, in press.

Petrenko, V.V., Smith, A.M., Brailsford, G. Riedel, K., Hua, Q., Lowe, D., Severinghaus, J.P., Levchenko, V., Bromley, T., Moss, R., Muhle, J., Brook E.J., 2008b. A new method for analyzing 14C of methane in ancient air extracted from glacial ice. Radiocarbon 50 (1), in press.

Price, P.B., 2007. Microbial life in glacial ice and implications for a cold origin of life. Fems Microbiology Ecology 59, 217-231.

Rabo, J.A., Elek, L.F., Francis, J.N., 1980. Cyclic two step process for production of methane from carbon monoxide. Patent no. US 4242103. Union Carbide Corporation (New York, NY), U.S.

Reeh, N., 1988. A Flow-Line Model for Calculating the Surface Profile and the Velocity, Strain-Rate, and Stress-Fields in an Ice-Sheet. Journal of Glaciology 34, 46-54.

Reeh, N., Oerter, H., Thomsen, H.H., 2002. Comparison between Greenland ice-margin and ice-core oxygen-18 records. Annals of Glaciology 35, 136-144.

Reimer, P.J., Baillie, M.G.L., Bard, E., Bayliss, A., Beck, J.W., Bertrand, C.J.H., Blackwell, P.G., Buck, C.E., Burr, G.S., Cutler, K.B., Damon, P.E., Edwards, R.L., Fairbanks, R.G., Friedrich, M., Guilderson, T.P., Hogg, A.G., Hughen, K.A., Kromer, B., McCormac, G., Manning, S., Ramsey, C.B., Reimer, R.W., Remmele, S., Southon, J.R., Stuiver, M., Talamo, S., Taylor, F.W., van der Plicht, J., Weyhenmeyer, C.E., 2004. IntCal04 terrestrial radiocarbon age calibration, 0-26 cal kyr BP. Radiocarbon 46, 1029-1058.

Rohde, R.A., Price, P.B., 2007. Diffusion-controlled metabolism for long-term survival of single isolated microorganisms trapped within ice crystals. Proceedings of the National Academy of Sciences of the United States of America 104, 16592-16597.

Rossler, K., Jung, H.J., Nebeling, B., 1984. Hot atoms in cosmic chemistry. Advances in Space Research 4, 83-95.

Rother, M., Metcalf, W.W., 2004. Anaerobic growth of Methanosarcina acetivorans C2A on carbon monoxide: An unusual way of life for a methanogenic archaeon. Proceedings of the National Academy of Sciences of the United States of America 101, 16929-16934.

Schaefer, H., Whiticar, M.J., Brook, E.J., Petrenko, V.V., Ferretti, D.F., Severinghaus, J.P., 2006. Ice record of delta C-13 for atmospheric CH4 across the Younger Dryas-Preboreal transition. Science 313, 1109-1112.

Severinghaus, J.P., Sowers, T., Brook, E.J., Alley, R.B., Bender, M.L., 1998. Timing of Abrupt Climate Change at the End of the Younger Dryas Interval from Thermally Fractionated Gases in Polar Ice. Nature 391, 141-146.

Smith, A.M., Levchenko, V.A., Etheridge, D.M., Lowe, D.C., Hua, Q., Trudinger, C.M., Zoppi, U., Elcheikh, A., 2000. In search of in-situ radiocarbon in Law Dome ice and firn. Nuclear Instruments & Methods in Physics Research Section B-Beam Interactions with Materials and Atoms 172, 610-622.

Sowers, T., 2006. Late quaternary atmospheric CH4 isotope record suggests marine clathrates are stable. Science 311, 838-840.

Stenstrom, T., 1970. On the chemical fate of nascent 11C atoms induced by irradiation of water and aqueous solutions with 185 MeV protons. PhD Thesis, University of Uppsala, Sweden, Uppsala, 190 pp.

Stuiver, M., Grootes, P.M., Braziunas, T.F., 1995. The GISP2 delta O-18 climate record of the past 16,500 years and the role of the sun, ocean, and volcanoes. Quaternary Research 44, 341-354.

Tsunogai, U., Nakagawa, F., Gamo, T., Ishibashi, J., 2005. Stable isotopic compositions of methane and carbon monoxide in the Suiyo hydrothermal plume, Izu-Bonin arc: Tracers for microbial consumption/production. Earth and Planetary Science Letters 237, 326-340.

van der Borg, K., van der Kemp, W.J.M., Alderliesten, C., de Jong, A.F.M., Lamers, R.A.N., 2001. In-situ radiocarbon production by neutrons and muons in an antarctic blue ice field at Scharffenbergbotnen: A status report. Radiocarbon 43, 751-757.

van der Kemp, W.J.M., Alderliesten, C., Van Der Borg, K., De Jong, A.F.M., Lamers, R.A.N., Oerlemans, J., Thomassen, M., Van De Wal, R.S.W., 2002. In situ produced C-14 by cosmic ray muons in ablating Antarctic ice. Tellus Series B-Chemical and Physical Meteorology 54, 186-192.

van der Kemp, W.J.M., Alderliesten, C., van der Borg, K., Holmlund, P., de Jong, A.F.M., Karlof, L., Lamers, R.A.N., Oerlemans, J., Thomassen, M.,van de Wal, R.S.W., 2000. Very little in situ produced radiocarbon retained in accumulating Antarctic ice. Nuclear Instruments & Methods in Physics Research Section B-Beam Interactions with Materials and Atoms 172, 632-636.

van de Wal, R.S.W., Vanderborg, K., Oerter, H., Reeh, N., Dejong, A.F.M., Oerlemans, J., 1990. Progress in C-14 Dating of Ice at Utrecht. Nuclear Instruments & Methods in Physics Research Section B-Beam Interactions with Materials and Atoms 52, 469-472.

van Roijen, J., Van Der Borg, K., DeJong, A., Oerlemans, J., 1995. A correction for in-situ C-14 in Antarctic ice with (CO)-C-14. Radiocarbon 37, 165-169.

Walter, K.M., Edwards, M.E., Grosse, G., Zimov, S.A., Chapin III, F.S., 2007. Thermokarst Lakes as a Source of Atmospheric CH4 During the Last Deglaciation. Science 318, 633 - 636.

Walter, K.M., Zimov, S.A., Chanton, J.P., Verbyla, D., Chapin, F.S., 2006. Methane bubbling from Siberian thaw lakes as a positive feedback to climate warming. Nature 443, 71-75.

Wang, Y.H., Jacob, D.J., 1998. Anthropogenic forcing on tropospheric ozone and OH since preindustrial times. Journal of Geophysical Research-Atmospheres 103, 31123-31135.

Wang, Y.J., Cheng, H., Edwards, R.L., An, Z.S., Wu, J.Y., Shen, C.C., Dorale, J.A., 2001. A high-resolution absolute-dated Late Pleistocene monsoon record from Hulu Cave, China. Science 294, 2345-2348.

Weidick, A., Oerter, H., Reeh, N., Thomsen, H.H., Thorning, L., 1990. The Recession of the Inland Ice Margin During the Holocene Climatic Optimum in the Jakobshavn-Isfjord Area of West Greenland. Global and Planetary Change 82, 389-399.

Yiou, F., Raisbeck, G.M., Baumgartner, S., Beer, J., Hammer, C., Johnsen, S., Jouzel, J., Kubik, P.W., Lestringuez, J., Stievenard, M., Suter, M., Yiou, P., 1997. Beryllium 10 in the Greenland Ice Core Project ice core at Summit, Greenland. Journal of Geophysical Research-Oceans 102, 26783-26794.

Chapter 6:

Summary of main accomplishments and outlook for future work

6.1 Summary of main accomplishments of the Ph.D. project

- Established an easily accessible, unlimited archive of ancient ice dating to the last glacial termination at the Pakitsoq ice-margin ablation site in West Greenland.
- Established a detailed ice and gas chronology for the section of the outcrop spanning the last glacial termination.
- Demonstrated that records of $\delta^{18}O_{ice}$, $\delta^{18}O_{O2}$ and $\delta^{15}N_{N2}$ in this ice are well preserved.
- Demonstrated that records of $[CH_4]$ are well preserved in most of the ice, but alterations are present in some sections.
- Developed a system capable of extracting 30 – 35 L STP of occluded air from glacial ice in just a few hours, without contamination from ambient air, without significant isotopic fractionation of the gases, and without alteration of CH_4 ($[CH_4]$ blank < 4 ppb).
- Found an aluminum surface treatment (chemical polishing + anodizing) which results in near-total elimination of procedural $[CH_4]$ blank associated with the aluminum surface.
- Developed a method for processing low-$[CH_4]$ air (such as ancient air from glacial ice) for CH_4 isotopic analyses. Eliminated carbon memory in the air processing line and reduced the processing blank to 0.23 ± 0.16 μg of 23.57 ± 16.22 pMC carbon by the use of a small amount of platinized quartz wool as the CH_4 combustion catalyst.

- Achieved quantitative removal of CO and eliminated the possibility of ^{14}C interference from ^{14}CO in the air samples through the use of the Sofnocat reagent.
- Reduced graphitization times for small (10 – 45 μg C) CO_2 samples from up to 4 days to ≤ 80 min by employing a colder, more effective water vapor trap (-65˚C instead of – 39˚C).
- Reduced graphitization blanks to an unprecedentedly low value of 0.03 μg of 100 pMC carbon.
- Achieved an overall $^{14}CH_4$ processing blank of 0.75 ± 0.38 pMC for ~20 μg, ^{14}C-free air samples with [CH_4] of 500 ppb.
- Successfully measured $^{14}CH_4$ in 14 air samples extracted from last-glacial-termination ice, finding higher-than-expected values for all samples.
- Determined the most likely $^{14}CH_4$ for an in-situ CH_4 contaminant affecting some of the samples and applied appropriate corrections to sample $^{14}CH_4$.
- Determined that direct cosmogenic production of $^{14}CH_4$ molecules in glacial ice is the most likely mechanism for the observed $^{14}CH_4$ elevation over maximum expected values, possibly providing the first detection of cosmogenic $^{14}CH_4$ in a natural setting.
- Performed measurements of $^{14}CO_2$ in the ancient air samples.
- Performed measurements of ^{14}CO in the ancient air samples, finding surprisingly low values of 0 – 8 ^{14}CO molecules per gram of ice, which

suggested that most or all cosmogenic ^{14}CO produced in the accumulation zone had somehow been lost.

- Applied a speculative correction for cosmogenic $^{14}CH_4$ production to the results. The corrected results suggest no substantial changes in the fossil CH_4 fraction for the YD-PB transition, which argues against substantial clathrate involvement. The corrected results also suggest that 80 – 100% of the OD – Bølling CH_4 transition was driven by ^{14}C-free methane sources. This result depends heavily on the applied corrections. It is thus speculative and remains to be confirmed.

6.2 Outlook for future paleo $^{14}CH_4$ work

Measurements of deep ice core $\delta^{13}CH_4$ from Greenland and comparisons to the Pakitsoq $\delta^{13}CH_4$ record should allow a test of the integrity of Pakitsoq YD, Transition, PB and OD ice for $[CH_4]$, and either confirm or remove the need for the in-situ CH_4 correction which has so far increased $^{14}CH_4$ uncertainties by a factor of 2 or more. We therefore recommend that such a study is conducted. Further $^{14}CH_4$ work should be done at ablation sites where absolutely no in-situ CH_4 production takes place. This should be possible at cold blue-ice sites in Antarctica, such as Taylor glacier (Aciego et al., 2007). It may also be possible at other ice-margin sites in Greenland where the ice layers have not interacted with subglacial sediment.

Cosmogenic $^{14}CH_4$ production, if real (as is suggested by our results), presents a ubiquitous obstacle to paleo $^{14}CH_4$ reconstructions. Production at both the

accumulation and ablation zone for each sampling site must be carefully investigated and quantified before accurate corrections can be made. A test is currently planned to see whether cosmogenic $^{14}CH_4$ is produced and retained in the top few meters of the firn at Summit, Greenland.

References

Aciego, S.M., Cuffey, K.M., Kavanaugh, J.L., Morse, D.L., Severinghaus, J.P., 2007. Pleistocene ice and paleo-strain rates at Taylor Glacier, Antarctica. Quaternary Research 68, 303-313.